Nonlinear Rigid Block Dynamics

Thesis by
Peter Pich

In Partial Fulfillment of the Requirements
for the Degree of
Doctor of Philosophy

California Institute of Technology
Pasadena, California

1995
(Submitted December 12, 1994)

Acknowledgments

I would like to thank the California Institute of Technology for making it possible for me to visit the US and study here.

I would like to thank my advisor, Dr. John Hall. He suggested the problem which became my thesis topic and he guided me through the whole project. I appreciate all the time he has given me over the years and I am grateful for his advice, support and patience during this endless process.

I would like to thank Dr. Stephen Wiggins for his directions and suggestions in the work on chaotic aspects of the problem.

Finally, I want to thank two of my fellow students: Maurice van Putten and Blair Zajac. Maurice helped me a lot not only with discussions, advice and even with office space but also by listening to my presentations and simply by being interested in the problem. Blair helped me with almost anything related to computers. He introduced me to the world of Sparcstations, Unix, and the C language. He provided the latest software and he also functioned as an on-line computer help. Finally he proofread the whole thesis.

I also want to thank Jurij Levin for his useful ideas and help in the final stages of the project.

.

Abstract

Motion of a block on flat ground under the influence of gravity is studied.

A general model is introduced for the free motion of a rectangular, rigid block on a continuous, perfectly elastic foundation. The model includes friction forces between the block and foundation and allows for sliding, rocking and flight of the block. Solutions are obtained through numerical integration. A three parameter study is carried out, namely as a function of aspect ratio, r, coefficient of friction, μ, and non-dimensional stiffness, k_-, for various initial conditions.

Dominant types of response are identified and the stability of the block against overturning and its tendency to fly are studied. For initial conditions with sufficient energy, critical curves are found in the (k_-, r) parameter space which define a transition between a flight and no flight region. For initial conditions with sufficient energy there also exists a critical curve in the same parameter space which separates a region of overturning from a region where the block does not overturn.

Chaos is found in the flight region of the (k_-, r) parameter space for sufficiently high r. Poincare maps and Liapunov exponents are computed to document the existence of chaos.

Contents

List of Tables

List of Figures

Chapter 1

Introduction

Why study rigid block dynamics?

Rigid block dynamics is a rewarding subject. A simple, common object like a rectangular block can behave in a variety of different ways when interacting with even such a simple environment as an elastic half space.

Consider the following 'experiment.' Take a rectangular block composed of a hard material having dimensions 1x5x10 cm (i.e. a brick.) Place the block on a flat surface, for example a table. Rotate the block a little with one corner remaining on the table and release it. Depending on the block's $\frac{height}{width}$ ratio you will observe quite different behavior. To be more specific: if the block's dimensions in the plane of rotation are $\frac{height}{width} = \frac{10}{1}$ the block will rock back and forth a few times. The rotation amplitude will get smaller and eventually the block stops moving. If the dimensions are $\frac{height}{width} = \frac{10}{6}$ the block will bounce only once, jump forward and immediately stop. If $\frac{height}{width} = \frac{5}{10}$ the block is likely to clear the table and fly shortly before stopping. In the first described case it took a few seconds, while in the latter two cases the block stops almost immediately. The moral is that the block displayed qualitatively different behavior due to the change of only one parameter - its aspect ratio.

It is our goal to develop a simple model of the block simulating to some extent real world behavior, such as the situation described above. Studying dynamics of a rigid block is interesting from a purely academic perspective: finding and understanding why and how a simple block may behave in a complicated way.

At the same time, the subject of rigid block dynamics definitely has a wide application. Many man made objects are block-like: starting with a box of matches and ending with a high rise building. An immediate application of considerable importance is performance of rectangular structures or

objects during an earthquake. Some important questions arising in this context are: Will the given rectangular object overturn when subjected to a certain ground acceleration? How can we prevent overturning? What will be the acceleration of the object during the earthquake induced motion? Is the block going to slide? What will be the final displacement?

Objects, whose earthquake response is of prime interest to engineers, include towers, nuclear reactors, base isolated buildings, statues, monuments, and on a smaller scale, laboratory or hospital equipment, computers, precious museum pieces ... and the list goes on. Undoubtedly, the reader can think of other examples.

Previous work

Rigid objects overturned in an earthquake can be seriously damaged, say when a TV set or computer overturns and falls down from a shelf. They can also hurt people, as when a piece of factory machinery falls on somebody. Due to importance of such earthquake related issues most studies in rigid block dynamics were geared towards earthquake applications.

Previous studies dealt mostly with *forced* vibrations and could be divided along two lines of research. The first line of research, represented mainly by the work of *Psycharis* [1991] and *Yim and Chopra* [1983], considered SDOF (single degree of freedom) structures on an elastic foundation. The structure, subjected to horizontal ground motions, was attached to a rigid mat. The mat was allowed to uplift. The foundation was represented by two spring damper elements placed at each corner of the foundation mat or by continuous spring damper elements distributed over the entire mat width. The main goal was to study the influence of foundation mat uplift on earthquake response.

The second line of research, undertaken by many authors, considered a rigid block rocking on rigid ground, where impact treatment was based on the assumption that the angular velocity after impact equals the angular velocity before impact times a restitution coefficient ranging from 0 to 1. Among the more recent publications, we highlight a complex investigation done by *ShentonIII* [1990] and by *Jones and ShentonIII* [1990]. The authors developed a model of the block allowing for motion in any of five modes of response: rest, slide, rock, slide rock, and free flight. The block was excited by a harmonic force or by impulsive periodic loading. For the interested reader, *ShentonIII* [1990] also includes a detailed survey of previous research on the subject. Other articles in the field include *Koh and Spanos* [1986], *Spanos and Koh* [1984], *Andreaus* [1990], *Matsui et al.* [1991] and a series of articles by Hogan [*Hogan*, 1994a], [*Hogan*, 1992b], [*Hogan*, 1992a], [*Hogan*, 1994b].

Research on chaotic aspects of rigid block dynamics has been recently presented by *Yim and Lin* [1991b], *Yim and Lin* [1991a] and, in analytical treatment, by *Bruhn and Koch* [1991].

Our model and objectives of work

We model a rigid block moving on an elastic ground in 2 dimensions. Naturally, a 3-dimensional study would be more realistic and very interesting but far more difficult so we leave it just as a possibility for future work. To our knowledge, no study in 3 dimensions has been published so far.

The block is rectangular and rigid in our model. The foundation is a continuous, elastic half space commonly called a Winkler foundation. Interaction between the two is realized by a vertical foundation reaction force and by a horizontal friction force resisting motion of the block along the foundation surface. We do not put any damper elements in the foundation and do *not* apply an *external* time dependent *excitation* to the block. Energy can be dissipated only by friction forces.

The block does or does not slide horizontally depending upon the available friction force acting at its lowest corner. Such treatment results in a dynamical system switching between 4 and 6 dimensions. The equations of motion are different in the two cases, therefore we introduce the notion of 'contact' and 'slide' modes. Also, the special case of zero friction removes any horizontal force resulting in a 4-dimensional system. The block is allowed to fly as well. By defining appropriate transition conditions the block can switch to either of the modes or flight.

Thus, the formulated model combines an elastic continuous foundation, as in *Psycharis* [1991], *Yim and Chopra* [1983], with treatment allowing for motion in different modes, as in *ShentonIII* [1990]. The presence of an elastic foundation allows us to introduce fewer, but more general modes than in *ShentonIII* [1990].

We aim at creating a simple model which would allow for general, unrestricted types of motion and treat impact without a restrictive coefficient of restitution. Our objective then is to use the model for a general investigation of rigid block dynamics. While the present work is not concentrated around a specific area like earthquake engineering, the results are applicable to it. The reader can argue that since our model incorporates neither external excitation nor damping it little resembles motion of the block in an earthquake. But does a harmonic excitation describe earthquake ground motion better than a single initial pulse? An initial impulse can be translated into appropriate initial conditions, just like the ones we later call ic2.

The beauty of numerical simulations is that a model can be *easily* altered. Thus, we can add damping, make friction proportional to the square of velocity,... or even incorporate an external force on the top of existing code. It is a beauty of mechanics that a simple model, where all physics limits to $mx'' = f$ and the concept of friction, can show rich behavior - including chaos. Let us see that on the next pages.

Chapter 2

Analytical model

The physical system investigated consists of a block moving on a flat horizontal surface. The block is subjected to initial conditions such that it moves only in a fixed vertical plane. Motion of the block evolves under the action of gravity and interaction with the ground. The block and ground interact only when in direct contact with each other. There is no ground acceleration.

2.1 Model

2.1.1 Block, foundation and the range of motion

We model the physical system in 2 dimensions. The block is modeled as a rigid, rectangular block of height a and width b. The mass of the block is m and is distributed evenly in the block. Therefore, the center of gravity of the block is at its geometric center and its moment of inertia, I, about the center is given by $I = (a^2 + b^2)m/12$.

The ground is modeled as a Winkler foundation, only vertical stress, no shear, is considered. The foundation is elastic, and there is no viscous damping present. The stiffness constant characterizing the foundation flexibility is denoted as k. That means to hold a horizontal foundation strip of width dv at the depth s below the foundation surface we need to apply the force $df = ks \, dv$.

We assume range of motion such that at most two corners of the block sink under the foundation surface at a given time. Motion of the block is observed only up to a point of overturning. By the point of overturning we understand a position when the diagonal of the block is vertical. Only blocks with their height longer than or equal to their width, i.e., $a \geq b$ are considered.
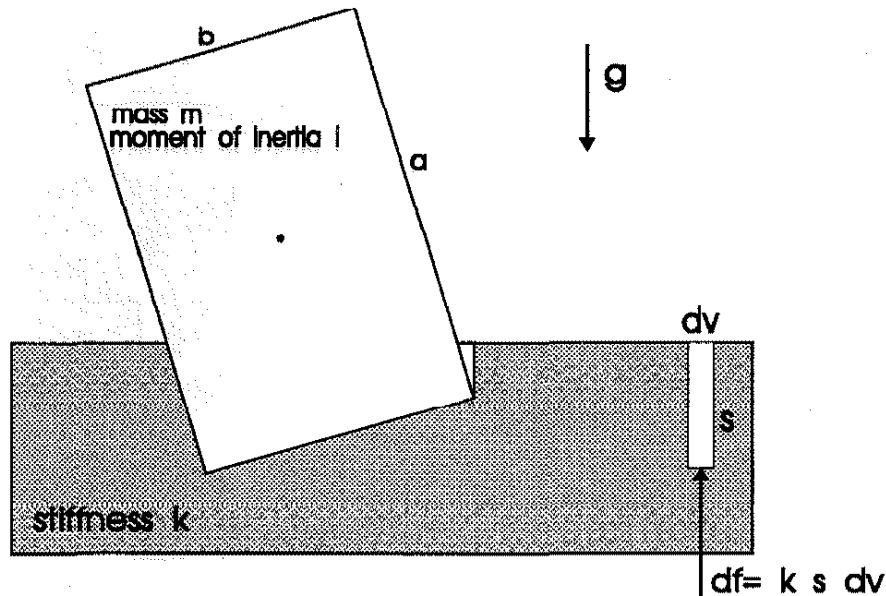
Figure 2.1: Block and foundation

2.1.2 Block foundation interaction

If the whole block is above the foundation, there is no interaction between the two.

When part of the block is below the foundation surface, interaction between the block and the foundation is modeled by two forces: the vertical R_y and the horizontal R_x.

The horizontal force R_x is the conventional friction force which resists the horizontal motion of the block along the foundation surface. It is the only horizontal force introduced in the system. We let R_x act only at the lowest corner of the block. This assumption simplifies the model and implies that no energy is lost while the block rotates about its lowest corner. Let the friction between the block and the foundation be characterized by a coefficient of friction μ, then $|R_x| \leq \mu R_y$.

The vertical force R_y is the resultant of all the vertical forces the foundation exerts on the block. These are the forces which push the block up out of the foundation. Now we determine the magnitude and the line of action of R_y. Refer to Figure 2.2 for the following derivation. Let us consider a connected rigid 2-D object with a piecewise smooth boundary sinking in a Winkler foundation. By the definition of a Winkler foundation, each foundation strip of infinitesimal width dv compressed to the depth s below the foundation surface will contribute an infinitesimal vertical force $df = ks\,dv$ pushing the object up. Vector summation of all such forces is R_y. We have

$$R_y = \int_{v1}^{v2} ks(v)dv = k \int_{v1}^{v2} s(v)dv.$$
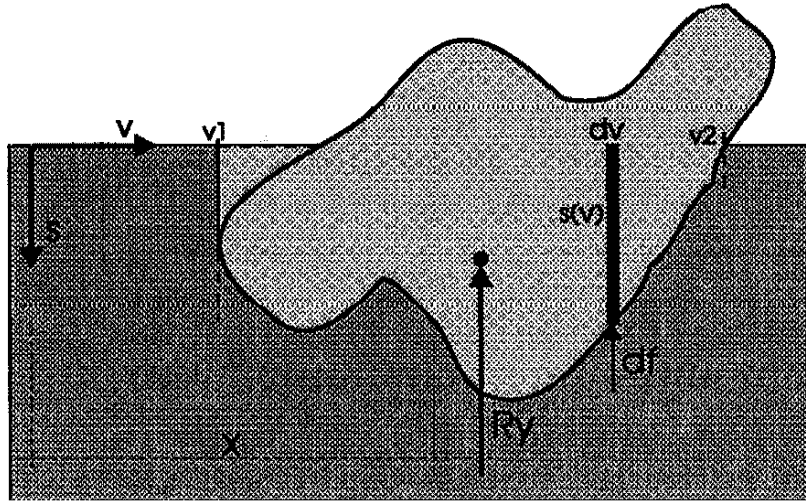
Figure 2.2: Winkler foundation

Let the position of the line of action of R_y be given by x with respect to the employed coordinate system. We find x from the moment equilibrium about the origin of the coordinate system:

$$R_y x = \int_{v1}^{v2} vks(v)\mathrm{d}v.$$

Clearly

$$x = \frac{\int_{v1}^{v2} vks(v)\mathrm{d}v}{R_y} = \frac{\int_{v1}^{v2} vs(v)\mathrm{d}v}{\int_{v1}^{v2} s(v)\mathrm{d}v}.$$

Thus, x is simply an x coordinate of the geometric center of the region, where the elastic foundation was displaced by a rigid object sinking in it. The vertical force R_y acts at the geometric center of that region.

Hereafter we refer to the region, where the elastic foundation was displaced by a rigid object, as the *Region*. In Figure 2.2, the *Region* is the part of the picture below the surface($s > 0$), lightly shaded. The magnitude of R_y is the area of the *Region* multiplied by the stiffness constant k. Note that *Region* consists not only of the part of the object under the surface, but also of any vertical gap between the object and the surface. In Figure 2.2, such a gap is of triangular shape and on the left side of the rigid object.

We can summarize our knowledge about R_y in the following: R_y is a vertical force larger than zero acting at the geometric center of the *Region*. Let the area of the *Region* be given by *area*, then $R_y = k\,area$.

2.1.3 Equations of motion
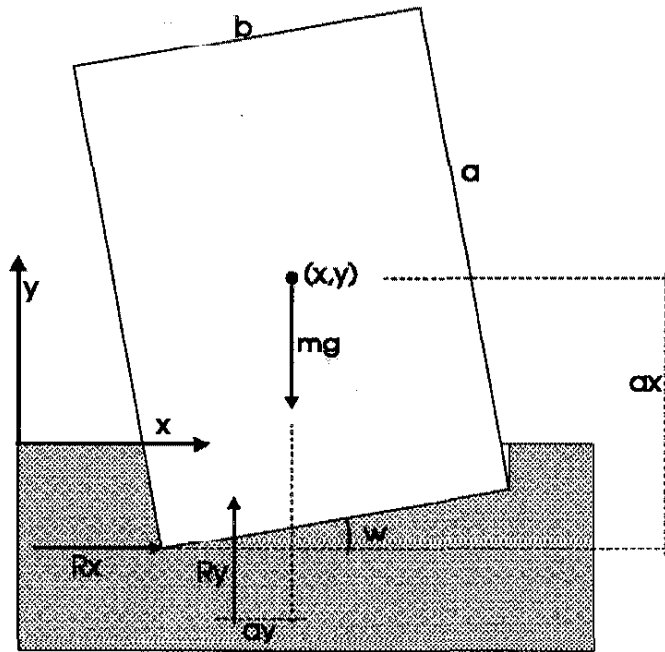
Figure 2.3: Block foundation interaction

The block is a rigid body moving in a 2-dimensional plane. To describe uniquely its motion, we need three variables, let us call them $x(t), y(t), w(t)$. Time t is the independent variable, $x(t)$ and $y(t)$ are the x and y coordinates of the center of the block in the usual Cartesian coordinate system. The x axis is aligned with the foundation surface and points to the right, the y axis points vertically up. The third variable, $w(t)$, is the angle of rotation of the block. The rotation angle $w(t)$ is measured from a horizontal line counterclockwise to the line passing through the bottom edge of the block.

Now we can write three simple equations of motion for the considered system. The equations, in terms of chosen variables, are:

$$
\begin{aligned}
m\ddot{x}(t) &= R_x \\
m\ddot{y}(t) &= R_y - mg \\
I\ddot{w}(t) &= R_x a_x + R_y a_y,
\end{aligned}
$$

where a_x is the difference between y (the y coordinate of the center of the block) and the y coordinate of the point where R_x acts. Similarly, a_y is the difference between x (the x coordinate of the center of the block) and the x coordinate of the point where R_y acts. Note that a_x is always positive but a_y can be negative to account for the correct sign of the moment $R_y a_y$.

2.1.4 Non-dimensional analysis

We rewrite the analytical formulation of the problem in a non-dimensional form. This will determine the relevant parameters in the problem, thus reducing the number of parameters needed. This approach also clarifies and simplifies the equations.

First we perform a non-dimensional analysis to determine how to combine existing parameters to form a smaller set of new non-dimensional parameters. Subsequently we introduce non-dimensional variables and rewrite the equations of motion in a non-dimensional form. From now on we work with only non-dimensional constants, parameters, variables and equations. All newly introduced variables and equations will be non-dimensional. As a notational convention, we attach an underscore $_$ to a symbol to distinguish it from its dimensional counterpart. For example, the x coordinate of the center of the block, x is a physical quantity length using unit meter. Its non-dimensional counterpart of unit 1 is x/a, described by a symbol $x_$. So $x_ = x/a$ and similarly $y_ = y/a$, etc. However, if there is no need to put $_$ at the end of a non-dimensional symbol to avoid double notation we do not do so. For example, the non-dimensional aspect ratio r given by $r = b/a$ does not need an underscore $_$ attached to it. Neither does the coefficient of friction μ or the angle w (measured in radians) which are from the outset of dimension 1.

The non-dimensional analysis is omitted here. We merely state results. Both the old and new parameters and variables are presented in Table 2.1. The derivative dx/dt with respect to time t is written as $\dot{x}(t)$, whereas the derivative with respect to non-dimensional time $t_$ is written as $x_'(t_)$. The original six parameters are reduced to three non-dimensional parameters: μ, r, $k_$. Only the variables $t, x, y, w, \dot{x}, \dot{y}, \dot{w}$ and their non-dimensional counterparts are presented in Table 2.1. All other variables are put in a non-dimensional form in a similar manner. For example, $R_{x_} = R_x/mg$. The new variables $x_, y_, w$ are functions of non-dimensional time $t_$. That is $x_ = x_(t_), y_ = y_(t_), w = w(t_)$. The new parameter $k_$ has a nice physical interpretation: a block of unit height will sink $1/k_$ units deep under the foundation surface when resting in a vertical static equilibrium. Now we can state the equations of motion in terms of the non-dimensional parameters and variables:

$$x_'' = R_{x_} \tag{2.1}$$

$$y_'' = R_{y_} - 1 \tag{2.2}$$

$$I_ w'' = R_{x_} a_{x_} + R_{y_} a_{y_}, \tag{2.3}$$

where $I_ = I/ma^2 = (1 + r^2)/12$.

	old	dimension	new	dimension
	a	m		
	b	m	$r = b/a$	1
Parameters	m	kg		
	g	m/s^2		
	μ	1	μ	1
	k	kg/ms^2	$k_- = kab/mg$	1
	t	s	$t_- = t\sqrt{g/a}$	1
	$x(t)$	m	$x_-(t_-) = x(t)/a$	1
	$\dot{x}(t)$	m/s	$x_-'(t_-) = \dot{x}(t)/\sqrt{ag}$	1
Variables	$y(t)$	m	$y_-(t_-) = y(t)/a$	1
	$\dot{y}(t)$	m/s	$y_-'(t_-) = \dot{y}(t)/\sqrt{ag}$	1
	$w(t)$	1	$w(t_-)$	1
	$\dot{w}(t)$	1/s	$w'(t_-) = \dot{w}\sqrt{a/g}$	1

Table 2.1: Parameters and variables

2.1.5   The right-hand side

To fully describe the analytical model we must express $R_{x-}, R_{y-}, a_{x-}, a_{y-}$ on the right-hand side of equations 2.1, 2.2, 2.3 in terms of the variables x_-, y_-, w.

First consider a simple case when the whole block is above the foundation. There is no interaction between the block and the foundation. Therefore $R_{x-} = R_{y-} = a_{x-} = a_{y-} = 0$.

In the other case, when a part of the block is under the foundation surface, we can evaluate R_{y-}, a_{x-}, a_{y-} solely from the geometry of our model. Directly from Figure 2.4 or 2.5, we see that

$$a_x(w) = a\cos(w)/2 + b\sin(w)/2 \qquad \text{for } w > 0.$$

Clearly for $w < 0$ the figure is symmetric and

$$a_x(w) = a\cos(-w)/2 + b\sin(-w)/2 \qquad \text{for } w < 0.$$

Thus, after dividing by a the formula for a_{x-} can be stated in a non-dimensional form

$$a_{x-}(w) = \cos(w)/2 + r\sin(|w|)/2,$$

which holds for any w.

Now we determine a_{y-} and $area_-$. We need to determine $area_-$ since $R_{y-} = k_- area_-$. We have to figure out the x coordinate of the geometric center of the *Region* to get a_{y-} and area of the *Region* to get $area_-$. The derivation is lengthy and therefore omitted, we only state formulas for a_{y-} and

*area_*. Formulas differ depending on whether only one or two of the corners are below the foundation surface. Declare:

position type **1**   exactly **one** corner of the block is under the surface
position type **2**   exactly **two** corners of the block are under the surface.

A drawing of a block in each position and corresponding formulas for a_{y-} and *area_* are shown in Figures 2.4 and 2.5. For a_{y-} the - sign holds for $w > 0$ and + sign holds for $w < 0$. The sign ensures the correct orientation of the turning moment $R_{y-}a_{y-}$. Let us verify the formulas for two special cases. For $w = 0$ we correctly get in position type **2**:

$$area_- = 1/2 - y_- \qquad\qquad a_{x-} = 1/2 \qquad\qquad a_{y-} = 0.$$

The position when exactly one corner is at the surface and exactly one is under the surface is both type 1 and type 2. In such a 'border' position, *area_* computed in type 1 must be equal to *area_* computed in type 2. Also a_{y-} must be the same computed in type 1 as in a type 2 position. Indeed, in 'border' position

type 1 $area_- =$ type 2 $area_- = \frac{r \sin |w|}{2 \cos w}$ and

type 1 $a_{y-} =$ type 2 $a_{y-} = \frac{r \cos w}{2} - \frac{\sin |w|}{2} - \frac{r \sin |w|}{3} \left(\frac{\cos w}{\sin |w|} - \frac{\sin |w|}{\cos w} \right)$.

Finally let us state the relations which hold $\forall\ y_-, w$:

$$
\begin{aligned}
area_-(y_-, w) &= area_-(y_-, -w) \\
area_-(y_-, w) &\geq 0 \\
a_{x-}(w) &= a_{x-}(-w) \\
a_{y-}(y_-, w) &= -a_{y-}(y_-, -w).
\end{aligned}
$$

These relations follow from the formulas for $area_-, a_{x-}, a_{y-}$ and are in accordance with the physical meaning of those quantities.

2.2   Modes

We have already determined a_{x-}, a_{y-}, R_{y-} in terms of y_-, w. In order to express the right-hand side of the equations 2.1, 2.2 and 2.3 in terms of the variables x_-, y_-, w we have yet to determine R_{x-}.

If the whole block is above the foundation surface, the block is in flight and $R_{x-} = 0$.

If not, then part of the block is below the surface and R_{x-} is the friction force resisting horizontal motion of the block along the foundation surface. The value of R_{x-} can be any real number satisfying $|R_{x-}| \leq \mu R_{y-}$
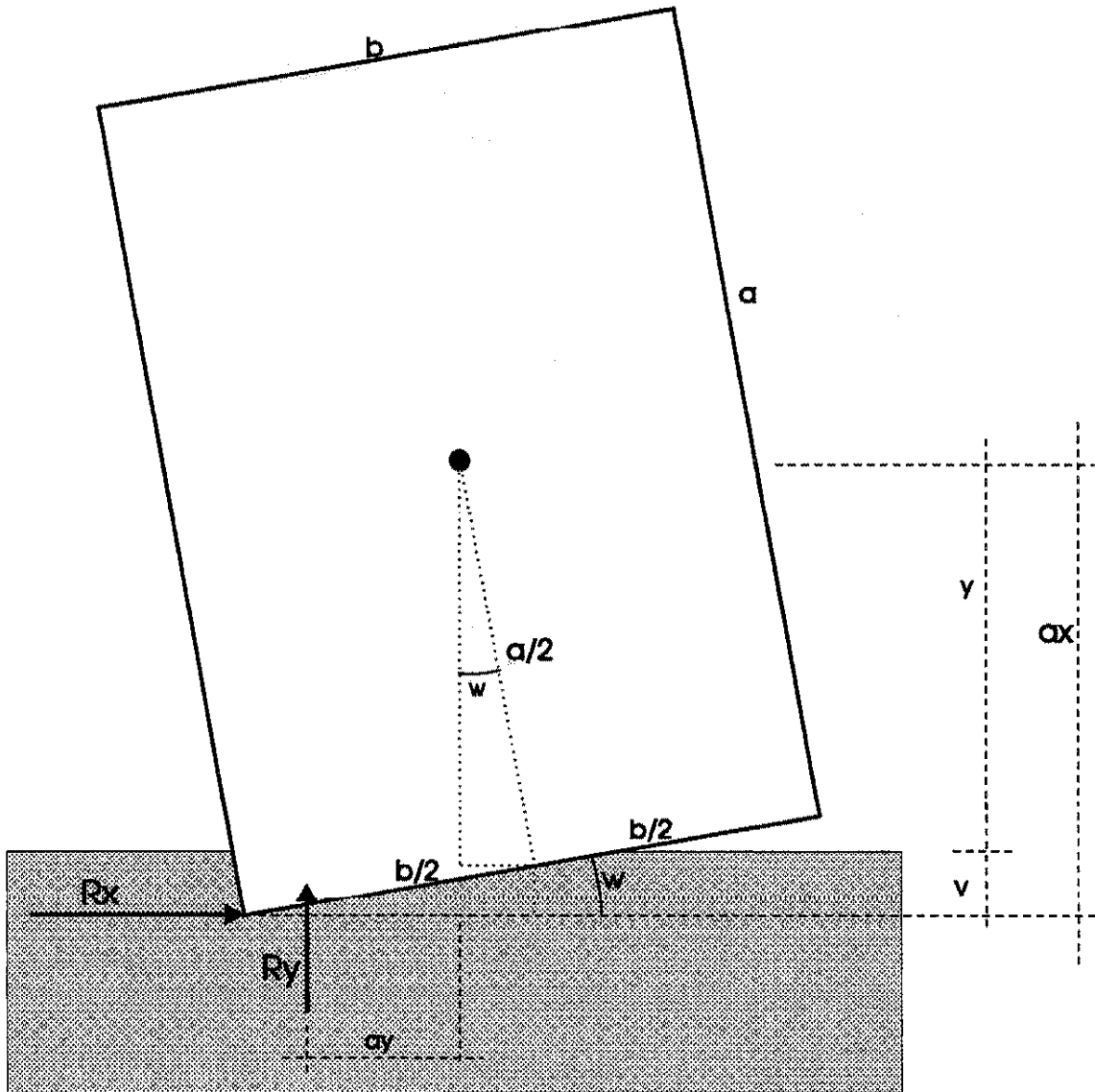
$$v_-(y_-, w) = \cos(w)/2 + r\sin(|w|)/2 - y_-$$

$$area_-(y_-, w) = \frac{v_-^2(y_-, w)}{2r\sin(|w|)\cos(w)}$$

$$\pm a_{y-}(y_-, w) = r\cos(w)/2 - \sin(|w|)/2 - v_-(y_-, w)/3 \left(\frac{\cos(w)}{\sin(|w|)} - \frac{\sin(|w|)}{\cos(w)}\right)$$

Figure 2.4: Position type 1
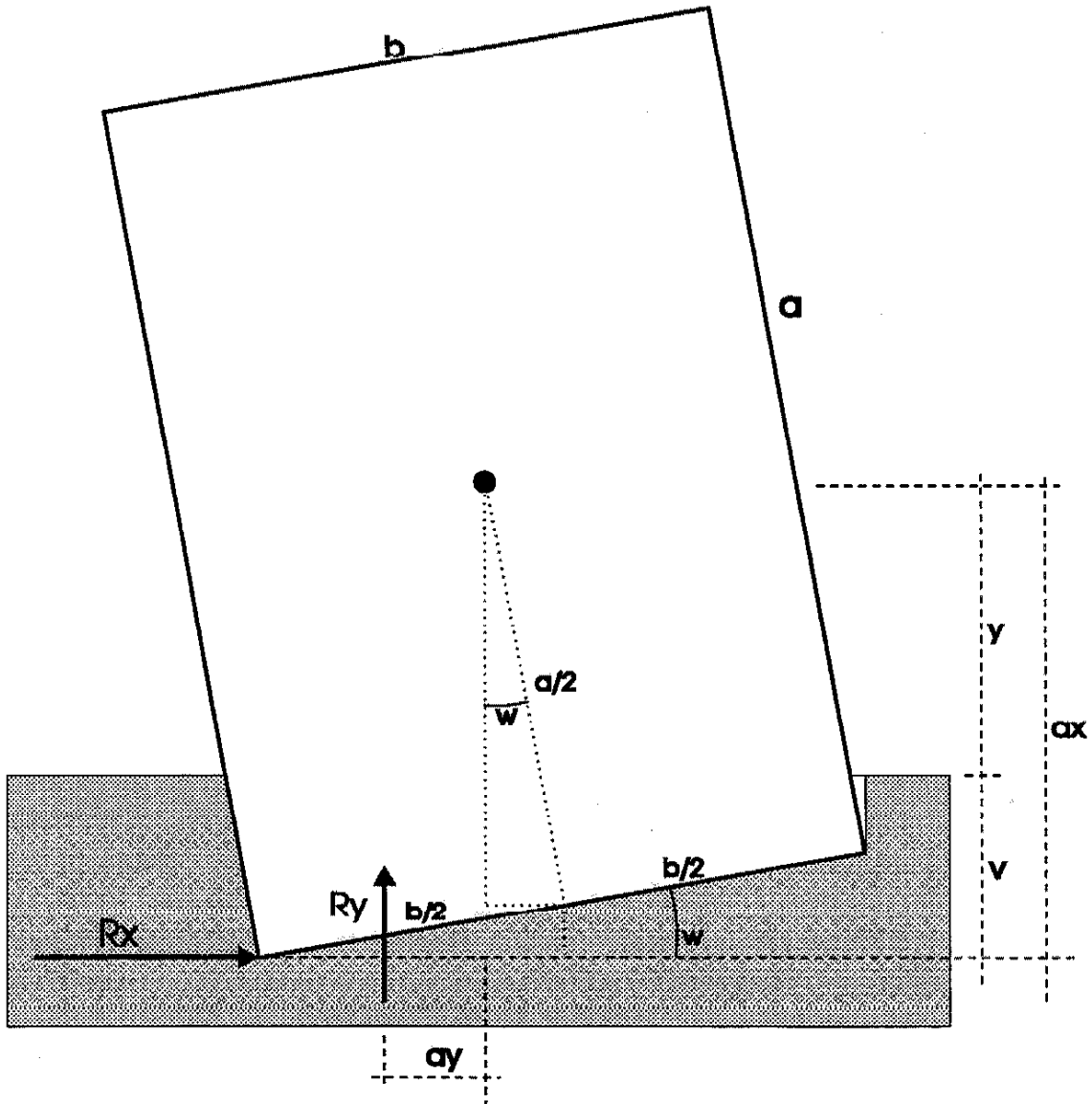
$$v_-(y_-, w) = \cos(w)/2 + r\sin(|w|)/2 - y_-$$

$$area_-(y_-, w) = (\cos(w) - 2y_-)\cos(w)/2 + \frac{\sin(|w|)}{2r\cos(w)}v_-{}^2(y_-, w)$$

$$\pm a_{y-}(y_-, w) = r\cos(w)/2 - \sin(|w|)/2 -$$

$$\frac{1}{3}\frac{r^2\cos^4(w)(3\cos(w)/2 - r\sin(|w|)/2 - 3y_-) - v_-{}^3(y_-, w)\sin^2(|w|)}{r\cos^3(w)(\cos(w) - 2y_-) + \sin(|w|)\cos(w)v_-{}^2(y_-, w)}$$

Figure 2.5: Position type **2**

Say the bottom of the block is sliding and the lowest corner of the block is moving to the right, that is in the positive x direction. Then there is a horizontal force R_{x-} acting at that corner against such motion, that is acting in negative x direction. The magnitude of R_{x-} is given by $R_{x-} = \mu R_{y-}$. Suppose the horizontal motion of the corner stops and block starts rotating about that corner. What will be the value of R_{x-} now? Furthermore, since the block rotates now about its corner, the variable $x_-(t_-)$ can be stated in terms of $w(t_-)$. One degree of freedom is lost.

Clearly one must account for different regimes (modes) of motion of the block. We introduce two basic modes of motion: **slide mode** and **contact mode**.

We will use frequently the terms 'lower left corner' and 'lower right corner.' When the block rests at a vertical position $w = 0$, we label its four corners as lower left and right, upper left and right corners, according to their physical position at the moment. The corner's label remains the same as the block moves even when the physical position of the corner may not correspond to the label at some time. For example, a corner labeled as the lower left corner will be still called lower left corner even when the blocks turns +90 degrees and the said corner is now physically the lower right corner. On the other hand, the term 'lowest corner' means exactly what it says. At a given time, the lowest corner is the corner positioned vertically lowest of all the corners.

2.2.1 Slide mode
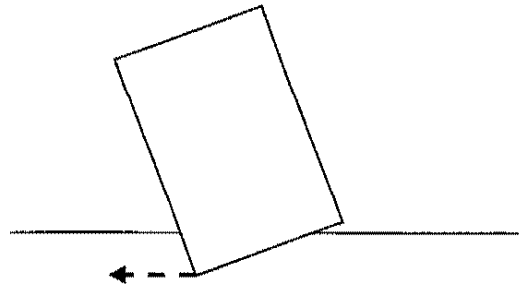
$x_l = $ x coordinate of the lower left corner
$x_r = $ x coordinate of the lower right corner
$w > 0 \quad x_l' = x_-' - 1/2(r\cos(w) - \sin(w))' \neq 0$
$w < 0 \quad x_r' = x_-' + 1/2(r\cos(-w) - \sin(-w))' \neq 0$

Figure 2.6: Slide mode

Definition:

The block is in **slide mode** if part of the block is below the foundation surface and at least one of the following is true:

i) horizontal velocity of the lowest corner is nonzero

ii) $\mu = 0$.

Sliding here does not imply purely horizontal translation of the block along the surface with $y_-' = 0$ and $w' = 0$. The block can move horizontally ($x_-' \neq 0$), vertically ($y_-' \neq 0$) and can also rotate about its center ($w' \neq 0$) while sliding. Case 1) is the usual way of slide mode engagement, when friction developed between the block and the foundation is too small to prevent sliding of the lowest corner (Figure 2.6). In the special case of $\mu = 0$ the lowest corner will move horizontally for most initial conditions. We state $\mu = 0$ case separately in ii) to define motion when $\mu = 0$ and $w(t_-) = w'(t_-) = 0$ also as slide mode. Such motion is a simple vertical oscillation of the upright block and the lowest corner does not move horizontally.

The horizontal force R_{x-} resisting the sliding acts at the lowest corner. Its magnitude is $R_{x-} = \mu R_{y-}$. The sign of R_{x-} is the opposite of the sign of the horizontal velocity of the lowest corner. We can substitute R_{x-} in equations 2.1, 2.3 with $\pm\mu R_{y-}$.

In the **slide mode** the equations of motion are

$$x_-'' = \pm\mu R_{y-} \tag{2.4}$$

$$y_-'' = R_{y-} - 1$$

$$I_-w'' = R_{y-}(\pm\mu a_{x-} + a_{y-}), \tag{2.5}$$

and the unknown variables are x_-, y_-, w.

2.2.2 Contact mode

Definition:

The block is in **contact mode** if part of the block is below the foundation surface and each of the following is true:

i) horizontal velocity of the lowest corner is zero

ii) $\mu > 0$.

The friction developed between the block and the foundation is large enough to prevent sliding of the lowest corner (Figure 2.7). The block can rotate about its lowest corner and move vertically ($y_-' \neq 0$) at the same time. We require $\mu > 0$ to prevent vertical oscillation of the block when $\mu = 0$ and $w(t_-) = w'(t_-) = 0$ from being classified as in contact mode.

The horizontal force R_{x-} resisting sliding acts at the lowest corner. Since the block rotates about one of its corners, the variables x_- and w are related. This will eliminate one of the equations of motion and determine R_{x-}.
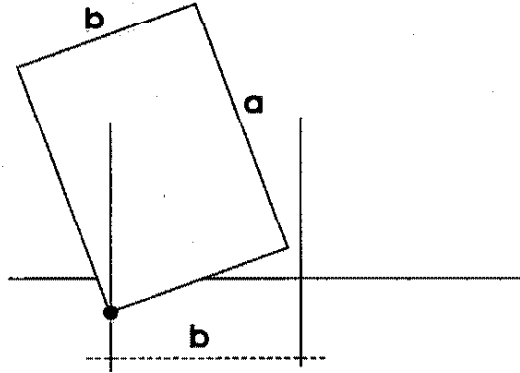
$x_l =$ x coordinate of the lower left corner
$x_r =$ x coordinate of the lower right corner
$w > 0$ $x'_l = 0 \Rightarrow x_-' = 1/2(r\cos(w) - sin(w))'$
      the lower left corner moves along the left vertical line only
      block rotates about the lower left corner
$w < 0$ $x'_r = 0 \Rightarrow x_-' = -1/2(r\cos(-w) - sin(-w))'$
      the lower right corner moves along the right vertical line only
      block rotates about the lower right corner

Figure 2.7: Contact mode

Let us assume $w > 0$, the block rotates about its lower left corner. Let the x coordinate of this corner be x_l, a constant. Then

$$x_- = x_l + (r\cos(w) - \sin(w))/2.$$

Differentiating the above equation twice with respect to t_- and recalling $x_-'' = R_{x-}$ (2.1) we get:

$$x_-'' = R_{x-} = w''(-\cos(w) - r\sin(w))/2 + w'^2(\sin(w) - r\cos(w))/2.$$

We substitute from the above equation for R_{x-} in equation 2.3 and solve for w'' to obtain

$$w'' = \frac{1/4w'^2(\sin(w) - r\cos(w))(\cos(w) + r\sin(w)) + R_{y-}a_{y-}}{I_- + 1/4(\cos(w) + r\sin(w))^2}.$$

A similar derivation can be easily done if $w < 0$, the block rotates about its lower right corner, whose x coordinate is x_r, a constant. Then

$$x_- = x_r - (r\cos(-w) - \sin(-w))/2.$$

Differentiating twice with respect to t_- and recalling $x_-'' = R_{x_-}$:

$$x_-'' = R_{x_-} = w''(-\cos(w) - r\sin(-w))/2 + w'^2(-\sin(-w) + r\cos(w))/2.$$

Substituting for R_{x_-} in equation 2.3 and solving for w'' we obtain

$$w'' = \frac{1/4w'^2(-\sin(-w) + r\cos(w))(\cos(w) + r\sin(-w)) + R_{y_-}a_{y_-}}{I_- + 1/4(\cos(w) + r\sin(-w))^2}.$$

Finally we can summarize this section. Since the block rotates about one of its corners, the variable x_- can be expressed in terms of w. The equation $x_-'' = R_{x_-}$ (2.1) is then used only to express R_{x_-} in terms of w. Now we can substitute for R_{x_-} in equation 2.3.

In the **contact mode**, the three equations of motion reduce to the following two:

$$
\begin{aligned}
y_-'' &= R_{y_-} - 1 \\
w'' &= \frac{\pm 1/4w'^2(\sin|w| - r\cos w)(\cos w + r\sin|w|) + R_{y_-}a_{y_-}}{I_- + 1/4(\cos w + r\sin|w|)^2},
\end{aligned}
\tag{2.6}
$$

where the $+$ sign relates to the case $w > 0$ and the $-$ sign to the case $w < 0$. The unknown variables are y_-, w.

2.2.3 Flight

Definition:

The block is in **flight** regime if the whole block is above the foundation surface.

There is no interaction between the block and the foundation: $R_{x_-} = R_{y_-} = a_{x_-} = a_{y_-} = 0$. The block is now just a free falling rigid body. The equations of motion 2.1, 2.2, 2.3 are simplified to:

$$
\begin{aligned}
x_-'' &= 0 \\
y_-'' &= -1 \\
I_- w'' &= 0.
\end{aligned}
$$

Given the initial conditions this can be solved analytically.

We call this regime of motion **flight**. However, we choose not to introduce flight as a new mode. We treat flight as a special case of the **slide mode**, as far as the equations of motion are concerned. Indeed, compare the equations of motion in slide mode (equations 2.4, 2.2, 2.5) and in flight (above). The flight equations are obtained from the slide equations merely by substituting

$R_{x-} = R_{y-} = a_{x-} = a_{y-} = 0$. Thus, the flight equations become a special case of the equations in slide mode.

2.2.4 Friction force in horizontal position

We have defined the friction force as a horizontal force acting at the lowest corner of the block. Say $w > 0$, then the block is tilted to the left and the friction force R_{x-} acts at the lower left corner. Now if the block passes through the horizontal position $w = 0$, the lower right corner becomes the lowest corner and R_{x-} acts there. Thus, as the block passes through the horizontal position, R_{x-} skips from one lower corner to the other. Since at that moment the two lower corners lie on a horizontal line, R_{x-} does not change its line of action. However, it could change the orientation or even magnitude. Now we examine if this happens.

In the **slide mode** $|R_{x-}| = \mu R_{y-}$ and R_{x-} acts against the horizontal motion of the lowest corner. At $w = 0$, the lower corners have the same horizontal velocity $x'_l = x'_r = x_-' + 1/2 w'$. Since R_{y-} is continuous through $w = 0$ and so is the horizontal velocity of the lowest corner, the friction force R_{x-} is also continuous through $w = 0$.

In the **contact mode** we compute R_{x-} for $w \leq 0$ and for $w \geq 0$ from the appropriate equations in section 2.2.2. At $w = 0$ we have

$$\text{if } w \geq 0 \quad R_{x-} = +rw'^2/2 \quad (-1 + \frac{1}{1 + 4I_-})$$
$$\text{if } w \leq 0 \quad R_{x-} = -rw'^2/2 \quad (-1 + \frac{1}{1 + 4I_-}).$$

Thus, R_{x-} changes its sign through $w = 0$, which results in a discontinuity on the right-hand side of equation 2.6.

2.2.5 Modes-summary

The flight regime holds when the whole block is above the foundation surface.

The block is in **slide mode** when it is not in flight and at least one of the following is true

    i) horizontal velocity of the lowest corner is nonzero

    ii) $\mu = 0$.

The block is in **contact mode** when it is not in flight and each of the following is true:

    i) horizontal velocity of the lowest corner is zero

    ii) $\mu > 0$.

2.3   Switching the modes

We have introduced two basic modes of motion: **contact mode, slide mode** and **flight** regime. We do not want to confine motion of the block to one mode only. The idea behind introducing different modes and regimes is to let the block switch freely between them, and to make the model more representative of actual behavior. Accordingly we have to define a process of switching between the modes. Let us list all such possible transitions:

contact→ slide	slide→ contact
contact→ flight	slide→ flight
flight→ slide	slide→ slide, when
flight→ contact	sliding direction changes.

2.3.1   Contact → slide, contact → flight

The block is moving in a **contact mode**. Then at a time t_- the state of the block is fully described by $y_-(t_-)$, $w(t_-)$, their first derivatives $y_-'(t_-)$, $w'(t_-)$ and a constant x_l or x_r. The block can switch from contact to either slide mode or flight regime.

contact → slide:	friction can no longer prevent sliding of the lowest corner
contact → flight:	the whole block leaves foundation surface

Table 2.2: Contact to either slide or flight

contact → slide: As the block moves in the contact mode we constantly monitor $R_{x-}(t_-)$ and $R_{y-}(t_-)$. In contact mode: $|R_{x-}(t_-)| < \mu R_{y-}(t_-)$. At the time when $|R_{x-}(t_-)|$ equals $\mu R_{y-}(t_-)$, the transition contact → slide occurs (Figure 2.8).

contact → flight: As the block moves in the contact mode at least some part of the block is under the foundation surface. We constantly monitor the y coordinate of the lowest corner of the block. Since the block partially sinks in the foundation, the y coordinate is negative. When the said y coordinate becomes zero, transition to flight occurs. At that moment, the block is just touching the foundation surface with its lowest corner.

Obviously in both cases, contact → slide and contact → flight, the equations of motion characterizing the dynamical system change from the contact equations 2.2, 2.6 to the slide equations 2.4, 2.2, 2.5. That means that a four-dimensional system (two second-order ODE's in contact mode) changes into a six-dimensional one (three second-order ODE's in slide mode). There is an additional degree of freedom in slide mode represented by the variables x_-, x_-'. We need to evaluate x_-, x_-' at the time of transition, t_{trans}. The values of the other variables, y_-, w, y_-', w', at the time of transition remain

criterion: $|R_{x-}| = \mu R_{y-}$

equations

2 ODE's
of 2nd order

3 ODE's
of 2nd order

variables

y_-, y_-'
w, w'

y_-, y_-'
w, w'
x_-, x_-'

at time t_{trans}

if $w > 0$ $x_- = x_l + (r\cos(w) - \sin(w))/2$
        $x_-' = 1/2(r\cos(w) - sin(w))'$
if $w < 0$ $x_- = x_r - (r\cos(-w) - \sin(-w))/2$
        $x_-' = -1/2(r\cos(-w) - sin(-w))'$

R_{x-} continuous

Figure 2.8: Contact $\rightarrow$ slide

unchanged. The contact mode still applies at the transition, so we can find $x_-(t_{trans}), x_-'(t_{trans})$ from the equations valid in contact mode.

$$w > 0 \quad x_- = x_l + (r\cos(w) - \sin(w))/2 \tag{2.7}$$

$$x_-' = 1/2(r\cos(w) - sin(w))',$$

$$w < 0 \quad x_- = x_r - (r\cos(-w) - \sin(-w))/2 \tag{2.8}$$

$$x_-' = -1/2(r\cos(-w) - sin(-w))'$$

The above expressions are evaluated at the time $t_- = t_{trans}$.

To complete the transition contact $\rightarrow$ slide, we need to determine which direction to apply the force R_{x-} when the block starts sliding. Right after the transition the lowest corner of the block moves left or right. We need to apply the horizontal friction force at sliding $R_{x-} = \pm\mu R_{y-}$ against that motion. That is, we need to determine the sign of R_{x-}. At the transition, we can compute the direction of R_{x-} assuming contact mode. Naturally R_{x-} will not change orientation through the transition; it will be continuous through the transition.

After the contact $\rightarrow$ flight transition the block is above the surface and $R_{x-} = R_{y-} = 0$. Therefore, we do not need to find the direction of R_{x-}. Contact $\rightarrow$ flight is actually unlikely to happen. Before the block leaves the foundation, the force R_{y-} usually becomes so small that R_{x-} in contact mode is greater than μR_{y-}. Thus, the transition contact $\rightarrow$ slide usually occurs before the flight.

2.3.2 Slide $\rightarrow$ contact, slide $\rightarrow$ slide and other transitions

If the block is moving in a **slide mode**, then at a time t_- the state of the block is fully described by $x_-(t_-), y_-(t_-), w(t_-)$ and their first derivatives $x_-'(t_-), y_-'(t_-), w'(t_-)$. A part of the block is below the foundation surface and the lowest corner moves in a horizontal direction. As the block slides we constantly monitor the horizontal velocity of the lowest corner of the block. When this velocity becomes zero, the lowest corner of the block comes horizontally to a stop and one of the two scenarios in Table 2.3 takes place.

slide$\rightarrow$ contact:	friction sufficient to support contact
slide $\rightarrow$ slide:	friction not sufficient to support contact
	the lowest corner continues sliding but in the other direction

Table 2.3: Slide to either contact or slide

Let us discuss the situation in more detail now. As the block slides the horizontal velocity of the

criterion to stop: if $w > 0$ $x'_l = x_-{}' - 1/2(r\cos(w) - sin(w))' = 0$
                    if $w < 0$ $x'_r = x_-{}' + 1/2(r\cos(-w) - sin(-w))' = 0.$

SLIDE $\rightarrow$ CONTACT

criterion: R_{x_-} computed in contact $< \mu R_{y_-}$
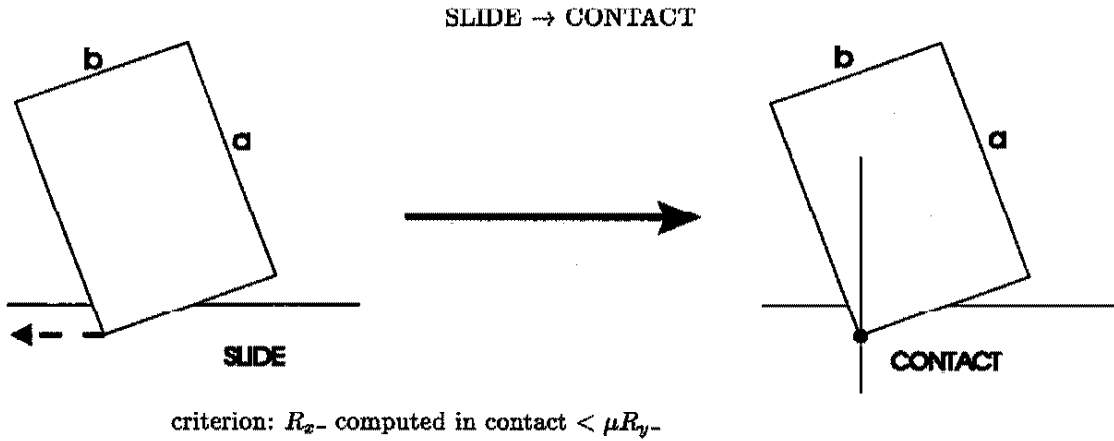
equations: 3 ODE's of 2nd order   2 ODE's of 2nd order
variables: $y_-, y_-{}'$ $y_-, y_-{}'$
            w, w' w, w'
            $x_-, x_-{}'$

Figure 2.9: Slide $\rightarrow$ contact

SLIDE $\rightarrow$ SLIDE

equations do not change
variables do not change
sliding direction reverses
R_{x_-} changes sign

criterion: R_{x_-} computed in contact $\geq \mu R_{y_-}$
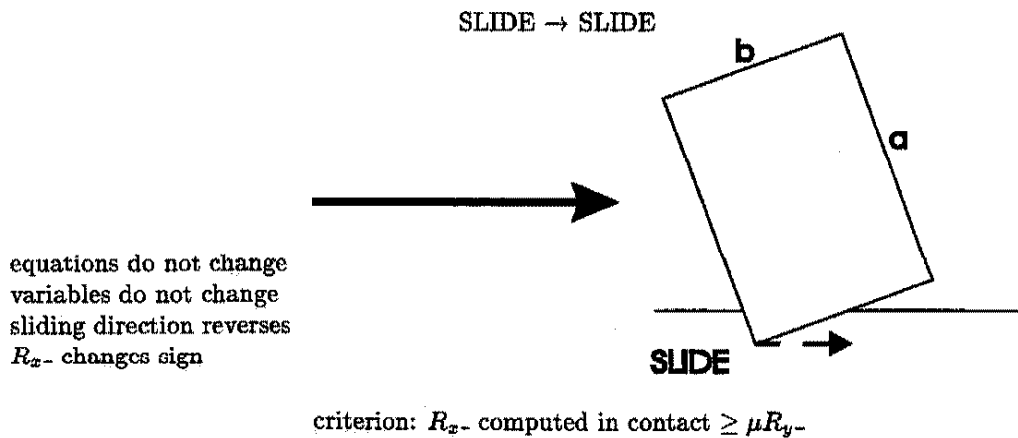
Figure 2.10: Slide $\rightarrow$ slide

lowest corner is given by:

$$\text{if } w > 0 \qquad x_l' = x_-' \quad 1/2(r\cos(w) - sin(w))' \neq 0$$

$$\text{if } w < 0 \qquad x_r' = x_-' + 1/2(r\cos(-w) - sin(-w))' \neq 0.$$

This velocity can be only positive or negative while the block is sliding. When the said velocity becomes zero, the lowest corner of the block stopped moving in a horizontal direction. At this time, we compute R_{x-} assuming contact mode. If $|R_{x-}| < \mu R_{y-}$, we let the block switch to a contact mode (slide $\rightarrow$ contact). If $|R_{x-}| \geq \mu R_{y-}$, we let the block continue in slide mode, reversing the direction of slide (slide $\rightarrow$ slide).

Slide $\rightarrow$ contact

Obviously, the equations of motion characterizing the dynamical system change from the slide equations 2.4, 2.2, 2.5 to contact equations 2.2, 2.6. That means that a six-dimensional system (three second-order ODE's in slide mode) changes into a four-dimensional one (two second-order ODE's in contact mode). One degree of freedom is lost. To keep track of the horizontal position of the block we only need to know the x coordinate of the lowest corner. That is a constant x_l or x_r, which can be obtained from the relations 2.7 and 2.8:

$$\text{if } w > 0 \qquad x_l = x_- - (r\cos(w) - \sin(w))/2$$

$$\text{if } w < 0 \qquad x_r = x_- + (r\cos(-w) - \sin(-w))/2.$$

The above expressions are evaluated at the time $t_- - t_{trans}$. Values of the variables y_-, w and their first derivatives y_-', w' carry over from contact to slide mode without change.

Slide $\rightarrow$ slide

The equations of motion do not change, neither do the variables. Only the sign of friction force R_{x-} reverses through the transition. The lowest corner was moving horizontally in either a positive or negative direction, came to a stop and then started moving in the opposite direction. We need to reverse the orientation of R_{x-} at the transition so that R_{x-} acts against the sliding motion after the transition as well as before. For example say $w > 0$, the lowest corner is the lower left corner and it is moving to the right, so the horizontal velocity of this corner is positive and friction force is $R_{x-} = -\mu R_{y-}$. Suppose now the horizontal velocity gets smaller and eventually becomes zero. The lower left corner stops moving in a horizontal direction. Suppose the friction is insufficient to keep

the corner from further sliding. The corner will move this time to the left, its horizontal velocity being negative. Then the friction force will be $R_{x-} = +\mu R_{y-}$. Thus, R_{x-} does not change magnitude through the slide → slide transition, it changes the sign.

Flight→contact, flight → slide

Either of the transitions can happen only at the instant of landing. At the landing we check horizontal velocity of the lowest corner, that is of the landing point. If this velocity is zero, we switch to contact. Usually though the said velocity will be nonzero and we switch to slide mode.

flight→contact: Transition same as in slide → contact.

flight → slide: Equations of motion and variables do not change at the instant of landing. We only have to determine direction of R_{x-} upon landing so that it acts against the horizontal motion of the lowest corner. Usually this direction is the same as the direction of R_{x-} when the block left the ground.

Slide →flight

The slide →flight transition we mention only for completeness. The equations and variables remain the same, nothing changes here.

2.4   Rigid block - rigid ground

In this section we consider a system consisting of a rigid block moving on rigid ground. Call such a system R-R as opposed to R-E system which consists of a rigid block moving on elastic foundation. In the preceding part of this chapter we defined a model for R-E system, derived the equations of motion and conceived the notion of different modes. Now we want to consider a model for R-R system for two reasons:

- the equations of motion in an R-R system can be used when determining some of the initial conditions in R-E system

- the R-R system will serve as a test case for the more general R-E system.

For this purpose, we do not need to fully work out the R-R model as done for the R-E model. Specifically, we do not need to treat impact. If we incorporated impact in the R-R model, we would derive another model for the considered dynamical system, similar to models already introduced by other authors [*Jones and ShentonIII*, 1990].

We observe the motion only for $w > 0$ and do not consider impact. The coordinate system, variables, parameters, definition of modes, and transition between them carry over from the R-E system model. Only the parameter k_- does not enter and the flight regime is not applicable anymore. The equations of motion can be derived from scratch or from the equations already stated for R-E model. The ground is rigid, therefore

$$y_- = (\cos w + r \sin w)/2$$

and the y_- degree of freedom is lost. We merely state equations of motion:

contact mode

$$w'' = -\frac{r\cos w - \sin w}{2I_- + (1 + r^2)/2} \tag{2.9}$$

slide mode

$$
\begin{aligned}
x_-'' &= \pm\mu R_{y-} \\
w'' &= \frac{(2 - w'^2(\cos w + r\sin w))(\mu(\cos w + r\sin w) - (r\cos w - \sin w))}{4I_- - (r\cos w - \sin w)(\mu(\cos w + r\sin w) - (r\cos w - \sin w))}.
\end{aligned} \tag{2.10}
$$

The reaction forces R_{x-}, R_{y-} are given by:

mode	force
contact	$R_x = -1/2(w'^2(r\cos w - \sin w) + w''(\cos w + r\sin w))$
slide	$R_{x-} = \pm\mu R_{y-}$
contact, slide	$R_{y-} = 1 - 1/2(w'^2(\cos w + r\sin w) - w''(r\cos w - \sin w))$.

Note, however, that R_{y-} is generally different in slide and contact mode, as w'' differs in each mode. In contact mode, the system is two-dimensional and we have one ODE of second order. In slide mode, the system is four-dimensional and we have two ODE's of second order. The equation of motion for y_- has been eliminated by expressing y_- explicitly in terms of w. Therefore in each mode, the dimension of the R-R system is smaller by two as compared to the R-E system.

Chapter 3

Numerical implementation

The equations of motion in both contact and slide mode are too difficult to solve analytically with the exception of a few special cases, such as free flight, or the periodic solution $w(t_-) = w'(t_-) = 0$.

The solution of the equations of motion can be obtained in the general case only by numerical methods. The equations of motion are autonomous ODE's of second order subjected to initial conditions. In contact mode there are 2 ODE's (2.2,2.6) and in slide mode there are 3 ODE's (2.4,2.2,2.5):

mode:	slide	contact
equations:	$x_-'' = f_x(y_-, w)$	
	$y_-'' = f_y(y_-, w)$	$y_-'' = f_y(y_-, w)$
	$w_-'' = f_{ws}(y_-, w)$	$w_-'' = f_{wc}(y_-, w)$
initial conditions:	$x_-(0) = x_0$	
	$x_-'(0) = x_0'$	
	$y_-(0) = y_0$	$y_-(0) = y_0$
	$y_-'(0) = y_0'$	$y_-'(0) = y_0'$
	$w(0) = w_0$	$w(0) = w_0$
	$w'(0) = w_0'$	$w'(0) = w_0'.$

Let us define

$$x_2 = x_-' \qquad y_2 = y_-' \qquad w_2 = w'.$$

Then the second-order system of equations can be written as a first-order system with twice the number of equations.

mode:	slide	contact
equations:	$x_-' = x_2$	
	$x_2' = f_x(y_-, w)$	
	$y_-' = y_2$	$y_-' = y_2$
	$y_2' = f_y(y_-, w)$	$y_2' = f_y(y_-, w)$
	$w' = w_2$	$w' = w_2$
	$w_2' = f_{ws}(y_-, w)$	$w_2' = f_{wc}(y_-, w)$
initial conditions:	$x_-(0) = x_0$	
	$x_2(0) = x_0'$	
	$y_-(0) = y_0$	$y_-(0) = y_0$
	$y_2(0) = y_0'$	$y_2(0) = y_0'$
	$w(0) = w_0$	$w(0) = w_0$
	$w_2(0) = w_0'$	$w_2(0) = w_0'.$

Thus, the problem at hand is identified as a standard initial value problem:

$$
\begin{aligned}
z' &= f(z) \\
z(0) &= z_0,
\end{aligned}
$$

where z and f are six-dimensional vectors in slide mode and four-dimensional in contact mode.

The equations of motion in flight are a special case of the equations of motion in slide mode. Therefore, when integrating the equations of motion, flight is treated as slide mode. For simplicity we choose not to solve the motion of the block in flight analytically.

There are number of numerical techniques to solve the above problem. We use a 5th-order Runge-Kutta integration scheme with automatic step size selection. The algorithm used is a slightly modified version of the *Press et al.* [1992] code. Computation is done on Sun Sparcstations. The code is written in C using 16 digit double precision variables.

3.1 Switching the modes

In chapter 2 we defined the contact and slide modes and the transition between them. The numerical implementation of the transition is mostly straightforward: we change the equations, evaluate x_-, x_-' and x_{l-} or x_{r-}, and determine the sign of R_{x-}. Finding the exact transition time, t_{trans}, is harder to solve numerically. The transition time is the time when a certain monitored quantity becomes

zero; in contact mode, when $|R_{x-}| - \mu R_{y-} = 0$, and in slide mode, when the horizontal velocity of the lowest corner becomes zero (that is $x_{r-}' = 0$ or $x_{l-}' = 0$).

Integration forward in one time step may result in conditions such that the current mode is no longer valid; the monitored value crossed zero. The time step could be quite long. For example, in Figure 3.1, the code passed t_{trans} while integrating from t_{i+1} to t_{i+2}. Only at the end of a time step (at t_{i+2} in Figure 3.1) does the code find out that the monitored quantity crossed zero.

y axis: monitored quantity

contact: $|R_{x-}| - \mu R_{y-}$
slide: x_{l-}' if $w > 0$
            x_{r-}' if $w < 0$
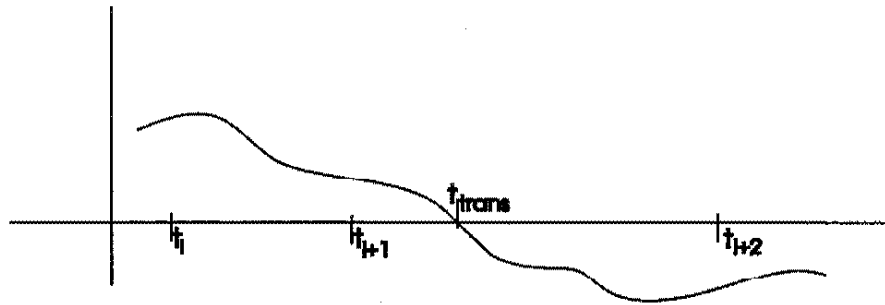
x axis: time

Figure 3.1: Iterative subroutines

We want to determine t_{trans} with machine accuracy. For this purpose we constructed simple iterative subroutines, CalcC_S for contact mode and CalcStop for slide mode. They both search for a zero crossing of the monitored quantity by successively halving the time interval. Say we find that the monitored quantity crossed zero within the interval (t_{i+1}, t_{i+2}), as in Figure 3.1. We halve the interval at $t_c = (t_{i+1} + t_{i+2})/2$ and determine at which of the two new intervals (t_{i+1}, t_c), (t_c, t_{i+2}), the monitored quantity crosses zero. We reiterate the above step until we have determined t_{trans} with machine accuracy.

The subroutine CalcC_S iterates to find t_{trans} when $|R_{x-}| = \mu R_{y-}$. The subroutine CalcStop iterates to find when the horizontal velocity of the lowest corner is zero. Thus, we use iteration to determine the transition time as accurately as possible in contact→slide, slide→contact, slide→slide.

In the case of flight→slide and slide→flight, we do not need to iterate to find t_{trans} since the equations of motion are the same for flight as for slide. In flight we keep track of direction of the horizontal motion of the lowest corner. When the block lands the friction force is correctly applied against that direction.

We do not iterate to find the exact transition time in the contact→flight transition. There are two reasons for this, both based on our experience. First, if the transition occurs, the time step

is already very small. Second, this transition rarely occurs. At the end of the time step when the block is completely above the surface we switch to flight. So we end up holding the block a tiny little bit longer in contact mode. Extensive testing showed this to be better than trying to iterate to the exact take off point.

CalcStop can be used in another rare transition: flight→contact. When the block lands, the code assumes it will continue in slide mode. The applied friction force may be large enough to push, in one time step, the lowest corner in the direction of the force. The code realizes this is incorrect, and it uses CalcStop to iterate back to a point when lowest corner is already below the surface but its horizontal velocity is still zero within machine accuracy. At such a point we then switch to contact.

CalcStop may be used more than once trying to find a suitable point for the flight→contact switch. Say the friction force points right. It pushes the lowest corner right during the landing time step. The corner incorrectly gains a positive horizontal velocity. The code discovers this at the end of the time step and uses CalcStop to iterate back. It may iterate back to a desired point below the surface where we can switch to contact. However, often with only one iteration CalcStop gets back to a point above the surface. Then the code switches the sign of friction force and the cycle is repeated. Using CalcStop once or twice is usually sufficient.

3.2   Initial conditions

We run the code with different initial conditions. Only x_0, the initial value of x_-, can be chosen arbitrary without any influence on the subsequent behavior of the block. Different x_0 merely shifts the origin of our coordinate system. We choose x_0 so that initially the lower left corner of the block is located at $x_- = 0$.

For most of this study, we use two sets of initial conditions. We call them initial conditions set 1 or ic1, and initial condition set 2 or ic2. Define $\alpha = \arctan(b/a)$, an angle between the diagonal of the block and its side. Then ic1 and ic2 are given by:

$ic1$ $w_0 = \alpha/2$ $ic2$ $w_0 = 0$

$w_0' = 0$ $w_0' = 6x_{-0}'/(1 + r^2)$

$y_{-0} = \text{`static`}$ $y_{-0} = \frac{1}{2} - 1/k_-$

$y_{-0}' = 0$ $y_{-0}' = 0.0001$

$x_{-0} = \frac{1}{2}(r\cos(w_0) - \sin(w_0))$ $x_{-0} = r/2$

$x_{-0}' = 0$ $x_{-0}' = 0.06.$

The set ic1 corresponds to a block tilted at an angle $w_0 = \alpha/2$. The tilted block is given zero

initial velocities and rests on the elastic foundation. By $y_{-0} = $ 'static' we mean that the block is not pushed down or pulled up, it just rests on the elastic springs under the action of gravity. We attempt to choose a y_{-0} such that the block will initially rotate about its lowest corner. To determine y_{-0} we assume momentarily that the foundation is rigid and calculate the resulting R_{x-}, R_{y-} in contact mode referring to the Rigid block-Rigid ground section. Comparing now R_{x-} and μR_{y-} we decide whether the block starts moving in slide or contact mode. If $|R_{x-}| > \mu R_{y-}$ the block starts in a slide mode and we recalculate R_{y-} appropriately assuming again rigid ground. Then

$$y_{-0} = \frac{\cos w_0 + r \sin w_0}{2} - \sqrt{2r \cos w_0 \sin w_0 R_{y-}/k_-}$$

The computed y_{-0} will be closer to the desired 'static' value when k_- is large.

The initial conditions ic2 correspond to a block resting upright on the foundation. A horizontal and a vertical force impulse are applied at the bottom of the block resulting in initial velocities stated above. Such initial condition can be viewed as a simplified simulation of an earthquake action on a free standing rectangular object.

3.3   Testing the code

We have defined the model of the block and foundation and discussed our implementation of the computer simulation code. We now check the integrity of the code against a known analytical solution and a simpler numerical solution.

Comparing R-E and R-R models

We expect close agreement between the dynamics of the R-R model and the R-E model with large k_-. We wrote a separate code for each model and ran it with initial condition set ic1, altering w_0 and the parameter set r, k_-, μ. We stopped the simulations when $w = 0$, since the R-R model was not designed to handle impact. Results of only two tests are presented in Figures 3.2 through 3.9.

	Figure	k_-	displayed RE x RR
first test	3.2	10^3	variables
ic1	3.3	10^4	$x_-, x_-', y_-, y_-', w, w'$
$r = 0.2$	3.4	10^5	
$\mu = 0.2$	3.5	10^6	
second test	3.6	10	
ic1 $w_0 = 0.8$	3.7	10^6	
$r = 2.0$	3.8	$10^7, 10^8, 10^9, 10^{10}$	forces
$\mu = 0.3$	3.9	$10^4, 10^5, 10^6$	R_{x-}, R_{y-}

Table 3.1: Test figures, comparison between RE, RR models

As expected, with increasing k_-, the response of the R-E model approaches the R-R model's response. For $k_- = 10^6$ the response of the two models is nearly identical. This is encouraging, since the two models are qualitatively different - to see that compare the equation of motion for w in the two models. In contact mode, compare equation 2.6 to equation 2.9 and in slide mode compare the equations 2.5 and 2.10. In the first test the block moves in contact mode only. The second test is more interesting: the block moves initially in contact mode, then its lowest corner starts sliding left, comes to a stop and slides to the right. In the second test we compare the response of the two models also by looking at the time, s_o, of the slide→slide transition, that is the time when the lowest corner came to a stop horizontally. As k_- increases, s_o computed in the R-E model converges to s_o computed in R-R model, as documented in Table 3.2.

	k_-	R-E model
	10^2	s_o=2.22580229
	10^3	s_n=2.30565954
	10^4	s_o=2.31704765
R-R model	10^5	s_o=2.32155059
s_o=2.32249567	10^6	s_o=2.32203630
	10^7	s_o=2.32239531
	10^8	s_o=2.32247161
	10^9	s_o=2.32248152
	10^{10}	s_o=2.32249325

Table 3.2: Test, time of slide→slide transition

Finally, we note an interesting difference between the two models. When the block switches its direction of sliding, the friction force R_{x-} changes sign. This introduces a discontinuity in w''. In the R-R model, the discontinuity in w'' implies a discontinuity in the vertical reaction force R_{y-}. In the R-E model, the discontinuity in w'' causes an oscillation in R_{y-}, whose amplitude increases with increasing k_- up to a certain point. This is a qualitative difference between the two models. In the R-E model, no matter how large k_- grows, a change in the direction of sliding will cause an oscillation in R_{y-}. We can view the oscillation as a result of an impulse in the turning moment caused by the change in direction of the friction force. The bottom of the block then oscillates vertically. In the R-R model, the change in the direction of sliding implies a simple jump in R_{y-}. Of course, adding damping to the R-E model would limit the R_{y-} oscillation. Figures 3.8 and 3.9 document discussion in this paragraph by plotting R_{x-}, R_{y-} for our second test case.

Periodic solution, $w(t_-) = w'(t_-) = 0$

We test the code against a known periodic solution where the block merely oscillates vertically, i.e., $w(t_-) = w'(t_-) = 0$ for all t_-. The code should be able to handle this special case and reproduce the

Figure 3.2: R-R, R-E model comparison - first test, $k_- = 10^3$

32

Figure 3.3: R-R, R-E model comparison - first test. $k_- = 10^4$

Figure 3.4: R-R, R-E model comparison - first test, $k_- = 10^5$

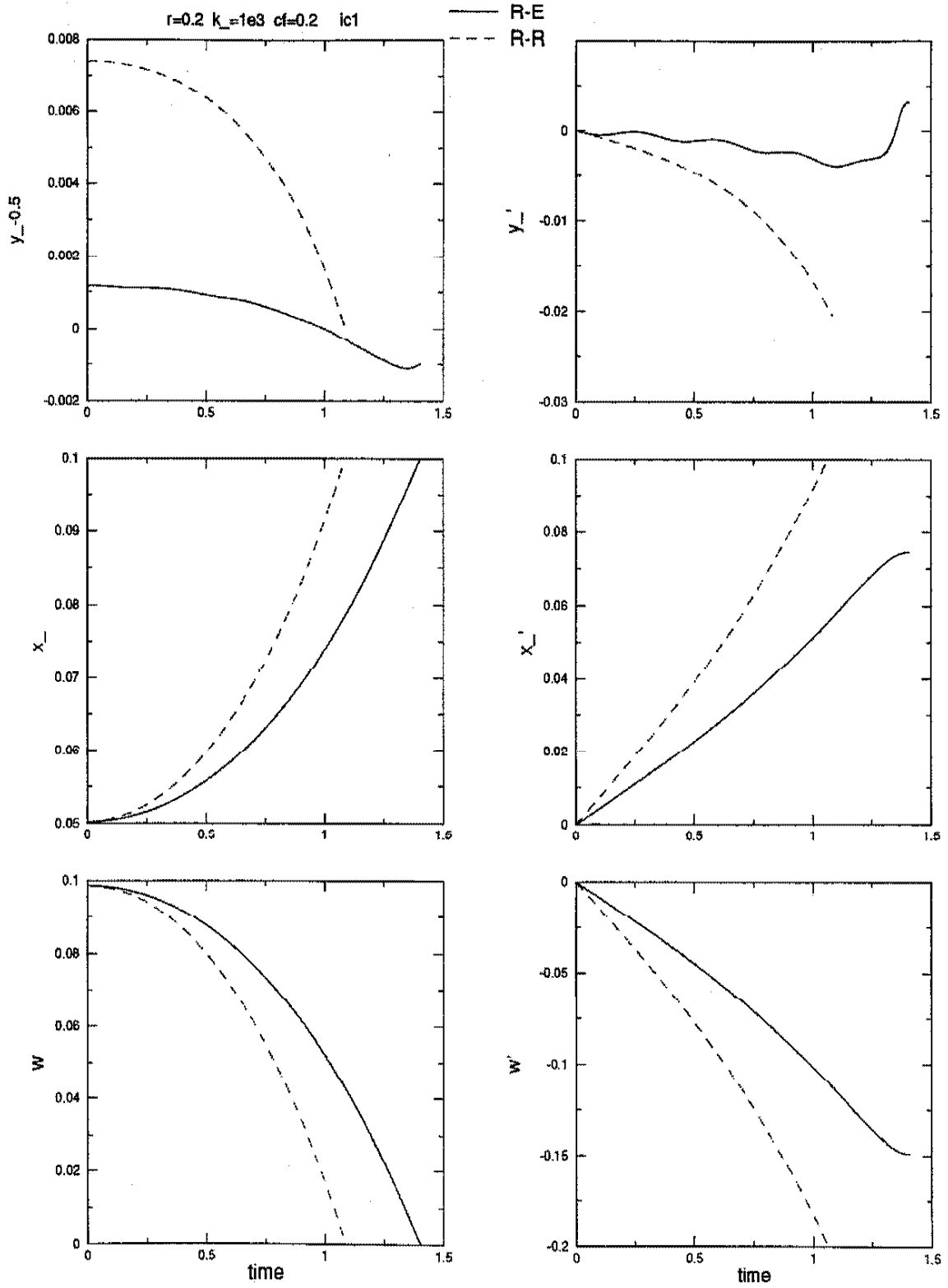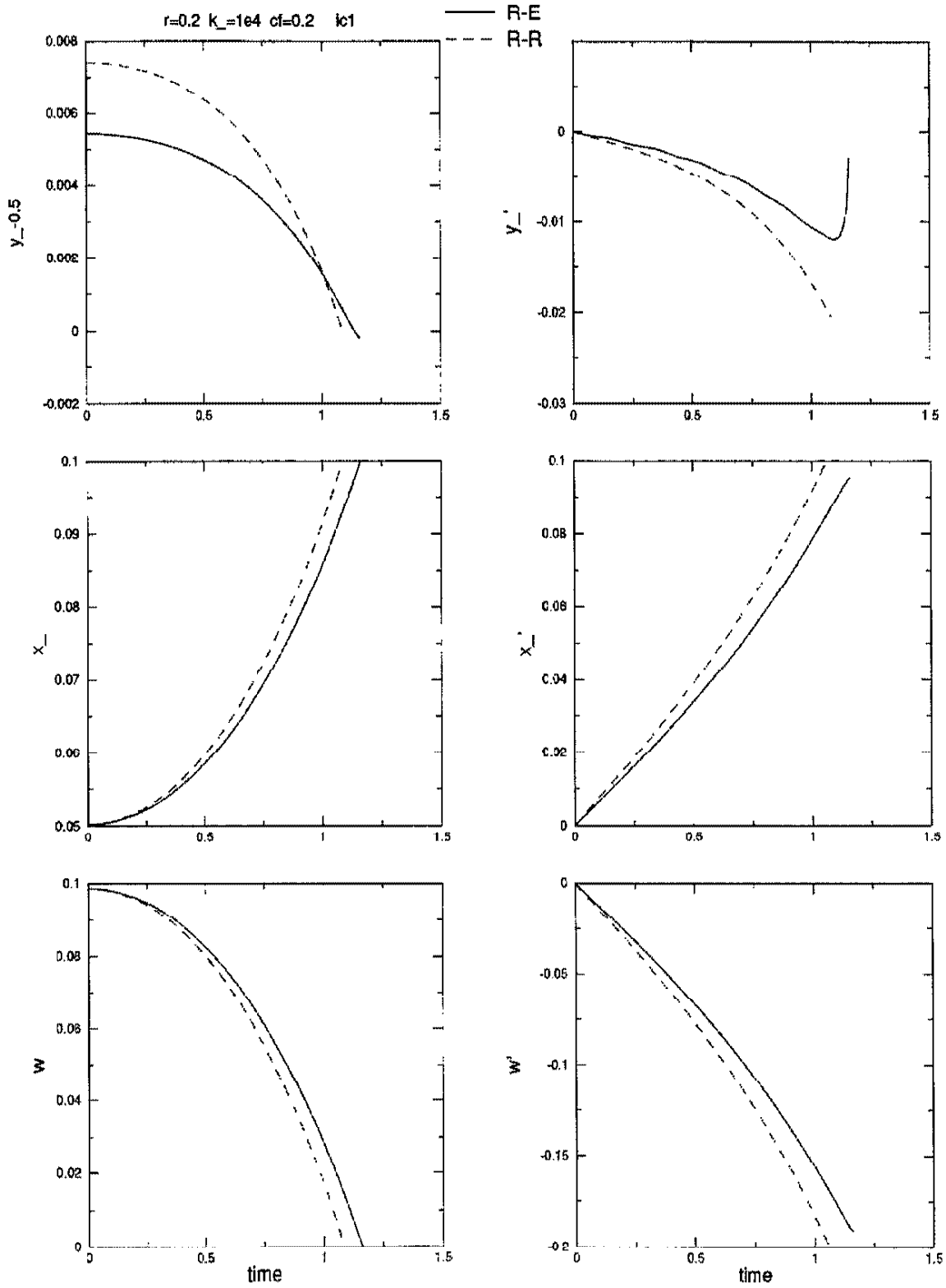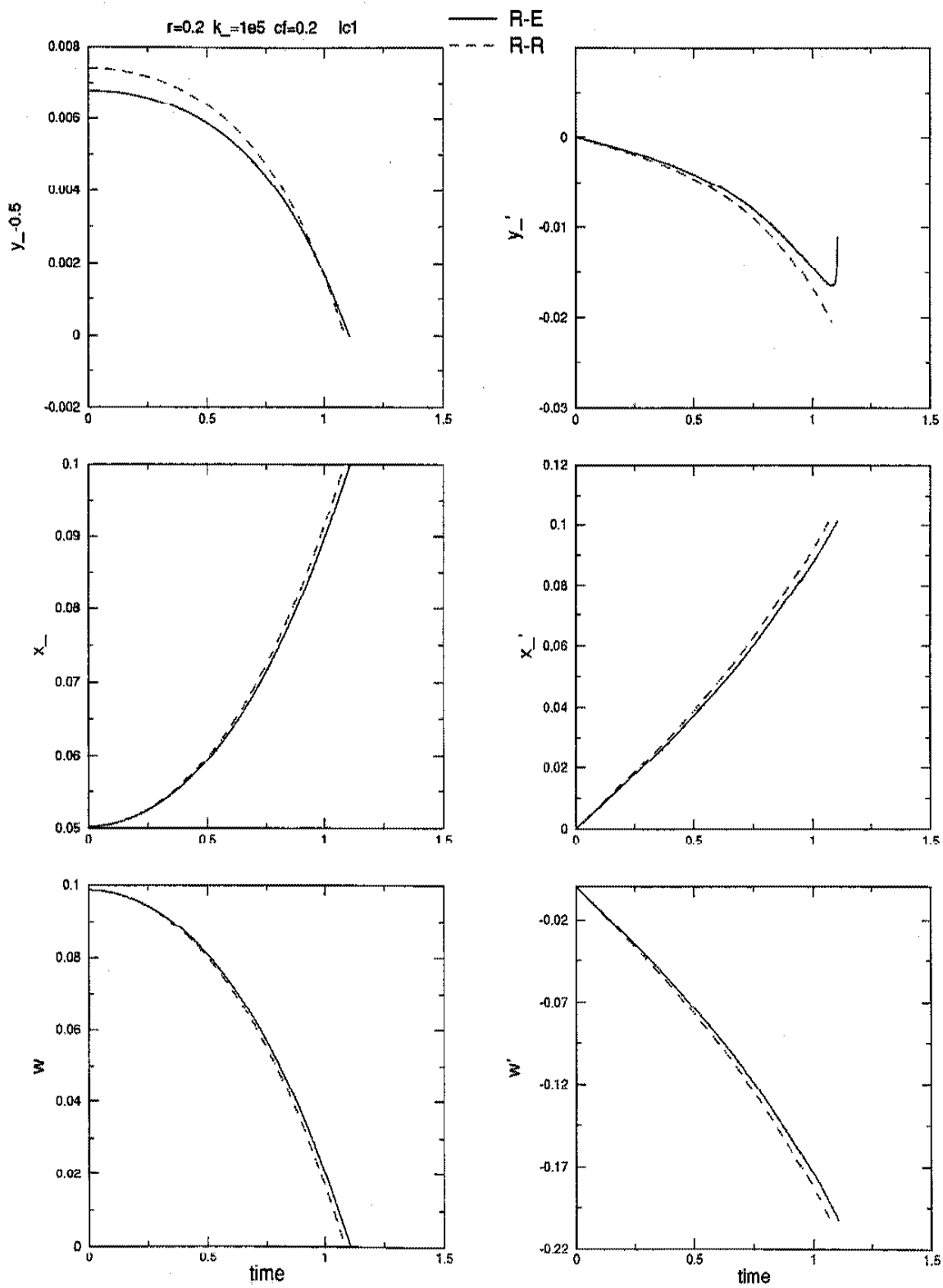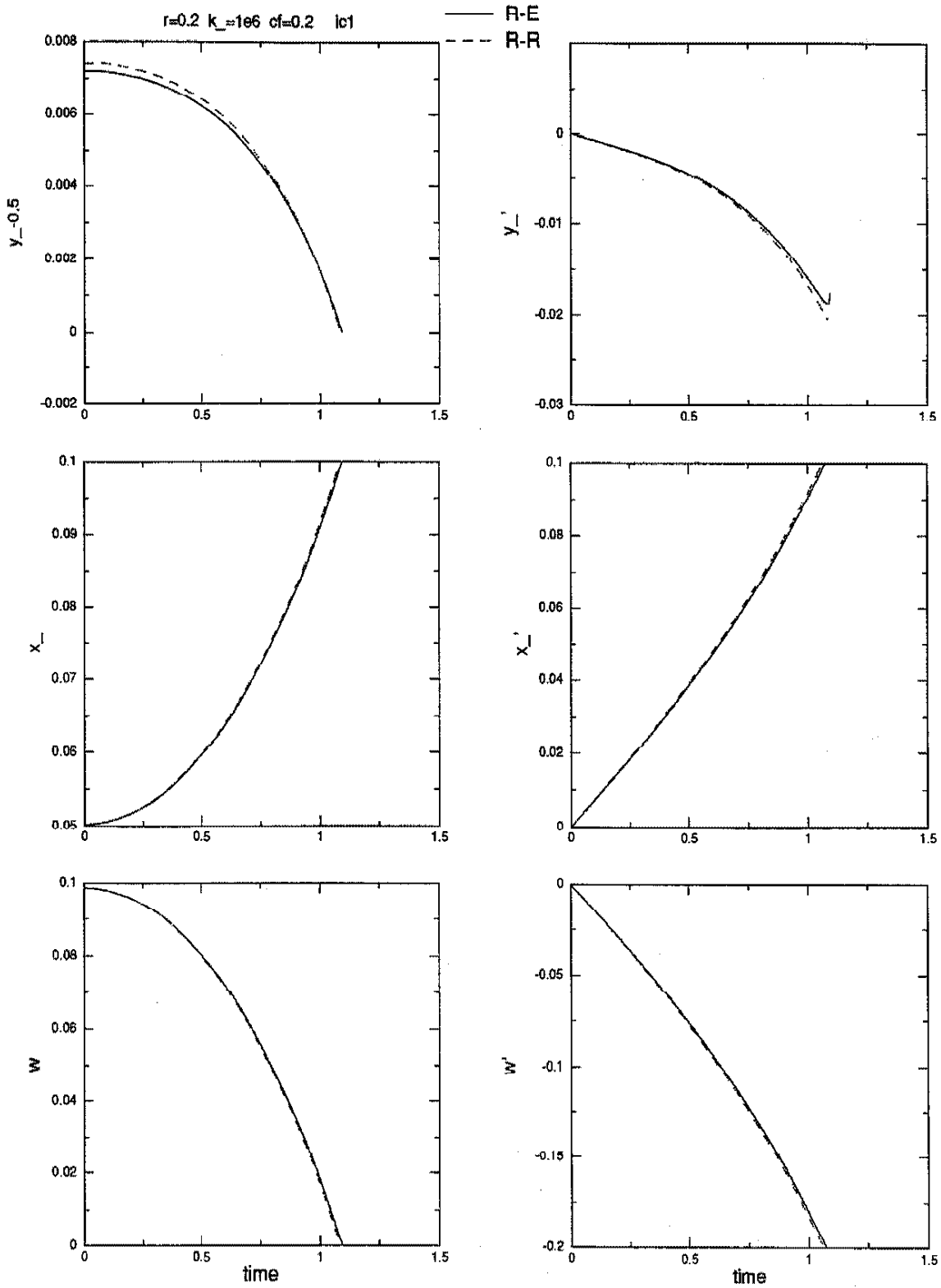Figure 3.5: R-R, R-E model comparison - first test, $k_- = 10^6$

Figure 3.6: R-R, R-E model comparison - second test, $k_- = 10$

Figure 3.7: R-R, R-E model comparison - second test, $k_- = 10^6$
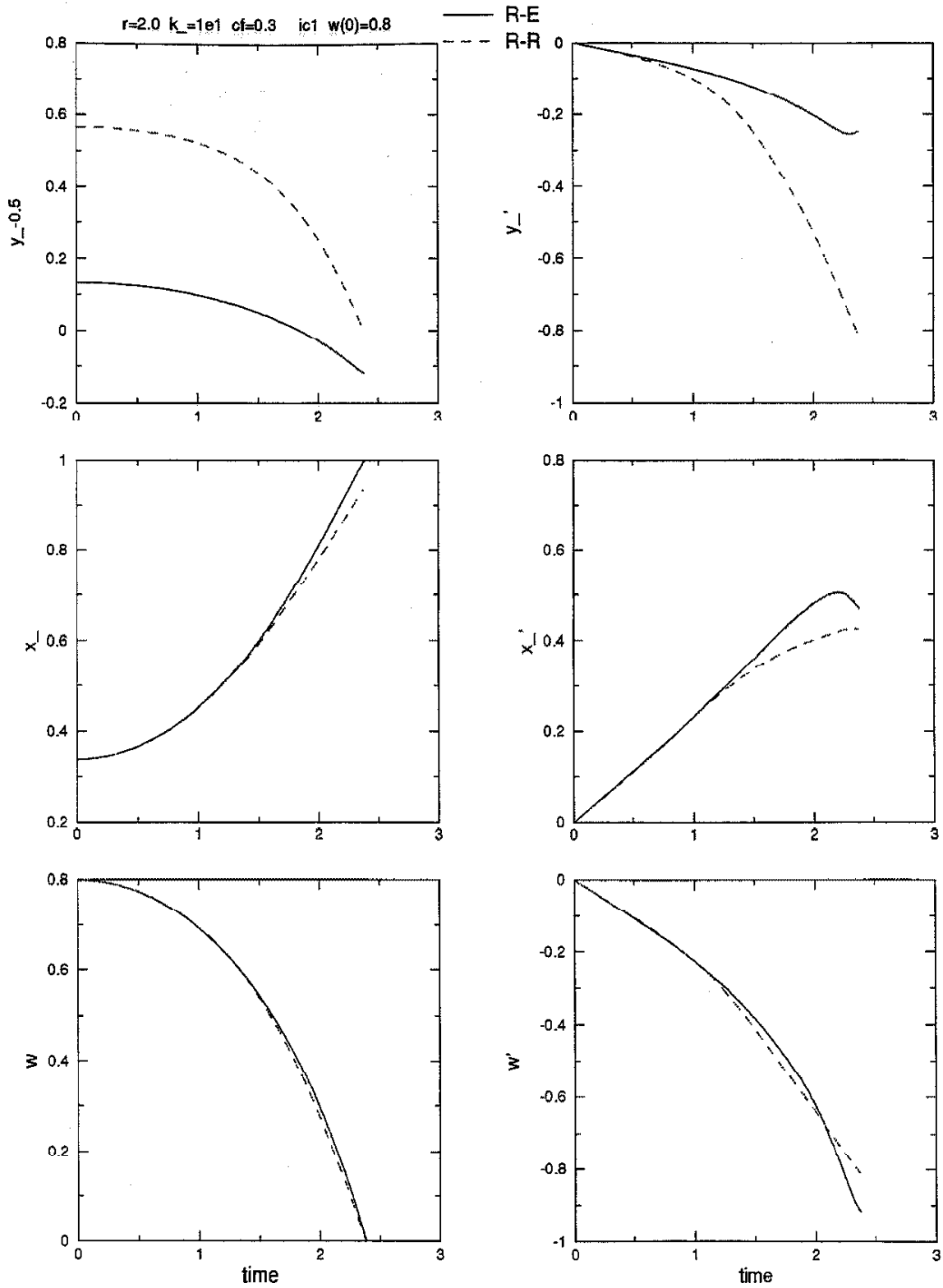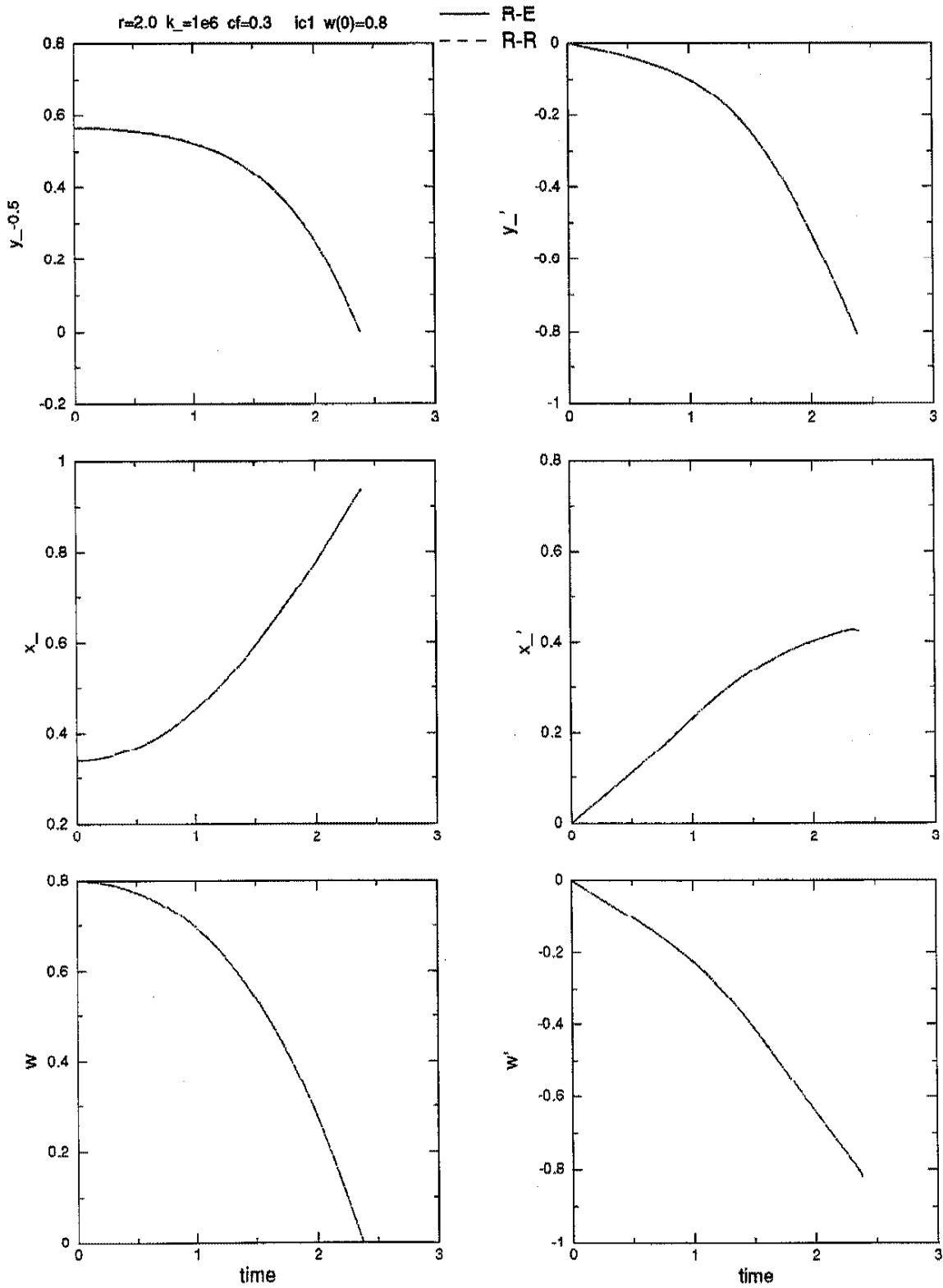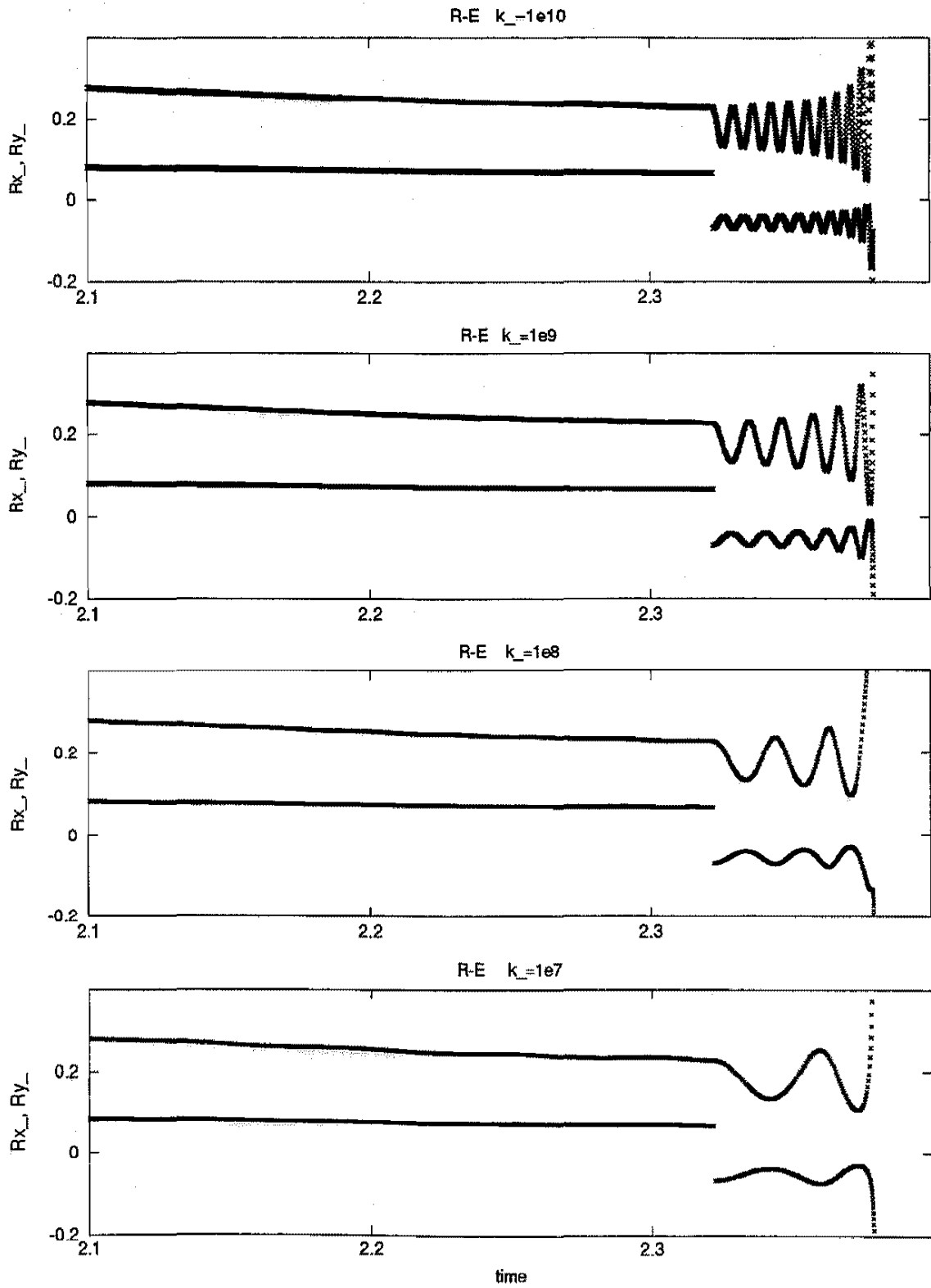
R-E k_-=1e10

R-E k_=1e9

R-E k_=1e8

R-E k_=1e7

time

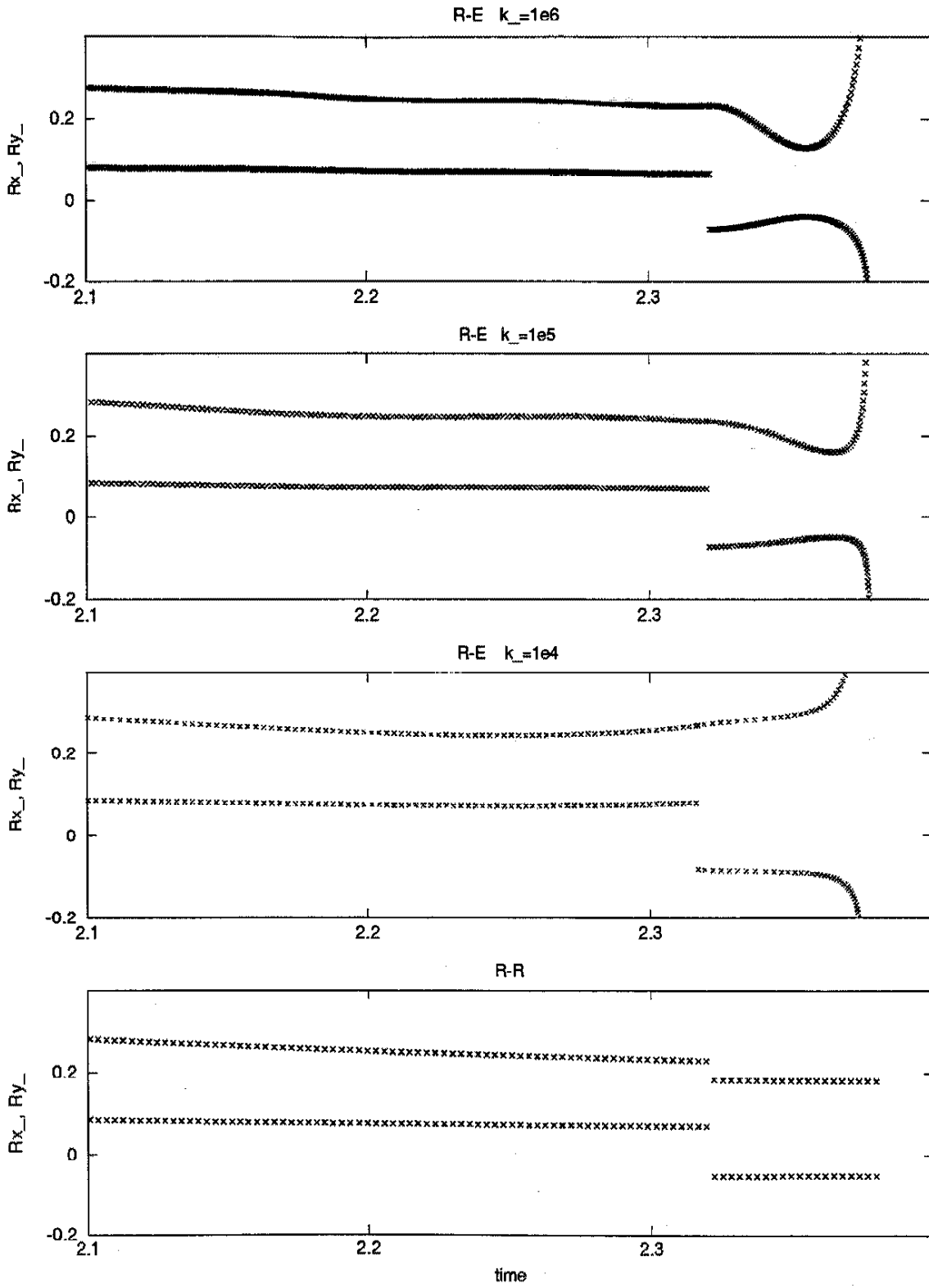Figure 3.8: Forces R_{x-}, R_{y-} for $r = 2.0, \mu = 0.3,$ ic1 $w(0) = 0.8$

Figure 3.9: Forces R_{x-}, R_{y-} for $r = 2.0, \mu = 0.3$, ic1 $w(0) = 0.8$

exact known solution. This simple case tests more than one might think at first glance. Specifying the initial conditions with sufficient energy, we ensure that the block will bounce off the surface - flight ensues. For $\mu > 0$ the block will move in contact mode and for $\mu = 0$ in slide mode when partially below the foundation surface. Above the foundation, the block is in its flight regime and the slide equations are employed. Thus, the transitions contact→flight, flight→contact and slide→flight, flight→slide are tested. The initial conditions we chose are:

$$x_{-0} = r/2 \qquad x_{-0}' = 0$$
$$y_{-0} = \tfrac{1}{2} - 3/k \quad y_{-0}' = 0$$
$$w_0 = 0 \qquad w_0' = 0,$$

which will guarantee flight no matter what set of parameters r, k_-, μ we use. Results for two test runs are presented in Figures 3.10 and 3.11. Our numerical solution is equal to the exact analytical solution.

In graphs of y_-, y_-' we plot discrete points at which a numerical solution was obtained. We can see how the code adjusts the time step size. Time steps are long in flight and short when block is interacting with the foundation springs. We also mark each usage of the iterative subroutine CalcStop by a circle plotted in the y_- graph. We see that for $\mu = 0$, CalcStop is never used. Transitions slide→flight and flight→slide do not require any additional computation for $\mu = 0$. CalcStop, however, is used each time the block lands for $\mu > 0$ to assist the flight→contact transition. When $\mu > 0$, a small amount of the horizontal force is applied to the block during the landing time step. As a result, at the end of the computation, w, w' are slightly perturbed, with values ranging from 10^{-17} to 10^{-20} instead of being identically 0. Identical zeros are obtained for w, w' in the case $\mu = 0$.

r=0.5 k_=1e5 cf=0.2

0=flight   1=contact
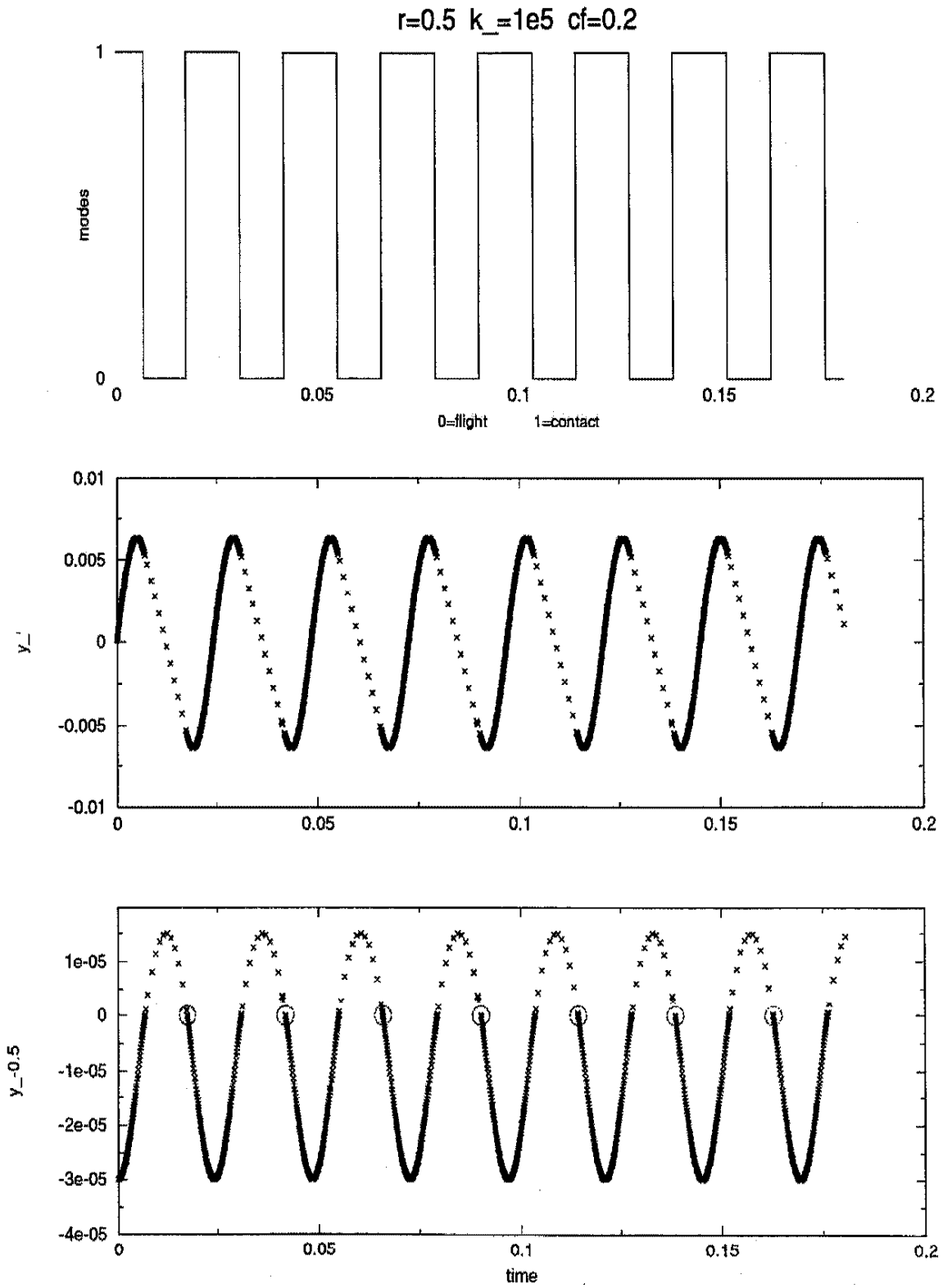
Figure 3.10: Vertical oscillation $\mu = 0.2$

r=0.5 k_=1e5 cf=0.0
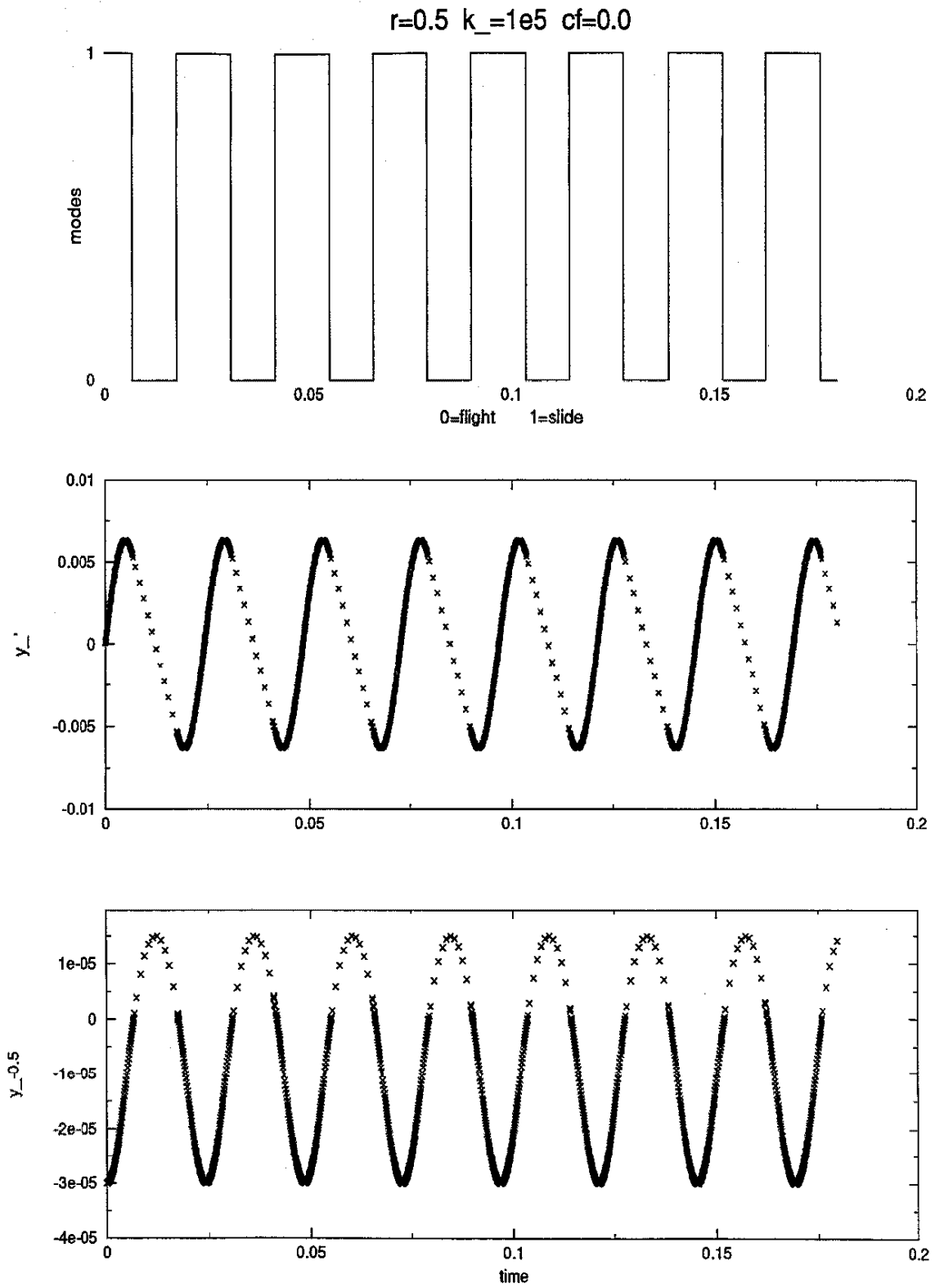
Figure 3.11: Vertical oscillation $\mu = 0.0$

Chapter 4

Parametric study

We ran the code and studied the dynamics of the block for various different parameters and initial conditions. The observed quantities were

- variables $x_-, x_-', y_-, y_-', w, w'$,

- mode as a function of time,

- energy.

We limit the study to following parameter ranges:

stiffness k_-	aspect ratio r (width/height)	coefficient of friction μ
2.0 to 10^7	$\frac{1}{30}$ to 1	0, 0.1, 0.2, 0.3

We did not introduce damping in the block-foundation system. However, energy can be lost in slide mode due to the friction force R_x. The system conserves energy if there is no friction, $\mu = 0$, or while the block is in flight, or while it is in contact mode.

mode or regime	flight	contact	slide $\mu = 0$	slide $\mu > 0$
energy	conserved	conserved	conserved	dissipated

The energy present in the block-foundation system consists of:

kinetic energy in the x direction	$x_-'^2/2$
kinetic energy in the y direction	$y_-'^2/2$
rotational kinetic energy	$I_- w'^2/2$
potential energy due to gravity	$y_- - 0.5$
potential energy of compressed springs	$\int\int_{Region} force_-/width_- \, dA_-$

To find the formula for the potential energy of the compressed springs, refer to Figure 2.2. We see that $\int\int_{Region} ks \, dA = \int_{v1}^{v2} \int_0^{s(v)} ks \, dsdv$. Carrying out the integration for the case of our rectangular

block is simple but lengthy. We merely state the resulting formulas:

block position	potential energy of compressed springs
block in flight	0
type 1	$\dfrac{k_- s_1^3}{6r \sin|w| \cos w}$
type 2	$\dfrac{k_-}{6r\sin|w|}(s_1^3/\cos w - s_2^3 \cos w),$

where $s_1 = \dfrac{\cos w}{2} + r\dfrac{\sin|w|}{2} - y_-,$ $\qquad\qquad\qquad s_2 = \dfrac{\cos w}{2} - r\dfrac{\sin|w|}{2} - y_-.$

Note that formula for type 2 correctly reduces to the type 1 formula when $s_2 = 0$. All the energies are stated in non-dimensional form.

4.1 Typical response

Some dominant types of response are presented in Figures 4.1, 4.2, 4.3, and 4.4. Presented computation was done using the initial conditions ic1. When both a generalized displacement and a generalized velocity are plotted in the same window, the smoother curve belongs to the displacement. The parameter μ is denoted as cf in figure headings.

In Figure 4.1, for initial conditions ic1, the block, after some transient rocking and sliding, settles down into steady-state motion. Variables x_-, y_-, w become nearly constant, with $w = 0, y_- = 0.5, x_- = 0.31$. Thus, the block is vertical, the bottom almost aligned with the foundation surface and it has slid significantly forward to $x_- = 0.31$. If the block settled down without sliding, then x_- would be $r/2 = 0.25$. Velocities x_-', w' are almost zero, only y_-' oscillates slightly as the block moves vertically. Even though y_- is nearly constant and the vertical oscillations are small, the block still escapes the foundation surface, flies and lands. Contact mode and flight regime regularly interchange. Slide mode occurs in steady-state only in between flight and contact mode and for a short time - when the block is landing or taking off. A lot of energy is dissipated by friction forces during the initial transient motion. Still referring to Figure 4.1, sudden changes in x_-', y_-', w' occur at the impact and constant values of x_-', w' occur in flight.

In Figure 4.2, the block moves in contact mode only. There is no flight or sliding. Therefore, we do not include a plot of the modes against time. The block is not restricted to the contact mode, it just does not switch to slide mode or flight. The block rocks steadily back and forth. An oscillation in the y direction is induced after the first impact. The amplitude of the y oscillation remains almost constant between two subsequent impacts, it can change though at the impact. Energy is conserved.
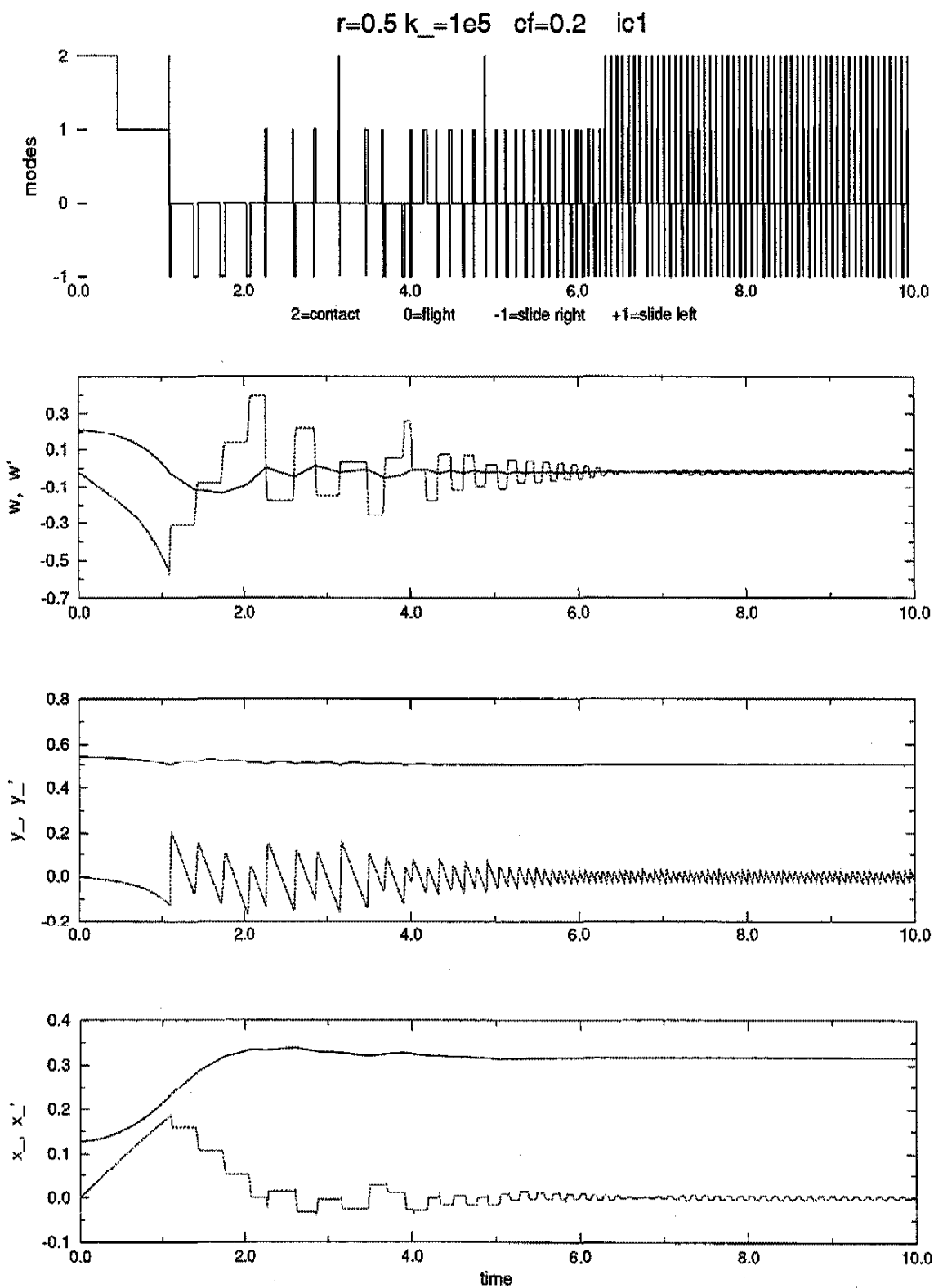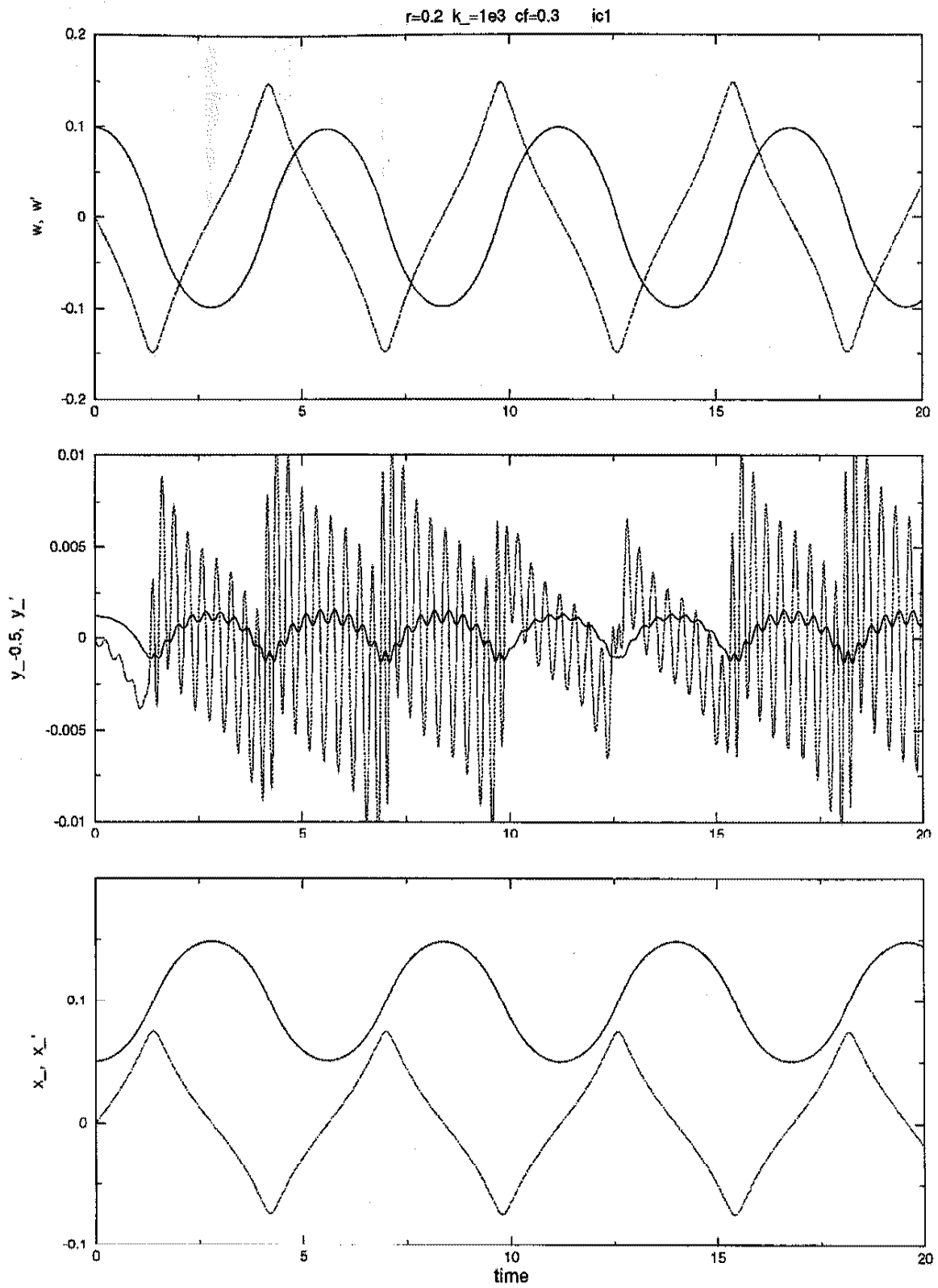
Figure 4.1: Block settles down

r=0.2 k_=1e3 cf=0.3   ic1

Figure 4.2: Steady rocking

Figure 4.3: Tall block

r-0.5 k_=1e5 cf=0.0   ic1

0=flight   3=slide
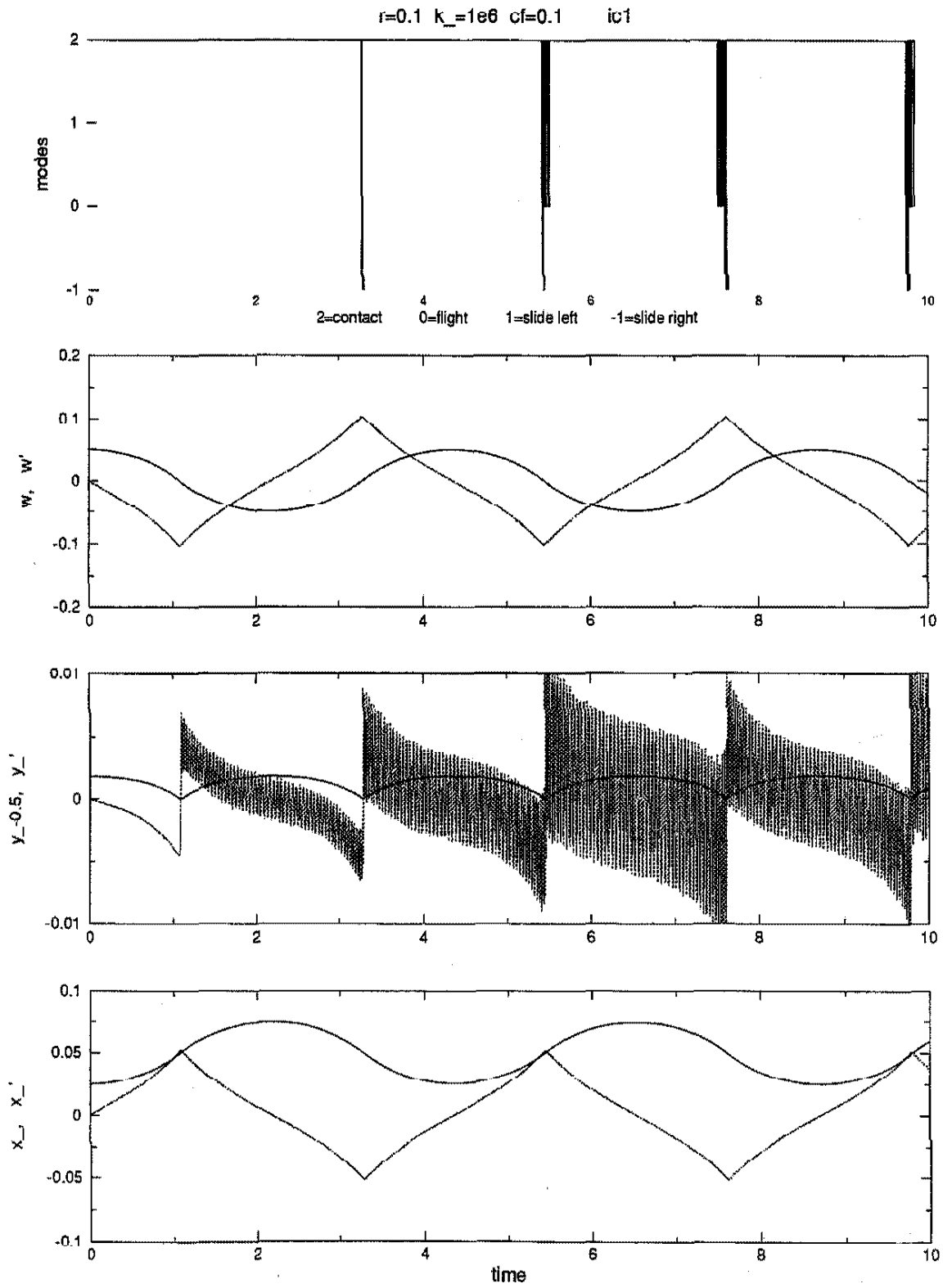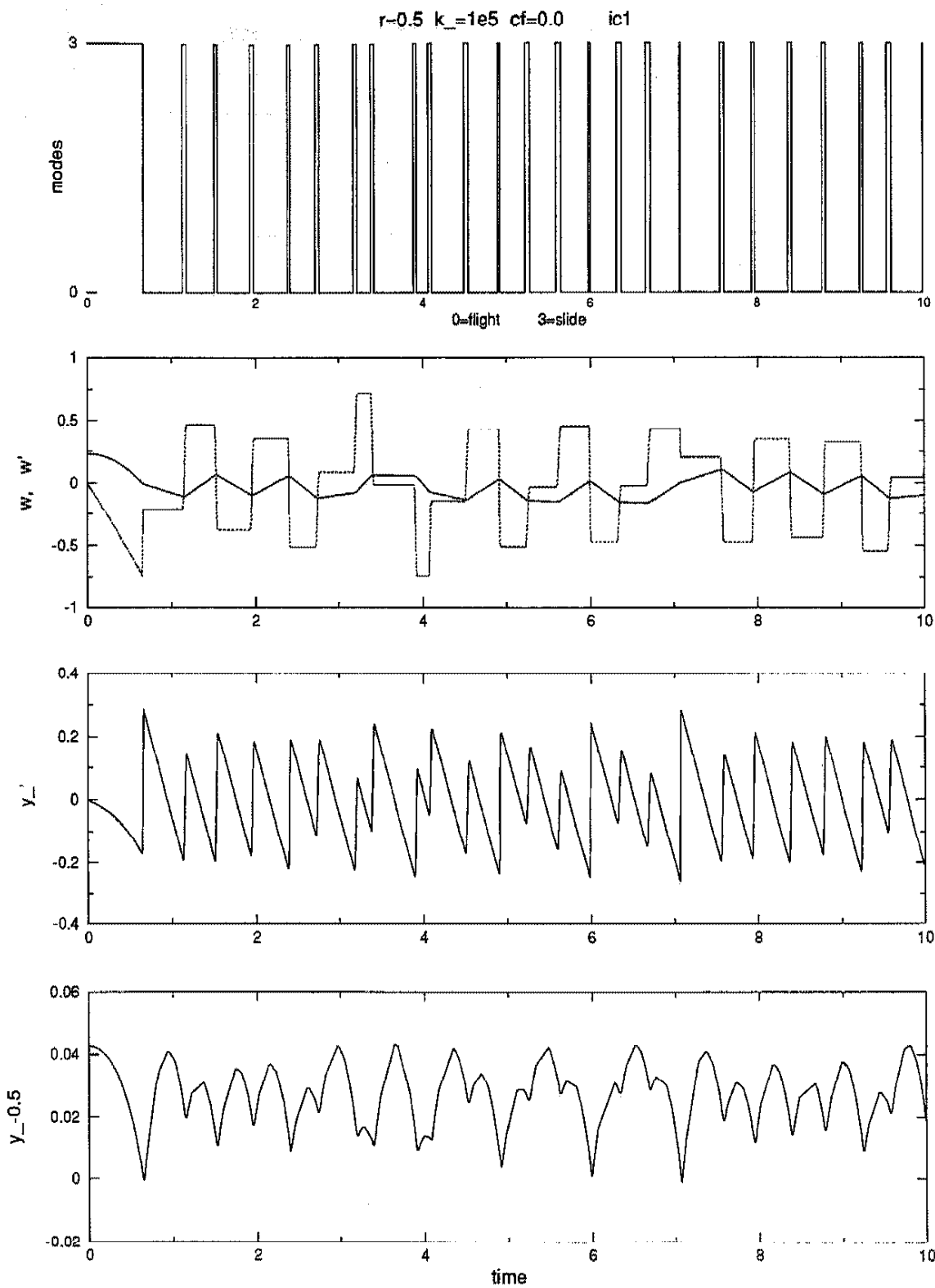
Figure 1.4: $\mu = 0$

In Figure 4.3, the foundation is stiffer. Impacts are harder and occur during a shorter time interval. The block moves mostly in contact mode. There is no flight or sliding at the first impact around a time of 1. The block slides and flies for a short time during the second and each subsequent impact. Again, the y oscillation is induced at the first impact, and again its amplitude remains almost constant between two subsequent impacts and can change at the impact. Comparing this to Figure 4.2, the y oscillation has a much higher frequency. Dissipation of energy in the system is minimal.

In Figure 4.4, the block moves with zero friction, $\mu = 0$. There are no horizontal forces acting on the block. The horizontal velocity, $x_-'(t_-)$, of the block is constant and equal to the initial velocity $x_-'(t_-) = x_{-0}'$, which is zero in this case. Without loss of generality, we can assume $x_-'(t_-) = 0$ and $x_-(t_-) = 0$ for all parameter sets with $\mu = 0$. Thus, the case of zero friction is qualitatively different and the x degree of freedom is lost. The code, however, still integrates in x even for $\mu = 0$ and it arrives at correct constant values for both $x_-(t_-), x_-'(t_-)$. Although the other two parameters k_-, r are the same as in Figure 4.1, the behavior of the block for $\mu = 0$ is completely different. The block never settles down and it never moves in contact mode. Flight and sliding take place and the block rocks and moves vertically. The block spends most of time in flight while impacts occur during a small time interval. Again, constant values of w' in Figure 4.4 correspond to flight. Energy is conserved in the system.

4.2 Flight

The purpose of our parametric study is to determine the response of the block in (μ, k_-, r) parameter space. We have to identify the dominant types of response and regions in the parameter space where such type of response occurs.

We start with the single most distinct type of response - flight. Through extensive numerical simulations, we will determine the range of initial conditions and parameters μ, k_-, r resulting in flight. However, before starting the numerical simulations we try to estimate the flight region analytically based on a simple energy criterion. The analytical approach will serve as a verification of the numerical results and will give us more insight.

4.2.1 Flight region - analytical estimate

Initial conditions with low energy will not allow flight and the block will merely sit on the springs, barely moving, and never leaving the foundation surface. Flight can occur only if the total initial

Figure 4.5: Flight region - lower bound
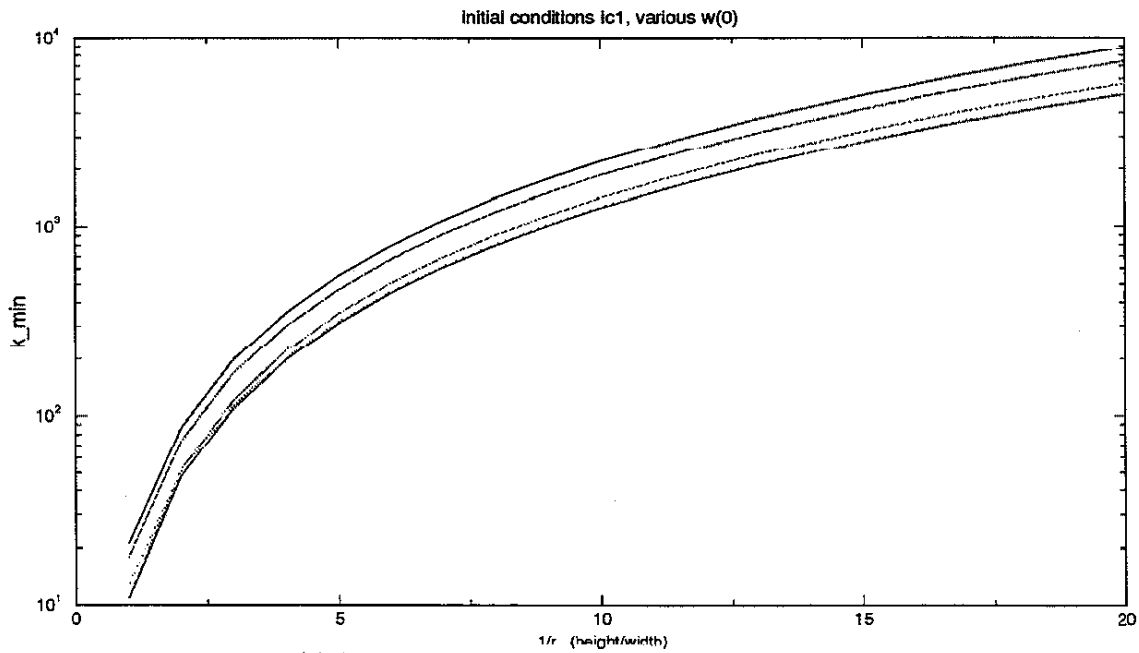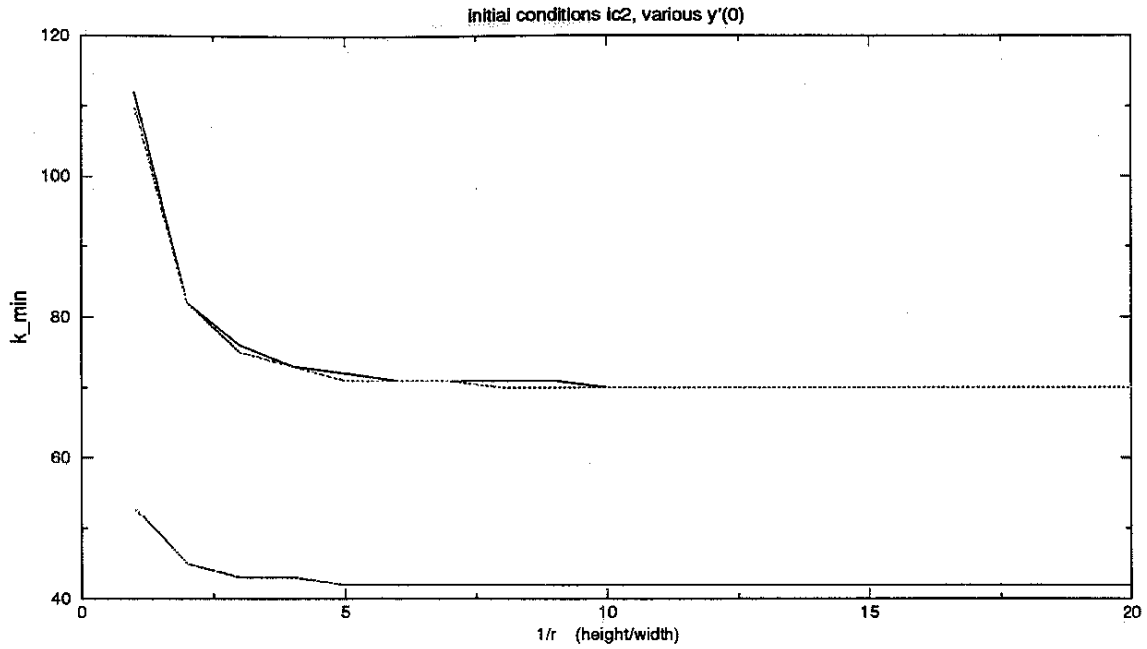
top:	curves $k\_min(r)$ for initial conditions:	ic2
		ic2 $y\_'(0) = 0.01$
		ic2 $y\_'(0) = 0.1$
bottom:	curves $k\_min(r)$ for initial conditions:	ic1 $w(0) = \alpha/5$
		ic1 $w(0) = \alpha/4$
		ic1 $w(0) = \alpha$
	ordering of curves in plot	ic1 $w(0) = \alpha/1.2$
	same as in the list	ic1

energy is sufficient to lift the block above the surface. Suppose no energy is lost during the motion, then the initial energy must be equal to or larger than the energy of the block in flight. The minimum energy the block can have in flight is zero. Thus, for the block to fly, the initial conditions with the total energy larger than zero are necessary. If the initial energy is zero and the block moves conserving energy, it could arrive at a vertical position, its bottom aligned with the surface, and all velocities zero. This is the situation when the block clears the surface requiring the least amount of energy. If the initial energy is less than zero, the block can never leave the foundation. If the initial energy is larger than zero, the block could fly. However, the block mostly leaves the surface tilted and with some kinetic energy. Some energy may also be dissipated before the block reaches the surface, so initial energy just larger than zero does not guarantee flight. Thus, the minimum initial energy necessary but not sufficient for flight is zero. Note that zero happens to be the minimum necessary energy due to the definition of potential energy. If we defined potential energy as y_-, the minimum energy required for flight would be 0.5.

The initial energies are given by the initial conditions, which in turn may depend on the parameters μ, k_-, r. Given a set of initial conditions we evaluate the total initial energy at different points in the μ, k_-, r parameter space. If for specific choice of parameters this energy is negative the block can never fly. If this energy is positive the block could possibly fly. The set of all points in parameter space where block could possibly fly, will be called the **possible flight region**. The higher the initial energy, the more likely flight is. The possible flight region will contain a region where block does fly at some time, the **actual flight region**. In other words, the possible flight region is the lower bound of the actual flight region.

Now we determine the lower bound of the actual flight region for the initial conditions set ic1, ic2 and other similar initial condition sets. For example, ic1 $w(0) = \alpha/4$ is the set ic1 where the initial value of $w(0)$ is changed from $w(0) = \alpha/2$ to $w(0) = \alpha/4$. We find that block could fly for all k_- larger than the value we call k_-min, which depends on r and practically does not depend on μ. The block can never fly for k_- smaller then k_-min. Curves of $k_-min(r)$ are plotted in Figure 4.5 for various initial conditions. The actual flight region can be only above the curve.

4.2.2   Flight region - numerical simulation

We want to determine the actual flight region by numerical simulations. In the previous section, we defined the possible flight region as the set of all points in parameter space where the block initially has enough energy to leave the foundation. The actual flight region is then set of all points where the block really does fly at some time. The words 'some time' present a problem when we want to

determine the actual flight region by numerical simulations. We cannot compute the motion of the block indefinitely; every code has to stop at some finite time. If the block did not fly during that time, it could fly later.

Flight for fixed r, μ

To find out more about the flight behavior of the block, we start by plotting time to flight versus k_- for fixed r, μ. Figures 4.6 through 4.13 contain such plots for our favorite initial conditions ic1, ic2. For each k_- we observe motion of the block only till a certain time t_{-end}. For each plot r, μ and t_{-end} are constant. If the first flight occurs at some $t_- < t_{-end}$, we plot a point (k_-, t_-). If the block does not fly for any $t_- \leq t_{-end}$, we plot a point (k_-, t_{-end}).

Based on the time to flight figures we can draw a few conclusions about the behavior of the block which are independent of μ and valid for both ic1, ic2.

For a given r, the lowest stiffness for which the block flies is much higher than the k_-min determined by energy considerations.

As predicted by the energy considerations, the block's tendency to fly increases with stiffness k_-. In general, the block does not fly for low k_- and flies early on during its motion for high k_-. Values of low and high k_- depend strongly on r. Flight behavior for k_- between low and high values depends also on r. When the aspect ratio r is around 1, we find that for all k_- below a certain value, no flight occurs at all, but as k_- increases, flight occurs early on during the block's motion. So the block either does not fly at all or flies early on. For lower aspect ratios r (tall, thin blocks) we find a more gradual change in flight tendency. Again, for all k_- below a certain value no flight occurs at all, then for some higher k_-, flight occurs, however, the time of the first flight is rather late. As the value of k_- goes further up, the time of the first flight decreases, then increases and again decreases, increases...., forming sort of spikes when plotted against k_-. At the peak we find late or no flight, in the valley between spikes flight occurs early on. Spikes get smaller with higher k_- and eventually they disappear as the block constantly flies early on (Figure 4.6). Although the described phenomena is evident for both ic1 and ic2, the gradual change in flight tendency with increasing k_- is more pronounced for initial conditions ic1. On the other hand, for initial conditions ic2, the no-flight-or-early-flight behavior is more pronounced and occurs for a wider range of the aspect ratio r. (from $r = 1$ to approximately $r = 0.3$).

Also for low r, points indicating the time of first flight are spaced vertically in rows, suggesting that the first flight occurs during some regularly repeating event. This event turns out to be the passage of the block through the upright vertical position ($w = 0$). During the short time we observed
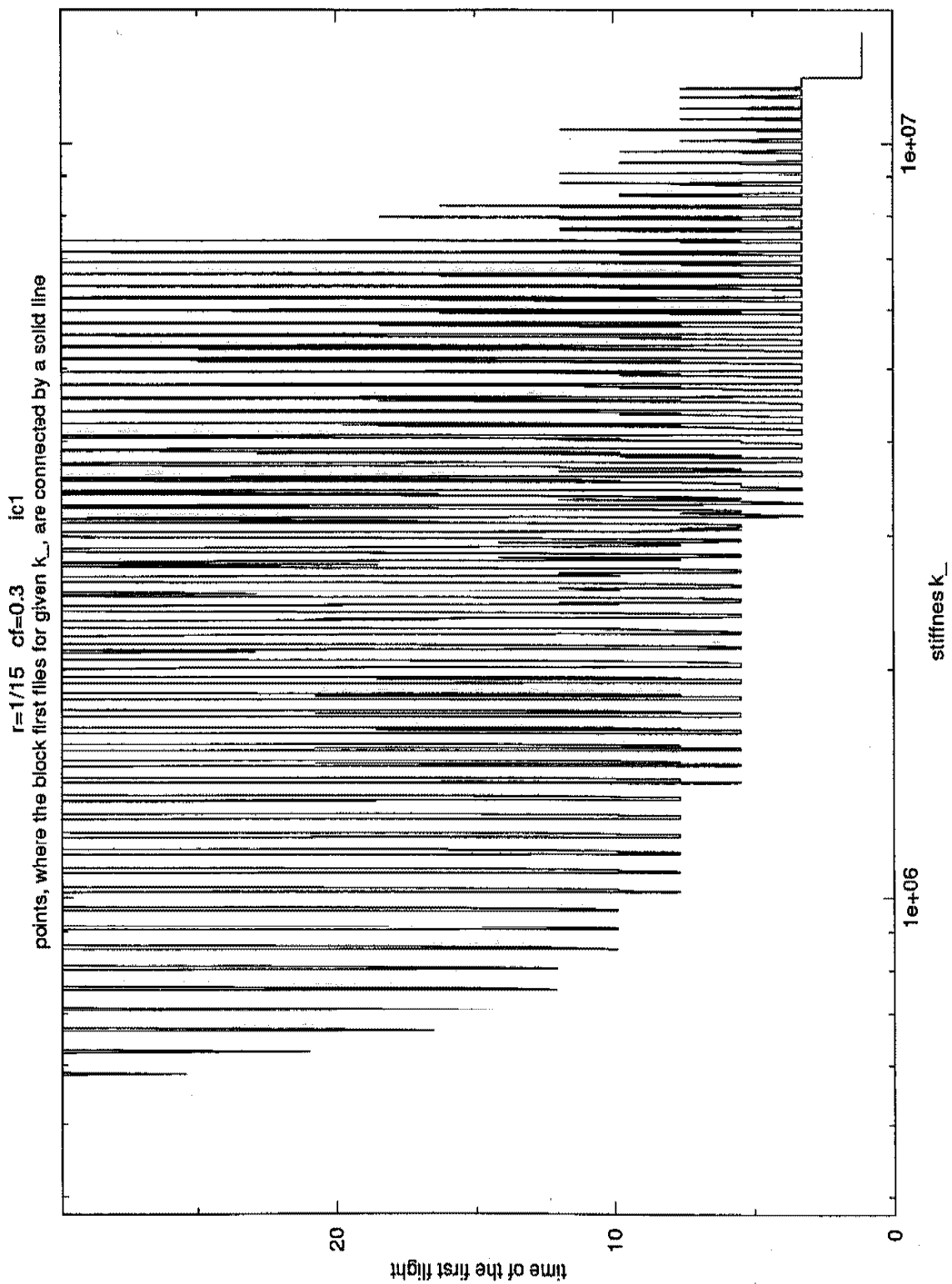
Figure 4.6: Time to flight, ic1, r=1/15
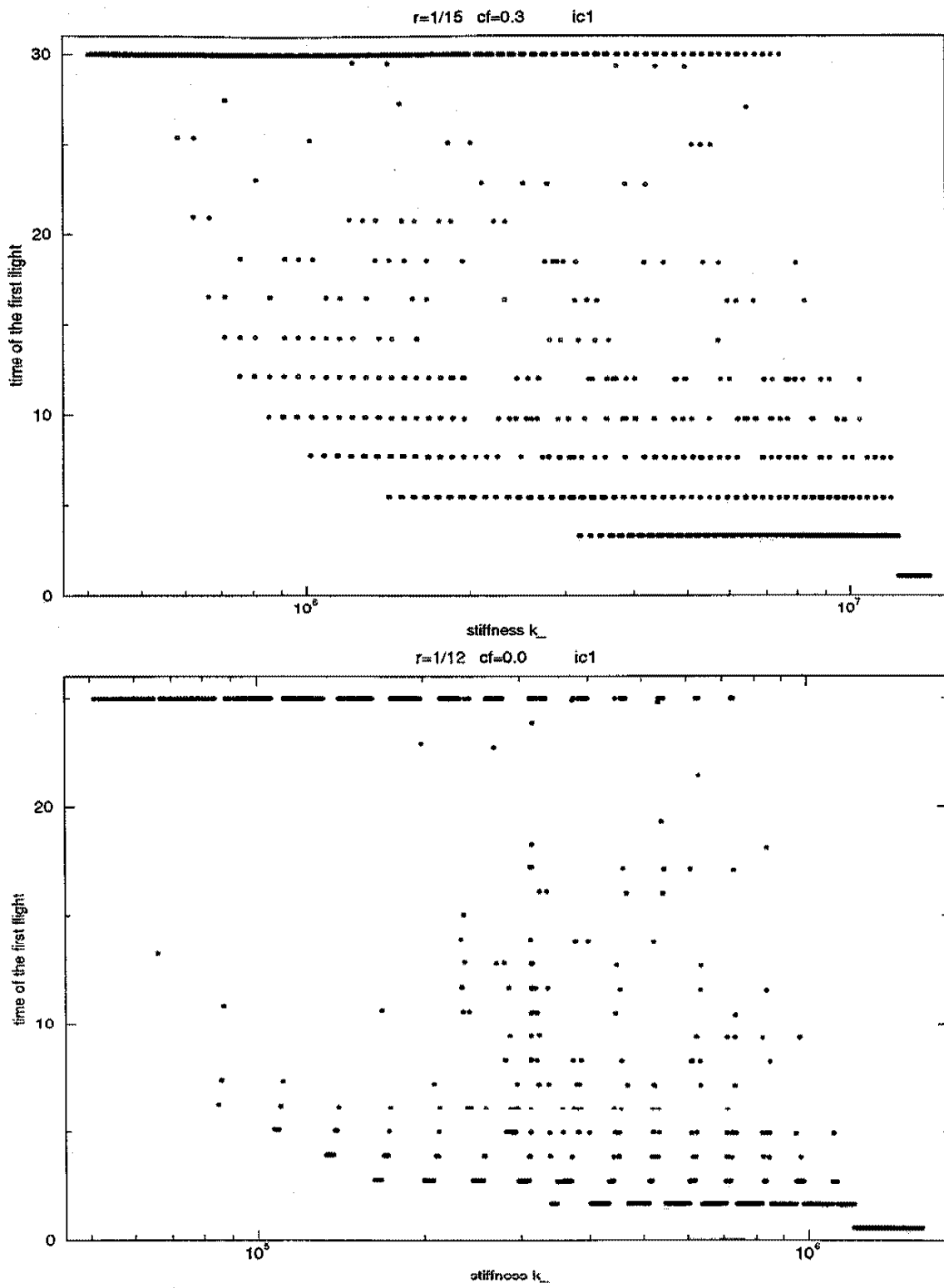
top: $t_{-end} = 30$, bottom: $t_{-end} = 25$

Figure 4.7: Time to flight, ic1, r=1/15, 1/12

top: $t_{-end} = 60$, bottom: $t_{-end} = 80$

Figure 4.8: Time to flight, ic1, r—0.1, 0.2
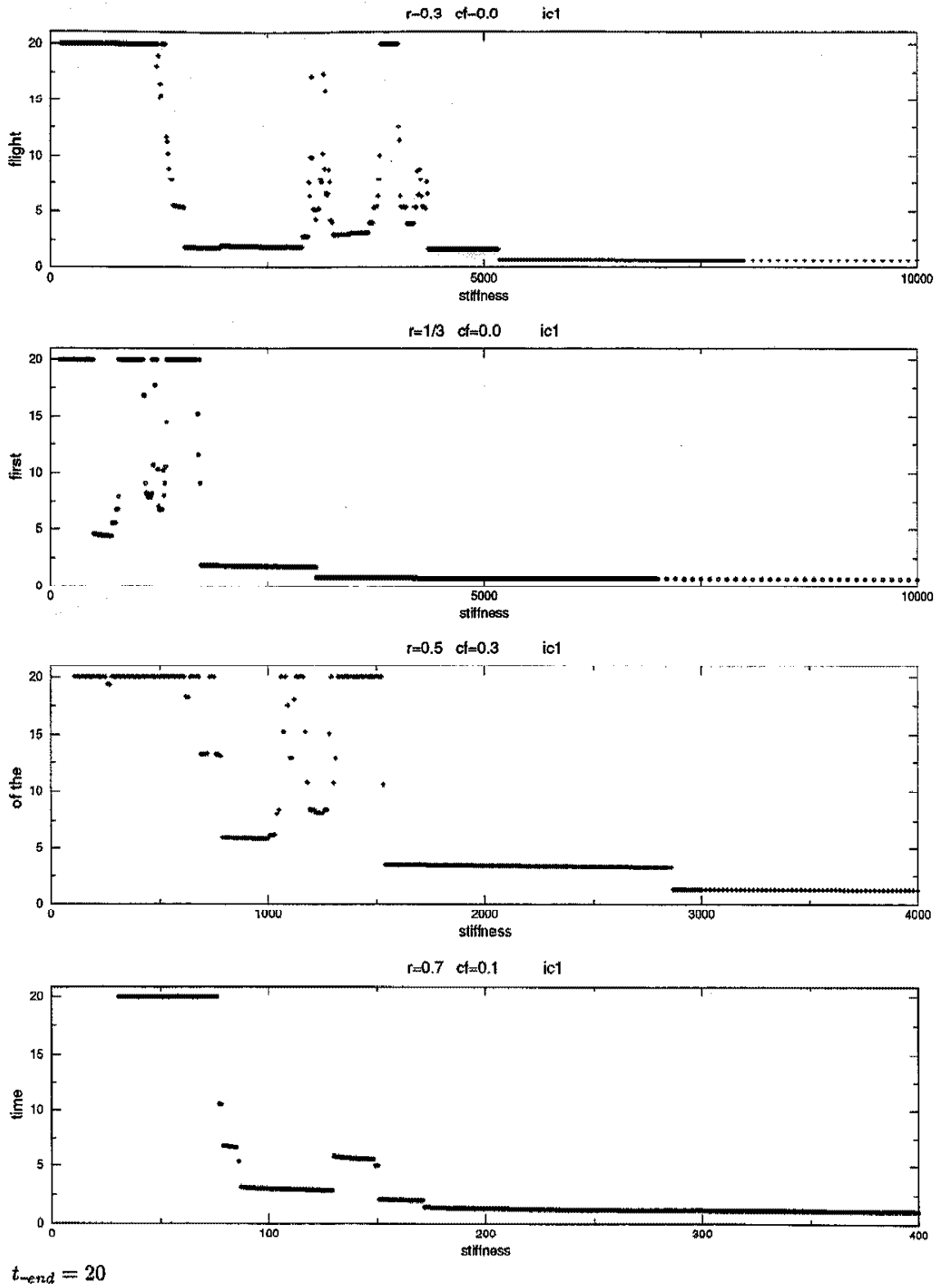
Figure 4.9: Time to flight, ic1, r=0.3, 1/3, 0.5, 0.7

r=0.9 cf=0.1   ic1

r=0.9 cf=0.0   ic1

r=0.9 cf=0.2   ic1

r=1 cf=0.3   ic1
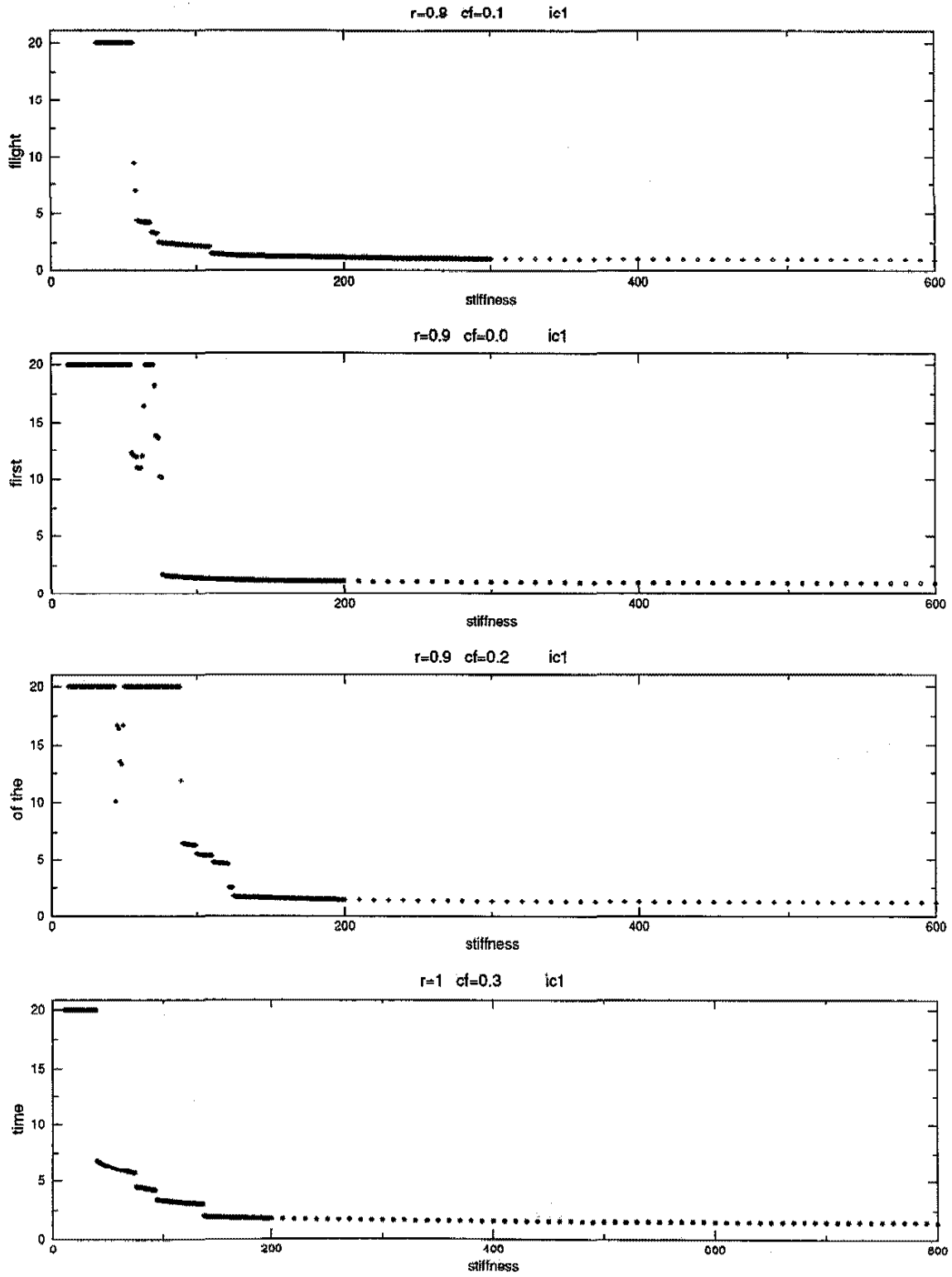
$t_{-end} = 20$

Figure 4.10: Time to flight, ic1, r=0.8, 0.9, 1
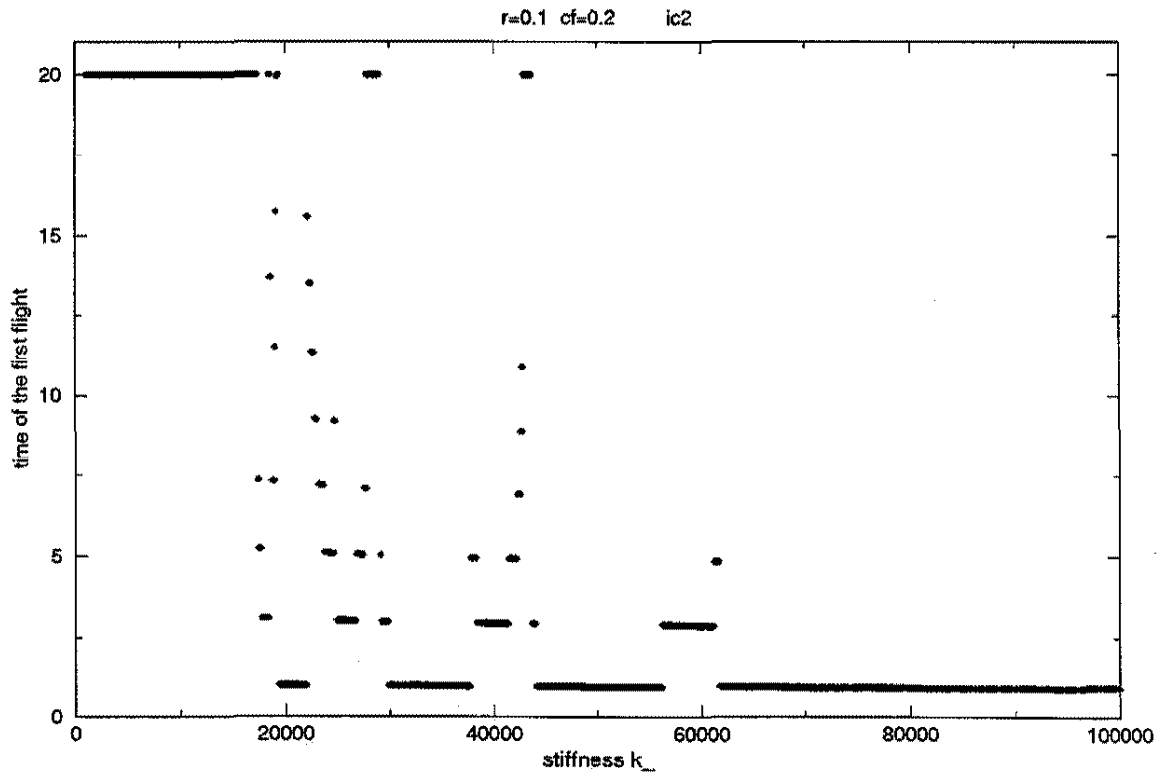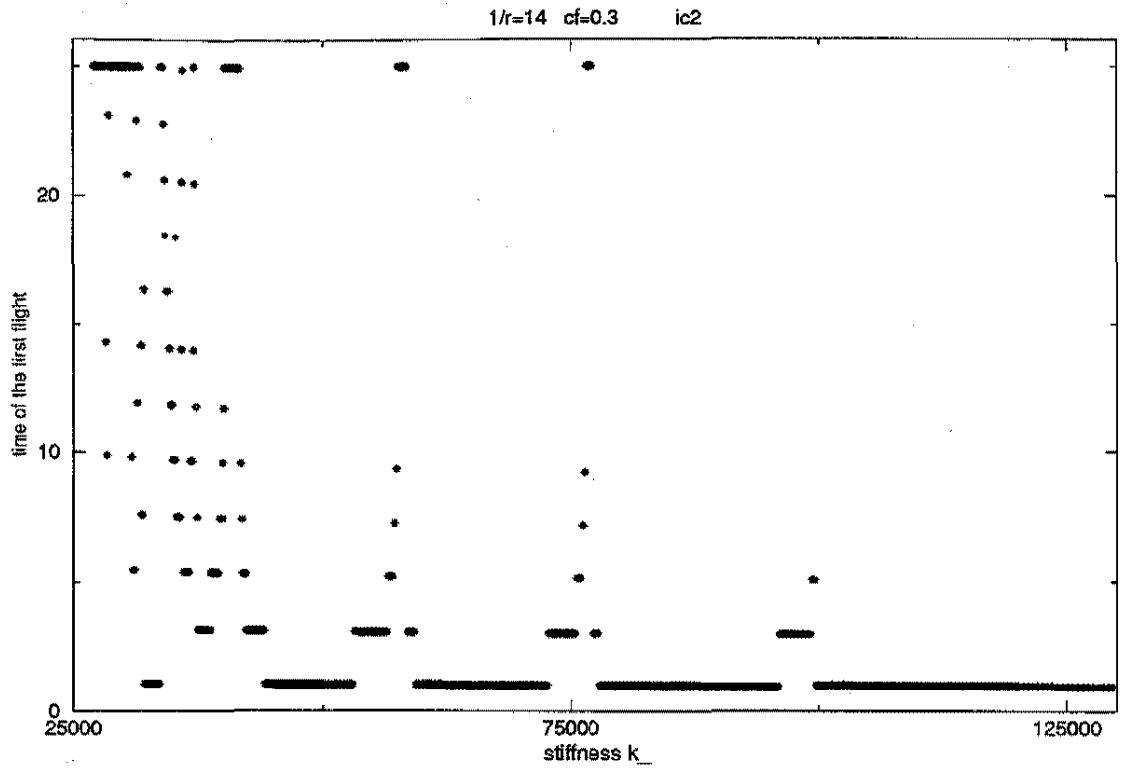
top: $t_{-end} = 25$, bottom: $t_{-end} = 20$

Figure 4.11: Time to flight, ic2, r=1/14, 0.1

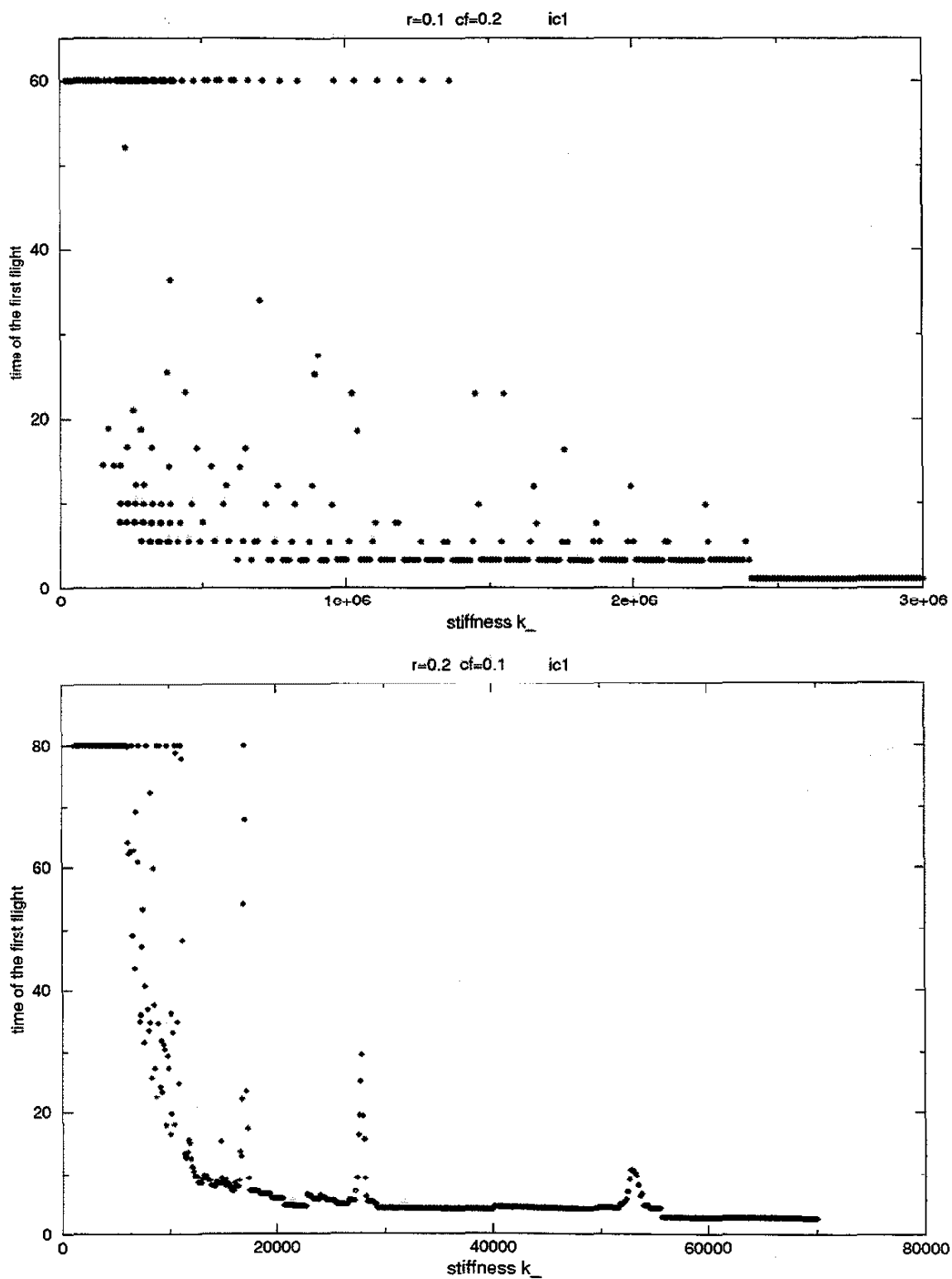bottom plot $t_{-end} = 12$, other $t_{-end} = 20$

Figure 4.12: Time to flight, ic2, r=1/7, 0.2, 1/3

Figure 4.13: Time to flight, ic2, r=0.5, 0.8, 1

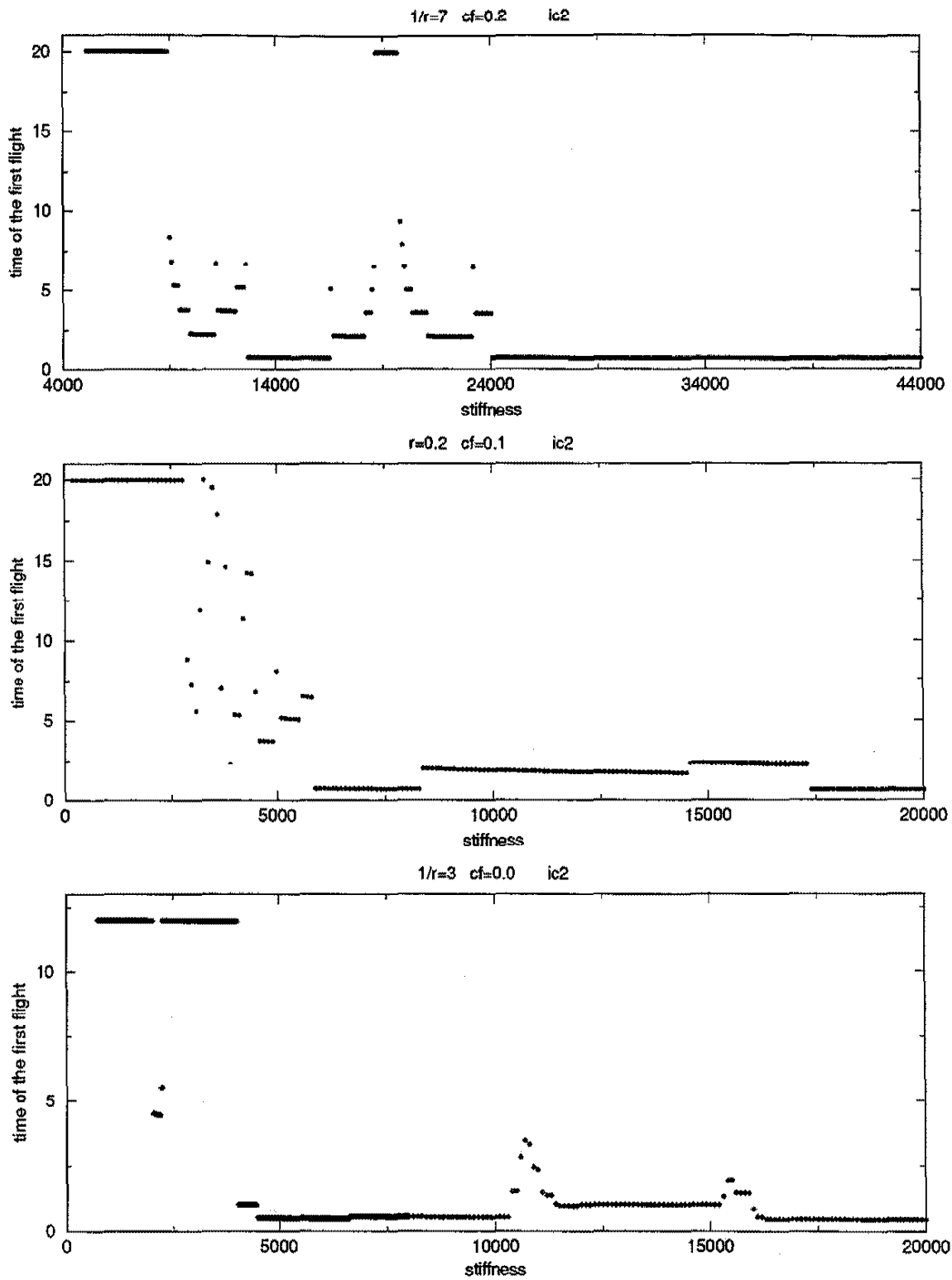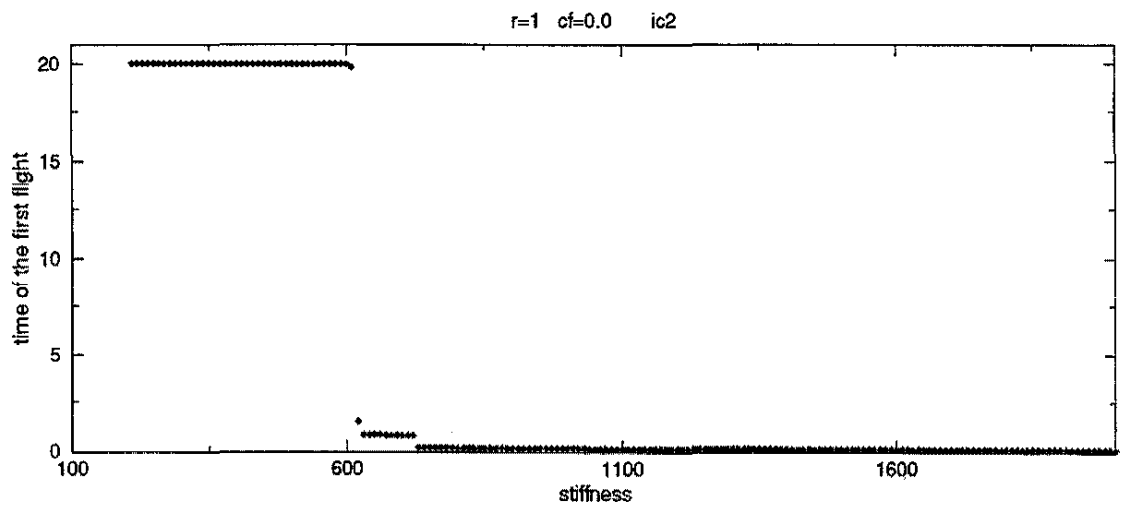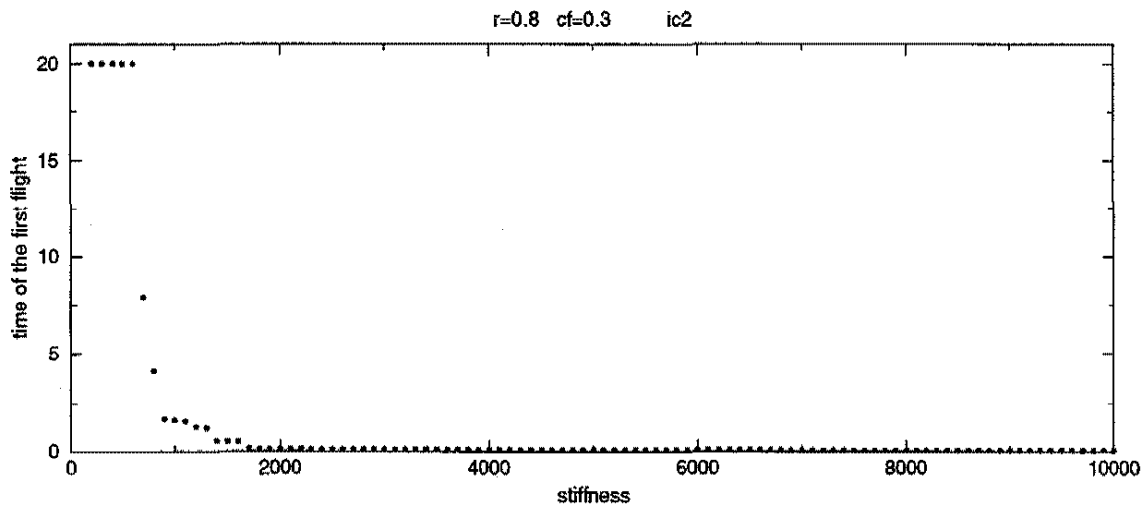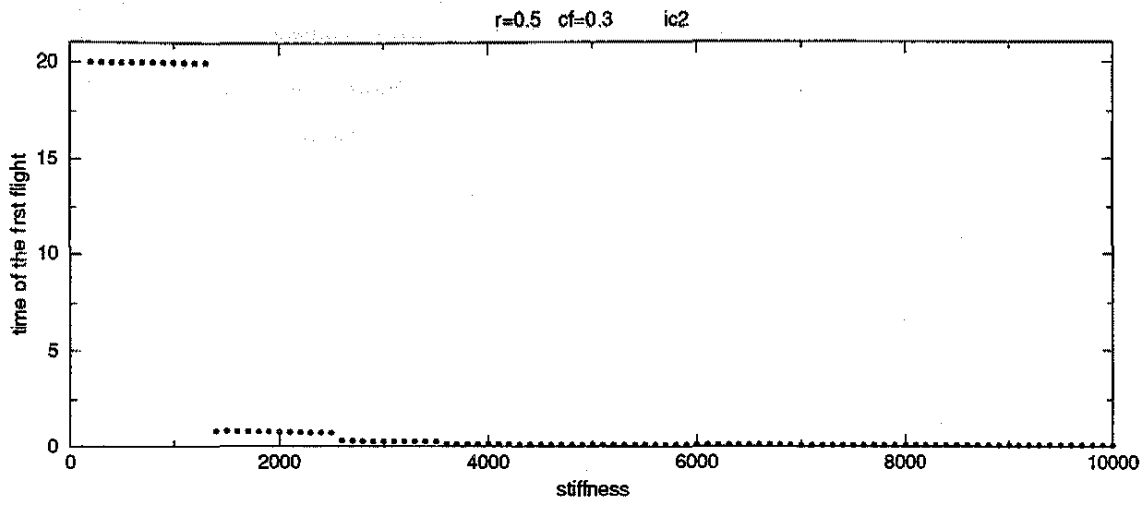$t_{-end} = 20$

its motion, the block was regularly rocking back and forth with a tendency to lift off when w was near zero, that is during impact. Note also that each plot in Figures 4.6 through 4.13 is ended by a continuous horizontal line positioned no higher than any previous point in the plot. This line corresponds to flight during the first impact. Continuity of the line implies that for all k_- larger than a certain value the block will always fly during the first impact. One can make even a stronger statement for initial conditions ic1: if for certain k_- the block flies during the first impact, it will do so for all larger k_-.

Flight in k_-, r parameter space

The flight behavior observed and described so far depends only weakly on the coefficient of friction μ. Relevant changes in flight behavior can be captured in the (k_-, r) parameter space. Also, based on energy considerations we do not expect much variation in the flight tendency for different μ. Therefore, we will numerically estimate the actual flight region in (k_-, r) parameter space for just a few different μ's. Since we cannot compute the motion of the block indefinitely, we cannot determine numerically the actual flight region defined as a set of all points in the parameter space where flight occurs at some time. We will instead determine in the (k_-, r) parameter space the low k_- region where block never flies, the No Flight Region, and the high k_- region where block always flies early on, the Early Flight Region. Plots in Figures 4.6 through 4.13 are for fixed r and μ, showing the block's tendency to fly along a single vertical line $r = constant$ in (k_-, r) parameter space. Knowing the flight tendency along few single lines $r = constant$ we can set a suitable criterion for establishing a critical curve, $k\_critical(r)$, separating the No Flight Region and a curve k_high separating the Early Flight Region.

Definition:

Consider arbitrary but fixed initial conditions and parameters μ, r. Let $k_n(r)$ be a stiffness such that for given initial conditions and for $\mu, r, \forall k < k_n(r)$, the block does not fly before completing the n-th pass through the vertical position $w = 0$. Then $k\_critical_n(r)$ is defined as supremum of all such numbers k_n.

The value of $k\_critical_n$ depends on the parameters μ, r and on the initial conditions. Dependence on r is stated explicitly in the definition as it is most distinct and of our prime interest. Criterion "before completing the n-th pass through the vertical position $w = 0$" can be stated briefly as "while $ihor < n$", where $ihor$ is an integer variable counting passages through $w = 0$. For initial conditions with $w(0) = 0$ the starting position also counts as a passage through $w = 0$, so $ihor = 1$ from the

start. For $n \to \infty$, the curve $k\_critical_n(r)$ will converge to a curve $k\_critical(r)$ separating the No Flight Region. Let us relate this definition to data displayed in time to flight versus $k\_$ plots for fixed r, μ. For example, in the bottom plot in Figure 4.7, the first flight occurs at time 13 for $k\_ = 6e4$ but flight during the first impact at time 0.55 is guaranteed for $k\_ \geq 1.2e6$. For that plot we have by our definition $k\_critical_3 = 1.63e5$, $k\_critical_2 = 3.41e5$ and $k\_critical_1$ does not exist since flight never occurs before the first passage through $w = 0$. Typically for initial conditions ic1, if the block flies during the first impact it does so shortly after passing through $w = 0$ but if the first flight occurs during the second, third or later impacts, it typically starts shortly before reaching $w = 0$.

Definition:

Consider arbitrary but fixed initial conditions and parameters μ, r. Let $kk(r)$ be a stiffness such that for given initial conditions and for $\mu, r, \forall k > kk(r)$ the block flies before or during the first impact. Then $k\_high(r)$ is defined as the infimum of all such numbers $kk(r)$.

The value of k_high depends again on the parameters μ, r and on the initial conditions. Again dependence on r is stated explicitly in the definition as the most distinct and interesting. For the initial conditions ic2, the criterion "before or during the first impact" is interpreted as "while $ihor < 2$." For initial conditions ic1 it is interpreted as "while $w' < 0$" if $k\_high(r)$ exists for such an interpretation. If not, then it is interpreted as "while $ihor < 2$". The reason for the different implementation of the "first impact" criterion is due to the nature of the initial conditions. For ic1, the first impact is usually finished while $w' < 0$. Only for r close to 1 does flight occur for very low stiffnesses, when the first impact is long and soft and the earliest our block can fly is at the end of the first impact when w' is already greater than 0.

In Figure 4.14, we plot $k\_critical_3(r)$ for the initial conditions ic1 (bottom plot) and ic2 (top plot). Each plot presents $k\_critical_3(r)$ for various coefficients of friction μ and an appropriate lower bounding curve k_min. At the bottom plot with ic1, the lowest curve is for $\mu = 0$. The other three curves which almost coincide are for $\mu = 0.1, 0.2, 0.3$. Thus, the block is a little more inclined to fly for zero friction and the flight tendency is practically independent of friction for $\mu = 0.1, 0.2, 0.3$. The curves $k\_critical_3(r)$ have the same shape as the lower bound k_min and the flight tendency is high for a square block and decreases with r, as the block gets tall and thin. The lower bound is orders of magnitude smaller than $k\_critical_3(r)$. At the top plot with ic2, the flight tendency is almost independent of μ for tall, thin blocks. For r between 1 and 1/6, the flight tendency depends somewhat on μ, but in contrast to ic1, the block does not tend to fly earlier for zero friction. The curves $k\_critical_3(r)$ are of similar shape, only more flat, compared to curves for ic1. The flight

tendency again decreases with r contrary to the prediction by ic2 lower bound k_min. The lower bound is a few orders of magnitude lower than $k\_critical_3(r)$, even more so than for ic1. Note that only one ic2 critical curve is computed up to $r = 20$, the other ic2 critical curves are shorter, each of different length. Reason for that will be explained in the Stability section.

In Figure 4.15, we plot $k\_critical_{10}(r)$ for initial conditions ic1 (bottom plot) and ic2 (top plot). Each plot presents $k\_critical_{10}(r)$ for various coefficients of friction μ and an appropriate lower bound curve k_min. The plots look very similar to the plots of $k\_critical_3(r)$ and all observations made there apply to $k\_critical_{10}(r)$ as well.

In Figure 4.16, we plot k_high, again for the initial conditions ic1 (bottom plot) and ic2 (top plot). Curves k_high for ic2 are slightly flatter and less smooth than k_high for ic1, but otherwise similar. For both ic1 and ic2, the flight tendency strongly decreases with r. The k_high curves also resemble $k\_critical$ curves. For both ic1 and ic2 we observe the same μ dependence as for $k\_critical$. For ic1, the lowest k_high curve is for $\mu = 0$, the other, coinciding when $r < 1/6$, are for $\mu = 0.1, 0.2, 0.3$. For ic2, zero friction does not result in a higher flight tendency.

Each plot in Figures 4.18 and 4.19 contains the $k\_critical_3, k\_critical_{10}$ and k_high curves. Figure 4.18 consists of four plots, all plots for initial conditions ic1, but each for different μ. Likewise Figure 4.19 consists of four plots, all plots for initial conditions ic2, again each for different μ.

By definition $k\_critical_{10}(r) < k\_critical_3(r) < k\_high(r) \; \forall \; r$, a fact reflected in plots in Figures 4.18 and 4.19. The two $k\_critical$ curves are close to each other in $(k\_, r)$ parameter space, indicating a fast convergence of $k\_critical_n$. For ic1 the two critical curves are nearly of the same shape over the whole observed range of r, one appears to be the other only shifted by a constant in plot's logarithmic scale. For ic2 the two $k\_critical$ curves nearly coincide when $r < 1/5$ and differ somewhat when $1/5 < r < 1$. Having k_high and $k\_critical$ in the same parametric plot gives a clear picture of flight tendency in the $(k\_, r)$ parameter space. The region above k_high we call the Early Flight Region - anywhere in that region the block will fly before or during the first impact. The region below $k\_critical_n$ we call the No Flight Region - anywhere in that region block will not fly while $ihor < n$. Finally, the region between k_high and $k\_critical$ is a transition between the two regions. We call this region the Flight Transition Region. Here the first flight occurs at various times: early, late or never. The vertical width of the Flight Transition Region appears constant in plot's logarithmic scale, it is approximately one order of magnitude. In other words for any given μ, r and initial conditions we have approximately $k\_high(r) = 10 \; k\_critical(r)$.

Flight - conclusions

In general, we can draw few conclusions valid for both ic1, ic2:

- The flight tendency depends strongly on the aspect ratio r and weakly on the friction μ

- The flight tendency decreases as the aspect ratio r decreases

- For any fixed r, the block never flies for k_- below a certain value called $k\_critical(r)$

- For any fixed r, the block always flies early for k_- above a certain value called $k\_high(r)$

- For any fixed r approximately $k\_high(r) = 10 \ k\_critical(r)$.

The curves $k\_high(r)$ presented in Figures 4.16 and 4.18 do not reach all the way to $r = 1$ for the initial conditions ic1. We recall that by the definition of k_high, we require the block to fly "before or during the first impact" for all $k > k\_high$. The said curves were computed for ic1 interpreting this criterion as "while $w' < 0$." When r is very close to 1, then k_high is not defined for the "while $w' < 0$" interpretation. Now we will use an alternate interpretation "while $ihor < 2$" to compute the remaining piece of k_high. In Figure 4.17 for initial conditions ic1, we present curves $k\_high(r)$ for an aspect ratio r between 1 and 1/5. Each plot is for different μ and each plot contains $k\_high(r)$ computed using "while $w' < 0$" and $k\_high(r)$ computed using the "while $ihor < 2$" interpretation. As expected for a given r, when $k\_high(r)$ computed by "while $w' < 0$" exists, it is higher. The two $k\_high(r)$ curves come together at an r coordinate, where $k\_high(r)$ computed by "while $w' < 0$" becomes undefined. Thus, $k\_high(r)$ computed by "while $w' < 0$" can be continuously extended into the r region where it does not exist by an alternate "while $ihor < 2$" interpretation of first impact criterion.

The last plot in the flight study, plot 4.20, shows a gray-scale image of the time to flight in the (k_-, r) parameter space, where darker shades represent longer time to flight.

4.3 Stability

In this section we study the stability of the block with aspect ratios $r \leq 1$. Although it is not explicitly repeated in each statement, the following observations, claims, and conclusions do not necessarily hold for the block of aspect ratio $r > 1$.

In all of the computer simulations in this thesis we observe the motion of the block only up to a point when its diagonal becomes vertical ($|w| = \alpha$.) If the block passes this position at some time we say that the **block overturns** and we stop the numerical computation. By the word **stability**
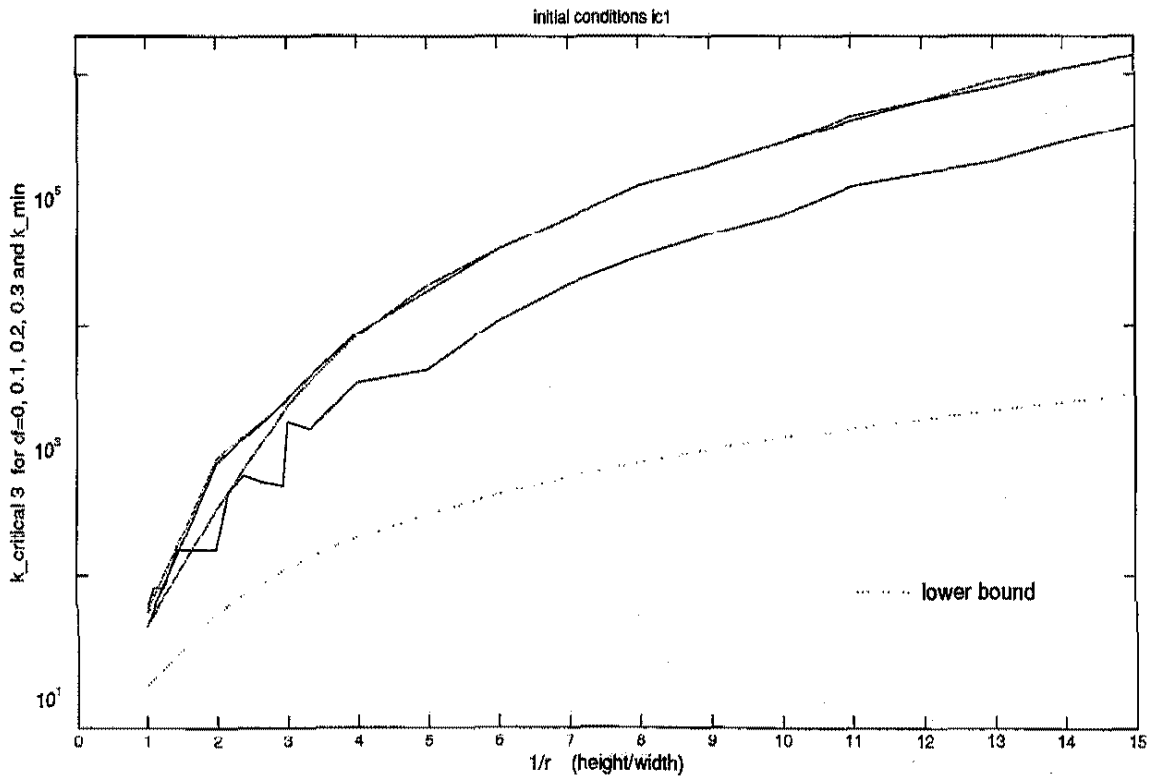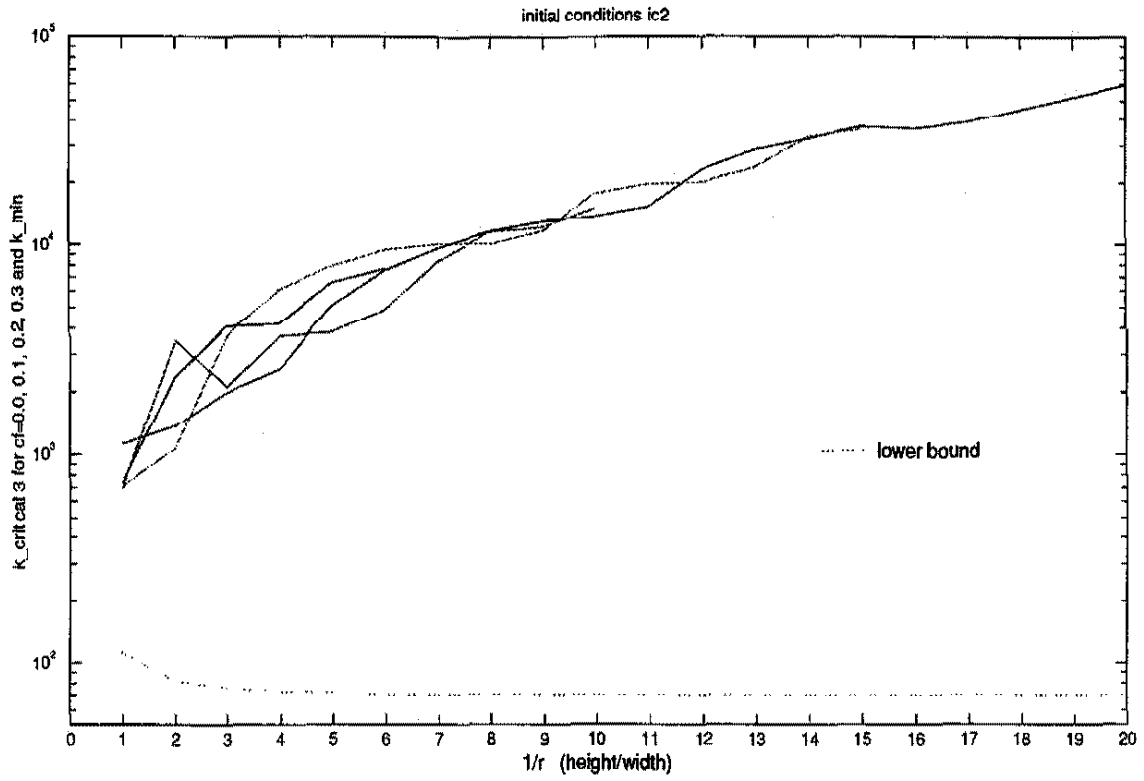
Figure 4.14: $k\_critical_3$
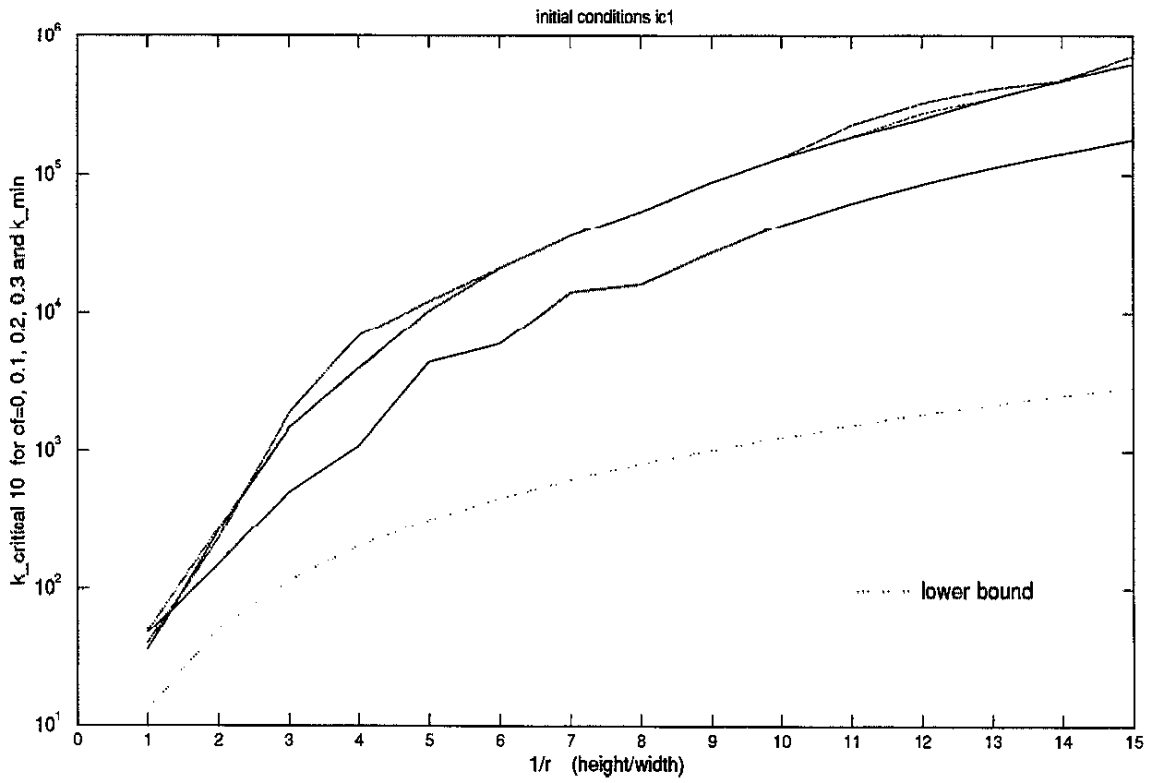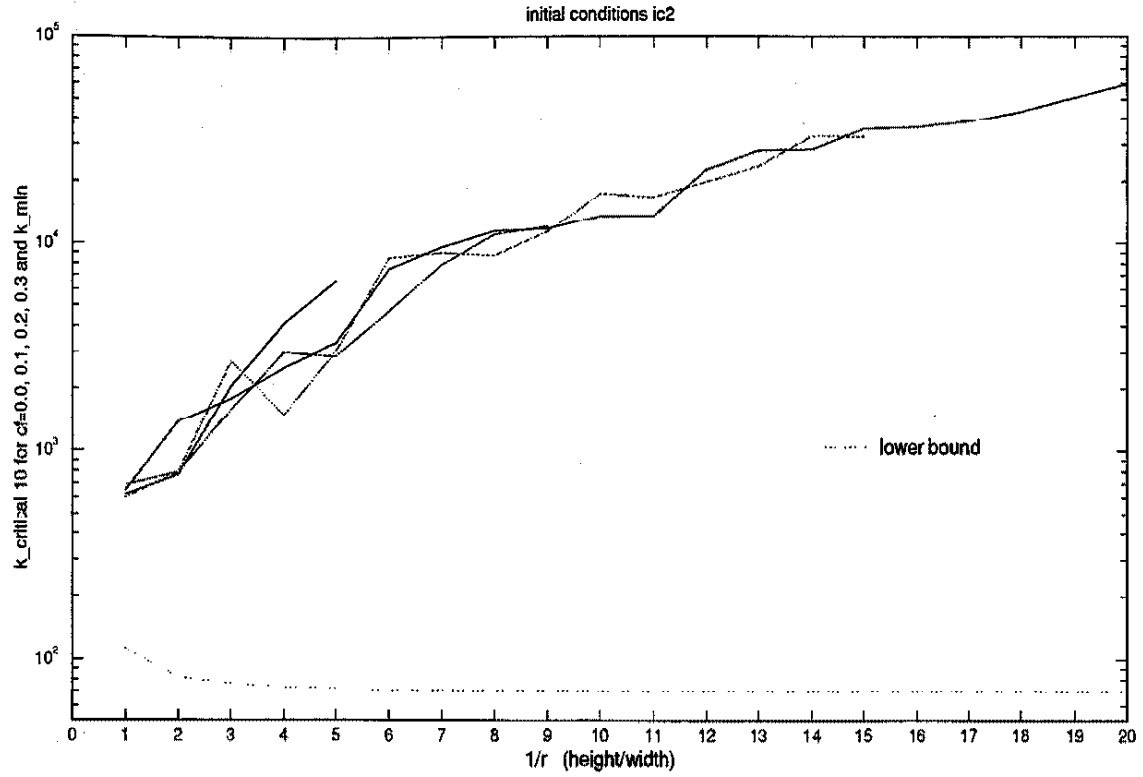
Figure 4.15: $k\_critical_{10}$
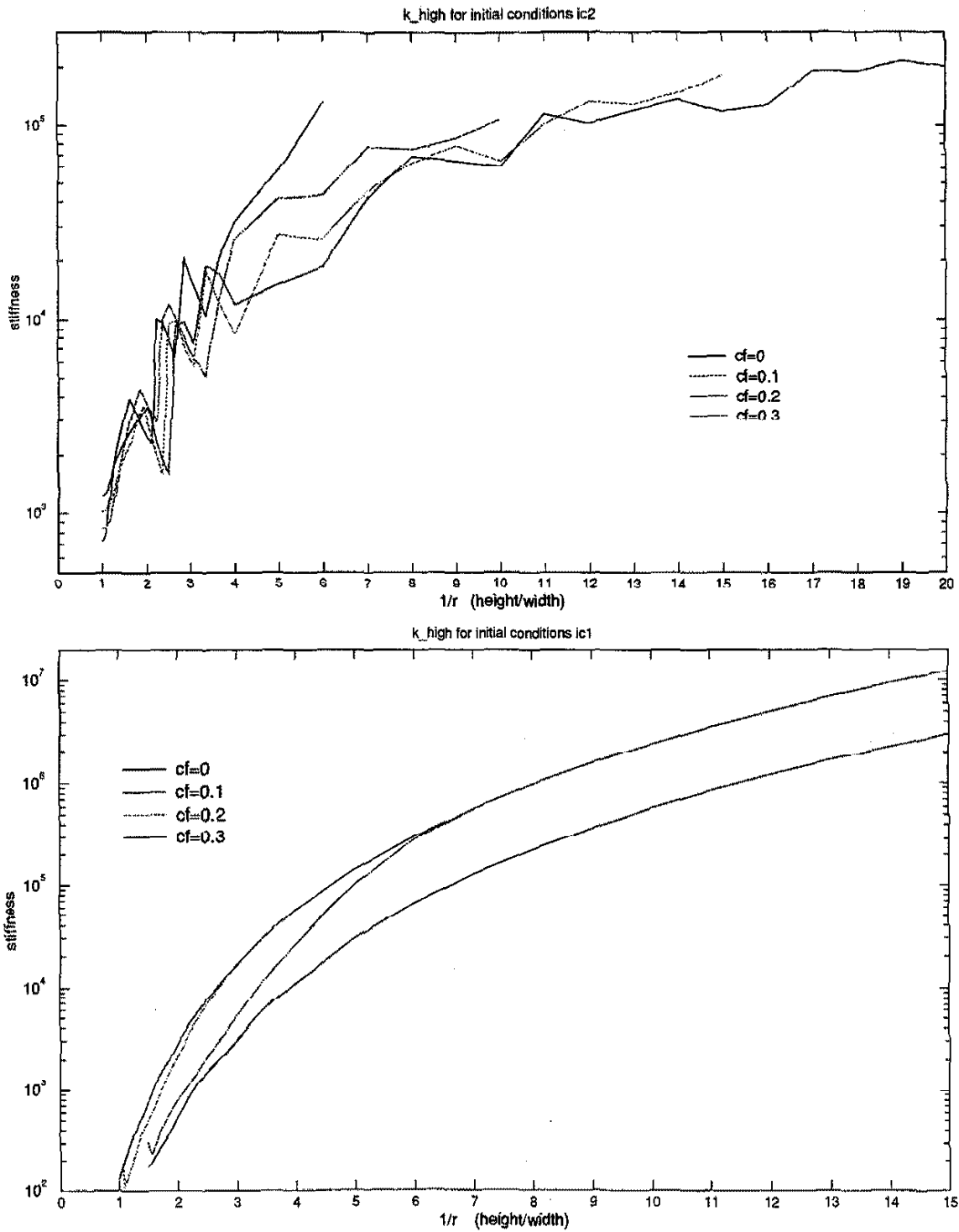
Figure 4.16: *k_high*

first impact criterion for ic2: while *ihor* < 2
first impact criterion for ic1: while $w' < 0$
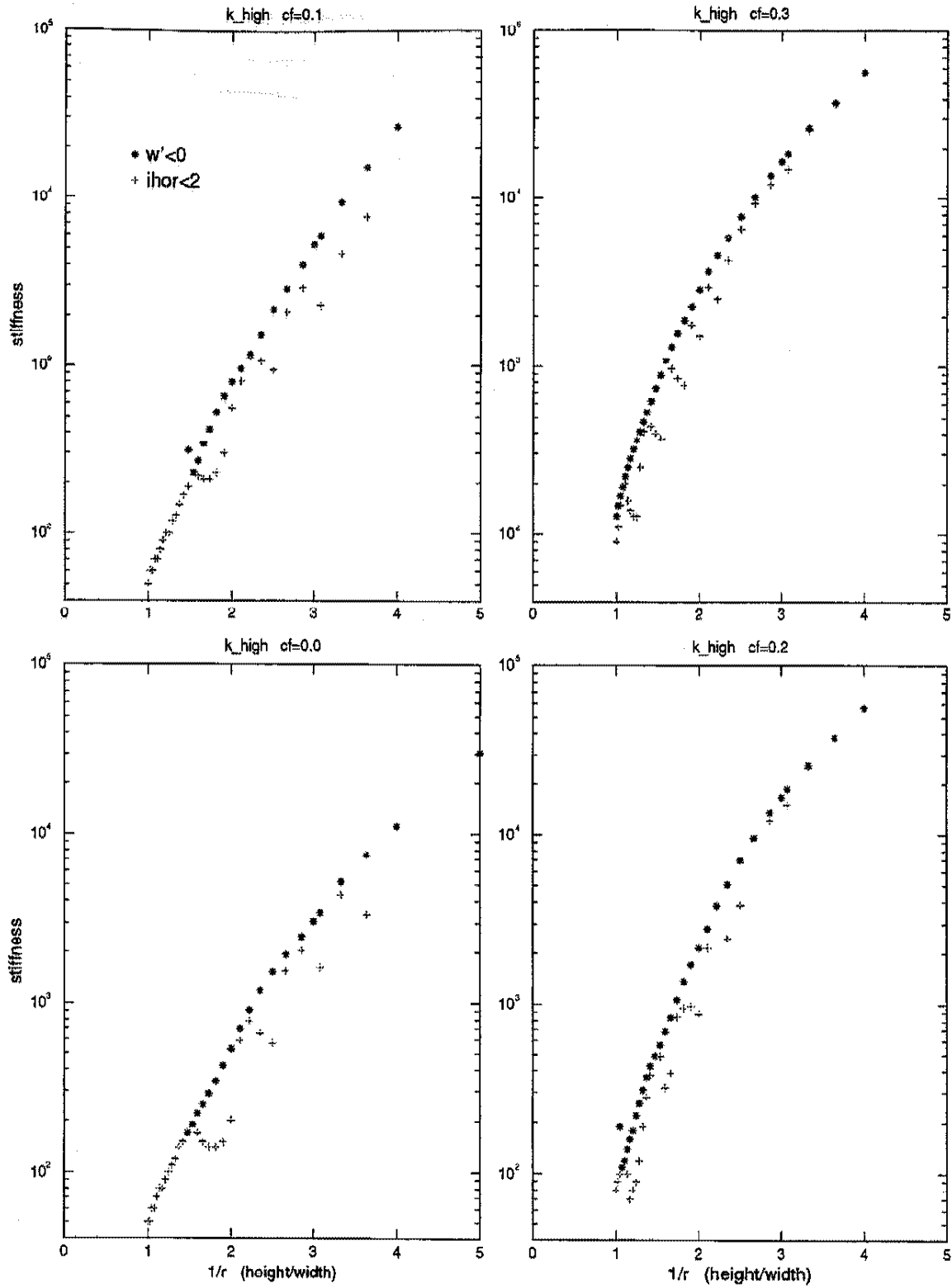
Figure 4.17: *k_high* for ic1 , $1 > r > 1/5$
first impact criterion: "while $w' < 0$", "while *ihor* < 2"

k_high, k_critical 3, k_critical 10 for initial conditions ic1
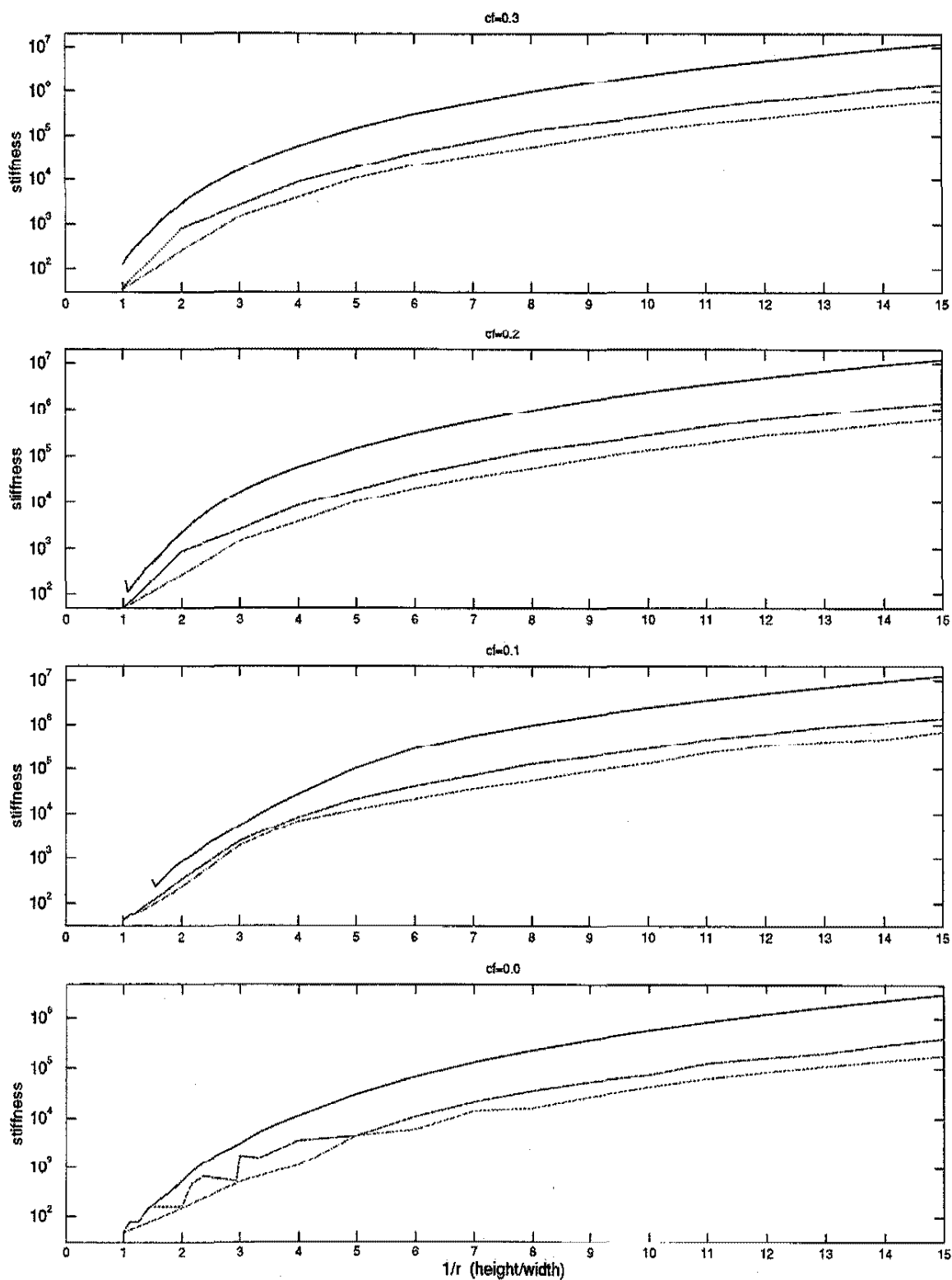
Figure 4.18: $k\_high, k\_critical_3, k\_critical_{10}$ for ic1

k_high, k_critical 3, k_critical 10 for initial conditions ic2

cf=0.3

cf=0.2

cf=0.1

cf=0.0

1/r (height/width)
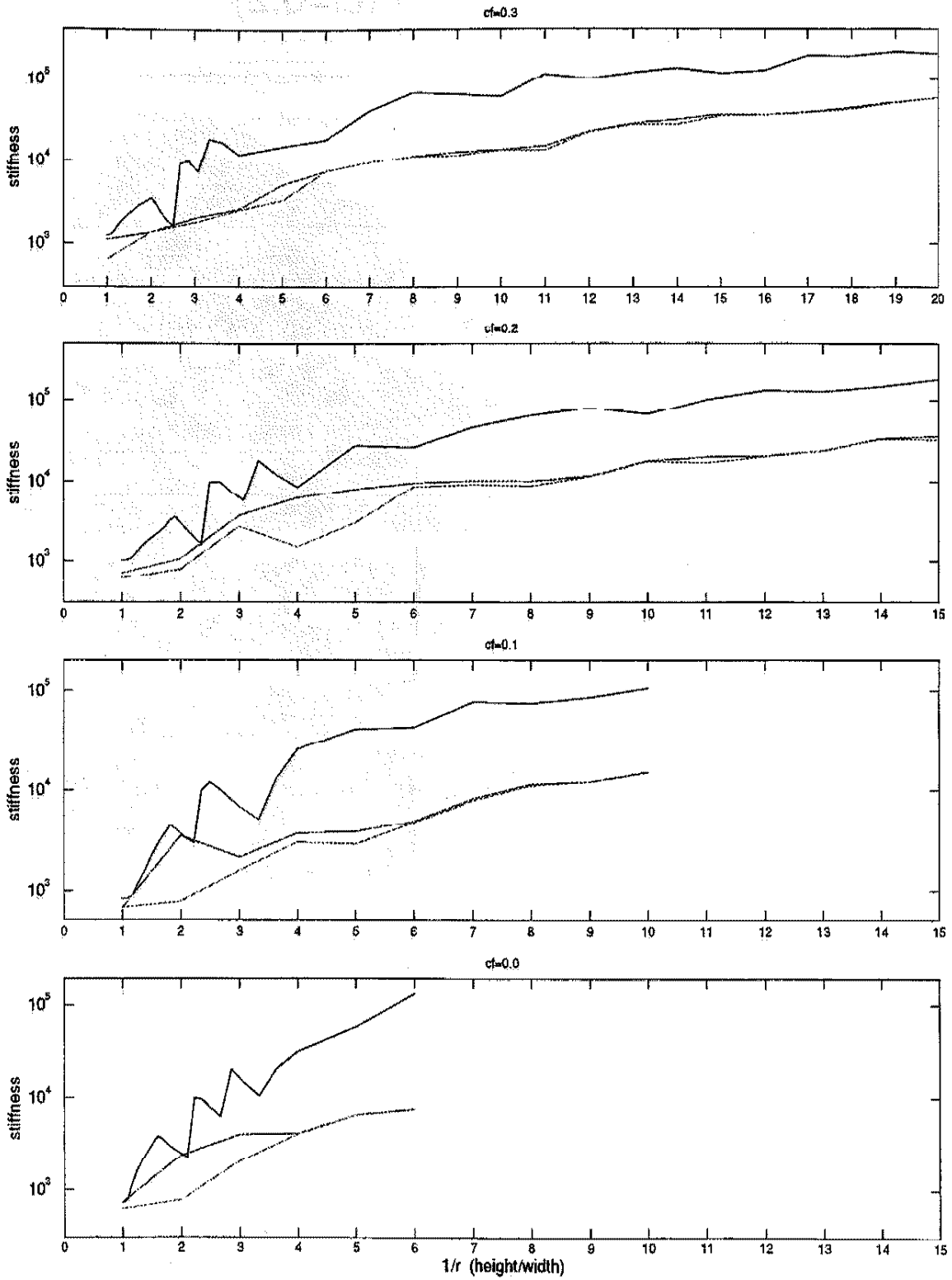
Figure 4.19: $k\_high, k\_critical_3, k\_critical_{10}$ for ic2
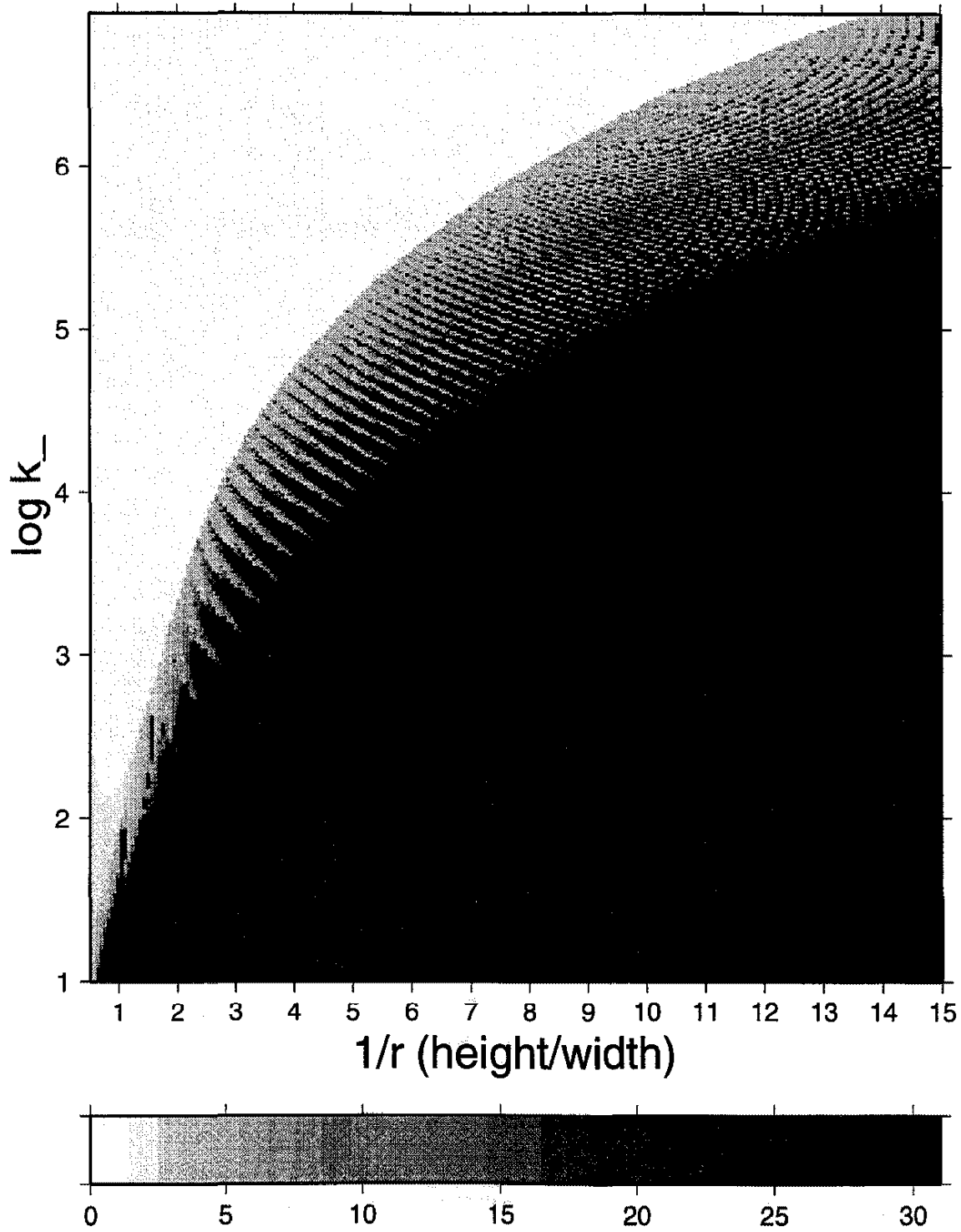
Figure 4.20: Gray-scale image of the time to flight in (k_-, r) parameter space, $\mu = 0.2$

we will mean the tendency of the block not to overturn. On the other hand, the words **stable** and **unstable** will be used to characterize the static **equilibrium** points of the block within $|w| \leq \alpha$. Reasons for the careful definition of seemingly obvious concepts will become apparent later. For example, we will show that the equilibrium $w = 0$ can be unstable but a block subjected to ic2 will never overturn!

Our effort in this section is to determine the parameter ranges resulting in overturning for the initial conditions ic1, ic2. However, we will not be satisfied with a mere "yes", "no" answer to a question: "does the block overturn at this point of parameter space for this set of initial conditions?" We also want to know the time when the block overturns, during which swing (or equivalently after how many passes through $w = 0$) did it overturn, if it did not overturn within the observed time, how likely it is to overturn later, etc. We will try to answer such questions in the subsections "Stability - initial conditions ic1" and "Stability - initial conditions ic2."

In the subsection "Static equilibrium," we will find static equilibrium positions of a rigid rectangular block on a Winkler foundation. In this study, our block does not move and such equilibrium positions depend only on the block's shape and the foundation model.

4.3.1 Stability - initial conditions ic2

Initial conditions ic2 impose a horizontal and a vertical force impulse at the bottom of the block, which is sitting straight up on elastic foundation in a static equilibrium. Since we keep the impulse constant, we expect intuitively that if the block gets sufficiently tall and thin, it will overturn. Numerical simulations described in this section confirm the intuitive suggestion and further show that stability depends on all three parameters: k_-, r, μ.

Similarly to flight studies, we will perform numerical simulations in the (k_-, r) parameter space for four different values of the coefficient of friction $\mu = 0, 0.1, 0.2, 0.3$. We start by studying the time when the block overturns versus the stiffness k_- for fixed parameters r, μ. For each k_- we note not only the absolute time when block overturned but also after how many passages through the vertical position $w = 0$ it occurred. We use the integer variable *ihor* to count the passages through $w = 0$. At time zero, the block is at a $w = 0$ position which is already counted, so *ihor* at time zero will be equal to one. Even though we study the time of overturning and the corresponding *ihor* for only a few fixed r, μ pairs, it will tell us a lot about general stability of the block. It will also give us a suggestion for a suitable way to study the global stability in the whole (k_-, r) parameter space.

Stability for fixed r, μ

Plots of time and *ihor* at overturning versus the stiffness k_- are displayed in Figures 4.21 through 4.28 for various fixed parameters r, μ. For each choice of r, μ we present two plots: the time of overturning versus the stiffness and *ihor* at the time of overturning versus stiffness. The two plots are always aligned vertically and share the same horizontal axis. For each k_- we run the code only till time 30. If the block overturns we plot the corresponding time and *ihor*. If it does not, we plot the final time 30 and *ihor* at that moment.

In interpreting the data plotted in the figures, the first evident observation is that stability of the block decreases with the aspect ratio r and increases with the stiffness k_-. Thus, the expected lower stability of tall, thin blocks is confirmed.

For very low aspect ratios, the block always overturns, no matter what k_- is. What "very low" r is, depends on the coefficient of friction μ. This simple kind of response is witnessed in Figure 4.24.

Furthermore, we find that for most of the presented runs there is a distinct, sharp border between the overturning region and the no overturning region. More specifically: there is a certain critical stiffness value such that for all k_- less than the value, the block always overturns and for any k_- larger than the value block never overturns. Among the test runs presented this is not true only for cases $\mu = 0.1, r = 0.092$ and $\mu = 0.2, r = 0.055$. A similar critical stiffness value exists here, however, for some k_- larger than the critical value, the block will overturn. Test runs like these two are rather hard to find though.

Thus, in all observed cases, if k_- is less than the critical value the block always overturns. The block overturns then only while *ihor* ≤ 2. That means the block will overturn before completing the third pass through the vertical position $w = 0$ or not at all.

Let us look now in more detail at, for example, Figure 4.25. The left-hand side of the plot is for $\mu = 0.2, r = 0.2$. Here, the block overturns only while *ihor* $= 1$. The time of overturning is about 2 and rises sharply as k_- approaches the critical value of about 150. Even then, when the block overturns at a late time, it still does so while *ihor* $= 1$. Once k_- is above the critical value, the block never overturns and the plotted *ihor* now gives the number of passages through vertical position completed at time 30 when the computation stops. For k_- just above the critical value, *ihor* sharply rises from 1. The above observation is explained by the physical meaning of the critical stiffness value: the critical stiffness value is a value for which block initially subjected to ic2 will forever approach an unstable equilibrium position where the block rests on one corner only. The block will not overturn and will not come back down to pass through $w = 0$. It will get closer and closer to an equilibrium position as time goes to infinity. The block's angular velocity w' does not change

Figure 4.21: Time, *ihor* at overturning for $\mu = 0, r = 0.4, 0.15$

Figure 4.22: Time, *ihor* at overturning for $\mu = 0.1, r = 0.3, 0.125$

Figure 4.23: Time, *ihor* at overturning for $\mu = 0.1, r = 0.096, 0.092$

Figure 4.24: Time, *ihor* at overturning for $\mu = 0.1, r = 0.08, 0.075$

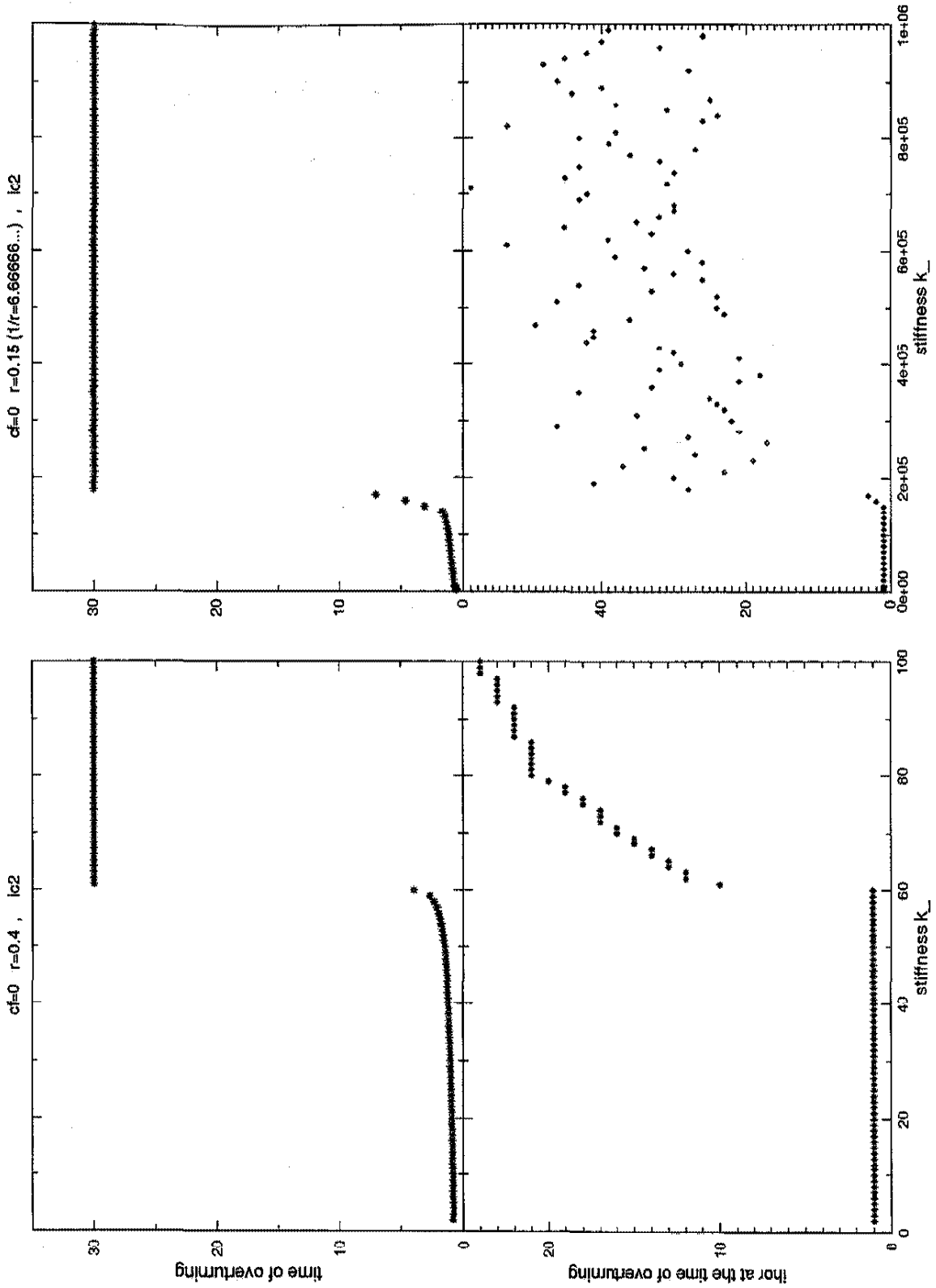Figure 4.25: Time, *ihor* at overturning for $\mu = 0.2, r = 0.2, 0.1$

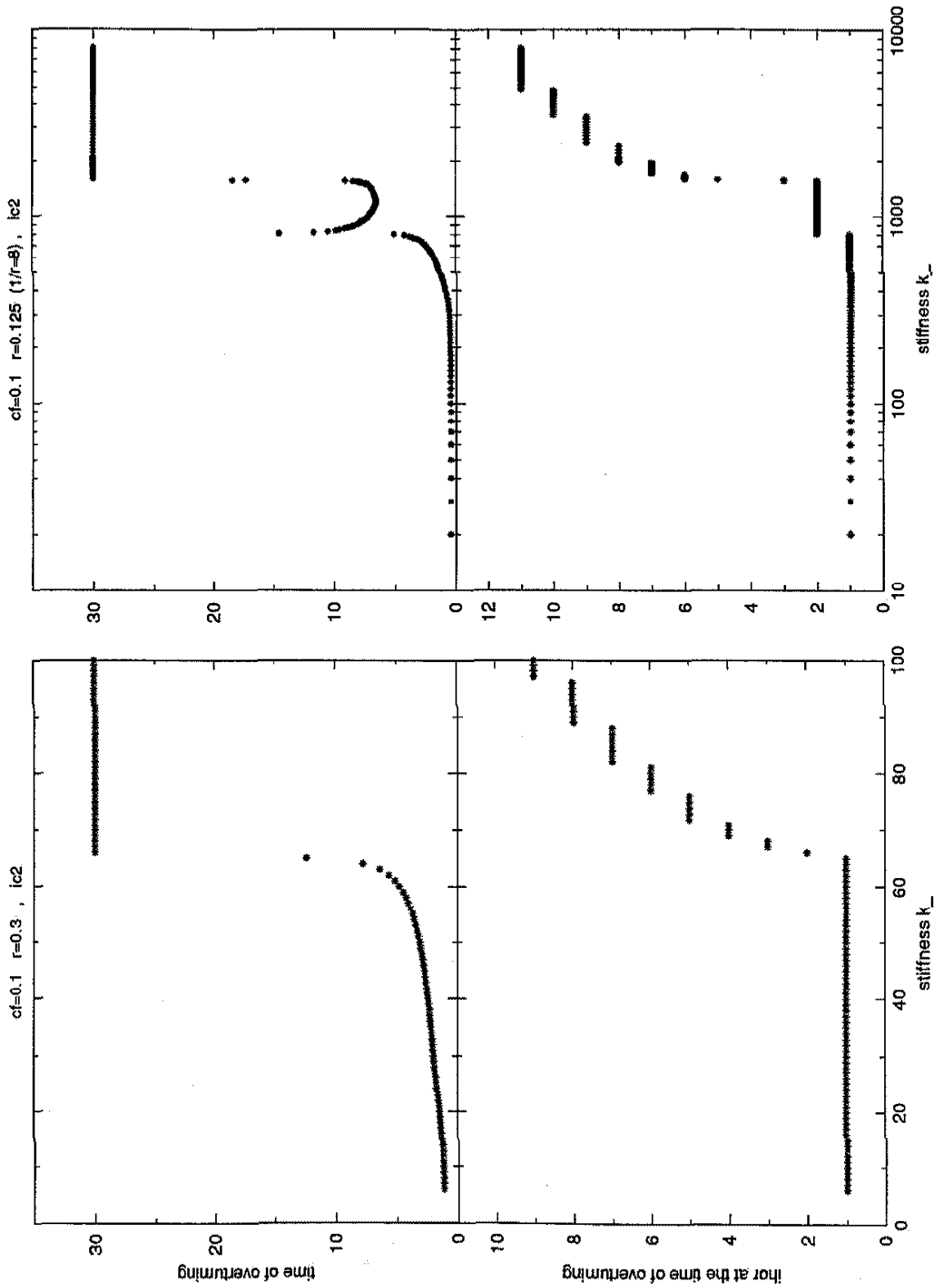Figure 4.26: Time, *ihor* at overturning for $\mu = 0.2, r = 0.06, 0.055$
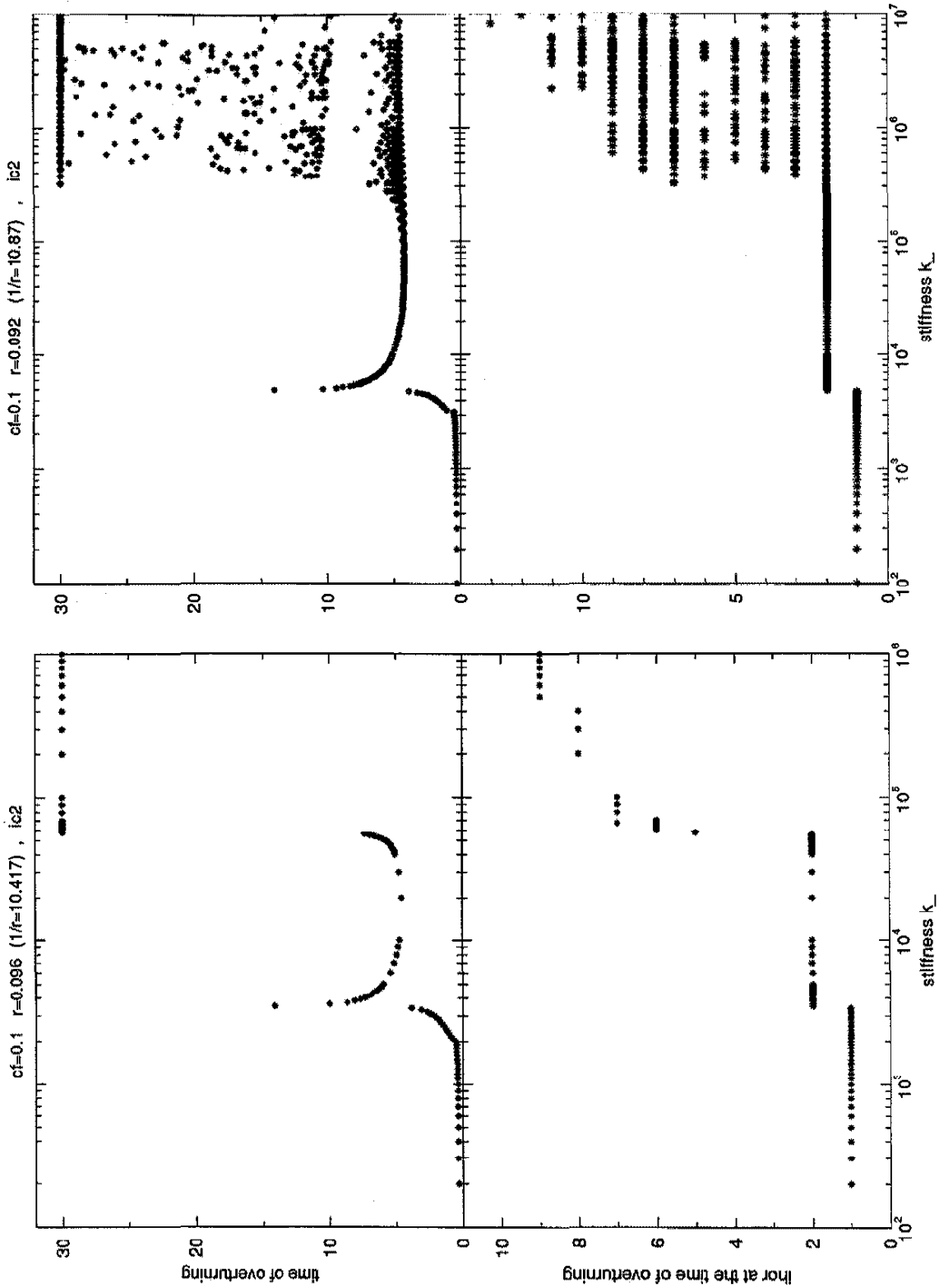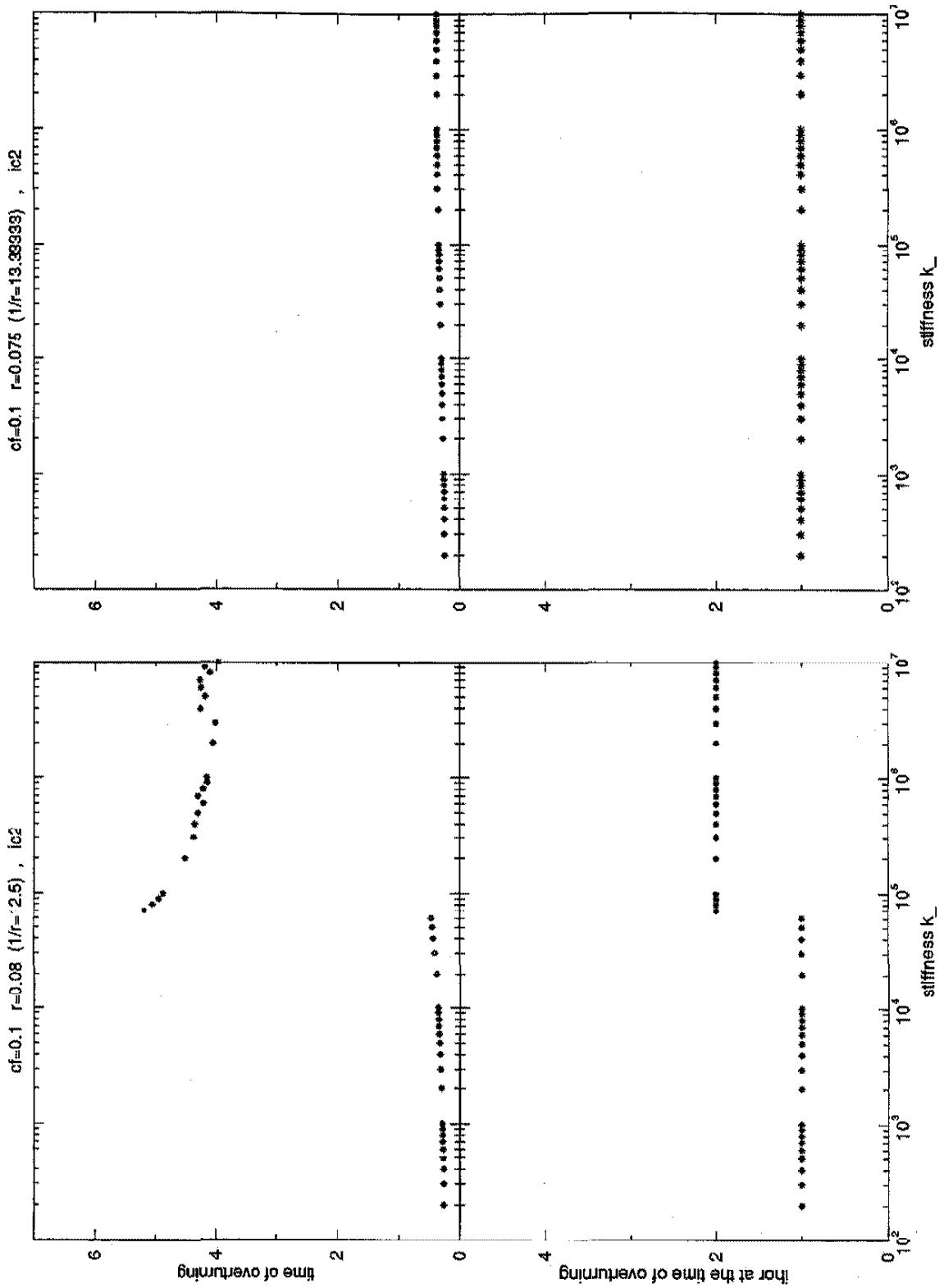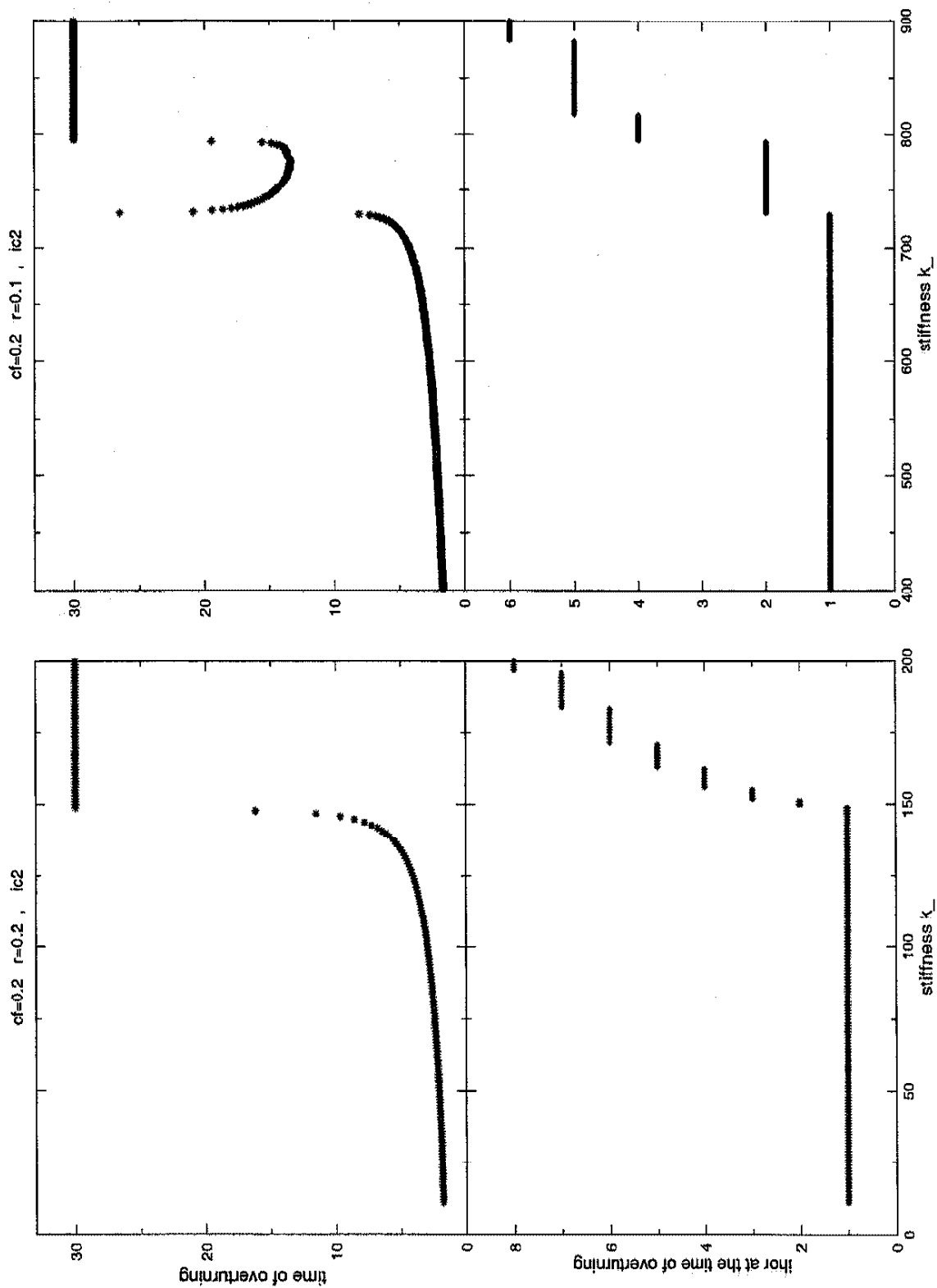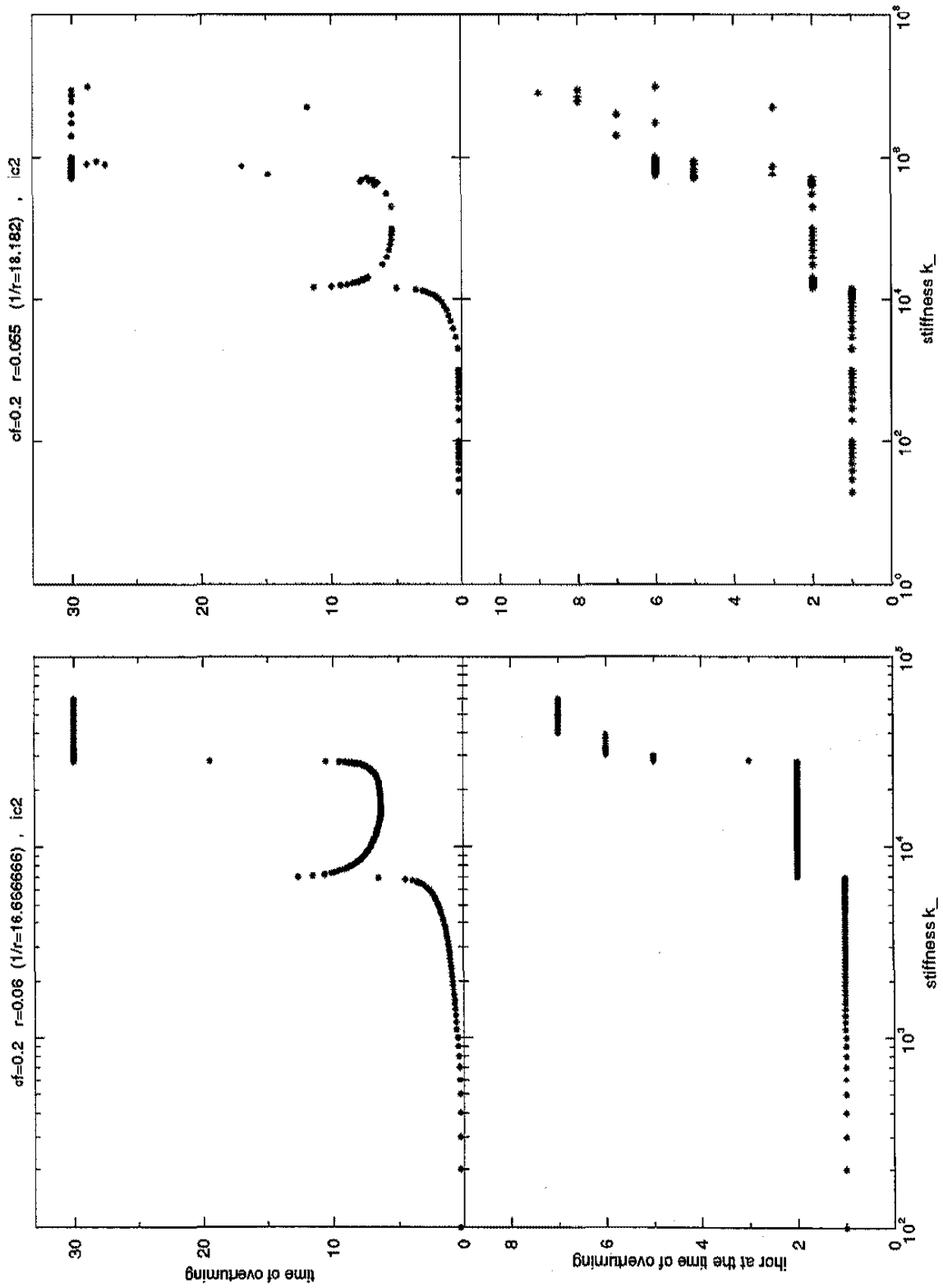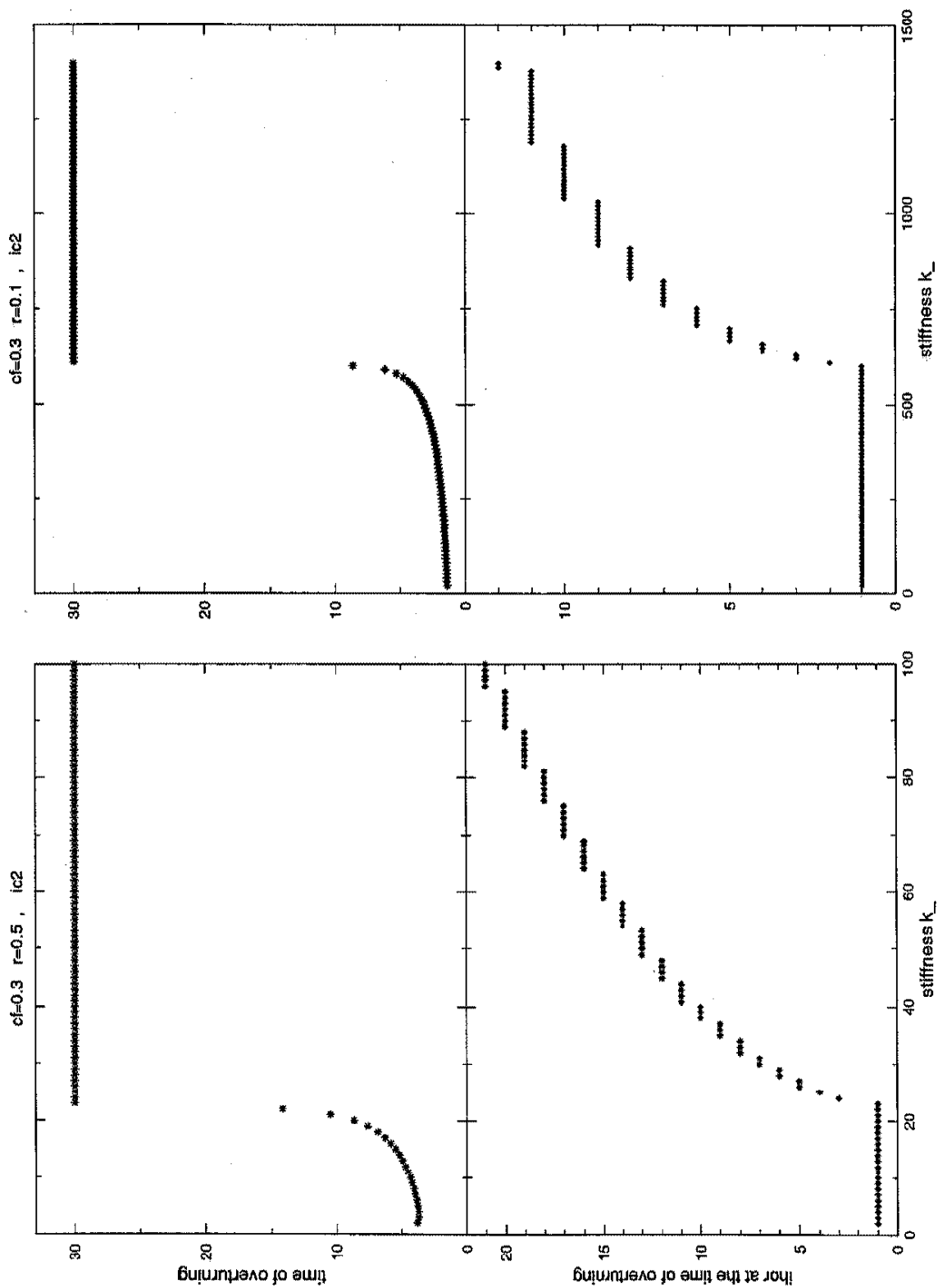
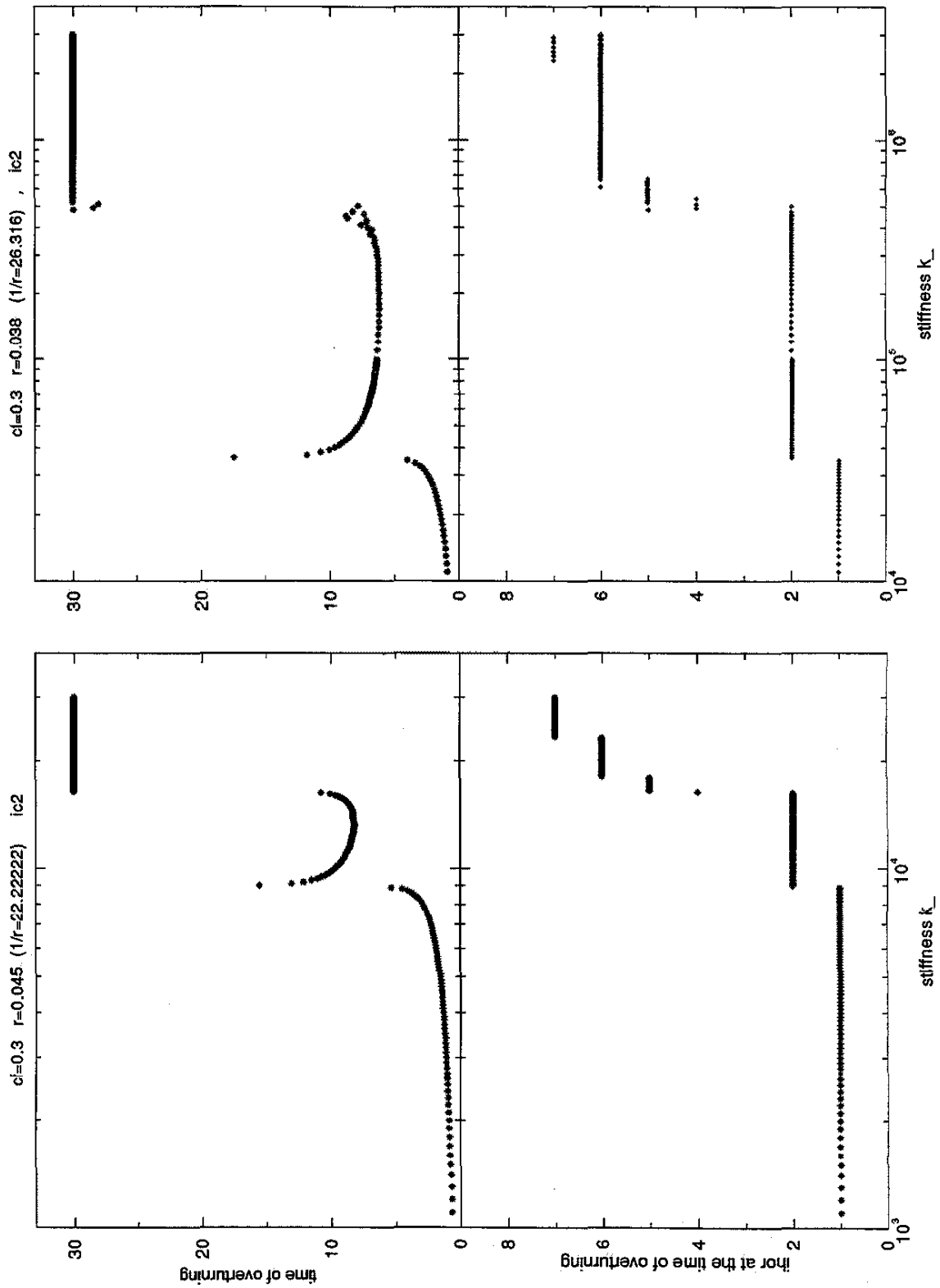Figure 4.27: Time, *ihor* at overturning for $\mu = 0.1, r = 0.5, 0.1$

Figure 4.28: Time, *ihor* at overturning for $\mu = 0.1, r = 0.045, 0.038$

sign and monotonically decreases. Thus, for k_- slightly less than critical, it takes a long time for the block to get past the equilibrium position- the block slowly approaches the equilibrium, eventually passing it at finite time and overturning. For k_- slightly above the critical value, the block again slowly approaches the equilibrium position, but never gets there. Here, w' changes sign and the block turns back. In most cases it will go on rocking. This is what we see in the plot, so for k_- right above the critical, *ihor* at the time of 30 is equal to only 2, 3 or 4. Rarely, the returning block gets stuck around another equilibrium, this time a stable one. Then the block never passes $w = 0$ and it oscillates around the stable equilibrium forever. The existence of such a stable equilibrium point is proved in a subsection on static equilibriums. The whole topic of stable and unstable equilibrium points will be studied there in great detail.

The plot on the right-hand side of Figure 4.25 is for $\mu = 0.2, r = 0.1$. Here, the block overturns while *ihor* = 1 but also while *ihor* = 2. For all k_- below 730, the block overturns while *ihor* = 1. The time at overturning is roughly 2-3, then rises sharply as k_- approaches 730. For k_- above 730, the time of overturning falls sharply to as low a value as 13 then rises up as k_- approaches a critical value of about 800. For k_- anywhere between 730 and 800, the block overturns while *ihor* = 2. For k_- above 800, the block never overturns. At each of the two stiffness values, 730 and 800, the behavior of the block qualitatively changes. The 800 is a critical value in sense discussed above - it divides the k_- axis into section where overturning occurs and a section where it does not. The 730 is a critical value in sense that it divides the overturning part further into an interval where block overturns while *ihor* = 1 and into an interval where block overturns while *ihor* = 2. The described behavior can be again explained by the physical meaning of the two critical values. For each of the two critical stiffness values, the block will approach an unstable equilibrium position as time goes to infinity. For the lower critical value it is the equilibrium position when $w > 0$. From the initial vertical position the block will tilt left forever: $w'(t_-) > 0 \; \forall t_-$ and $w'(t_- \to \infty) \to 0$. For the higher critical value the block will converge to the unstable equilibrium position with $w < 0$. The block initially turns with $w' > 0$, stops at some point and starts turning back with $w' < 0$. It passes through the vertical position $w = 0$, continues to turn with $w' < 0$, and approaches as time goes to infinity the unstable equilibrium position where $w < 0$.

The existence of unstable equilibrium points, and the corresponding critical stiffness values, explain why for k_- close to critical values, the block overturns in such a late time or why it takes so long to complete just 3 or 4 passes through $w = 0$. It is because for k_- near the critical value, block spends a long time near the unstable equilibrium point.

Stability in (k_-, r) parameter space

Now we want to study stability in the whole (k_-, r) parameter space. The foregoing discussion suggests that we find curves displaying critical stiffness versus r in (k_-, r) space. It also motivates the following definition of such critical curves:

Definition:

Consider the initial conditions ic2 and arbitrary but fixed parameters μ, r.

Let $k2(r)$ be stiffness such that $\forall k < k2(r)$, the block overturns before completing a 2-nd pass through the vertical position $w = 0$, that is while $ihor < 2$. Then the supremum of all such $k2(r)$ is defined as $k2_{stability}(r)$.

Let $k3(r)$ be the stiffness such that $\forall k < k3(r)$ not in an ϵ neighborhood of $k2_{stability}(r)$, the block overturns before completing its 3-rd pass through the vertical position $w = 0$, that is while $ihor < 3$. Then the supremum of all such $k3(r)$ is defined as $k3_{stability}(r)$.

Both $k2_{stability}(r)$ and $k3_{stability}(r)$ can be infinite; they can be also equal.

While we realize that the ϵ neighborhood in the definition needs to be described more accurately, we can only say ϵ is small compared to the difference between $k2_{stability}(r)$ and $k3_{stability}(r)$. To relate these definitions to the data plotted, let us consider Figure 4.25 discussed above. For $\mu = 0.2$ and $r = 0.2$, the critical stiffnesses $k2_{stability}$ and $k3_{stability}$ coincide at a value around 150. For $\mu = 0.2$ and $r = 0.1$, we have approximately $k2_{stability} = 730$ and $k3_{stability} = 800$.

Extensive numerical simulations establish the two critical curves, $k2_{stability}(r)$ and $k3_{stability}(r)$, in the (k_-, r) parameter space for $\mu = 0, 0.1, 0.2, 0.3$. The curves are displayed in Figure 4.29 for $\mu = 0, 0.1$ and in Figure 4.30 for $\mu = 0.2, 0.3$.

As follows from the definition, $k2_{stability}(r) < k3_{stability}(r)$ $\forall r$ and any fixed μ. Over the observed range, the critical stability curves monotonically increase with $1/r$. For $\mu = 0$ the two critical curves coincide. Plots for $\mu = 0.1, 0.2, 0.3$ are similar to each other. Any plot looks like the other two, only contracted or stretched along the horizontal axis. For $\mu > 0$, the two critical curves coincide when the block is close to a square, then slowly separate as $1/r$ increases. Both curves grow towards infinity at a certain aspect ratio r, the value of which is different for each curve and μ. The critical curves blow up also for $\mu = 0$. The aspect ratio r where $k2_{stability}(r)$ blows up we call $r2_s(\mu)$ and likewise r where $k3_{stability}(r)$ blows up we call $r3_s(\mu)$.

A plot of $r2_s(\mu), r3_s(\mu)$ is shown in Figure 4.31. For any r below $r2_s(\mu)$ (or equivalently for any $1/r$ above $1/r2_s(\mu)$), the block will overturn while $ihor = 1$ regardless of k_-. For any r between $r2_s(\mu)$ and $r3_s(\mu)$, the block will overturn while $ihor \le 2$ regardless of k_-. For r above $r3_s(\mu)$, the
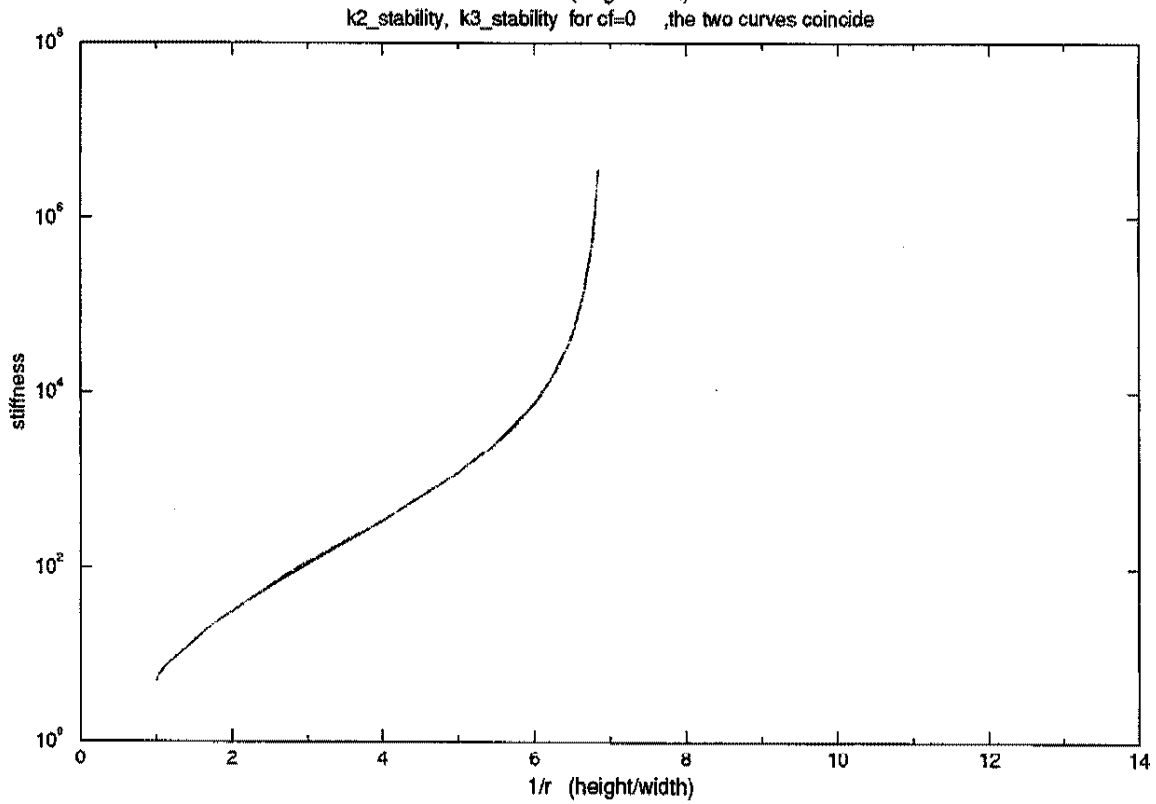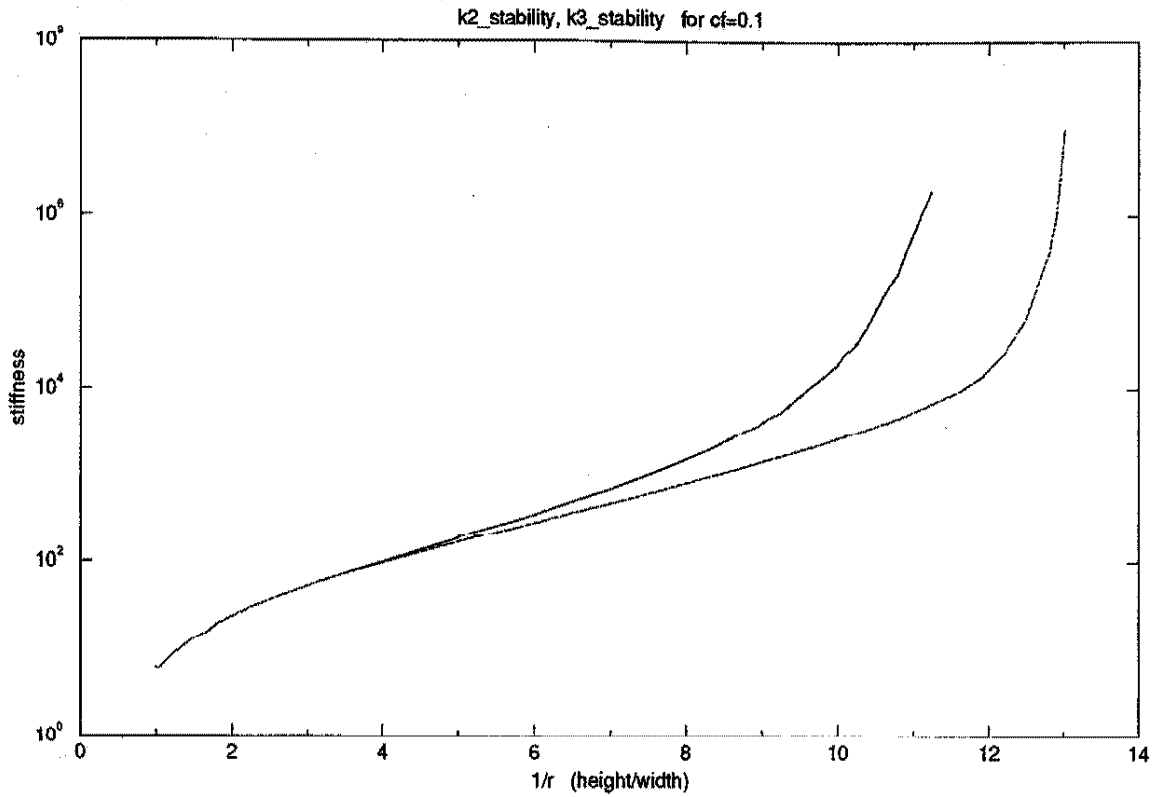
Figure 4.29: Critical stability curves, ic2, $\mu = 0, 0.1$
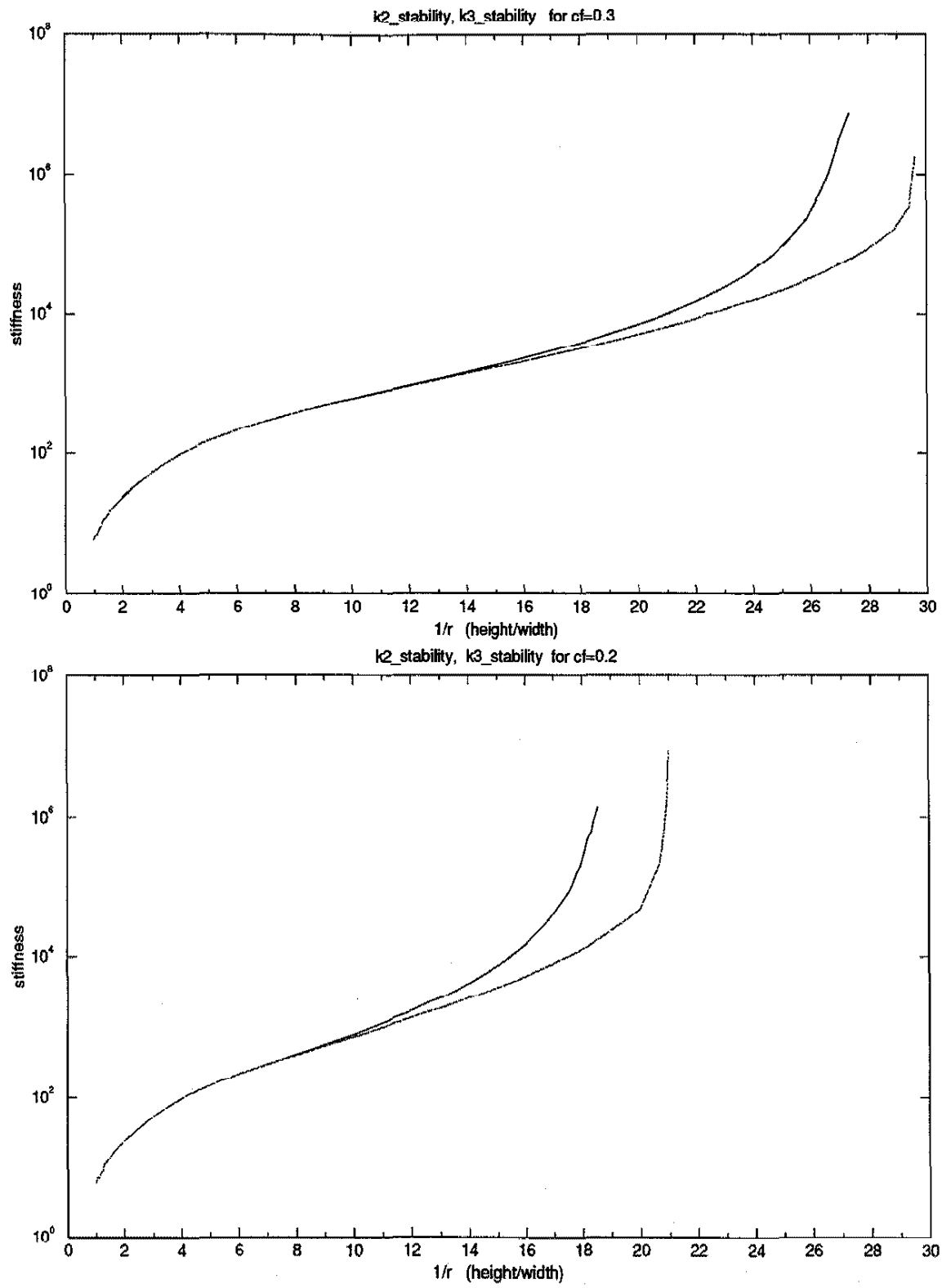
Figure 4.30: Critical stability curves, ic2, $\mu = 0.2, 0.3$

block does or does not overturn depending on k_-. For most r larger than $r3_s(\mu)$, the above defined critical stiffness $k3_{stability}(r)$ becomes a sharp stability border: the block overturns $\forall k_- < k3_{stability}$ and does not overturn for any $k_- > k3_{stability}$. Only rarely, for r just above $r3_s(\mu)$, can the block sometime overturn also for $k_- > k3_{stability}$. This is witnessed at the fixed μ, r plots: $\mu = 0.1, r = 0.092$ in Figure 4.23 and $\mu = 0.2, r = 0.055$ in Figure 4.26.

r2_s(cf), r3_s(cf)   ,   ic2
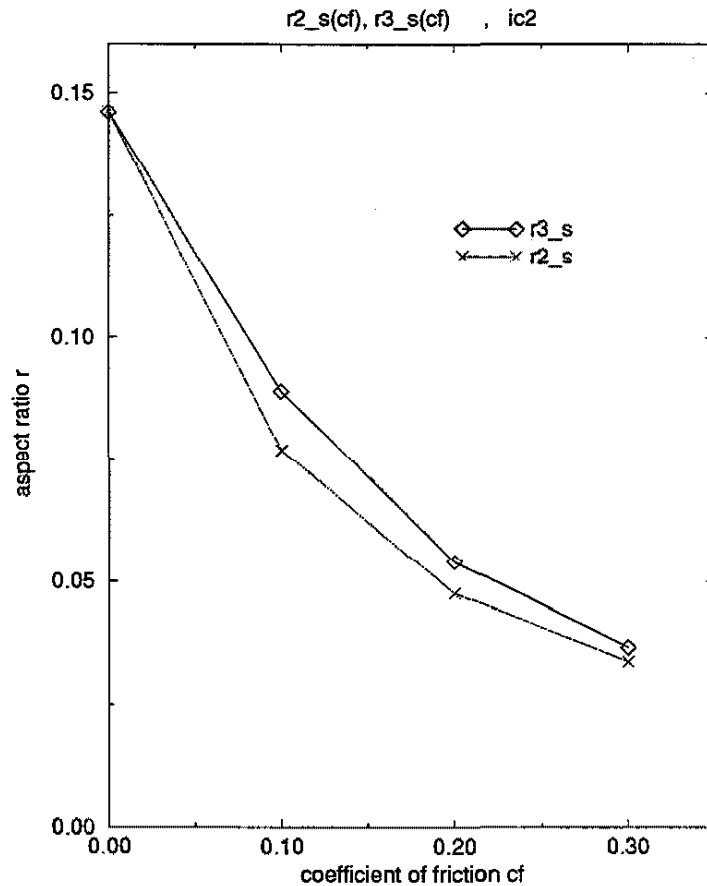
Figure 4.31: $r2_s(\mu), r3_s(\mu)$

Comparing to the block's flight tendency, points in the parameter space where the block overturns form a simpler, more compact region. We saw that for given r and μ, the block can fly at some k_-, then as we increase k_-, the block never flies, flies early, late again, never flies etc. In comparison, stability is with a few exceptions well behaved. Given r and μ, the block overturns for all k_- below a critical value and never overturns for any k_- above the value. That value can be infinite, in which case the block overturns for any k_-.

The few exceptions when stability is not nicely, simply behaved occur for a narrow range of r. Given such r and μ, again the block overturns for all k_- below some critical value. However, for some k_- above the critical value, the block can overturn too. As mentioned before, this occurs, for

example for $\mu = 0.1, r = 0.092$ in Figure 4.23 and $\mu = 0.2, r = 0.055$ in Figure 4.26. In those plots, for k_- above the critical value, a slight change in k_- makes a crucial difference in stability. In other words stability depends sensitively on parameter k_-. This sensitive dependence is a phenomena not limited to stability. It is also witnessed in Figure 4.21 for $\mu = 0, r = 0.15$, where $ihor(t_- = 30)$ depends sensitively on k_-. We commented shortly on sensitive dependence as it is apparent in some stability plots - we will investigate sensitive dependence more deeply in the chapter on chaos.

Stability ic2 - conclusions

- Stability of the block increases as the coefficient of friction μ increases

- Stability of the block decreases as the aspect ratio r decreases

- Stability of the block increases as the stiffness k_- increases

- The block always overturns, regardless of k_-, for all r less than a certain μ-dependent value

- If given a fixed r and μ, the block does not overturn for some k_- then it does not overturn for any k_- above a certain critical value and does overturn for all k_- less than that value. This is true for most but not all r

- If the block overturns it does so mostly during the first or second swing

4.3.2 Stability - initial conditions ic1

Initial conditions ic1 prescribe that the block is initially resting on springs inclined at an angle $w_0 = \alpha/2$ and that all of the initial velocities are zero. That is, the block is initially inclined half way to point of overturning. For this set of initial conditions, the block displays somewhat similar but far simpler stability behavior than for set ic2.

We will proceed in the same fashion as in case of the ic2 initial conditions. We will do numerical simulations in (k_-, r) parameter space for four different values of the coefficient of friction $\mu = 0, 0.1, 0.2, 0.3$. First we plot the time and $ihor$ at overturning versus stiffness k_- for fixed parameters r, μ. Just as for ic2, we observe the motion only up to time 30. If block overturns, we plot the corresponding time and $ihor$. If it does not overturn, we plot the final time 30 and $ihor$ at that moment. Only two such plots are presented in Figure 4.32. They show stability behavior typical for block subjected to ic1. If we vary the parameters μ and r in the ranges considered, we get plots which do not qualitatively change.

As for ic2, stability of the block decreases with the aspect ratio r and increases with the stiffness k_-. As for ic2, there is a distinct, sharp border between the overturning region and the region where
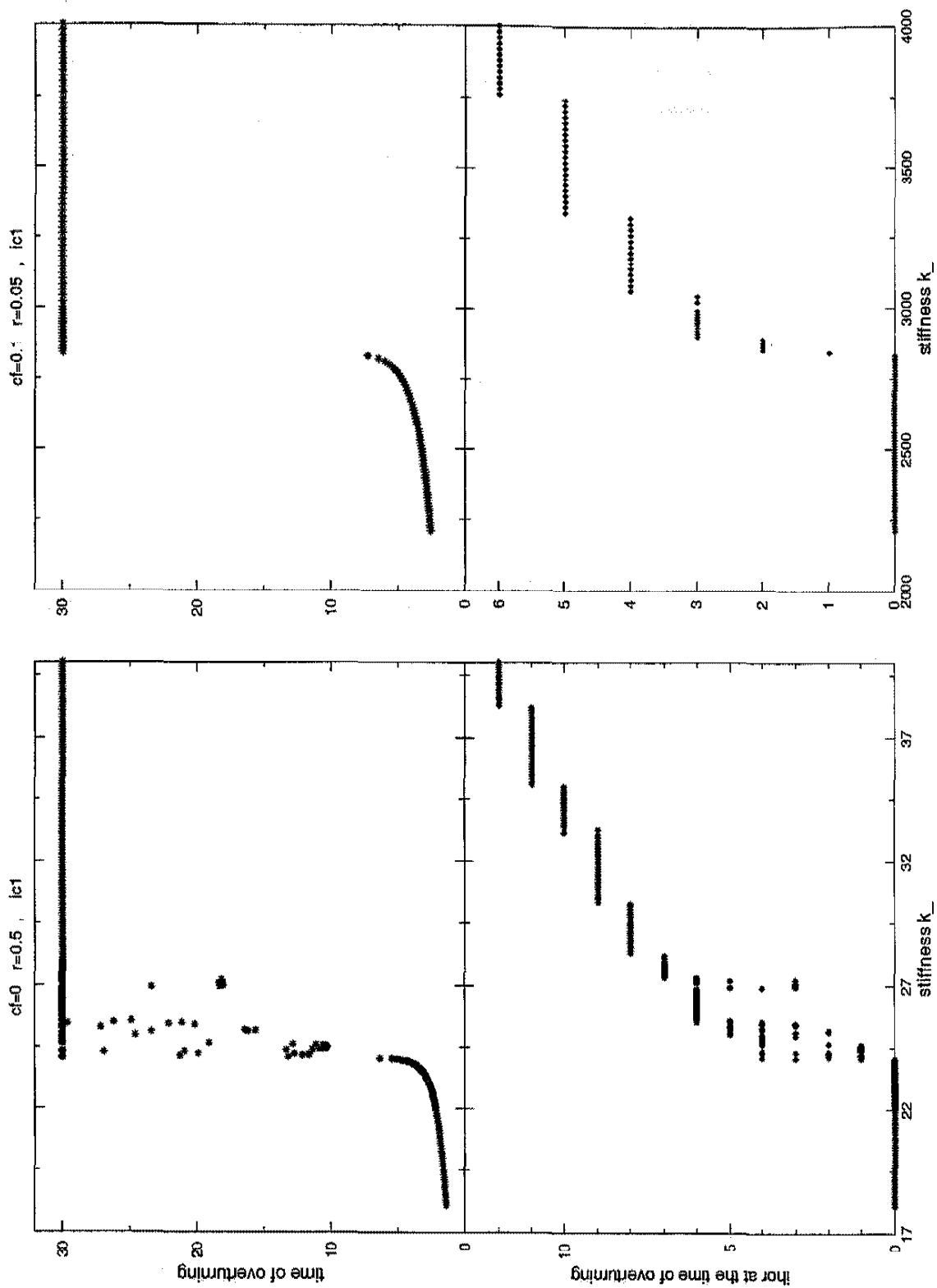
Figure 4.32: Time, *ihor* at overturning, ic1, $(\mu = 0, r = 0.5), (\mu = 0.1, r = 0.05)$

the block does not overturn. More specifically: there is a certain critical stiffness value such that for all k_- less than the critical value, the block overturns and for most k_- bigger than the critical value, the block does not overturn.

At the exceptional case, when block overturns at some k_- above the critical value, this k_- is close to critical and $\mu = 0$. We can possibly explain this by recalling the way the initial conditions ic1 are computed: based on block resting on rigid ground. When k_- is low, the initial conditions ic1 position the block high so that when motion starts the block not only rotates but also falls somewhat. Additional energy introduced to the system by initial conditions may result in overturning. The block overturns at k_- higher than critical only when this critical value is rather low which supports our explanation.

Unlike in case of block subjected to ic2, there does not exist an aspect ratio r for which the block always overturns regardless of k_-. Also, when k_- is below the critical value the block overturns when $ihor = 0$. That means the block on the foundation with less than critical stiffness never passes through the vertical position. From the initial position, $w = \alpha/2$, the block immediately overturns. Thus, there is only one critical stiffness value for ic1. At that critical k_- value the block is initially positioned very close to a static unstable equilibrium position.

To study stability in the whole (k_-, r) parametric space we define curves displaying critical stiffness versus r in (k_-, r) space.

Definition:

Consider the initial conditions ic1 and arbitrary but fixed parameters μ and r.

Let $k1(r)$ be the stiffness such that $\forall k < k1(r)$ the block overturns before completing its 1-st pass through the vertical position $w = 0$, that is while $ihor < 1$. Then the supremum of all such $k1(r)$ is defined as $k1_{stability}(r)$.

Numerical simulations establish a critical curve $k1_{stability}(r)$ in (k_-, r) parameter space for $\mu = 0, 0.1, 0.2, 0.3$. It turns out that these curves are essentially independent of μ. The curve is displayed in Figure 4.33. Over the observed range the critical stability curve monotonically increases with $1/r$. Comparing this to Figures 4.29 and 4.30 we see that the curves $k2_{stability}(r)$ and $k3_{stability}(r)$ computed for ic2 initially follow curve $k1_{stability}(r)$ computed for ic1. The smaller the μ the earlier they split and blow up.

The curve $k1_{stability}(r)$ divides the (k_-, r) parameter space into two regions. In the region below the curve the block always overturns right at the beginning of the motion. In region above the curve the block will not overturn most of the time. Only in few rare cases will the block overturn in that

region - when $\mu = 0$ and (k_-, r) is close above the curve, and r larger. We can close this subsection
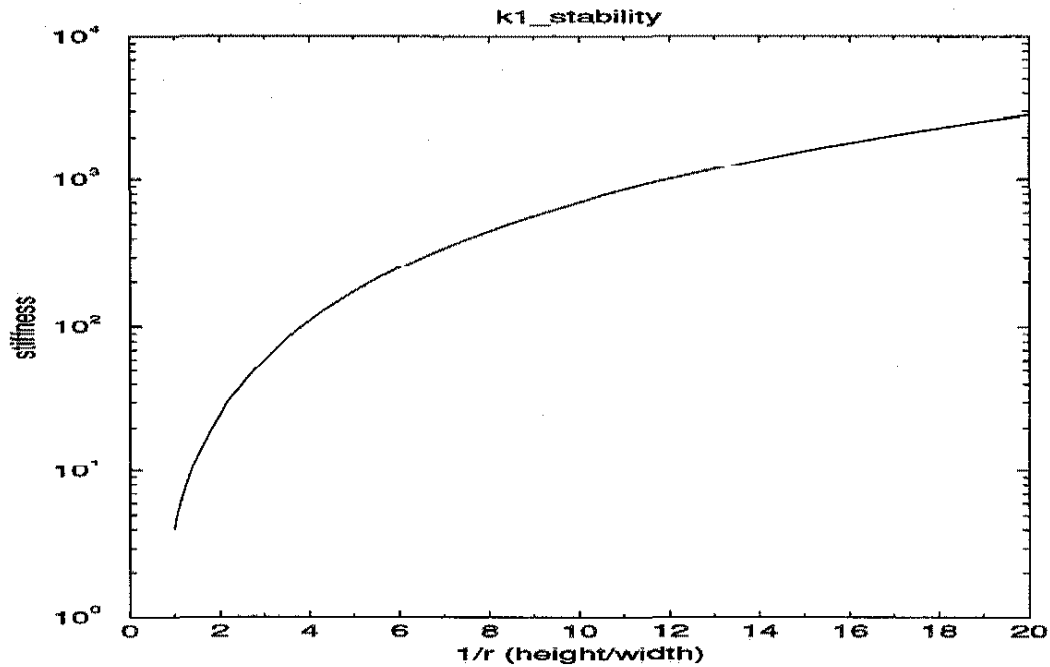
Figure 4.33: Critical stability curve, ic1

with our final conclusions on the stability behavior of a block subjected to the initial conditions ic1.

- Stability of the block is independent of the coefficient of friction μ

- Stability of the block decreases as the aspect ratio r decreases

- Stability of the block increases as the stiffness k_- increases

- For given r the block will overturn for all k_- below a certain critical value and will not overturn for most k_- above that value. this value is independent of μ

- If the block overturns it does so mostly during the very beginning of its motion

4.3.3   Static equilibrium

Consider a rigid block on a rigid foundation. Clearly, when the block rests on a foundation in a vertical position this is a stable equilibrium. When the block is positioned on a rigid foundation with its diagonal vertical, $w = \alpha$, it is in an unstable equilibrium. Consider now a rigid block on a Winkler foundation with stiffness k. If the stiffness k is high the equilibrium positions will be same as for rigid foundation. What happens for lower k? Are there any other equilibrium points? Does the existing stable equilibrium point at $w = 0$ remain stable? What role does the aspect ratio r play? These are the questions we will study and answer in this section.

Problem formulation
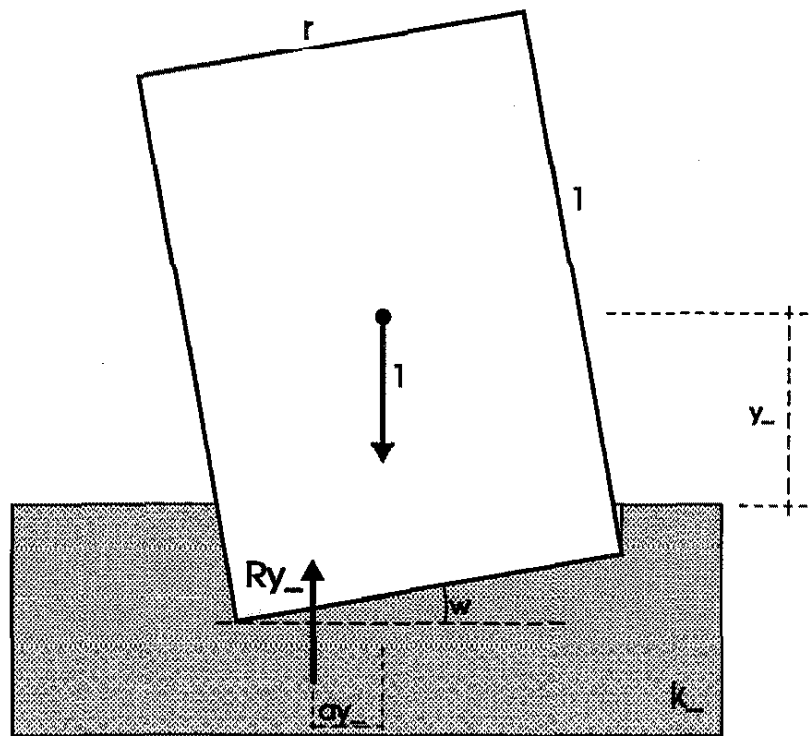
Figure 4.34: Equilibrium positions

We work with non-dimensional variables and parameters, keeping their names as introduced earlier. Thus, the gravity force is 1 and acts down at the center of gravity of the block. The resultant force pushing the block up is R_{y_-} and acts at the geometric center of the region in which foundation springs are displaced by the block (Figure 4.34). Distance between the two parallel forces is a_{y_-}. Both R_{y_-}, a_{y_-} are functions of y_-, w. We have $R_{y_-} = R_{y_-}(y_-, w)$ and $a_{y_-} = a_{y_-}(y_-, w)$. Equilibrium point is any position (y_-, w) satisfying both:

$$R_{y_-}(y_-, w) = 1$$
$$a_{y_-}(y_-, w) = 0.$$

We limit our equilibrium search to blocks with aspect ratios $r \leq 1$ and foundations with $k_- > 2$. Furthermore, we confine the search to angles w within range $0 < w < \alpha$. Since the geometry is symmetric in w this automatically covers angles $-\alpha < w < 0$. Note that looking at equilibria of a block with aspect ratio r for angles $0 < w < \alpha$ is equivalent to looking at equilibria of a block with aspect ratio $1/r$ for angles $\alpha < w < \pi/2$.

Solution technique

Formulas for $R_{y-}(y-, w)$ and $a_{y-}(y-, w)$ are stated in Figures 2.4 and 2.5. Due to their complexity we opt for a numerical solution. The problem is formulated in mathematical terms as:

Find zeros of a two-dimensional function of two variables $y-, w$ with parameters $k-, r$.

There are several numerical techniques to solve this rather standard problem. We could also determine the equilibrium by finding the local energy minimum or maximum of the block-foundation system. We do not use any standard numerical solver. We created an efficient code ourselves utilizing our knowledge of the function R_{y-}. This will prove useful later when we study the equilibrium positions in the whole $(k-, r)$ parameter space.

The function R_{y-} is monotonically decreasing in $y-$. Thus, given fixed w there is exactly one $y_R(w)$ such that $R_{y-}(y_R(w), w) = 1$. Then, for each w we can define a continuous function $arm(w) = a_{y-}(y_R(w), w)$. The problem is now reduced to finding zeros of $arm(w)$, a continuous function of one variable. In other words, we solve numerically $R_{y-}(y-, w) = 1$ for $y-$ as a function of w and substitute in $a_{y-}(y-, w) = 0$.

Equilibrium - fixed $k-, r$

The function $arm(w)$ is plotted for several specific parameter values in Figures 4.35 and 4.36. There are two plots in each row, both for the same parameters $k-, r$: on the left-hand side we show $arm(w)$ versus w and on the right-hand side we have a plot entitled energy. The energy plot shows $\int_0^w arm(q) * 1 \, dq$ versus w. But $\int_0^w arm(q) * 1 \, dq$ is equal to the work done when moving the block from $(y_R(0), 0)$ to $(y_R(w), w)$. Thus, the said integral gives the energy of the block-foundation system at $(y_R(w), w)$ assuming a zero energy level at $(y_R(0), 0)$.

At any w where $arm(w)$ becomes zero we have an equilibrium point. At that w the energy reaches a local minimum if it is a stable equilibrium and a local maximum if it is an unstable equilibrium. We can imagine a little ball rolling atop the curve in energy plot. If we put a ball on a 'hill' it will stay until slightly perturbed. If we put the ball in a 'valley' it will stay even if perturbed. The block would rock back and forth in the same way that the ball would roll.

The parameters $k-, r$ in Figures 4.35 and 4.36 were chosen to display qualitatively different kinds of equilibrium situation. Figure 4.35 shows $arm(w)$ and its corresponding energy plot for $r = 0.9$ and $k- = 4.5, 6.2, 100$. Figure 4.36 shows the same information for $r = 0.1$ and $k- = 500, 599.1, 2000$.

Fixing the aspect ratio at $r = 0.9$ we have for $k- = 100$ a stable equilibrium point at $w = 0$ and an unstable one near $w = \alpha$. This is a familiar situation - just like having a rigid block on rigid ground. The situation qualitatively changes when we lower the foundation stiffness to $k- = 6.2$.
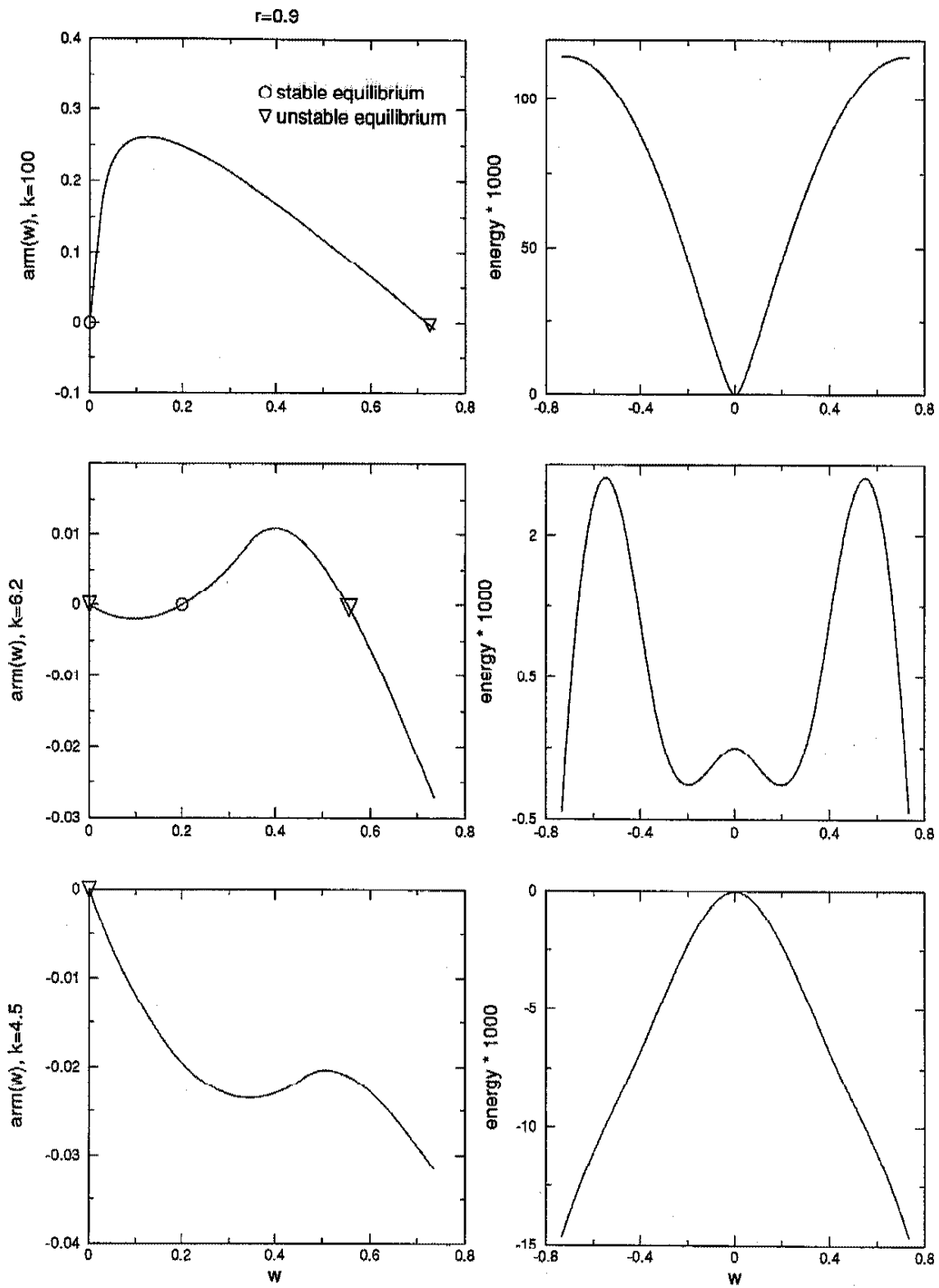
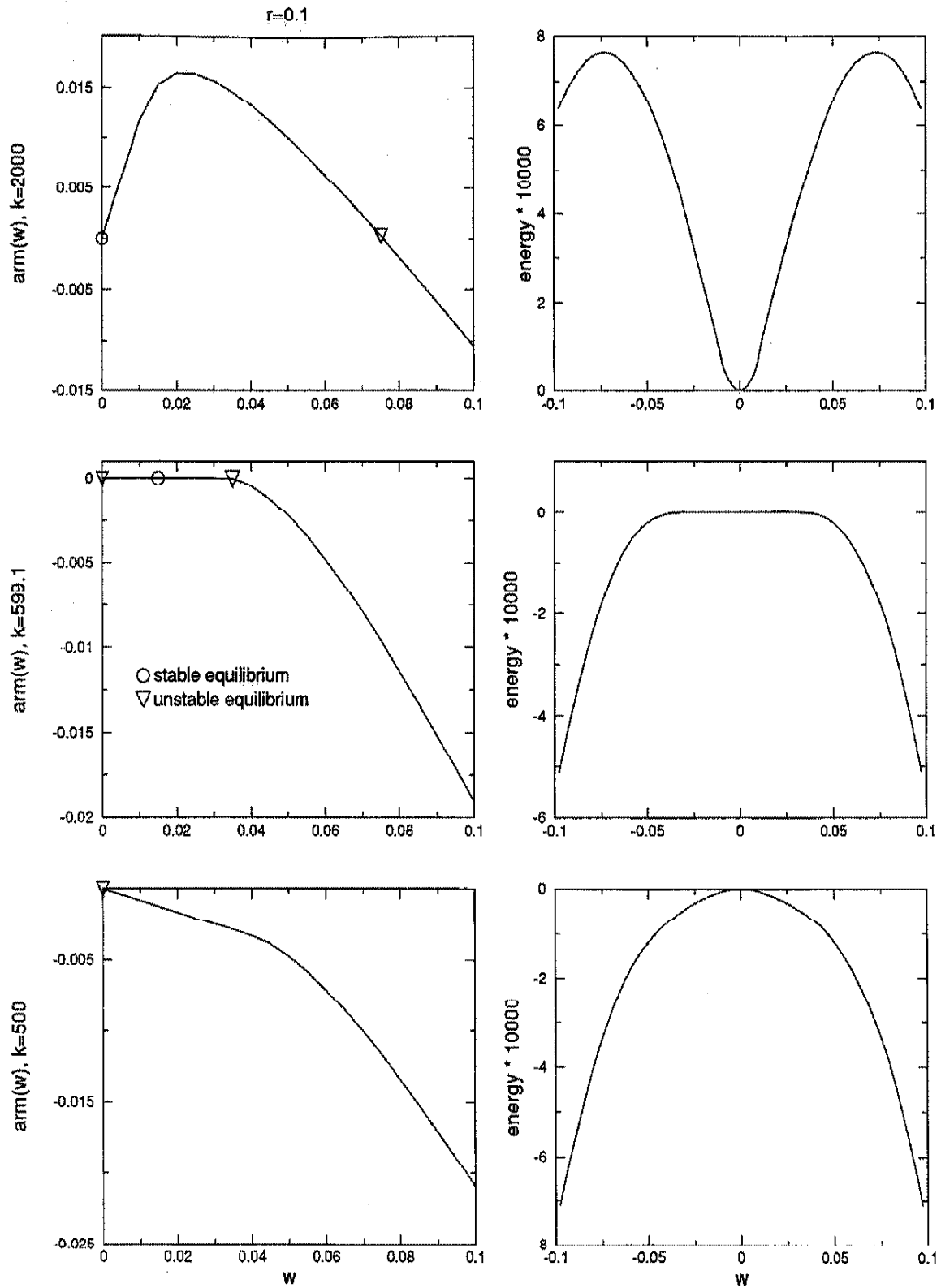Figure 4.35: $arm(w)$, energy at $(y_R(w), w)$ for $r = 0.9, k = 4.5, 6.2, 100$

Figure 4.36: $arm(w)$, energy at $(y_R(w), w)$ for $r = 0.1, k = 500, 599.1, 2000$

The equilibrium point at $w = 0$ becomes unstable, a new stable equilibrium point shows up at $w = 0.19950$, and the equilibrium point nearest the angle α remains unstable and moves to $w = 0.552$. Lowering the stiffness further to $k_- = 4.5$ while keeping r fixed at 0.9 we find things different again. There are no stable equilibrium points at all and only one unstable point at $w = 0$.

Changing now the aspect ratio to $r = 0.1$ we have for $k_- = 2000$ a stable equilibrium point at $w = 0$ and an unstable one near $w = \alpha$, again a familiar situation. Fixing r and lowering k_- to 599.1 we find that $w = 0$ equilibrium point is now unstable, a new stable equilibrium point appears at $w = 0.01433593$, and the old unstable point drops to $w = 0.034466552$. This sounds the same as the equilibrium scenario for the parameters $r = 0.9, k_- = 6.2$ - until we look at the plot. For $w < 0.034466552\, arm(w)$ gets so close to zero that we cannot see with the naked eye where in the plot $arm(w)$ actually crosses the zero line. Basically, the whole interval $-0.034466552 < w < 0.034466552$ becomes one large neutral equilibrium. This is reflected in the corresponding energy plot where the top of the 'hill' is wide and flat. Lowering k_- further to 500 there are no stable equilibrium points at all and only one unstable point at $w = 0$.

Equilibrium bifurcation - fixed r, varying k_-

An obvious question to ask now is: for $r = 0.9$ what happens to the equilibrium picture when k_- changes between the values 4.5, 6.2 ,100? At a more general level we ask to see the equilibrium points for a fixed r as the stiffness changes in the considered interval $k_- > 2$.

For fixed r we vary k_- in small increments starting at 2. For each k_- we compute all of the equilibrium positions w and determine whether they are stable or unstable. We plot the equilibria positions w versus k_- in Figure 4.37 for $r = 1, 0.95$, in Figure 4.38 for $r = 0.7, 0.5$, and in Figure 4.39 for $r = 0.2, 0.1$. For each r we present two horizontally aligned plots. The right-hand plot shows the equilibria positions w in the whole range $2 < k_- < 10^5$. The left-hand plot shows a magnification of the same data where the equilibrium situation qualitatively changes. The stable equilibrium points w are connected by a solid line, unstable by a dashed line. For reference we draw $w = \alpha$ as a dotted line in the plots.

Analyzing the data displayed in the plots we notice different equilibria behavior between $r = 1$ and any $r > 1$.

For any fixed $r > 1$ we observe the following: When k_- is high, $w = 0$ is a stable equilibrium point and $w = \alpha$ is an unstable one. As k_- gets smaller, $w = 0$ is still a stable equilibrium but the unstable equilibrium originally at $w = \alpha$ drops monotonically to smaller and smaller values of w. This is true for all k_- down to an r dependent stiffness value we call $k_{0s}(r)$. At $k_{0s}(r)$ an equilibria
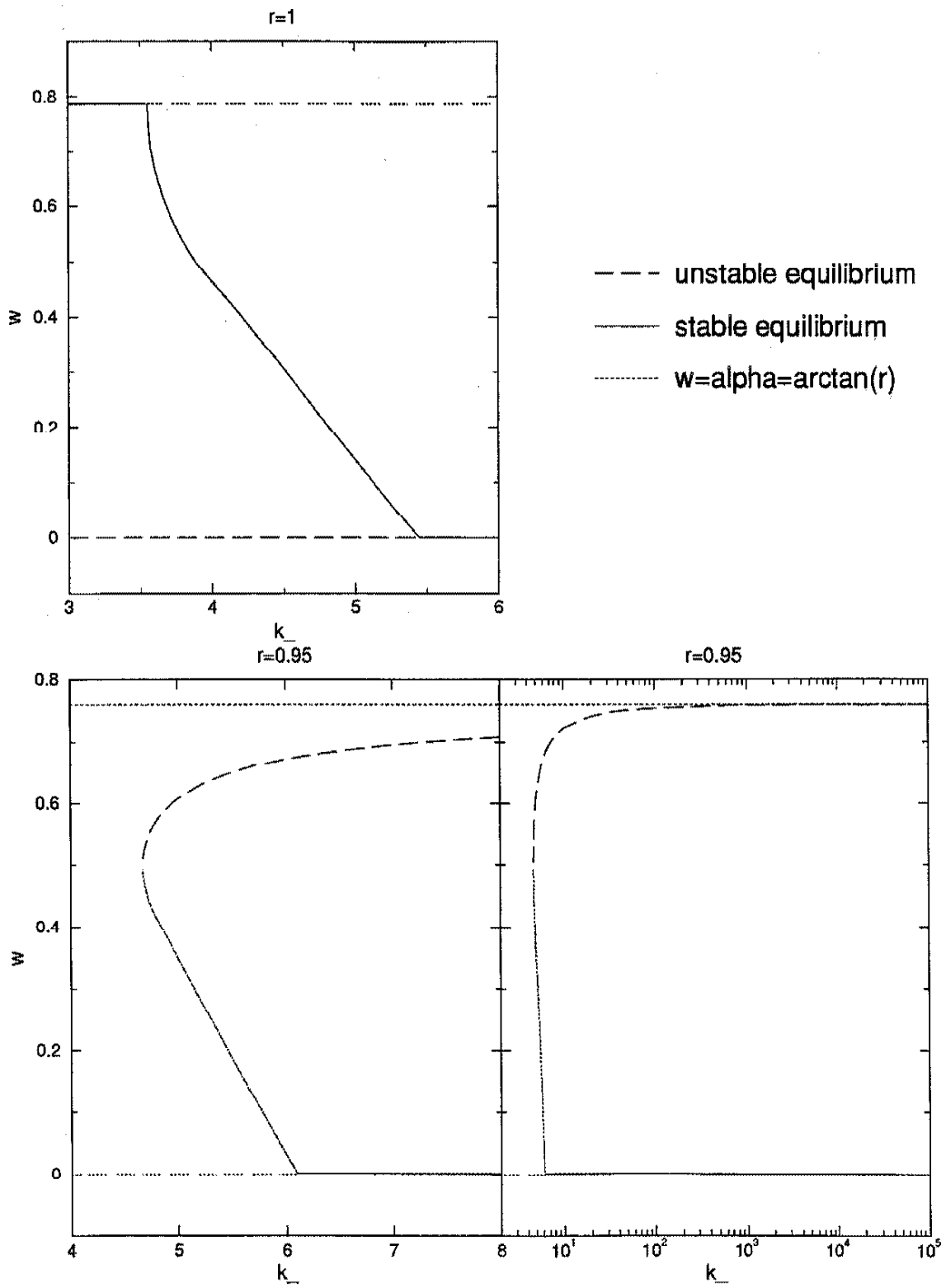
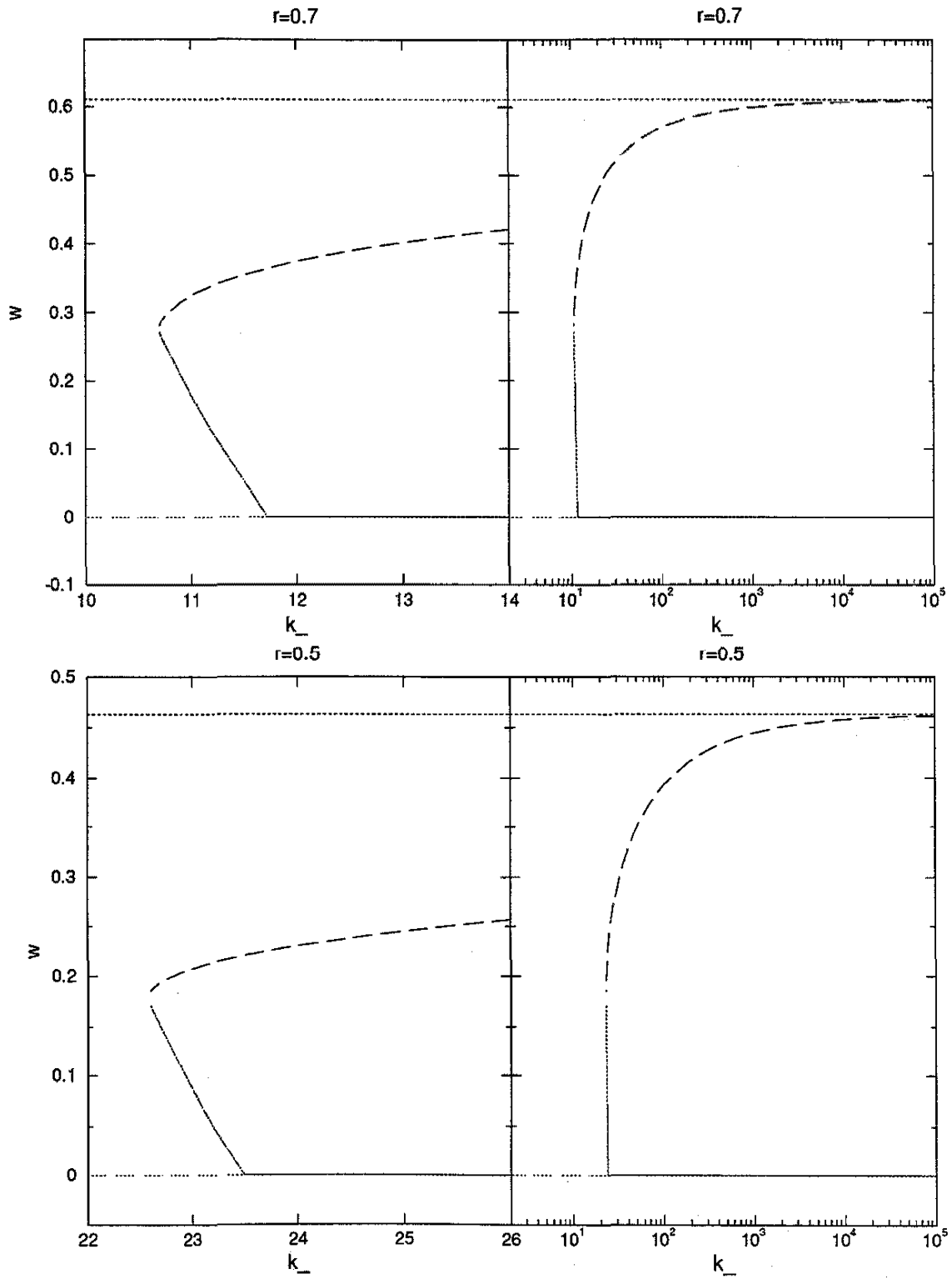Figure 4.37: Equilibrium bifurcation, $r = 1, 0.95$, varying k_-

Figure 4.38: Equilibrium bifurcation, $r = 0.7, 0.5$, varying k_-
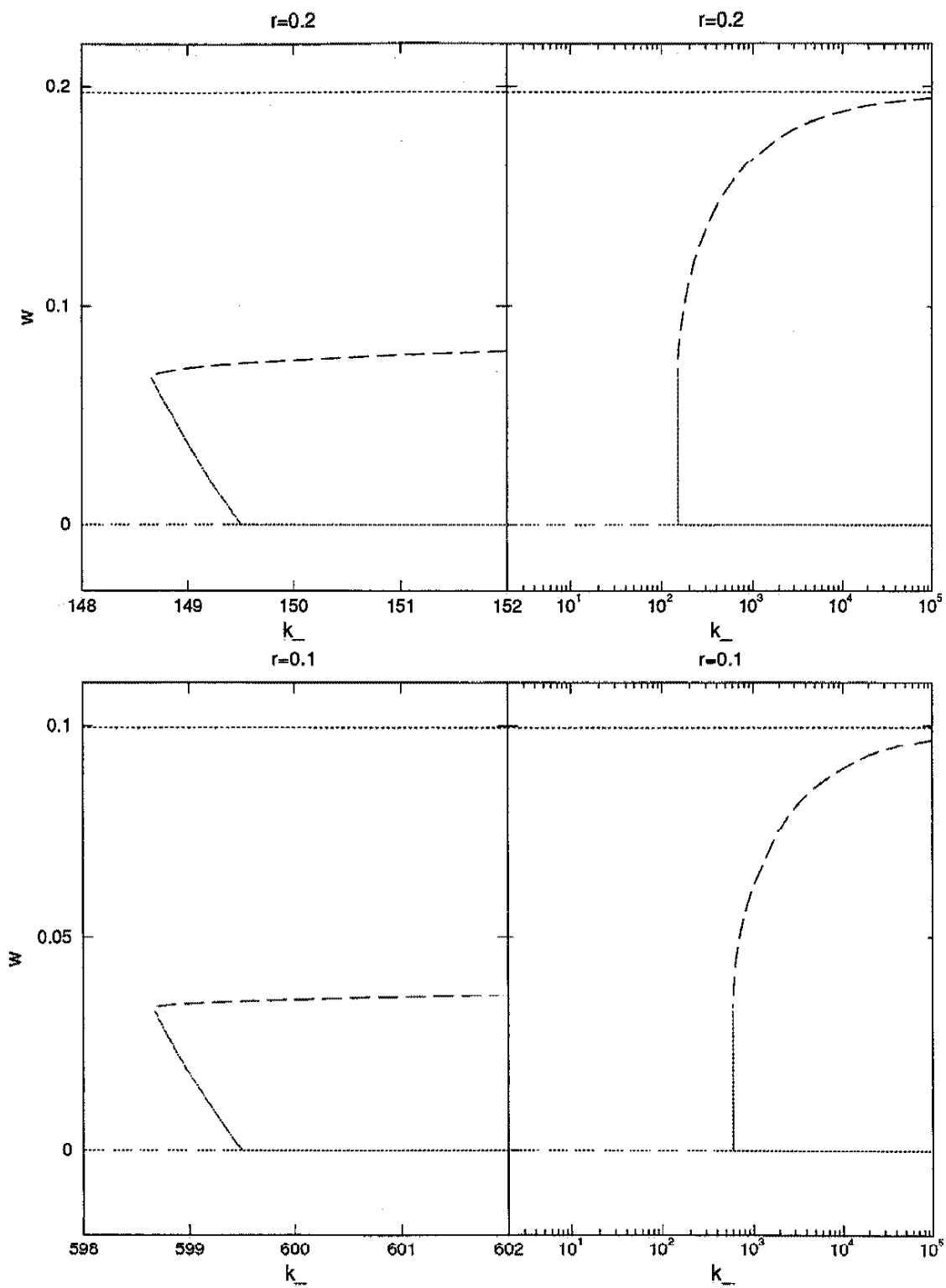
Figure 4.39: Equilibrium bifurcation, $r = 0.2, 0.1$, varying k_-

bifurcation occurs. The $w = 0$ equilibrium becomes unstable and another, new stable equilibrium is born at $w = 0$. When k_- is lowered further the new stable equilibrium branches off to higher w values. Thus, we have three equilibrium points now: an unstable one at $w = 0$, a stable at some higher w and another unstable one at even higher w. The latter equilibrium point is the unstable branch coming from $w = \alpha$. This situation persists for all k_- down to an r dependent value we call $k_{uns}(r)$. At $k_{uns}(r)$ the two higher branches meet and die. For all k_- below $k_{uns}(r)$ there is no stable equilibrium and only one unstable point at $w = 0$.

A square block, $r = 1$, is an exceptional situation. For high k_-, there is again a $w = 0$ stable equilibrium point and an unstable one at $w = \alpha = 0.7854$. However, when we lower k_- the unstable equilibrium point remains exactly at $w = \alpha = 0.7854$, unlike the case when $r > 1$. Again a new, stable equilibrium branch bifurcates from $w = 0$ at $k_{0s}(1) = 5.449$ and the $w = 0$ equilibrium point becomes unstable here. However, unlike the case $r > 1$, when the stable branch meets the unstable $w = \alpha$ branch at $k_{uns}(1) = 3.558$, they collapse into one stable branch. This stable branch continues exactly at $w = \alpha = 0.7854$, as k_- drops below the value $k_{uns}(1) = 3.558$.

Thus, for a square block, the equilibrium point $w = 0$ is stable $\forall k_- > k_{0s}(1) = 5.449$ and unstable $\forall k_- < k_{0s}(1) = 5.449$. The $w = \alpha = 0.7854$ equilibrium point is stable $\forall k_- < k_{uns}(1) = 3.558$ and unstable $\forall k_- > k_{uns}(1) = 3.558$. So interestingly, for soft springs, a square block resting with its diagonal vertical is at a stable equilibrium.

For $r = 1$ we get a stable equilibrium point at $w = \alpha$ below the value $k_{uns}(1)$. But for a block with r just slightly less than 1 we do not see any stable equilibrium points below the value $k_{uns}(r)$. Recall that we only looked at $w < \alpha$. Physical intuition says that when the stable and unstable equilibria branches meet and disappear at $k_{0s}(r)$ there is a new equilibria branch born at some value $w > \alpha$. We do not investigate this further.

Equilibrium bifurcation in (k_-, r) parameter space

We have already obtained plots of the equilibrium position w against k_- for several specific aspect ratios r. For each r we found two critical k_- values where equilibrium bifurcation occurred. We called these critical values $k_{0s}(r)$ and $k_{uns}(r)$.

Now we want to determine $k_{0s}(r), k_{uns}(r)$ as a function of r. We will consider aspect ratios in the interval $0.05 < r < 1$. Knowledge of $k_{0s}(r), k_{uns}(r)$ as functions of r will tell us where different kinds of equilibrium behavior occur in the whole (k_-, r) parameter space. First let us make a precise definition of both functions.

Definition:

Consider a rigid block of aspect ratio $r < 1$ on a Winkler foundation with stiffness $k_- > 2$. Consider the equilibrium positions of the block only at angles $0 < w < \alpha = \arctan(r)$. Fix r.

Let $ks(r)$ be a value such that $\forall k_- > ks(r)$ the equilibrium point $w = 0$ is stable. Then $k_{0s}(r)$ is an infimum of all such values $ks(r)$.

Let $ku(r)$ be a value such that $\forall k_- < ku(r)$ there are no stable equilibrium points. Then $k_{uns}(r)$ is supremum of all such values $ku(r)$.

Both $k_{0s}(r), k_{uns}(r)$ are plotted in Figure 4.40. The curves $k_{0s}(r), k_{uns}(r)$ nearly coincide in the top plot with logarithmic scale. Therefore, we plot the difference between the two curves in a lower plot. The difference $k_{0s}(r) - k_{uns}(r)$ is 1.891 at $r = 1$, then falls quickly to about 0.8 and remains almost constant for tall, thin blocks. Thus, the distance between the two bifurcation points remains nearly constant as the block gets taller and thinner.

The $k_{uns}(r)$ curve divides the (k_-, r) parameter space into two regions. The region below the curve has no stable equilibrium points and every point in region above the curve has a stable equilibrium point at some w. Again we remind ourselves this refers to equilibria in the interval $|w| < \alpha$.

The nice, smooth shape of $k_{0s}(r)$ suggests that we try to find a polynomial to approximate $k_{0s}(r)$. A few attempts yield a simple expression $6/r^2 - 0.5$ which fits $k_{0s}(r)$ with remarkable accuracy. At the lower picture in Figure 4.40 we also plot $6/r^2 - 0.5 - k_{0s}(r)$. It is practically equal to zero. The remarkable fit suggests we try to derive $6/r^2 - 0.5$ analytically.

It is possible, indeed. We recall the formula for $a_{y_-}(y_-, w)$ stated in Figure 2.5:

$$\pm a_{y_-}(y_-, w) = r\cos(w)/2 - \sin(|w|)/2 - \frac{1}{3}\frac{r^2\cos^4(w)(3\cos(w)/2 - r\sin(|w|)/2 - 3y_-) - v_-^3(y_-, w)\sin^2(|w|)}{r\cos^3(w)(\cos(w) - 2y_-) + \sin(|w|)\cos(w)v_-^2(y_-, w)},$$

where $v_-(y_-, w) = \cos(w)/2 + r\sin(|w|)/2 - y_-$. Consider a block resting on a foundation at equilibrium position $y_- = 0.5 - 1/k_-, w = 0$. Tilt the block a small amount $w = \epsilon$. We can assume that y_- does not change. Then the equilibrium point $w = 0$ is neutral when

$$a_{y_-}(0.5 - 1/k_-, \epsilon) = 0.$$

When solving the equation we assume that $\sin\epsilon = \epsilon$ and $\cos\epsilon = 1$ and neglect all terms with second or higher powers of ϵ. After some algebra the equation simplifies, the first power of ϵ cancels out and we arrive at:

$$k_-^2 r^2 - 6k_- + 3 = 0.$$
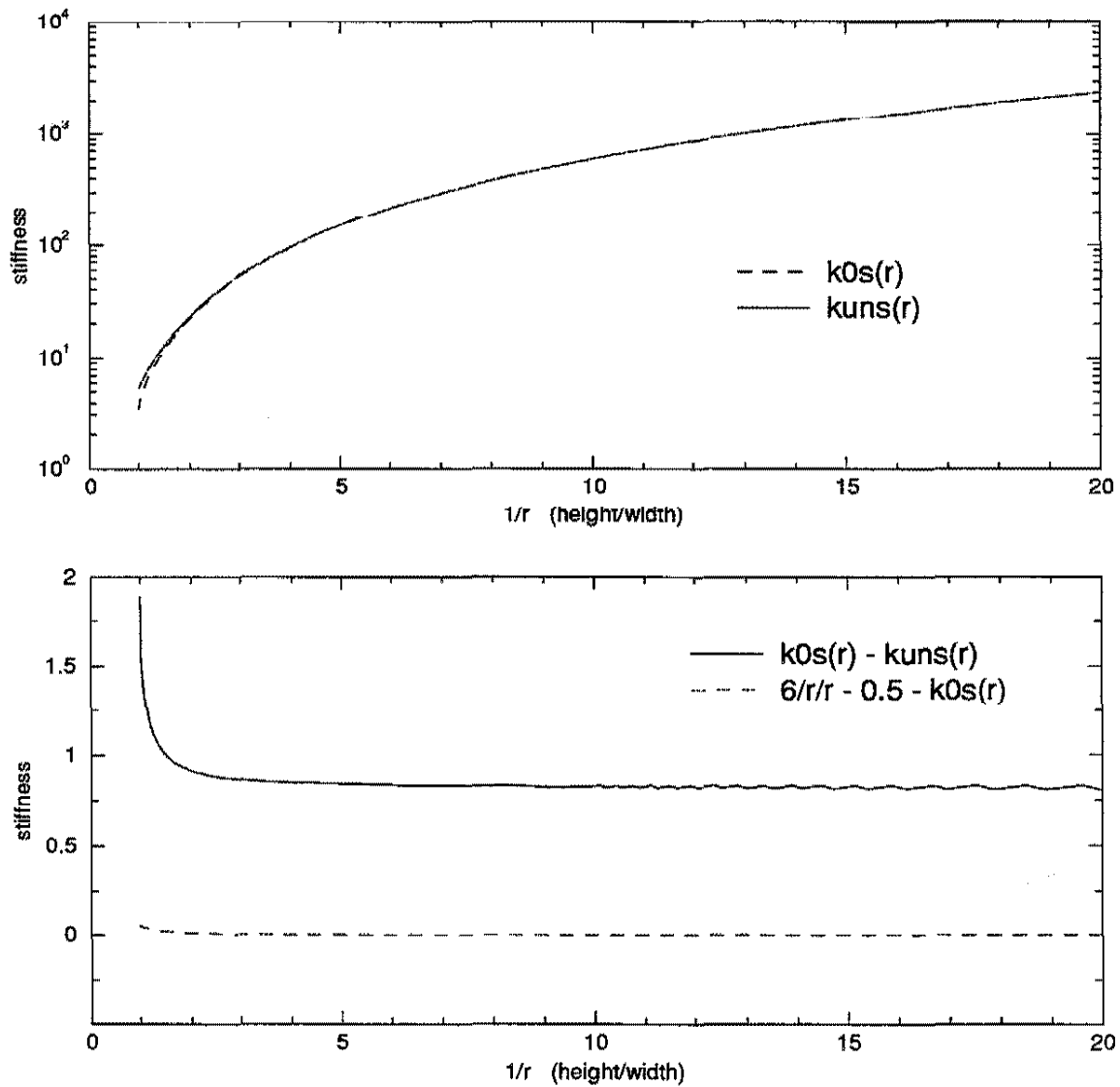
Figure 4.40: Equilibrium bifurcation in (k_-, r) parameter space

When solving for k_- we make the additional assumption that r^2 is small and replace the expression $\sqrt{3 - r^2}$ by $\sqrt{3} - \frac{r^2}{2\sqrt{3}}$. The solution is then given by:

$$k_{-1} = 0.5 \qquad\qquad k_{-2} = \frac{6}{r^2} - 0.5.$$

We disregard the first solution, $k_{-1} = 0.5$, because the whole block would be under the foundation surface. Our model assumes at most two corners of the block are under the surface. The second

solution is the one we were looking for. Thus,

$$k_{0s}(r) = \frac{6}{r^2} - 0.5$$

is the stiffness value, where for a given r, equilibrium point $w = 0$ is neutral. For larger k_-, the equilibrium point $w = 0$ will be stable and for smaller k_- it will be unstable.

Equilibrium - conclusions

The following conclusions apply to a block with an aspect ratio $r < 1$ on Winkler foundation with stiffness $k_- > 2$ for equilibria positions in the interval $|w| < \alpha$.

- The equilibrium point at $w = 0$ is stable for all k_- larger than $k_{0s}(r) = \frac{6}{r^2} - 0.5$ and unstable for all k_- lower than $k_{0s}(r)$

- There is no stable equilibrium point for any k_- lower than $k_{uns}(r)$ and there is a stable equilibrium point for all k_- larger than $k_{uns}(r)$. The value of $k_{uns}(r)$ is about 0.8 less than $k_{0s}(r)$

- At $k_{0s}(r)$ and $k_{uns}(r)$, equilibria are born or die. Bifurcation occurs

- There is exactly one equilibrium point for any k_- smaller than $k_{uns}(r)$, there are three equilibrium points for any k_- between $k_{uns}(r)$ and $k_{0s}(r)$, and there are two equilibrium points for any k_- larger than $k_{0s}(r)$

The fact that there are no stable equilibrium points for any k_- smaller than $k_{uns}(r)$ is reflected in our dynamic analysis. The $k2_{stability}(r)$ and $k3_{stability}(r)$ curves computed for ic2 follow $k_{uns}(r)$ closely before blowing up. The $k1_{stability}(r)$ curve computed for ic1 is almost identical to $k_{uns}(r)$, only little higher.

Equilibrium - applications

We discussed equilibria of a rigid block, assuming it is a rectangular rigid block with uniform density as defined in the beginning of this thesis. Looking back at this section we realize our equilibria discussion applies to a much larger class of rigid objects. The block does not have to be uniform since the moment of inertia I_- does not enter the discussion. The whole object does not have to be rectangular. The discussion applies to any rigid object with the following properties:

1) the part of the object which is below the foundation surface must be part of some rectangle, and

2) the center of gravity of the object when projected straight at the bottom edge is in the middle between the two lower corners.

Then the aspect ratio r of the object will be $\frac{l_1}{2l_2}$, where l_1 is width of the bottom edge and l_2 is the distance from center of gravity to the bottom.

A possible application of this static equilibria analysis lies in the area of civil engineering. We could estimate k_- that best approximates given foundation soil properties and conclude that buildings of lesser aspect ratio than $k_{0s}^{-1}(k_-)$ cannot exist on a given foundation. Cities and countries put a large amount of effort and take pride in constructing tall buildings. The simple equilibria analysis suggests that the mere height may not be the main limiting factor in constructing tall structures. More important is how slim the structure gets. We realize that real soil foundations do not behave exactly like our investigated elastic model. The immediate conclusions regarding the stability of tall structures may be oversimplified. However, the presented equilibria approach could be developed further towards civil engineering applications. A more realistic model could be considered for foundations, for structures, etc. We believe such analysis would yield valuable results on the stability of tall structures.

We have to mention another interesting application. If the block is tilted and both lower corners are under the foundation surface, then the triangular area between the higher of the two corners and the surface contributes to an upward force pushing the block out. Referring to Figure 4.34 or 2.5, it is the white triangle outside of the block. We let the said triangle contribute to the reaction force since the springs cannot 'bend around' the corner.

Suppose now that the contribution of the said triangular area does not strongly influence the equilibria of the block. Then we simply take $k_- = \frac{\rho_{liquid}}{\rho_{block}}$ and relate the whole analysis to the equilibria of blocks floating on water. Indeed, we can see garbage cartons floating on water declined from vertical. It would be interesting and not very difficult to redo the analysis with a model which does not include the said triangle, that is with a liquid foundation model.

4.4 Long term response

This section is a direct continuation of the 4.1 section. We will be looking at the behavior of the block subjected to the initial conditions ic1, ic2 for various different parameters, trying to identify the dominant types of response. In section 4.1 we looked at the behavior of the block for times 0 to 10 or 20. Now we study the motion of the block to times of order 100 or 1000. We observe the motion for large times t_- to find out whether the response changes for large t_- and if it does how.

Unlike in section 4.1, we do not plot the variables $x_-, x_-', y_-, y_-', w, w'$ versus time. We present

phase space plots of y_-' versus y_- and w' versus w. Plots of x_-' versus x_- are often not included. If the whole motion takes place in contact mode, x_- is just a function of w for all times. If $\mu = 0$, the block moves only in slide mode but its motion in the x direction is trivial. So we can take $x(t_-) = 0$ without loss of generality. In these cases or when we simply feel the x_-' versus x_- plot does not show anything worth displaying, we omit it.

Furthermore, we present plots of energy versus time. We plot all five of the energy components defined earlier: kinetic rotational, translational in x, in y, and gravitational potential, potential of the springs. We plot the energy averaged over one swing instead of plotting the energy continuously at each time step. By swing we understand that part of the block's motion which occurs between two subsequent changes of the sign of angular velocity w'. So, if rocking were periodic, one period would consist of two swings. To average the energy we numerically integrate the energy over the whole swing using a trapezoidal rule and divide it by the time length of that swing. We average each of the five energy components. The averaged energy for a given swing is plotted at the end of that swing. We call averaged energy components as follows:

averaged kinetic energy in x direction	ave_x'
averaged kinetic energy in y direction	ave_y'
averaged rotational kinetic energy	ave_w'
averaged gravitational potential energy	ave_y
averaged potential energy of compressed springs	ave_k.

The response presented in the form of the said phase space and energy plots is shown in Figures 4.41 through 4.55. Each figure shows the response of our system for a given choice of parameters μ, k_-, r. Each figure presents phase space plots of y_-, y_-' and w, w'. At the bottom of a plot the averaged energy versus time is shown. Rarely, we include the phase space plot of x_-, x_-'. Table 4.1 contains a list of figures with parameters and initial conditions given for the figure and a brief description of the response type in the figure. Figures are listed in the table in order they appear in this thesis.

In phase space we plot the discrete points along trajectories at constant time intervals. Since the motion is observed for a long time, drawing trajectories with a continuous solid line would result in an overcrowded picture - essentially just a black spot. Plotting discrete points may not show the geometry of the trajectories well. But it will show a region in phase space where trajectories move for given initial conditions. The presented phase space plots are a projection of this region onto the y_-, y_-' and w, w' planes. Then on top of the dotted region we sometimes draw an initial or a typical trajectory with a solid line - but only for a short time, just enough to display the geometry of a trajectory.
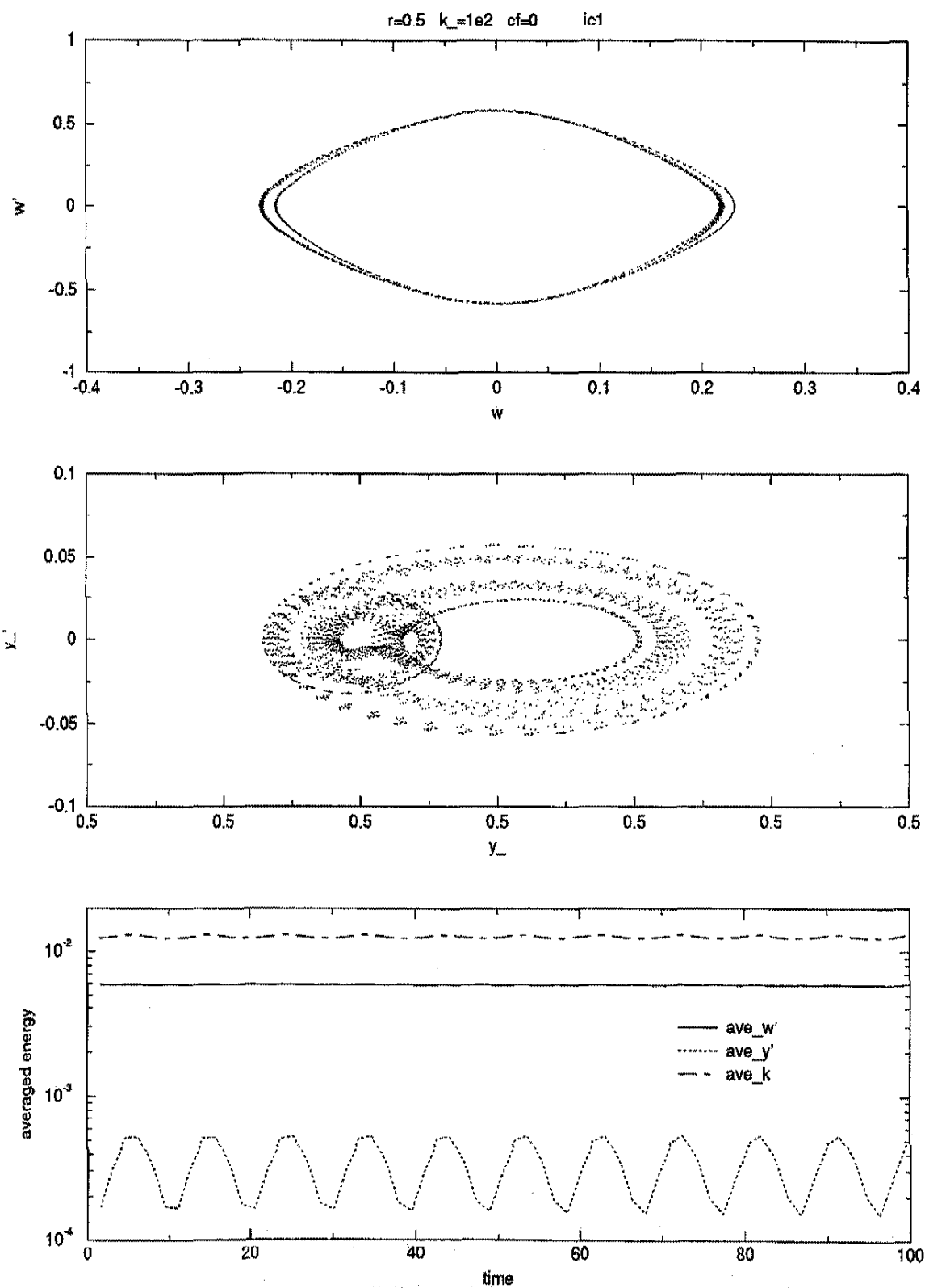
Figure 4.41: Steady rocking $r = 0.5, k_- = 1e2, \mu = 0$, ic1
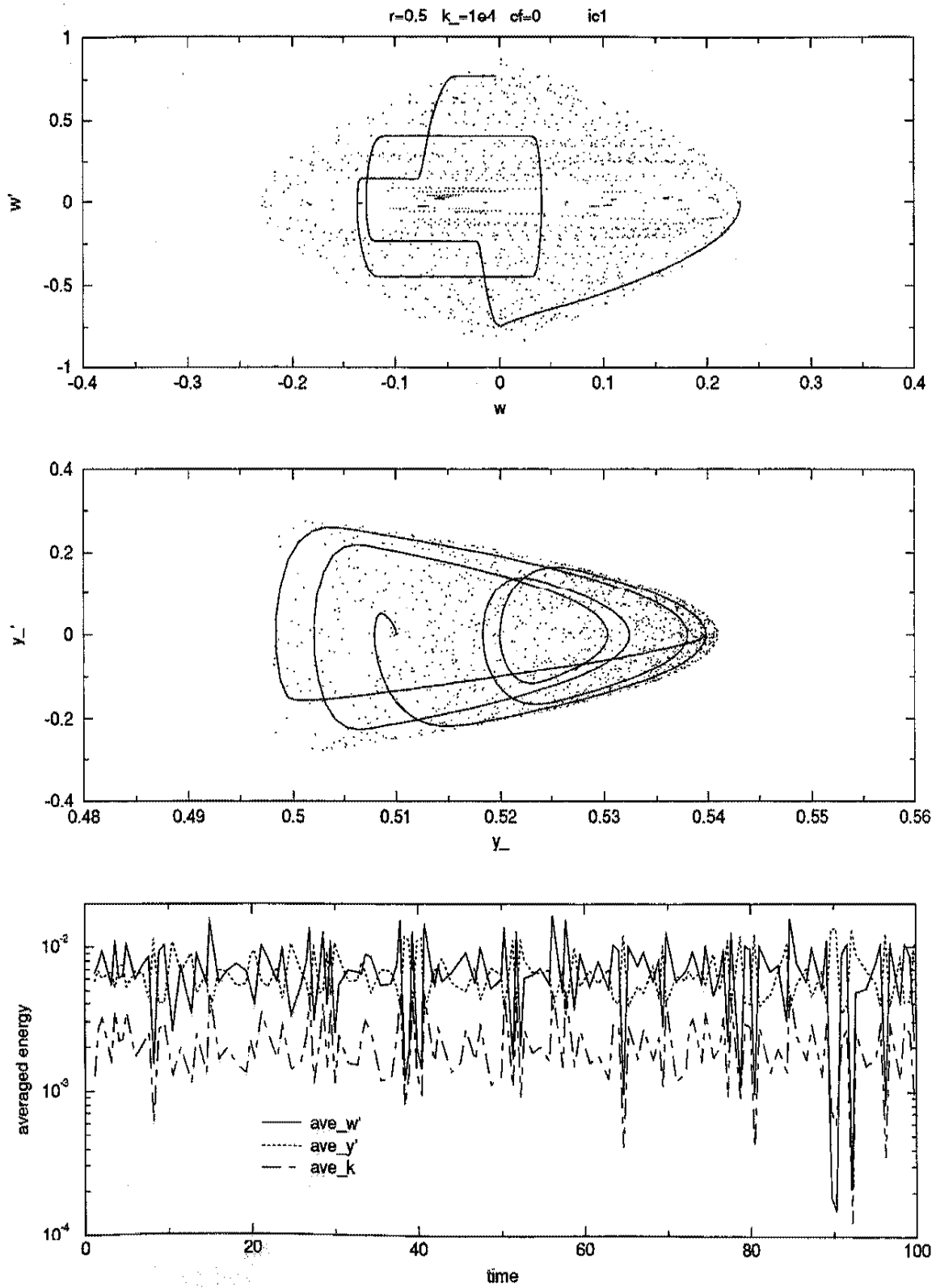
Figure 4.42: Zero friction rock flight $r = 0.5, k_- = 1e4, \mu = 0$, ic1

Figure 4.43: Rock to Vertical $r = 0.1, k = 1e6, \mu = 0$, ic1

Figure 4.43: Rock to Vertical $r = 0.1, k_- = 1e6, \mu = 0$, ic1

Figure 4.44: Steady rocking $r = 0.5, k_- = 1e2, \mu = 0$, ic2
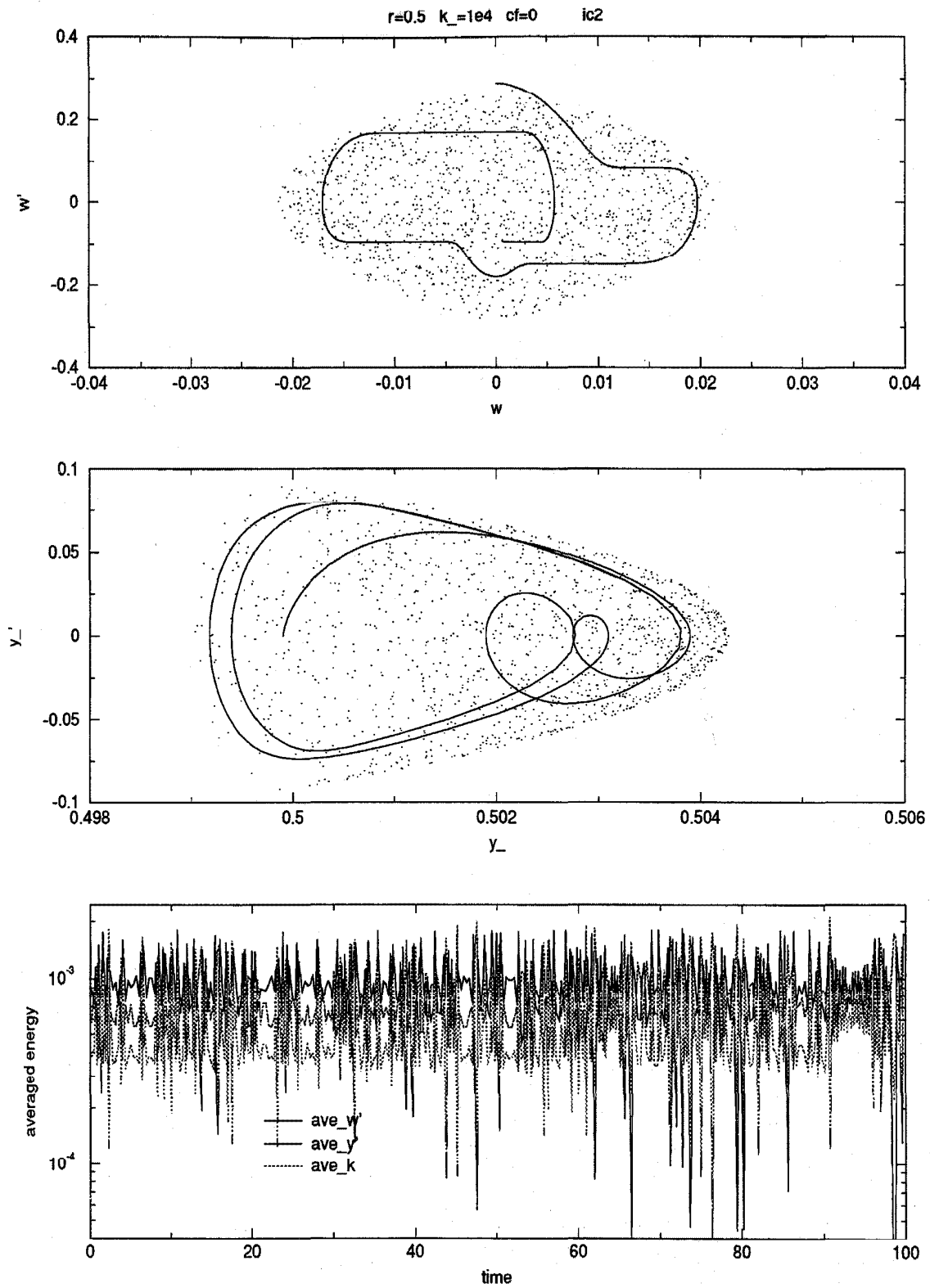
Figure 4.45: Zero friction rock flight $r = 0.5, k_- = 1c4, \mu = 0$, ic2
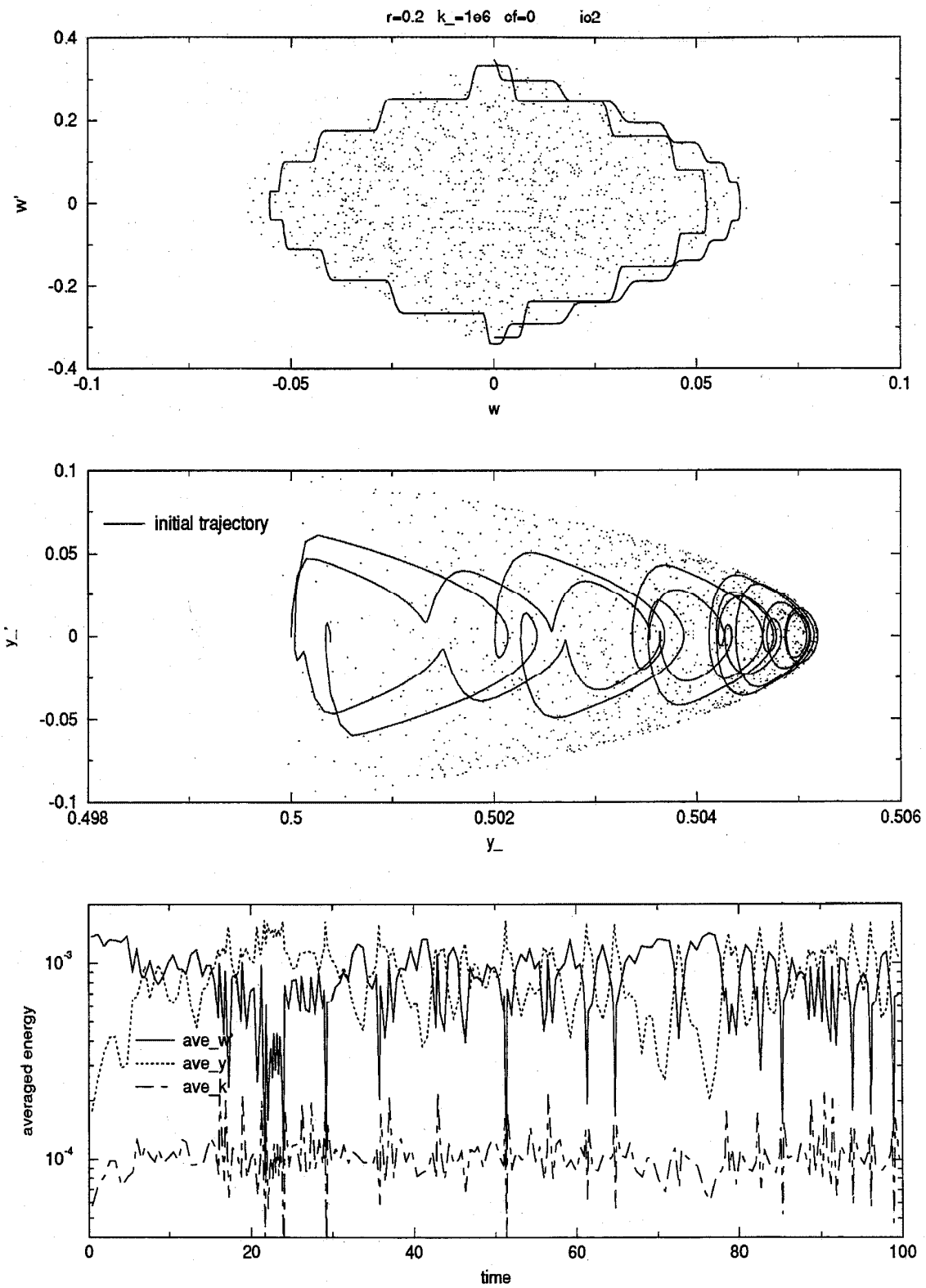
Figure 4.46: Rock to vertical $r = 0.2, k_- = 1e6, \mu = 0$, ic2
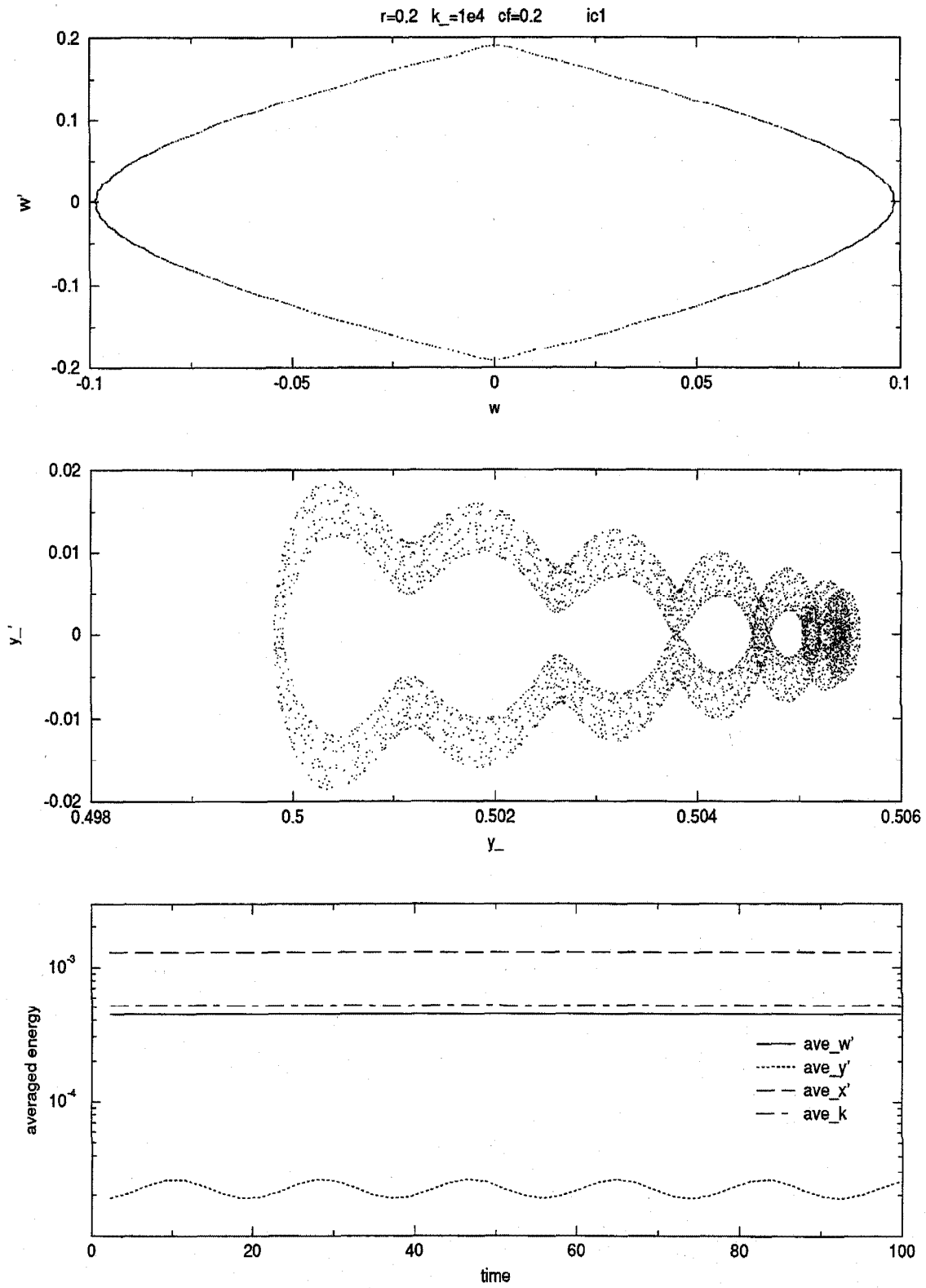
Figure 4.47: Steady rocking $r = 0.2, k_- = 1e4, \mu = 0.2$, ic1
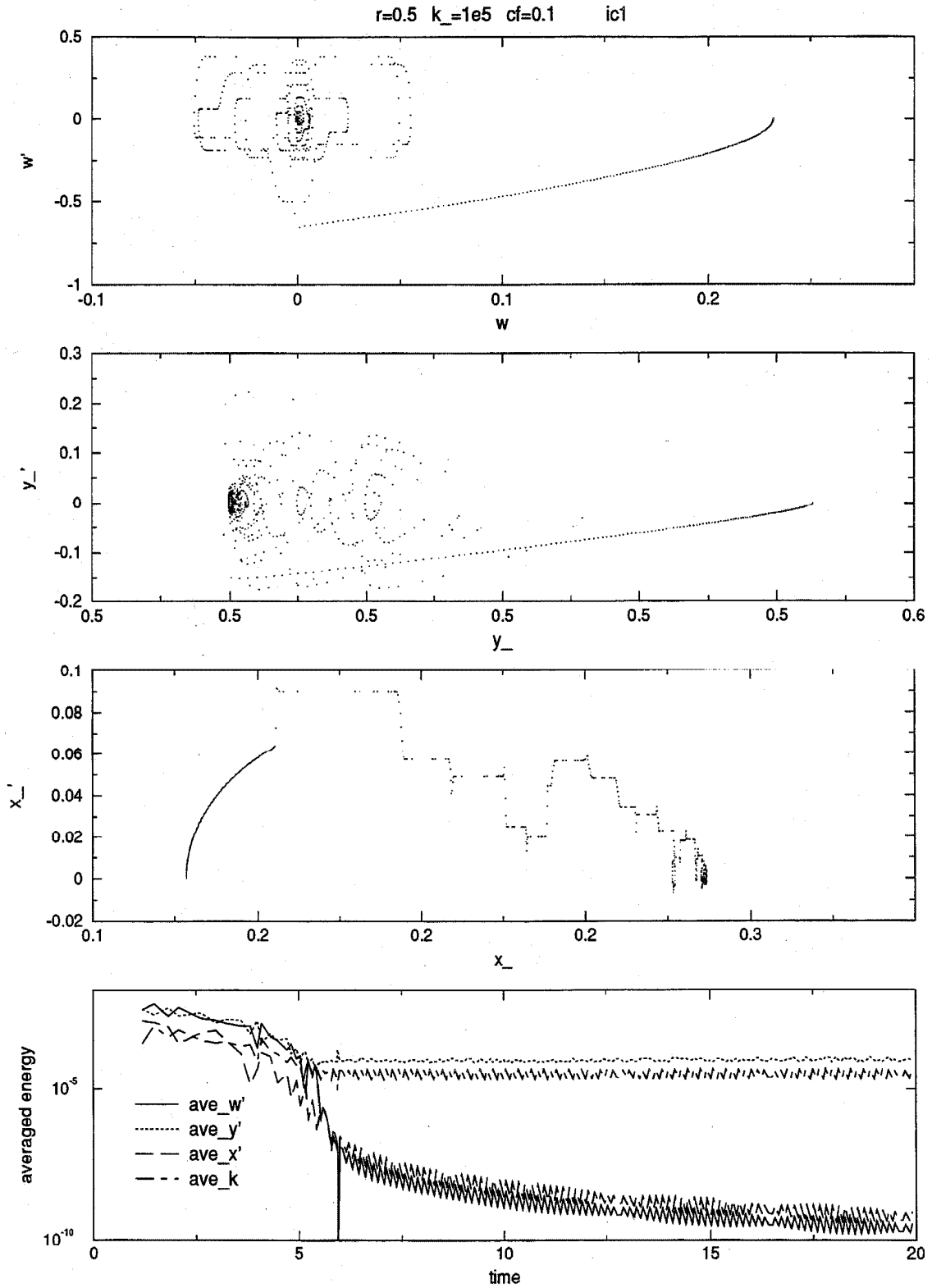
Figure 4.48: Settle down $r = 0.5, k_- = 1e5, \mu = 0.1$, ic1
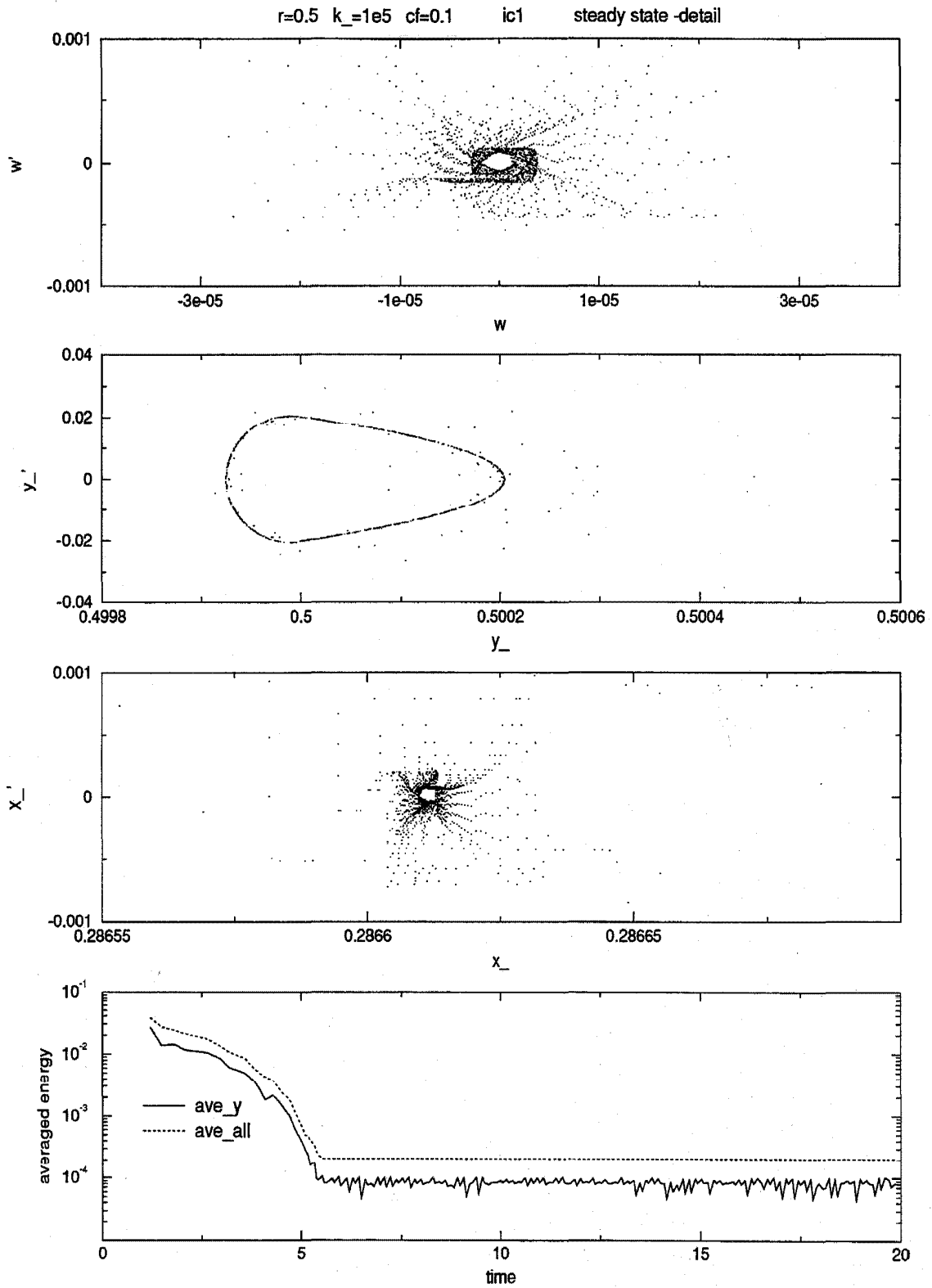
Figure 4.49: Detail of the previous figure $r = 0.5, k_- = 1e5, \mu - 0.1$, ic1

Figure 4.50: Rock to Vertical $r = 0.2, k_- = 1e5, \mu = 0.3$, ic1
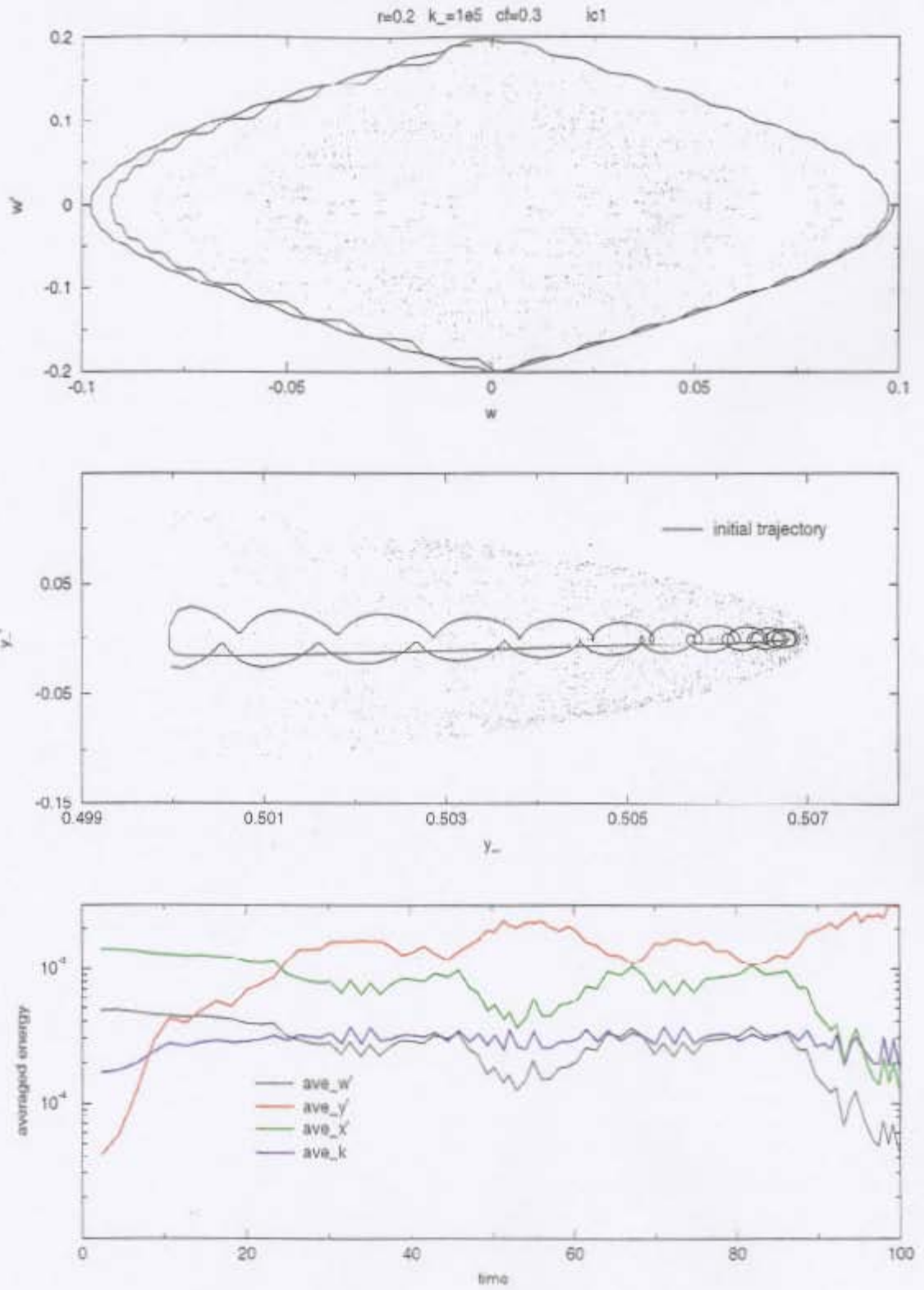
Figure 4.50: Rock to Vertical $r = 0.2, k_- = 1e5, \mu = 0.3$, ic1
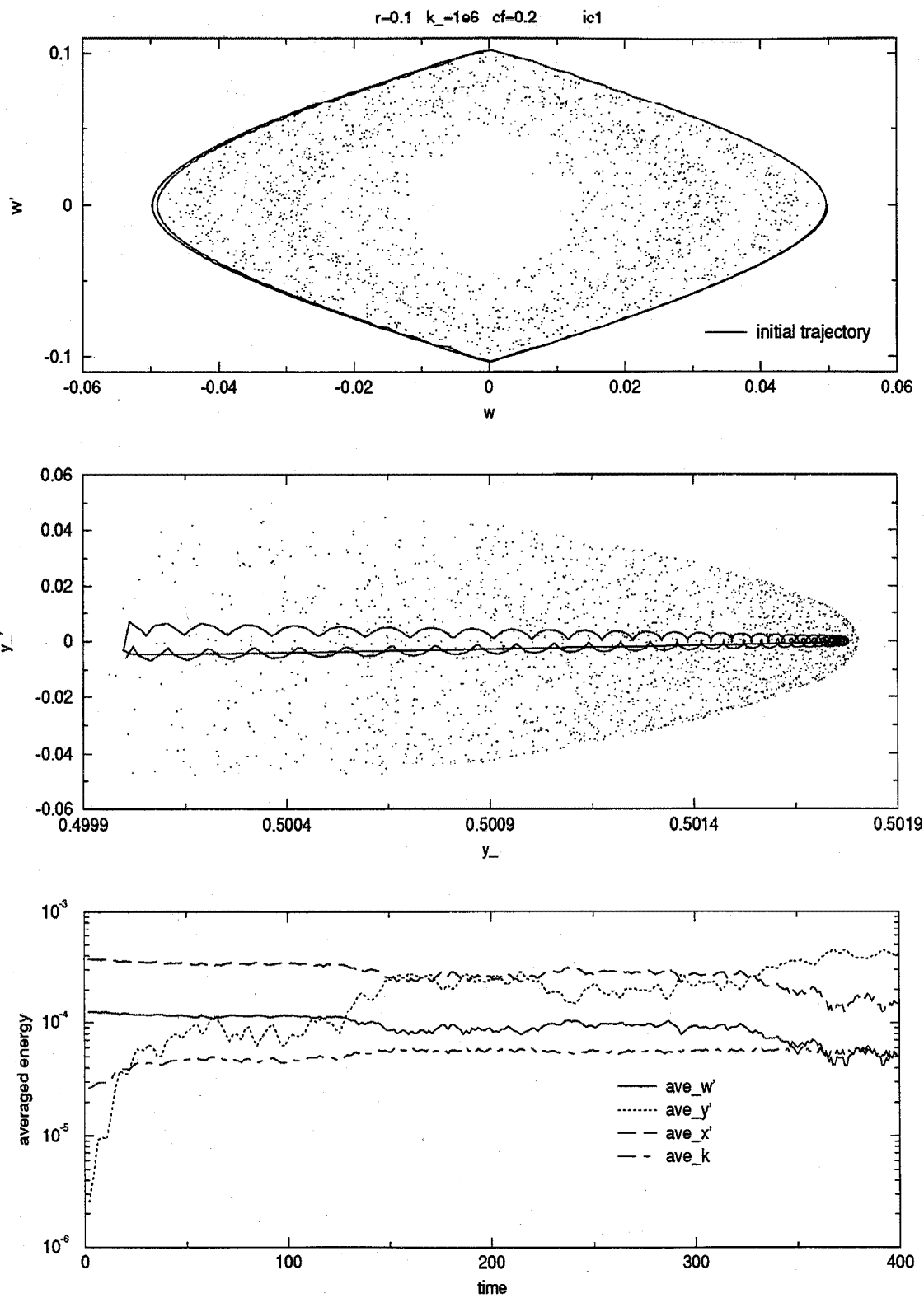
Figure 4.51: Rock to vertical $r = 0.1, k_- = 1e6, \mu = 0.2$, ic1
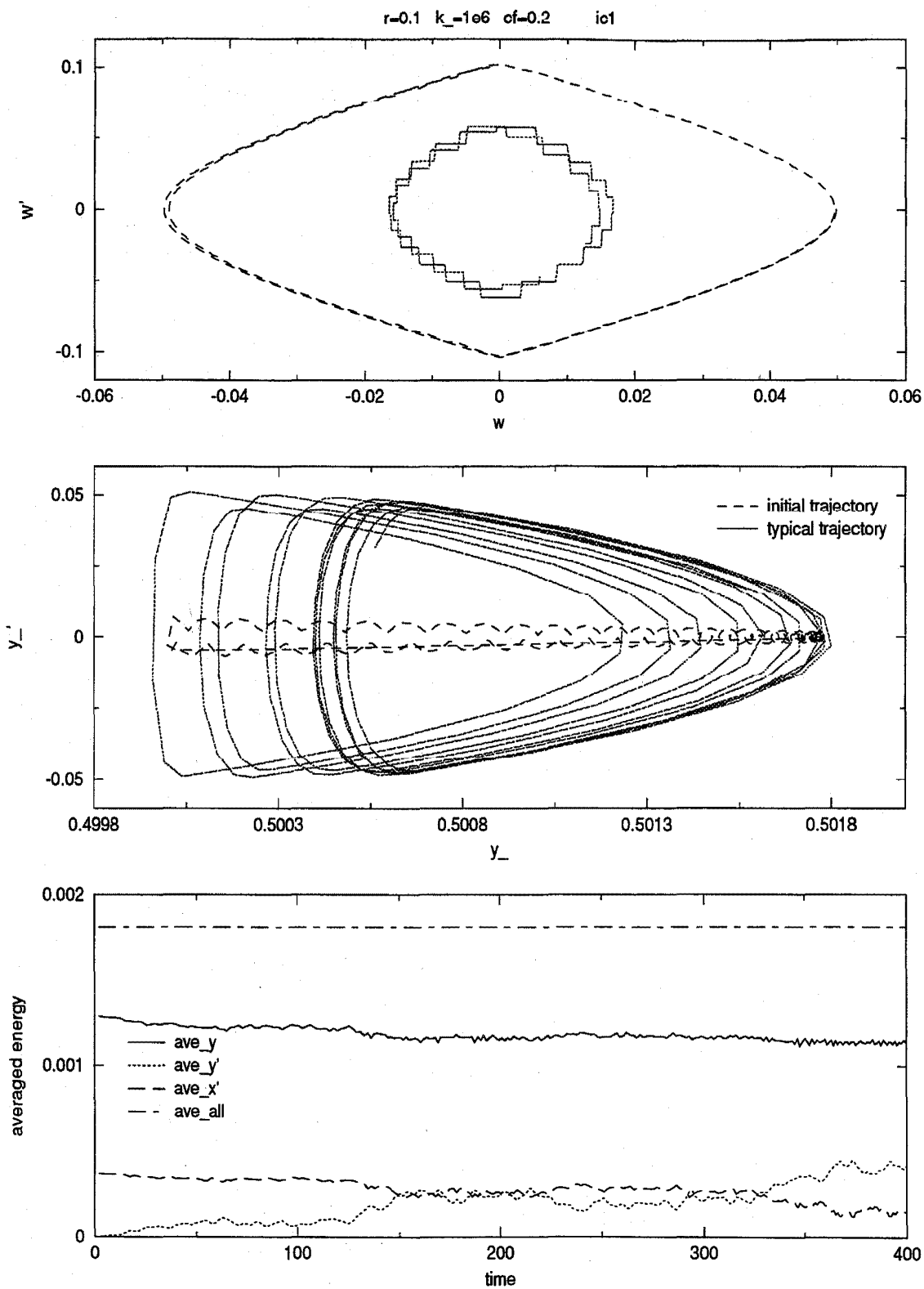
Figure 4.52: Rock to vertical $r = 0.1, k_- = 1e6, \mu = 0.2$, ic1

r=0.3 k_=1e2 cf=0.2   ic2
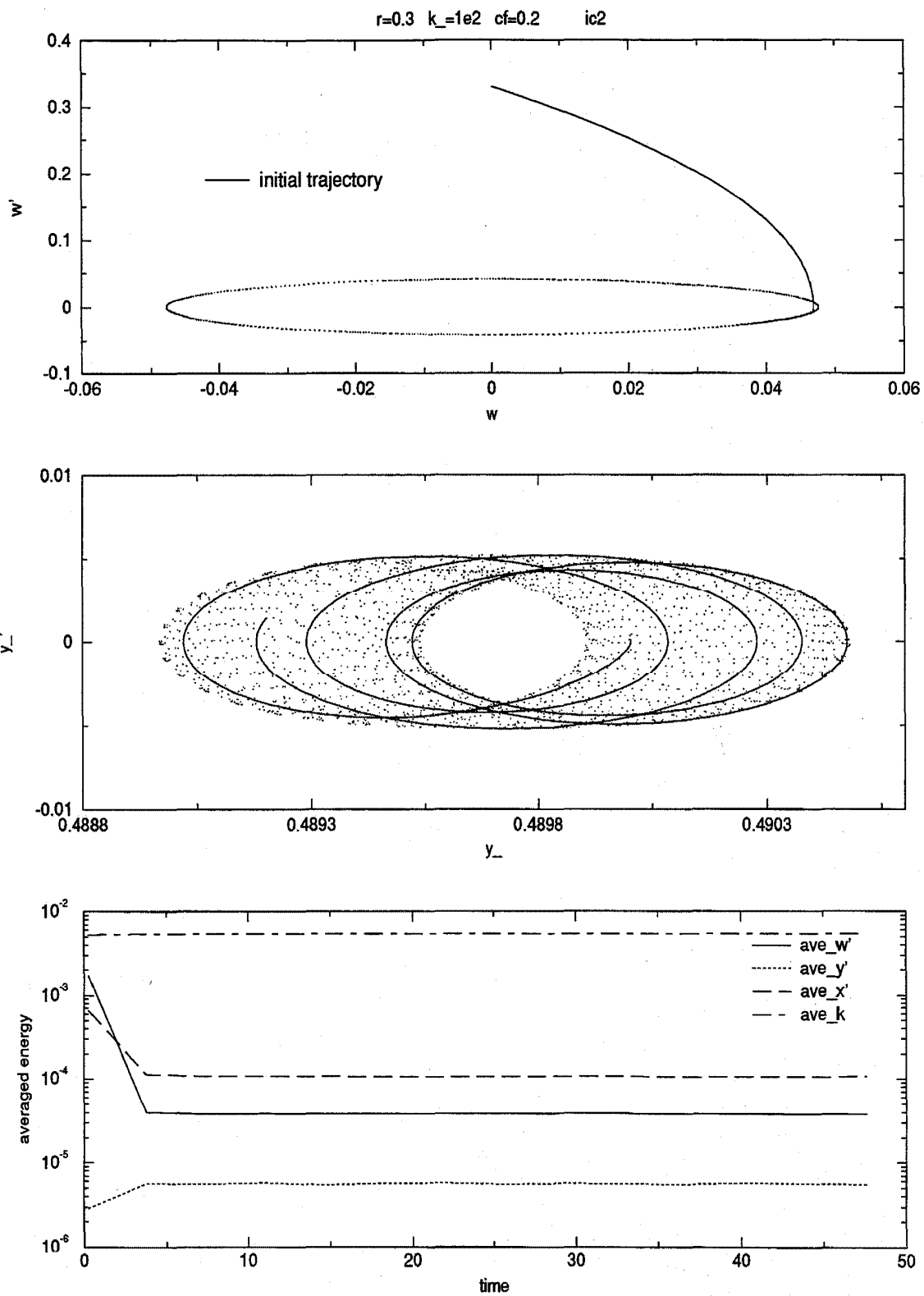
Figure 4.53: Steady rocking $r = 0.3, k_- = 1e2, \mu = 0.2$, ic2

r=0.2 k_=1e4 cf=0.1   ic2
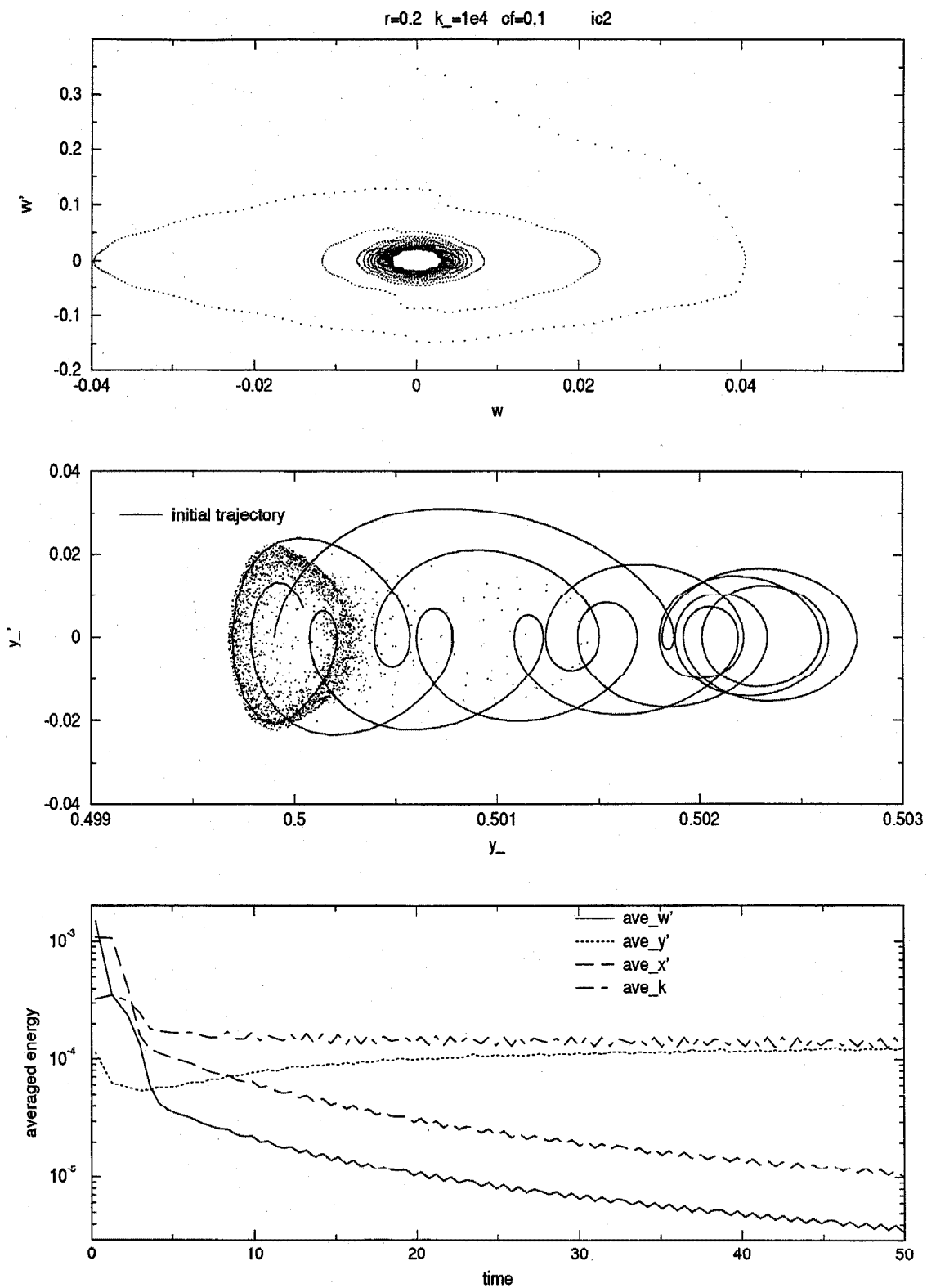
Figure 4.54: Settle down $r = 0.2, k_- = 1e4, \mu = 0.1$, ic2

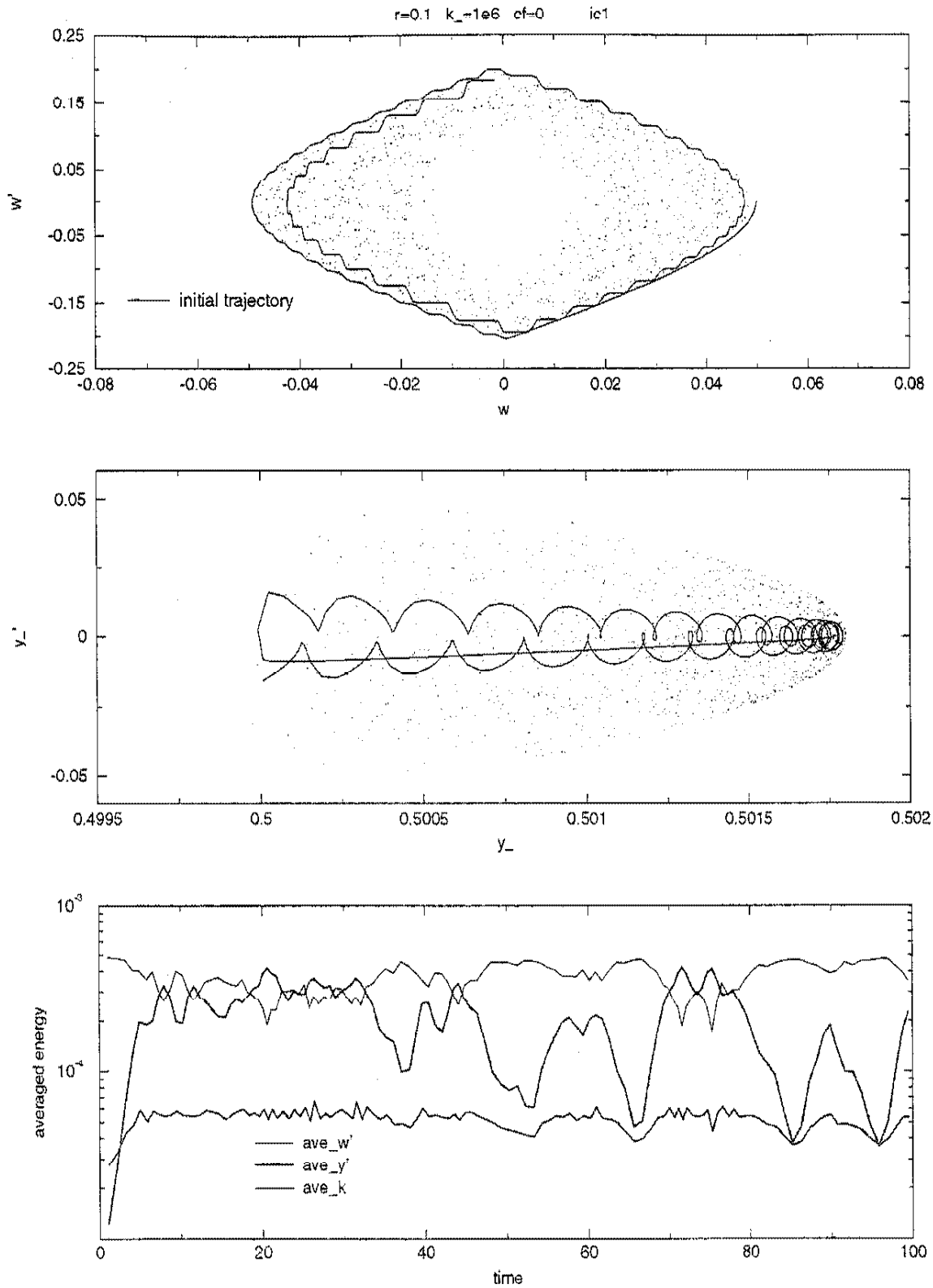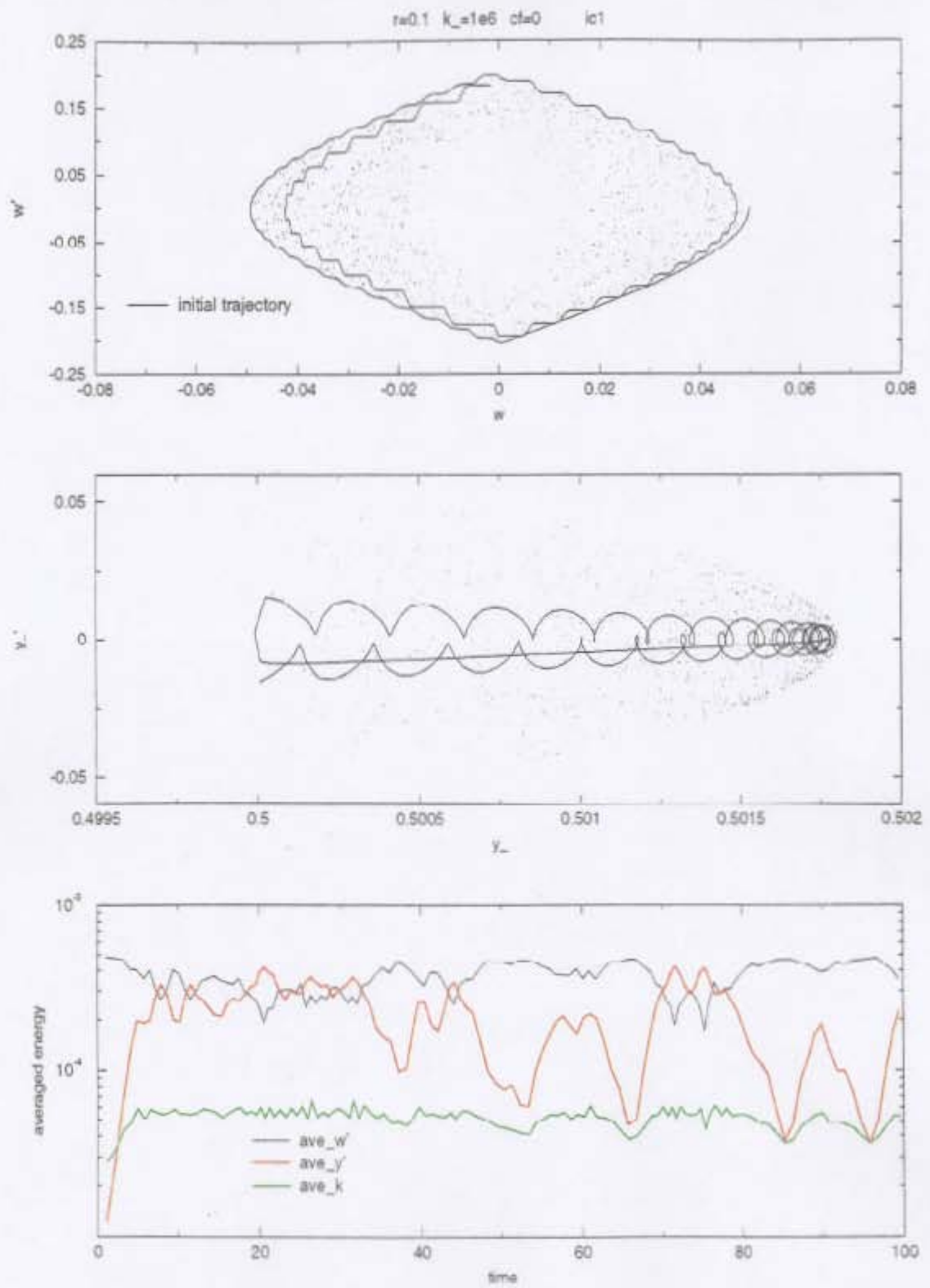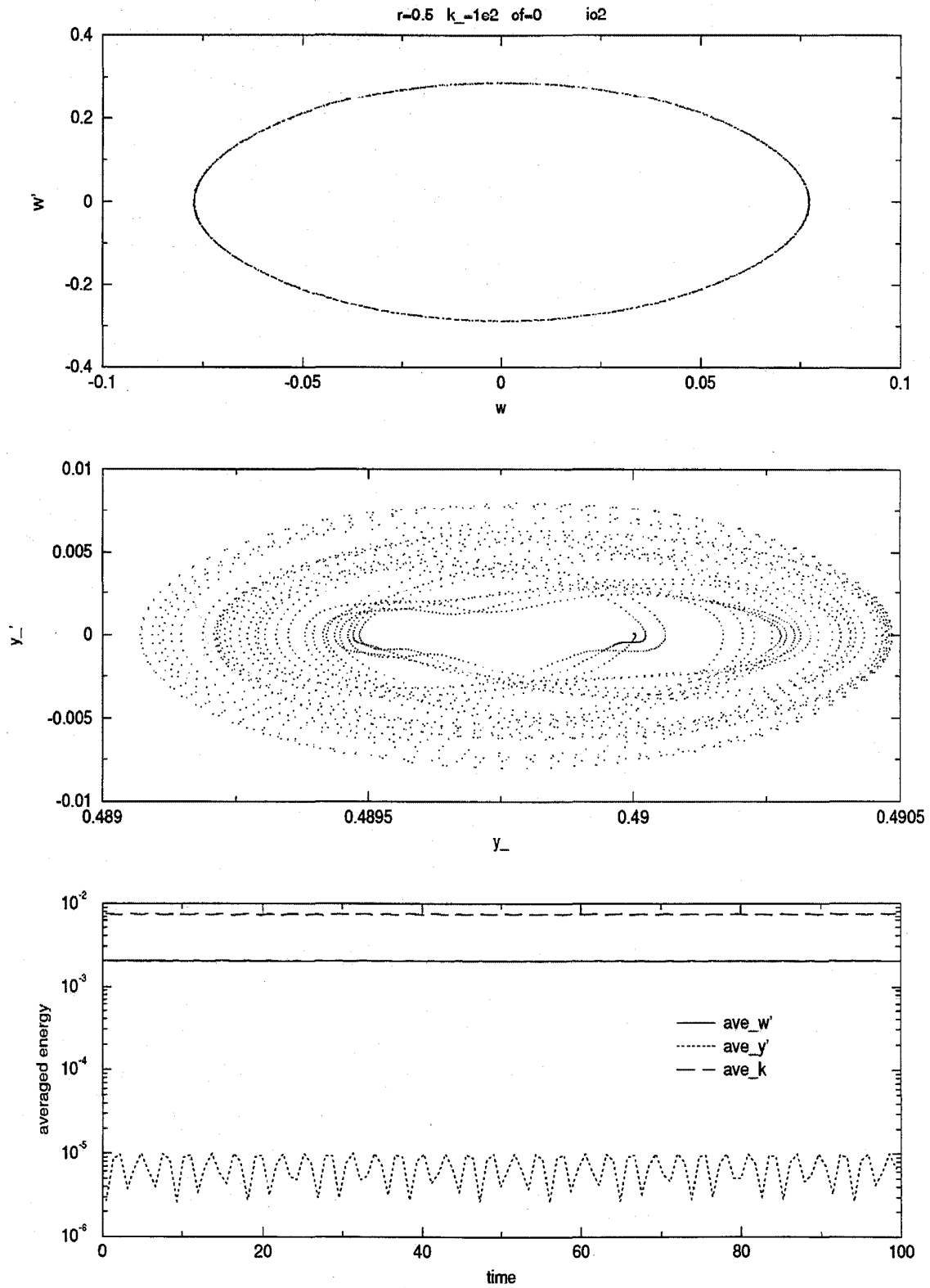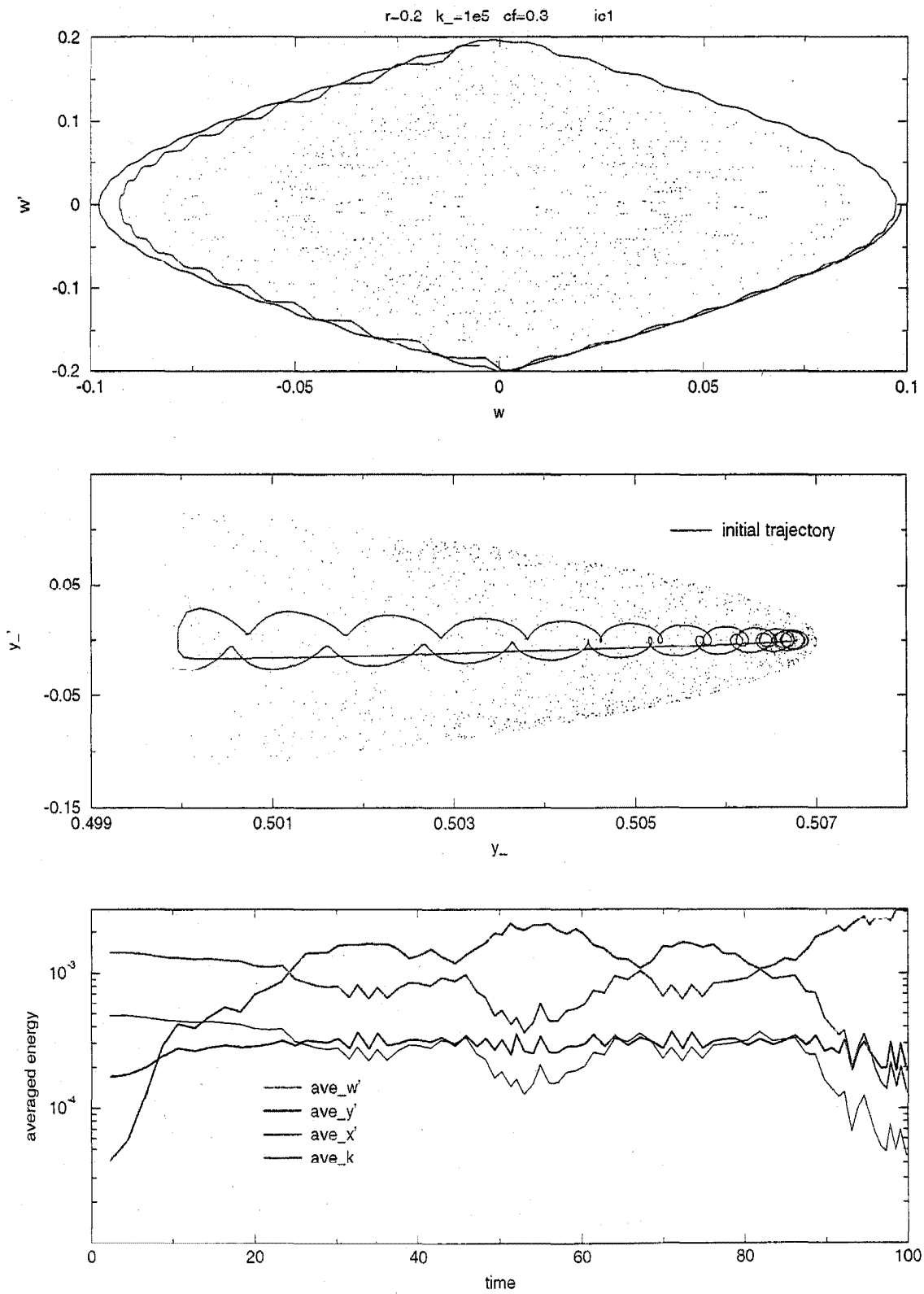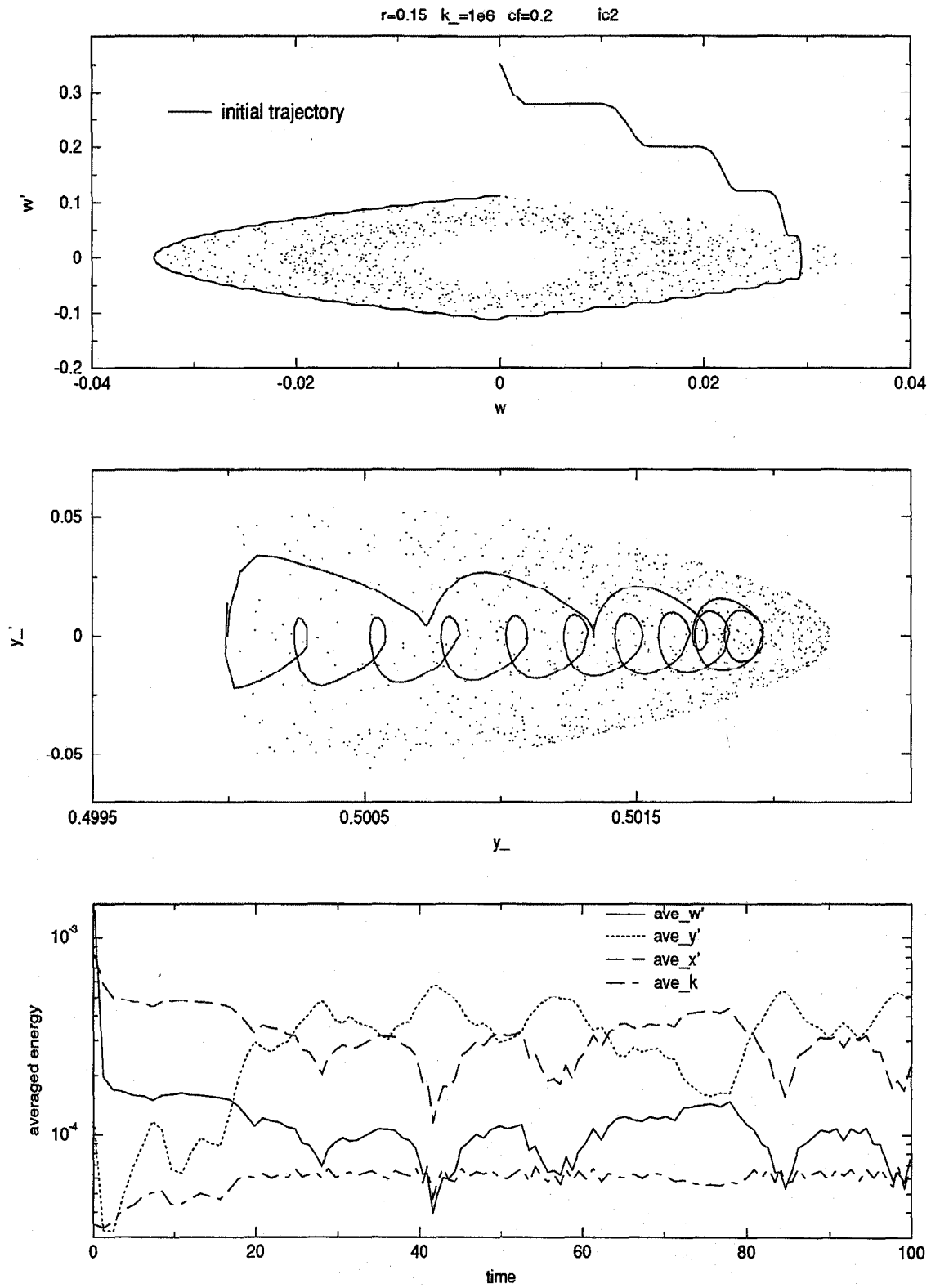Figure 4.55: Rock to vertical $r = 0.15, k_- = 1e6, \mu = 0.2$, ic2

Figure	μ	r	k_-	initial conditions	response type
4.41	0	0.5	10^2	ic1	Steady rocking
4.42	0	0.5	10^4	ic1	Zero friction rock-flight
4.43	0	0.1	10^6	ic1	Rock to vertical
4.44	0	0.5	10^2	ic2	Steady rocking
4.45	0	0.5	10^4	ic2	Zero friction rock-flight
4.46	0	0.2	10^6	ic2	Rock to vertical
4.47	0.2	0.2	10^4	ic1	Steady rocking
4.48	0.1	0.5	10^5	ic1	Settle down
4.49	0.1	0.5	10^5	ic1	Settle down
4.50	0.3	0.2	10^5	ic1	Rock to vertical
4.51	0.2	0.1	10^6	ic1	Rock to vertical
4.52	0.2	0.1	10^6	ic1	Rock to vertical
4.53	0.2	0.3	10^2	ic2	Steady rocking
4.54	0.1	0.2	10^4	ic2	Settle down
4.55	0.2	0.15	10^6	ic2	Rock to vertical

Table 4.1: Long term response figures list

Dominant response types

When the block does not overturn we can divide the response of the system into four dominant types:

$$\text{dominant response types:} \quad \begin{array}{l} \text{Steady rocking} \\ \text{Settle down} \\ \text{Zero friction rock-flight} \\ \text{Rock to vertical.} \end{array}$$

Each of response types occurs for both initial conditions ic1 and ic2. Its occurrence depends mainly on the parameters μ, r, k_-. The four response types above correspond to the types of response discussed in section 4.1 when studying the short term behavior of the block. Description of the four dominant types now follows one by one.

4.4.1 Steady rocking response

This type of response occurs for any μ in the No Flight Region of the (k_-, r) parameter space. In other words, it occurs for smaller values of k_- when the block does not fly. No other type of response occurs in the No Flight Region so we could call the Steady rocking response the No flight response. The block will forever rock back and forth in a quasiperiodic motion. For ic1 the averaged energy components slightly oscillate around a certain constant value and the total energy is conserved. The

same holds for ic2 once a short transient period is passed. Thus, the block moves in a steady-state motion from the beginning when subjected to ic1 and after some transient, energy losing period when subjected to ic2. However, the motion is not periodic, at least not on the time scale the block was observed. While the oscillation in the w, w' plane seems to fall on a closed orbit, the vertical y_-, y_-' oscillation of the block changes in time creating nice patterns. The time length of a swing remains almost constant with only a slight sinusoidal like oscillation. See Figure 4.57 for a typical swing length plot.

4.4.2   Settle down response

This type of response occurs only for coefficients of friction μ greater than 0. It can take place when the aspect ratio is between $0.2 < r < 1$ and for higher k_-, in the region where the block already flies. During the initial transient motion, which also includes flight, the block loses almost all energy due to friction forces. Then it settles down into a small steady-state vertical oscillation, while motion in the x_-, x_-' and w, w' planes is practically eliminated. Even though the vertical oscillation in a steady-state is small, the block still periodically lifts off the surface and flies shortly. The transient, energy dissipating motion is rather short, roughly up to time 5 during which the block rocks back and forth about 5 to 10 times. Dramatic loss of the energy is reflected in the plots of the averaged energy. The total averaged energy decreases at least one order of magnitude. Elimination of the angular rotation is also evident in a sharp decline of averaged rotational kinetic energy ave_w'. As the block settles down, its swings get shorter and shorter. See Figure 4.57 for a typical swing length plot. The time length of a swing falls practically to zero during the transient part of the motion.

For initial conditions ic2, the Settle down response is in some ways similar to the Steady rocking response. In both cases, the system loses energy during its initial transient motion and then settles in a steady-state oscillation. The difference is that in the Settle down response, the block flies during both transient and steady-state motion, whereas in the Steady rocking response the block almost never flies. Furthermore, in the Settle down response, much more energy is lost and the steady-state angular motion is smaller. Steady-state trajectories in the y_-, y_-' plane practically form a simple closed orbit (Figure 4.56).

In both the Settle down and the Steady rocking response types, the block will move in a steady-state motion after a short transient period. In the other two response types, Zero friction rock-flight and Rock to vertical, the block will never settle into steady-state motion.

4.4.3 Zero friction rock-flight response

This type of response occurs only for coefficients of friction $\mu = 0$. We can view it as a counterpart of the Settle down response in a case of zero friction. It takes place in a similar region in the (k_-, r) parameter space (for aspect ratios in the range $0.2 < r < 1$ and larger k_-, such that the block flies). Since there is no friction, energy is conserved. The block never settles down into steady-state motion. It will rock back and forth, move vertically, and fly in a random manner for all times. We do not see any regularity in the behavior or any trend as in the two response types discussed above. Graphs of the averaged energies wiggle in time in an unpredictable fashion. Also, the length of the swing changes rather unpredictably (Figure 4.57).

Initial trajectories travel through the whole dotted region in the phase space plots. This is different than in the Rock to vertical response type.

4.4.4 Rock to vertical response

This type of response occurs for any μ. It takes place for r below approximately 0.2 and large k_-, such that the block flies. This corresponds to a tall, slender block on a hard foundation. The following description of the Rock to vertical response type holds for initial conditions ic1. We observe the same behavior for ic2 only after a short initial energy dissipation.

If $\mu > 0$ the block moves in the beginning mostly in contact mode with short flights during impact. As time increases, flights get longer and more frequent and the contact mode less dominant. However, in any time the slide mode, with its consequent energy dissipation, is limited to a very short time between the flight and contact modes. Thus, energy is almost conserved. If $\mu = 0$, the energy is entirely conserved and we also observe more and longer flights as time increases.

The initial trajectories travel through specific parts of the dotted region in the phase space plots. In the w, w' plane, they travel along the circumference of the dotted region. In the y_-, y_-' plane, they oscillate close to a horizontal line of symmetry of the dotted region. As time progresses, the trajectories move away from their initial paths. In the w, w' plane, trajectories start on the boundary of dotted region and then spiral towards the inside. In the y_-, y_-' plane, trajectories start along a horizontal line of symmetry but then stretch out vertically and spread out across the whole dotted region. This is best illustrated in Figure 4.52 where an initial, as well as a typical, trajectory are drawn in the same picture.

Furthermore, throughout the motion, energy is transfered between different energy components. In the beginning of the motion, the y kinetic energy rises which in turn is balanced by decreasing gravitational potential, x kinetic and rotational kinetic energies. The energy subsequently flows

between different components. The initial energy distribution is not regained. Thus, the y kinetic energy and the potential energy of springs will almost always be higher than they were initially. The x kinetic, the rotational kinetic energy, and the gravitational potential energy are almost always lower than they were initially. The sharp rise of the y kinetic energy right at the beginning of motion is seen clearly in Figures 4.50 and 4.51. The kinetic y energy rises significantly during first 5-8 swings. This energy rise is accompanied by decreasing length of the swings (Figure 4.57).

The three described phenomena, increasing flight time, the difference in initial and later trajectories and the energy transfer are all related. They suggest that a tall block on a hard foundation will rock less but oscillate more vertically during the initial motion, all that with energy practically conserved.

Consider now a simple, real world experiment. We slightly incline a tall, slender block on a flat, hard surface and release it. It rocks less and less over time and all motion quickly dies. One would think that it rocks less only because energy gets dissipated. The described numerical simulation suggests that a tall block has a natural tendency to right itself even when energy is conserved. Thus, the decreasing rocking motion in our experiment may be natural to a large extent and not caused by energy dissipation. Of course later, when the block tends to oscillate more vertically, dissipation takes over and motion disappears.

The Rock to vertical response does not settle into a steady-state. However, unlike the Zero friction rock-flight response, we observe an initial trend toward purely vertical motion.

4.4.5 Response types - summary

We have identified four dominant types of response in the long term behavior of the block subjected to the initial conditions ic1 and ic2. We roughly characterize each of them in the following table.

response type	flight	steady-state	energy	description
Steady rocking	no	yes	conserved	smooth rocking
Settle down	yes	yes	dissipated a lot	motion almost dies slight y oscillation
Zero friction rock-flight	yes	no	conserved	random rocking,flight
Rock to vertical	yes	no	almost conserved	long time energy transfer

For ic2 some energy is dissipated even in Steady rocking and Rock to vertical response types. This dissipation occurs only in the beginning of the motion and for a short time.
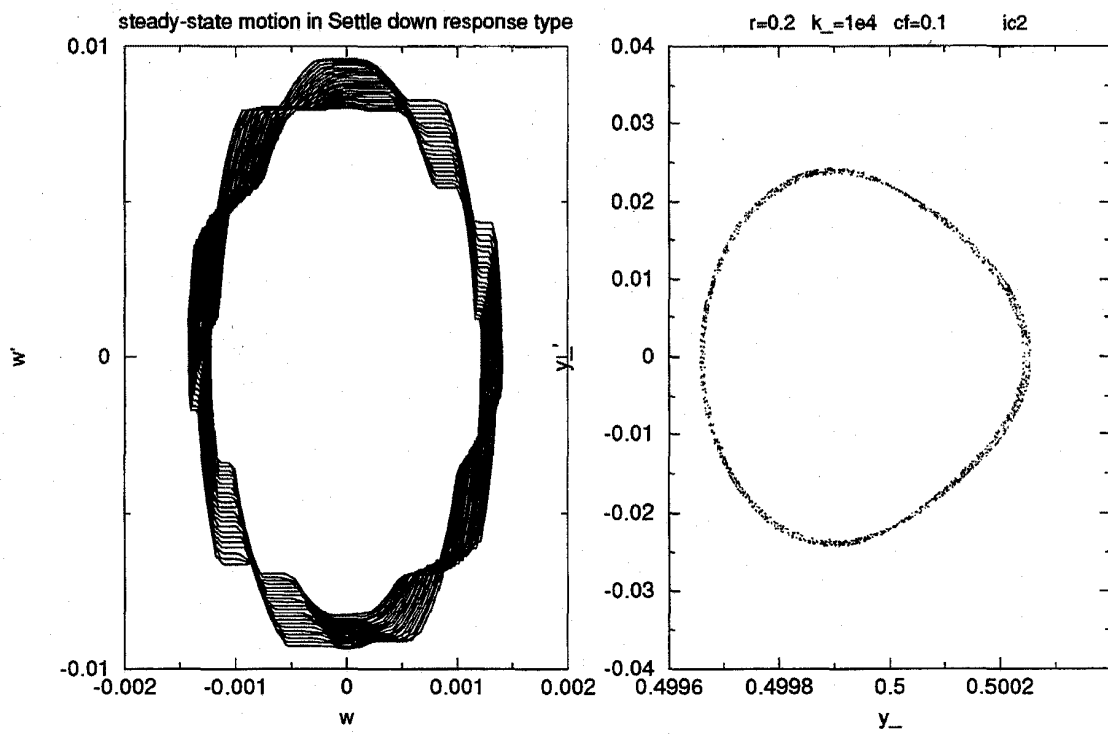
Figure 4.56: Settle down response type: steady-state motion
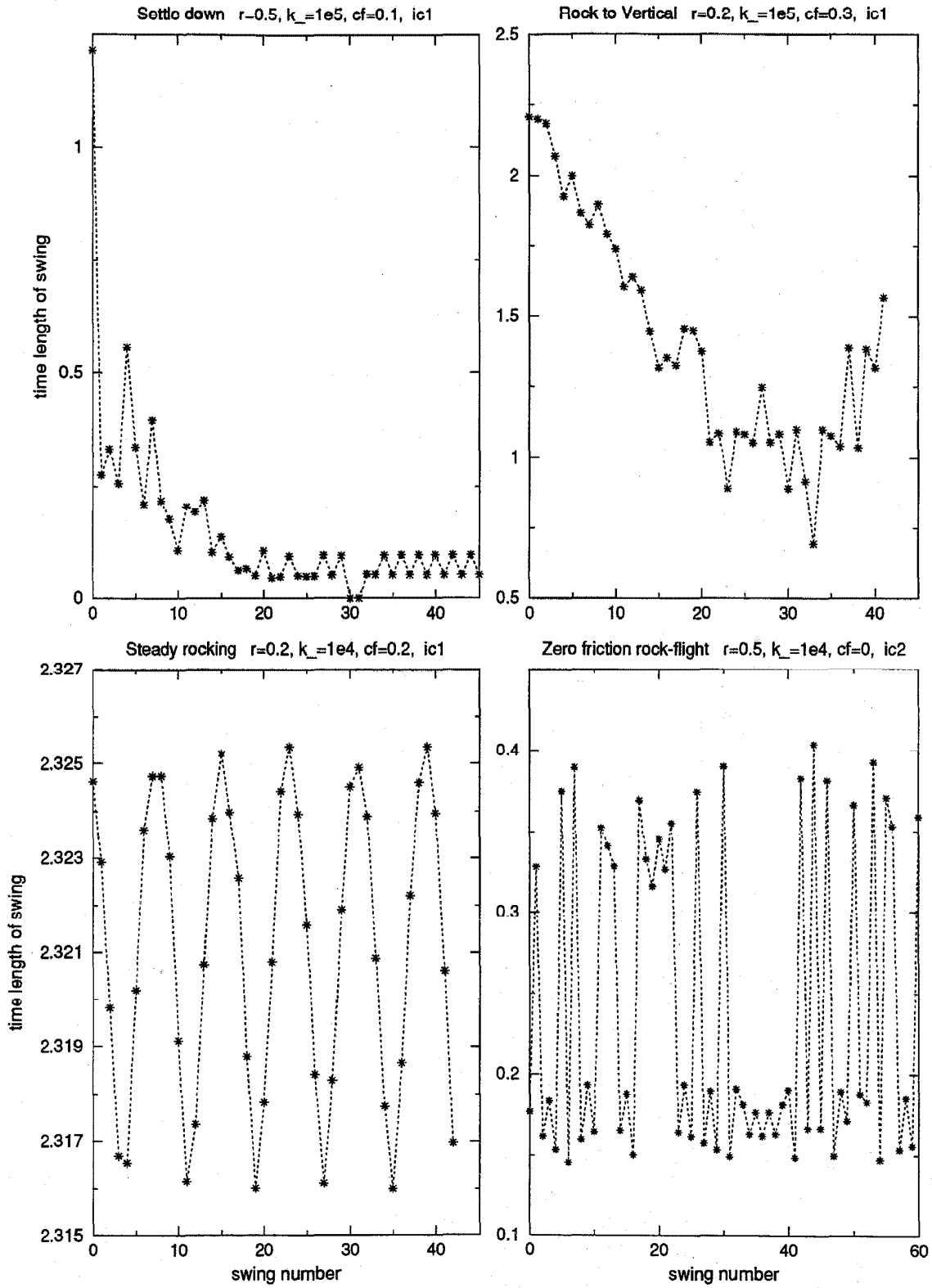
Figure 4.57: Swing time length for different response types

Chapter 5

Sensitive dependence, chaos

Sensitive dependence on initial conditions and parameters in *forced* rigid block dynamics has been already reported in a few publications. The authors *Aslam et al.* [1980] describe experimental shaking table tests:

> ......similar tests using simulated earthquake motions were not exactly repeatable
>
> ...Unlike a linear elastic problem, the rocking problem is very sensitive to small changes
>
> ...a small change in the value of ν (coefficient of restitution) completely changes the time history response under the same ground motion ...

Bruhn and Koch [1991] analyze a simple model of a rocking block subjected to periodic forcing. They prove *analytically* the existence of Smale horseshoe chaos in the dynamics by calculating intersections of stable and unstable manifolds of periodic solutions.

The dynamical system we consider in this thesis is not subjected to external forcing; only *free* vibration of the block is analyzed. In this chapter we provide *numerical evidence of chaos* in such dynamical system ,i.e., *in the initial value problem.*

5.1 Energy conservation and phase space

Phase space of the considered dynamical system is either 4- or 6-dimensional. Conservation and dissipation of energy restrict the set of all possible states of the dynamical system in the appropriate phase space. In other words, the energy considerations restrict motion of the block to a certain subset of the whole 4- or 6-dimensional phase space. Dissipation is possible only in a 6-dimensional space. Energy is conserved in a 4-dimensional space. In either case, trajectories cannot escape a

compact set given by initial conditions:

$$6 \text{ dimensions:} \quad \text{total energy}(x_-', y_-, y_-', w, w') \quad \leq E$$

$$4 \text{ dimensions:} \quad \text{total energy}(y_-, y_-', w, w') \quad = E,$$

where E is the initial energy.

If the system is 6-dimensional we have friction forces. Friction will allow for only a finite x_- variation, meaning $|x_-(t_-) - x(0)| < constant$ $\forall t_-$. The $constant$ is always finite and depends on the initial conditions and parameters. The block cannot travel too far since even a small amount of friction stops it effectively. The system is also invariant under x_- translation so we can consider x_- only in the interval $|x_-| < constant$. We argue that variation in x_- is finite to support the claim that trajectories in a 6-dimensional space cannot escape a compact set given by initial conditions. Thus, all trajectories of a 6-dimensional system will lie on or inside a 4-dimensional surface given by the following equation

$$y_- - 0.5 + \frac{x_-'^2}{2} + \frac{y_-'^2}{2} + \frac{I_- w'^2}{2} + ek(y_-, w) = E, \qquad (5.1)$$

where $ek(y_-, w)$ is the potential energy of compressed springs. The 4-dimensional surface can move in the finite interval $-constant < x_- < +constant$.

If the system is 4-dimensional the situation is simpler. The block is either in the contact mode or the friction is zero. In each case, the energy is conserved and the variables x_-, x_-' do not enter the problem. All trajectories lie strictly on a 3-dimensional energy surface given by equation 5.2 in the $\mu = 0$ case and by equation 5.3 in the contact mode case.

$$\mu = 0: \qquad y_- - 0.5 + \frac{y_-'^2}{2} + \frac{I_- w'^2}{2} + ek(y_-, w) \quad = \quad E \ (5.2)$$

$$\text{contact mode:} \qquad y_- - 0.5 + \frac{(\frac{1}{2}(r \cos w - \sin w)')^2}{2} + \frac{y_-'^2}{2} + \frac{I_- w'^2}{2} + ek(y_-, w) \quad = \quad E \ (5.3)$$

So we know that in a 4-dimensional phase space all trajectories lie on some 3-dimensional energy surface and that in a 6-dimensional phase space all trajectories remain on or within some 4-dimensional energy surface. But the presented phase space plots are in 2-dimensional w, w' and y_-, y_-' planes. Therefore, we would like to know the projection of the energy surfaces 5.1, 5.2, and 5.3 onto our 2-dimensional planes. A bit of algebra shows that the projection of any of the three energy surfaces 5.1, 5.2, and 5.3 onto the y_-, y_-' plane is given by:

	y_-, y_-' projection	y_- range
$E \geq 0$	$y_- - 0.5 + \frac{y_-'^2}{2} \leq E$	$0 \leq y_- - 0.5 \leq E$
	$y_- - 0.5 + \frac{y_-'^2}{2} + \frac{k_-(y_- - 0.5)^2}{2} \leq E$	$-\frac{1+\sqrt{1+2Ek_-}}{k_-} \leq y_- - 0.5 \leq 0$
$E \leq 0$	$y_- - 0.5 + \frac{y_-'^2}{2} + \frac{k_-(y_- - 0.5)^2}{2} \leq E$	$-\frac{1+\sqrt{1+2Ek_-}}{k_-} \leq y_- - 0.5 \leq \frac{-1+\sqrt{1+2Ek_-}}{k_-}$

Projection of the energy surface 5.2 onto the w, w' plane is different than the w, w' projection of 5.3. Formulas for both projections are given in the following table:

surface	w, w' projection	
5.2, $\mu = 0$	$y_R(w) - 0.5 + \frac{I - w'^2}{2} + ek(y_R(w), w)$	$\leq E$
5.3, contact	$y_R(w) - 0.5 + \frac{w'^2}{2}(\frac{1}{4}(r \sin w + \cos w)^2 + I_-) + ek(y_R(w), w)$	$\leq E$,

where $y_R(w)$ was defined in the section on static equilibria as a function satisfying $R_{y_-}(y_R(w), w) = 1$. Equivalently, this definition of $y_R(w)$ means that given w

$$ek(y_R(w), w) + y_R(w) - 0.5 \leq ek(y_-, w) + y_- - 0.5 \quad \forall y_-$$

To put it in words: $y_R(w)$ makes the combined potential energy of the system minimal for a given w. We do not state in an analytical form the w range admissible for a given value of E. This will depend on y_R which we compute only numerically.

Projection of the 4-dimensional surface 5.1 on the w, w' plane will be in general equal to the w, w' projection of 5.2 surface. However, if energy dissipation in the 6-dimensional system is very small then the trajectories will be effectively limited to a smaller set than 5.1, a set whose w, w' projection is equal to the projection of the 5.3 surface. This happens when the block spends most of its time in the contact mode and in flight. Then the system is 6-dimensional but sliding is limited to very short periods during take off and landing and results in only negligible energy dissipation. Such behavior can be seen in the Rock to vertical response.

5.1.1 Projected energy surface and trajectories

Since trajectories must stay on the energy surface they must also stay within its projection on the y_-, y_-' and w, w' planes. Thus, the numerically computed trajectory projected onto the y_-, y_-' and w, w' planes should stay for all times within the analytically derived projection of the energy surface.

We present computed trajectories projected onto the y_-, y_-' and w, w' planes by plotting in constant time intervals discrete points lying on a trajectory. All such trajectory 'dots' should stay within the relevant energy surface projection. Let us verify this by looking at specific examples in

Figures 5.1 and 5.2 where we present w, w' and y_-, y_-' phase space plots for each of the four discussed response types. Indeed in both Figures trajectories stay within the projected energy surface.

An important point to be made here is what part of the projected energy surface the trajectories occupy. For the Steady rocking and Settle down response types in Figure 5.1 the trajectories travel only through a small fraction of the admissible energy surface. On the contrary, for the Rock to vertical and Zero friction rock flight response types in Figure 5.2 the trajectories travel through the whole area of the projected energy surface. However, the fact that trajectories densely fill the whole projection of the surface does *not* imply that they densely fill the whole energy surface itself. In other words, the filled surface projection is a necessary but not sufficient condition for a filled surface itself. We can view it only as a good indication that the trajectories travel densely through the whole energy surface.

5.2 Sensitive dependence

In some subset of the parameter space (μ, k_-, r) even a slight change in a numerical value in the problem will cause a large solution difference later in time. This numerical value can be any of the initial conditions, the integrator time step selection parameter eps, the value of parameters μ, k_-, r etc. The author originally thought this was simply a programming error [Ames et al., 1993]. After long testing, checking and improving of the code, a different conclusion was reached. The code works fine and the trajectory separation is caused by a small initial change in a numerical value. This is a natural property of the dynamical system. The system exhibits *sensitive dependence* on initial conditions.

We give a brief example of the observed sensitive dependence on the initial conditions. We run the code using the parameter values $\mu = 0, k_- = 10^5$, and $r = 0.3$ with the initial conditions ic1. The second run is for the same setting, only the initial y_-' is changed from 0 to 10^{-10}. We stop the computation at time $t_- = 20$ and present results in the following table. In both runs the first flight

$\mu = 0 \quad k_- = 1e5 \quad r = 0.3$	initial conditions ic1	initial conditions ic1, $\ y_-'(0) = 1e - 10$
first flight at $w(20)$ $y_-(20)$ $ihor(20)$	$t_- = 0.604$ $-9.5108e - 02$ $5.1023e - 01$ 25	$t_- = 0.604$ $-3.8973e - 03$ $5.0924e - 01$ 33
$\max_{0 < t_- < 20} \lvert E - E(t_-) \rvert$	$1e - 9$	$1e - 9$

Table 5.1: Sensitive dependence on initial conditions - example

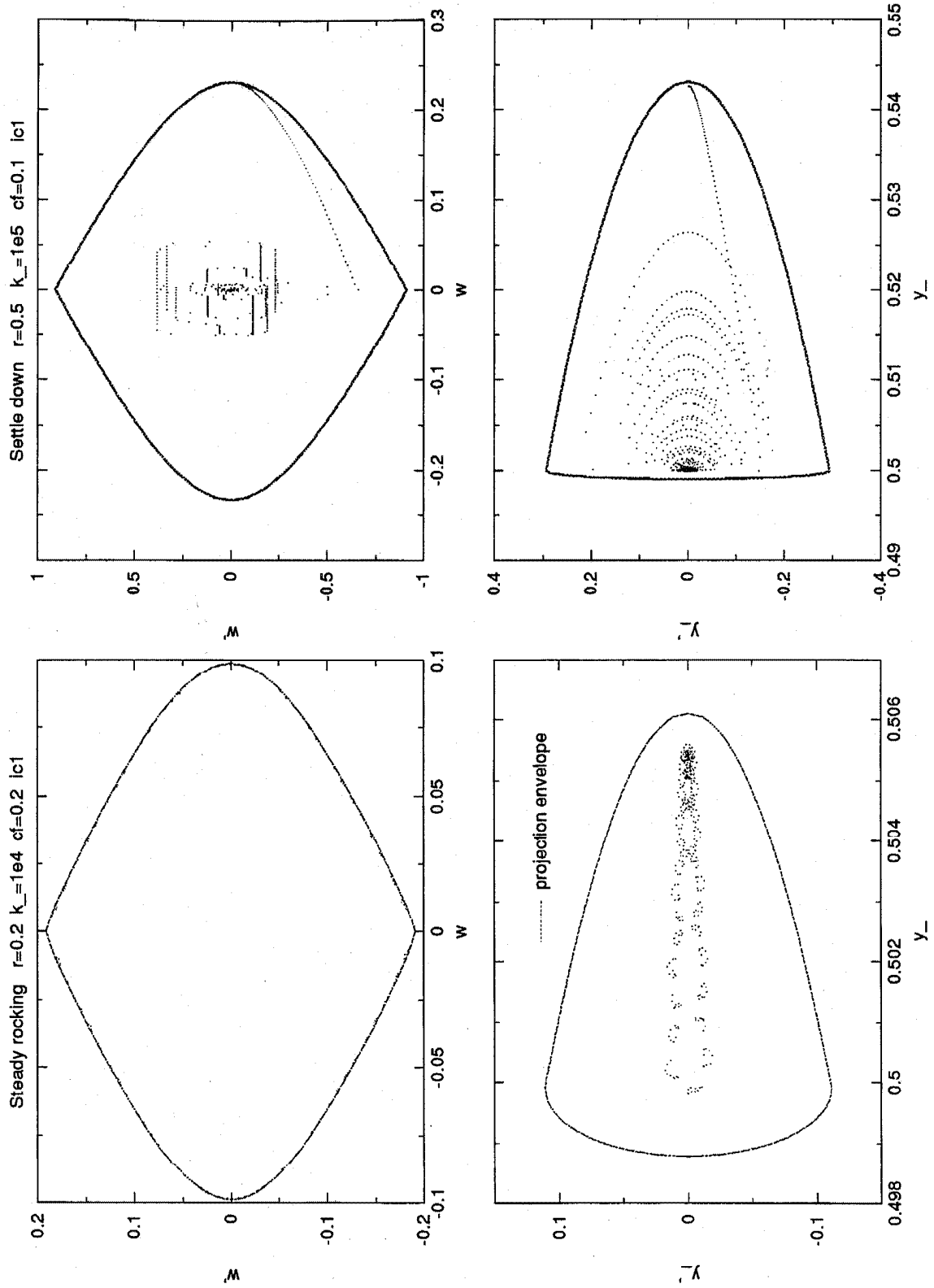occurs at time 0.604. However, at time 20 the values of the variables y_- and w differ completely

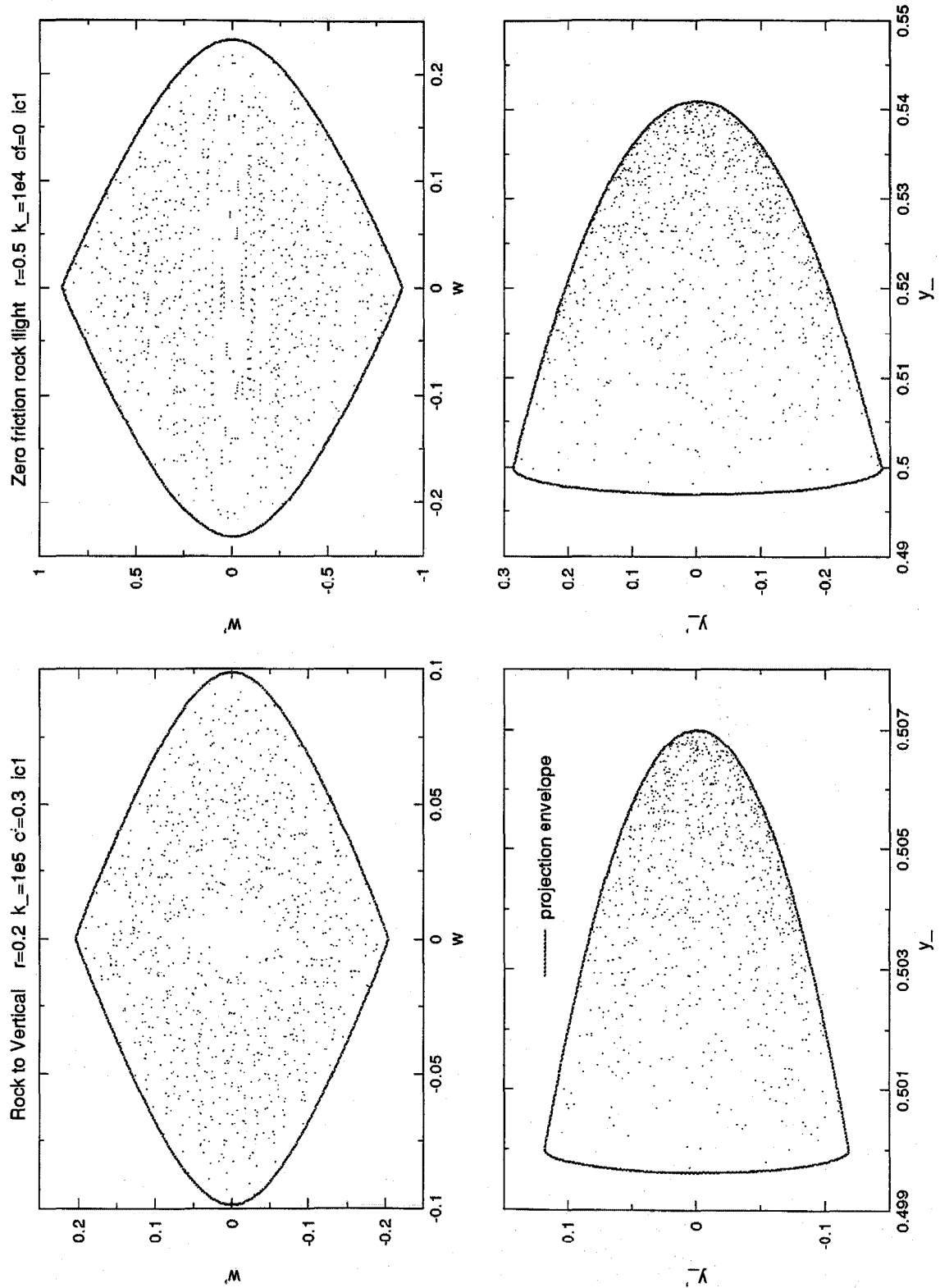Figure 5.1: Energy surface and trajectories : Steady rocking, Settle down

Figure 5.2: Energy surface and trajectories: Rock to vertical, Zero friction rock flight

in the two runs. Also, *ihor*(20) tells us that in the first run the block passed through the $w = 0$ position 25 times whereas in the second run 33 times. Thus, a very small change in the initial condition ($y_0' = 0$ in first run and $y_0' = 10^{-10}$ in the second) results quite quickly in a separation of the two solutions. The solutions become quite different, they are not just out of phase. At the same time we note that the total energy is well conserved in each numerical solution. The largest difference between the initial energy E and the total energy $E(t_-)$ at time $0 < t_- < 20$ is of order 10^{-9}. The initial energy $E = E(0) = 1.586403e - 02$ is of order 10^{-2} so the 7 first digits in the total energy are the same throughout the computation. Conservation of energy is an independent check of the numerical solution. It gives us increased confidence that the described separation of initially close trajectories is due to a natural *sensitive dependency on the initial conditions contained in the mathematical formulation of the system* and not due to an incorrect numerical implementation.

We ought to do more though to claim sensitive dependence. We will use two techniques widely accepted as strong evidence of chaotic behavior. We will study a Poincare map of our dynamical system and we will compute a Liapunov exponent along a trajectory.

5.2.1 Poincare map

A Poincare map is a classical technique for analyzing continuous dynamical systems. The technique cuts an n-dimensional phase space of the dynamical system along an $n - 1$-dimensional surface and then studies the intersections of solution curves with the said surface. This way, continuous-time flow of the n-dimensional system is replaced with an $n - 1$-dimensional discrete map. Advantages of such an approach are a dimensional reduction of the system and possible insightful display of global dynamics of the system. An important point is the selection of the $n - 1$-dimensional cutting surface. For a precise definition and examples of a Poincare map we refer the reader to *Wiggins* [1990] and *Guckenheimer and Holmes* [1983].

In our study a natural choice for the cutting surface is the $w = 0$ hyper plane. The said hyper plane is 3-dimensional in the case of a 4-dimensional space and 5-dimensional in the case of a 6-dimensional space. Thus, in more loose terms, we will be taking snapshots of the moving block each time it passes through the upright vertical position.

We run into the same problem when presenting results as in case of continuous trajectories. How do we display the results from a 3- or 5- dimensional space on 2-dimensional plots? We will project the intersection points from a 3-dimensional hyper plane $(y_-, y_-', w = 0, w')$ onto two planes: y_-, y_-' and y_-, w. We will employ the same projection also in case of a 5-dimensional hyper plane $(y_-, y_-', w = 0, w', x_-, x_-')$ simply forgetting about x_-, x_-' dimensions. Our experience shows that

including plots in x_-, x_-' plane does not give any more relevant information. In the interesting cases, when we suspect chaos, the dynamical system is 4-dimensional, as in the Zero friction rock flight response, or 'almost' 4-dimensional as in the Rock to vertical response.

A trajectory is computed in discrete time steps. It may pass through the cutting hyper plane in a large time step, especially when block is in flight. Therefore, we add to our code a subroutine which computes the intersection of a solution curve with the said hyper plane within machine accuracy.

5.2.2 Liapunov exponent

A Liapunov exponent tells us about the contraction or the expansion of the phase space in direct vicinity of a specific orbit. It tells us at what rate two trajectories starting initially very close to each other will separate. The following definition is from *Wiggins* [1990]: Consider a dynamical system

$$\dot{x} = f(x), \qquad x \in \mathcal{R}^n$$

with the initial condition $x(0) = x_0$. The system is linearized about its solution $x(t)$ by

$$\dot{\xi} = Df(x(t))\, \xi, \qquad \xi \in \mathcal{R}^n.$$

Let $X(t)$ be the fundamental solution matrix of the linearized system and $e \in \mathcal{R}^n$. Then the Liapunov exponent LE in the direction e along the orbit through x_0 is defined as:

$$\text{LE}(x_0, e) = \lim_{t \to \infty} \sup \frac{1}{t} \log \frac{\|X(t)e\|}{\|e\|}. \qquad (5.4)$$

We can view the Liapunov exponent as a time average of the real parts of the eigenvalues of $X(t)$. The dependence on x_0 appearing on the left-hand side of equation 5.4 enters the right-hand side through $X(t)$. The Liapunov exponent LE does not depend on the point x_0 itself; it is an asymptotic quantity and it depends on the *orbit* passing through x_0. So we should view x_0 in the definition of the Liapunov exponent as an orbit label rather than a point.

The Liapunov exponent depends by definition on a particular direction e. Thus, in general for a different direction e, the Liapunov exponent will be different. For a given orbit of an n-dimensional system there exists no more than n different Liapunov exponents.

If we choose the direction e arbitrarily and compute LE from the definition we are almost certain to get the maximal (largest) Liapunov exponent. Simplifying somewhat we would like to compare the convergence to the maximal LE for almost any e to a more familiar situation from linear algebra:

consider the iteration $v_{i+1} = A\, v_i$, where A is a $n \times n$ matrix and v_i an n dimensional vector. For almost any initial choice of v_0 the vector v_i will converge as $i \to \infty$ to the eigenvector belonging to the largest eigenvalue. In a similar fashion, for almost any choice of e, the vector $X(t)e$ will converge to and follow the direction of maximal stretch in $X(t)$ as $t \to \infty$. Consequently, the computed LE will be the largest Liapunov exponent. Only if we choose the vector e to be exactly orthogonal to the direction of maximal stretch in $X(t)$ then we compute an LE other then largest.

In a practical numerical setting the LE computed simply from the definition 5.4 will always be the largest one. This is due to fact that any computer implementation will produce perturbations from $X(t)\, e$. These perturbations are amplified in the direction of maximal stretch in $X(t)$ and eventually the vector $X(t)\, e$ will line up in that direction.

The described convergence to a maximal LE for almost any e is great if we merely want to compute the largest Liapunov exponent. However, it makes computation of the remaining Liapunov exponents more difficult.

Application to the considered dynamical system

In our study, we care to compute only the maximal Liapunov exponent. If for a certain orbit this exponent is positive, then phase space in the immediate vicinity of this orbit expands, indicating sensitive dependence. If the maximal Liapunov exponent is zero, phase space does not expand in the immediate vicinity of the orbit and the trajectories which start close together stay close together and there is no sensitive dependence on initial conditions near the given orbit.

We do not address in the definition 5.4 whether the solution $x(t)$ exists for all times. This is true for the dynamical system considered, since trajectories lie on the energy surface - a compact, bondaryless manifold. Also, the supremum in the definition 5.4 may be dropped in the context of our dynamical system as the limit $\lim_{t \to \infty}$ exists.

We write our own code to compute the Liapunov exponent along a given trajectory of the considered dynamical system. Without going into details of the code structure we refer the reader to *Parker and Chua* [1989] and *Benettin et al.* [1980] who discuss thoroughly practical Liapunov exponent computation. Other references we used on the subject of Liapunov exponents include *Wiggins* [1990], *Wolf et al.* [1985] and *Zaremba* [1992].
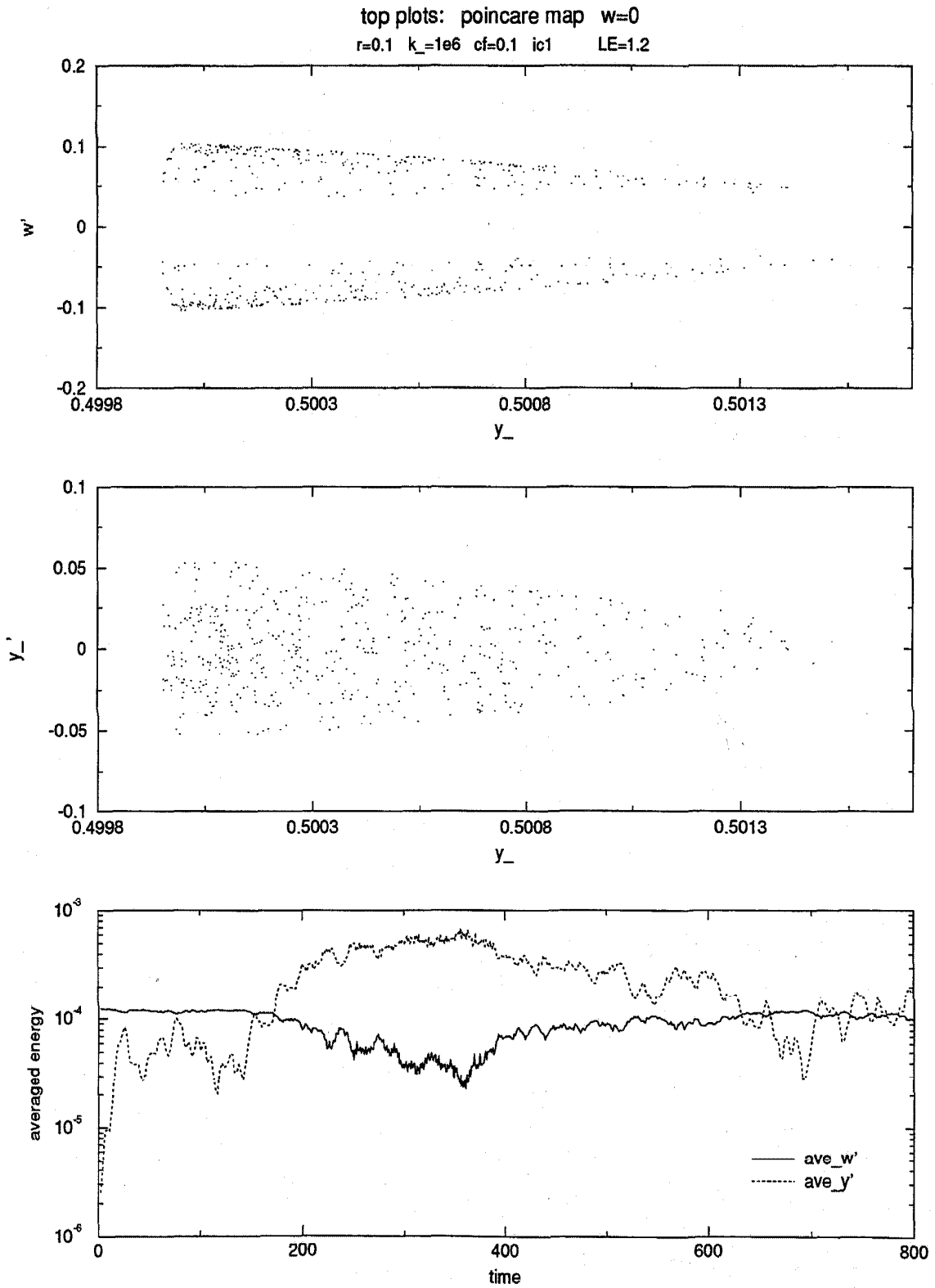
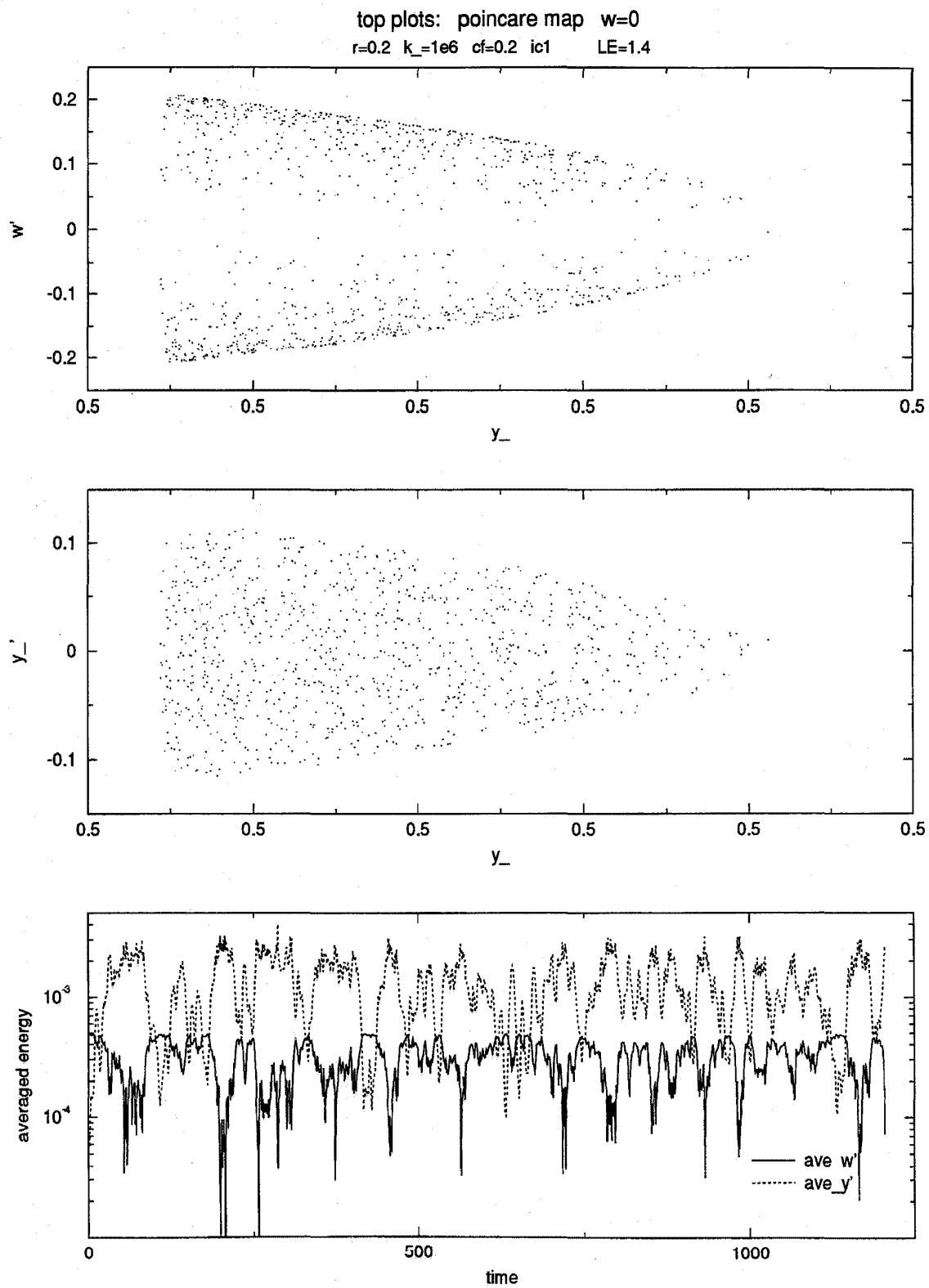Figure 5.3: Poincare map - Rock to vertical response type

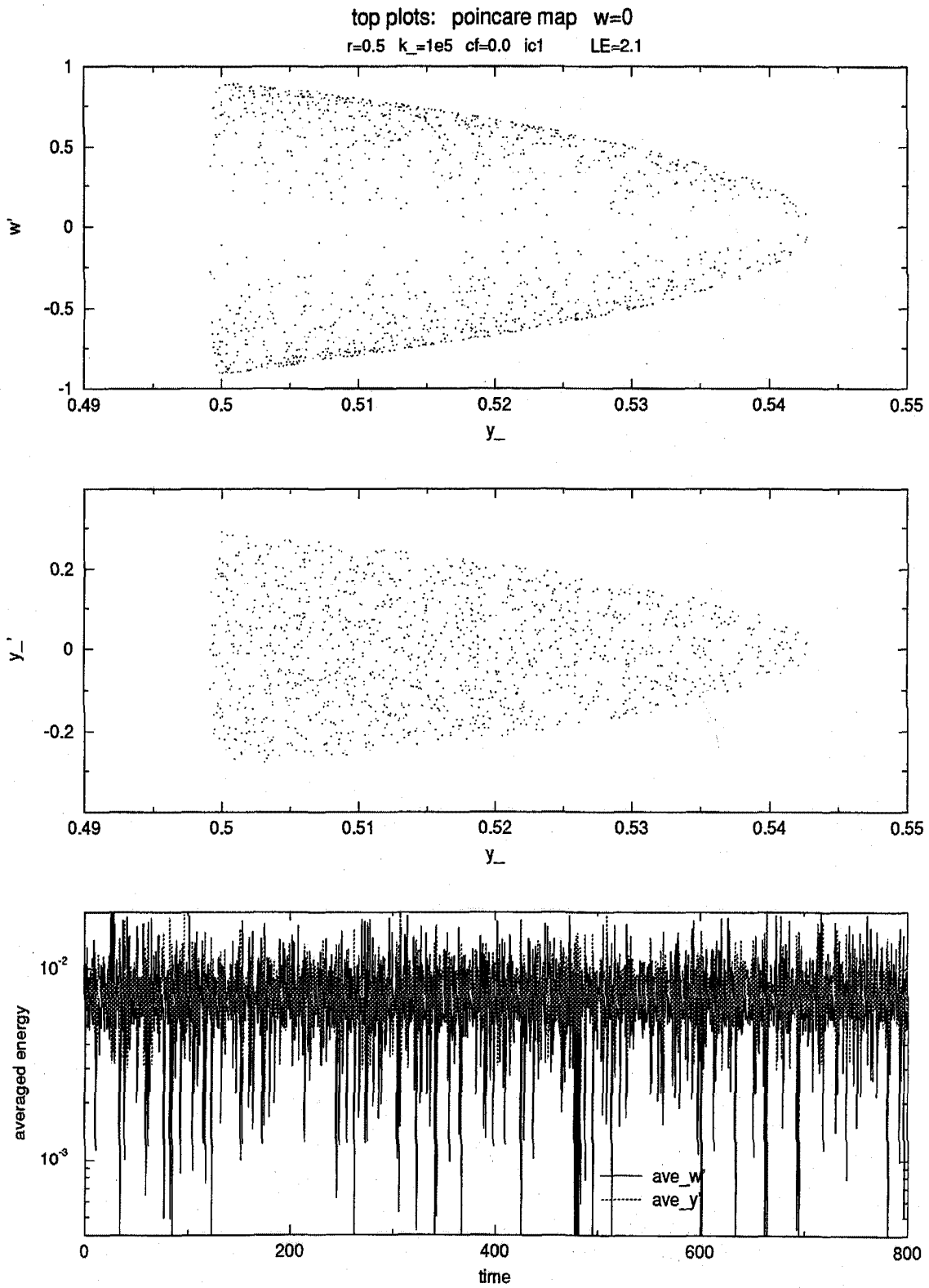Figure 5.4: Poincare map - Rock to vertical response type

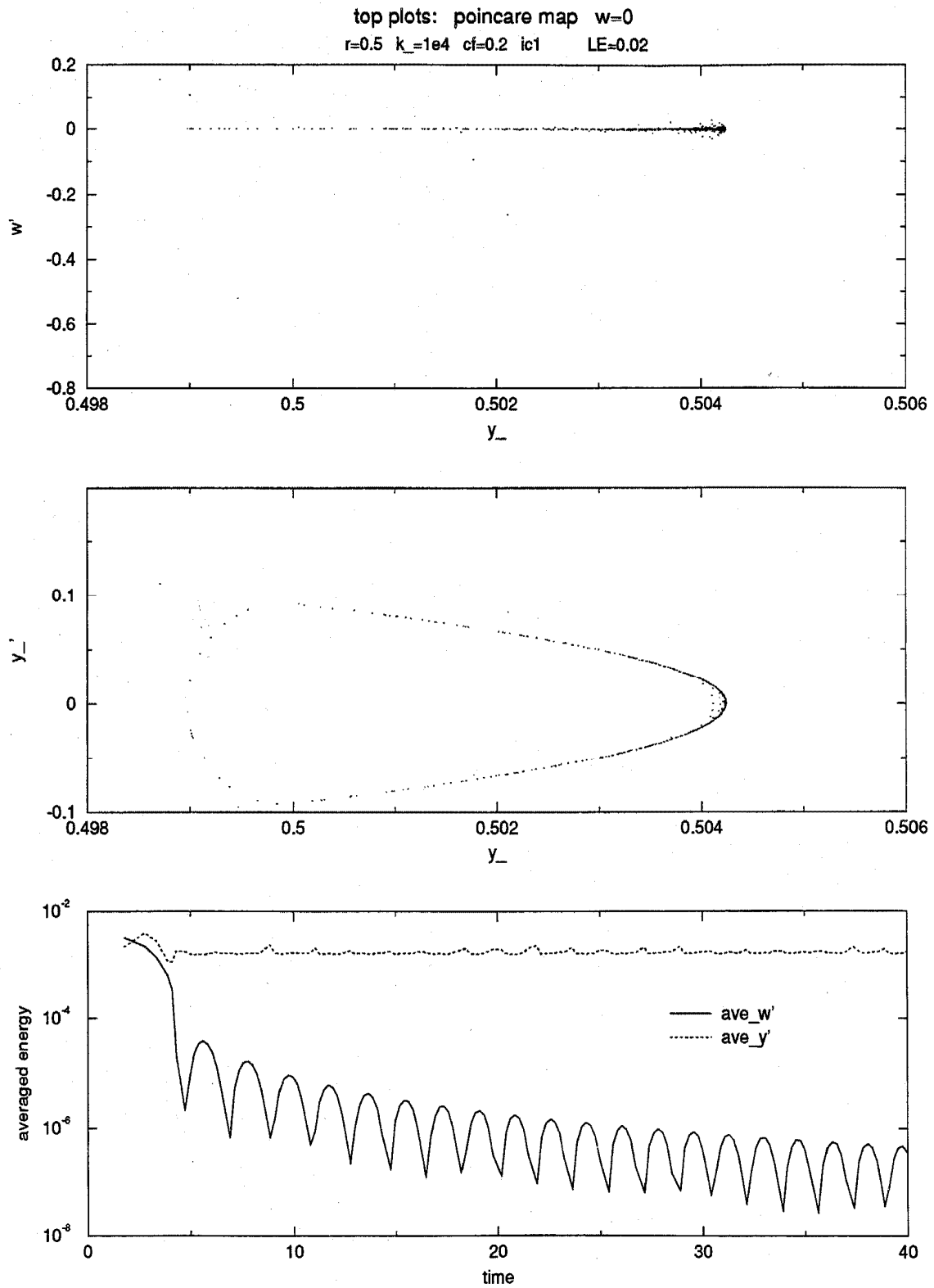Figure 5.5: Poincare map - Zero friction rock flight response type

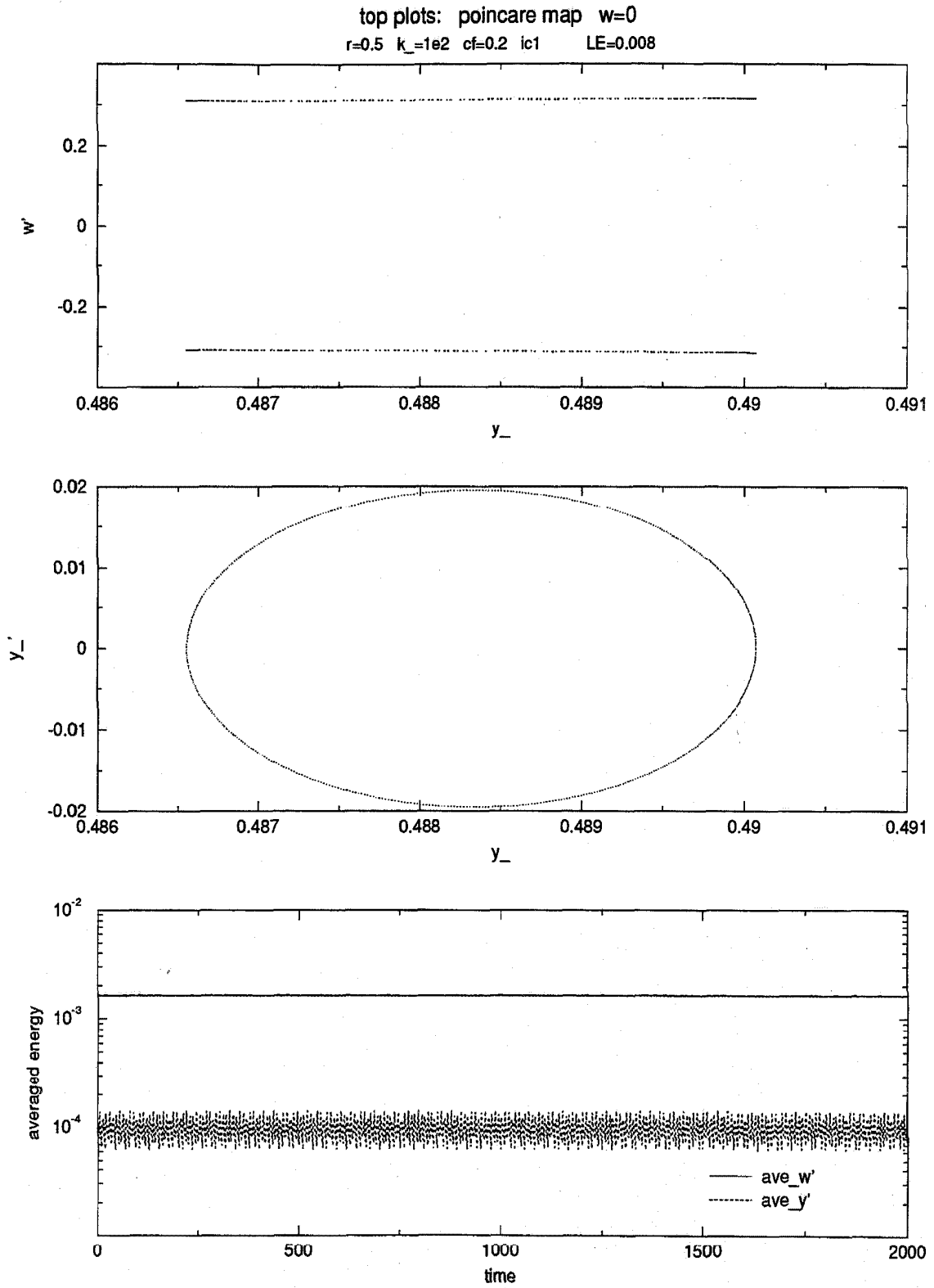Figure 5.6: Poincare map - Settle down response type

Figure 5.7: Poincare map - Steady rocking response type

5.3   Chaos

5.3.1   Chaos - initial conditions ic1 and ic2

In the beginning of section 5.2 we observed that the considered dynamical system exhibited suspected sensitive dependence on the initial conditions in *some* subset of the parameter space (μ, k_-, r). Then we introduced the notion of the Poincare map and the Liapunov exponent. We now use these two numerical techniques to support the claim of sensitive dependence and to show the underlying chaotic structure in the system. We will also specify more closely in *what* subset of the parameter space we observe chaotic structure.

For now we limit our computation of the Poincare map and the Liapunov exponent to trajectories starting with the initial conditions ic1. The results are presented in Figures 5.3 through 5.7. The top two plots of each figure display the Poincare map through the $w = 0$ hyper plane projected onto the planes y_-, y_-' and y_-, w'. The bottom plot shows again the averaged energy versus time, this also tells us up to what time we computed the Poincare map. The title of each figure notes the Liapunov exponent LE for the given orbit. Each figure is for a specific set of parameters, which are chosen so that we present in the five figures all four response types described in the section Long term response.

Response type Rock to vertical is presented in Figure 5.3 and 5.4 and response type Zero friction rock flight in Figure 5.5. We discuss the two at the same time as the computed Poincare maps show a striking resemblance. The Liapunov exponent is larger than 1 for each orbit, even larger than 2 when $\mu = 0$. The computed Poincare map does not create a simple geometric structure, it does not even follow any pattern. The computed intersection points are scattered randomly in phase space. This situation persists as we increase the computation time. The solution trajectory does not converge to any attracting set. It wonders endlessly through the phase space tied to the energy surface E since the energy dissipation is zero or negligible. The solution trajectory seems to travel throughout the whole energy surface although it visits less frequently the area where w' is close to zero.

Response type Settle down is presented in Figure 5.6. The computed Liapunov exponent is close to zero. The Poincare map quickly converges to a simple geometric figure in each projection plane: almost a straight line in y_-, w' and a pear shape in the y_-, y_-' plane. The corresponding steady-state motion is a permanent vertical oscillation with slight angular rotation.

Response type Steady rocking is presented in Figure 5.7. The computed Liapunov exponent is practically zero. All points in this Poincare map fall on two straight lines in the y_-, w' plane and on

an ellipse in the y_-, y_-' plane. The corresponding motion is steady-state rocking.

Thus, in the Rock to vertical and the Zero friction rock flight response types the computed Liapunov exponent indicates a local expansion in the vicinity of the orbit and therefore sensitive dependence on the initial conditions. The Poincare map shows no pattern; the points are scattered randomly indicating a chaotic like motion. On the contrary, in the Settle down and Steady rocking response types the computed Liapunov exponent is close to zero, indicating that the trajectories stay close together if they start close together. The Poincare map creates a simple geometric figure documenting a predictable, simpler type of motion.

The preceding discussion and presented plots were for the initial conditions ic1. We could present similar plots in each response type for the initial conditions ic2 and repeat the discussion above. The only difference for ic2 is an initial energy dissipation when $\mu > 0$. However, the initial dissipation will not change the structure of the Poincare maps.

Chaos ic1 and ic2 - where in parameter space

We have shown a sensitive dependence on the initial conditions ic1 and ic2 and the underlying chaotic structure of the dynamical system at *some* points in the parameter space. For the same initial conditions at *other* points of the parameter space our dynamical system exhibits simple, predictable behavior. Naturally, we want to know where in the parameter space we get chaotic like motion and where we do not - again still limited to initial conditions ic1 and ic2.

When we discussed Poincare maps and Liapunov exponents at specific points in parameter space we referred to that point by the response type it exhibited. We did so somewhat prematurely but for a reason: earlier described response types divide the parameter space into chaotic and non chaotic zones. The response types Rock to vertical and Zero friction rock flight exhibit chaotic structure. The response types Settle down and Steady rocking display simpler, predictable dynamics. Trajectories in these two response types occupy a small subset of the admissible energy surface or, in the case of dissipation, a small subset of the region inside that surface.

Chaotic motion occurs in the parameter space where the corresponding response types reside. The 'chaotic' response types reside, roughly speaking, anywhere in the actual flight region if $\mu = 0$ and in the $r < 0.2$ subset of the actual flight region if $\mu > 0$. For a more precise location of the subset of the (k_-, r) parameter space exhibiting chaotic like motion for ic1 and ic2, see the parametric Figures 6.1 and 6.2 in the final Conclusions section.
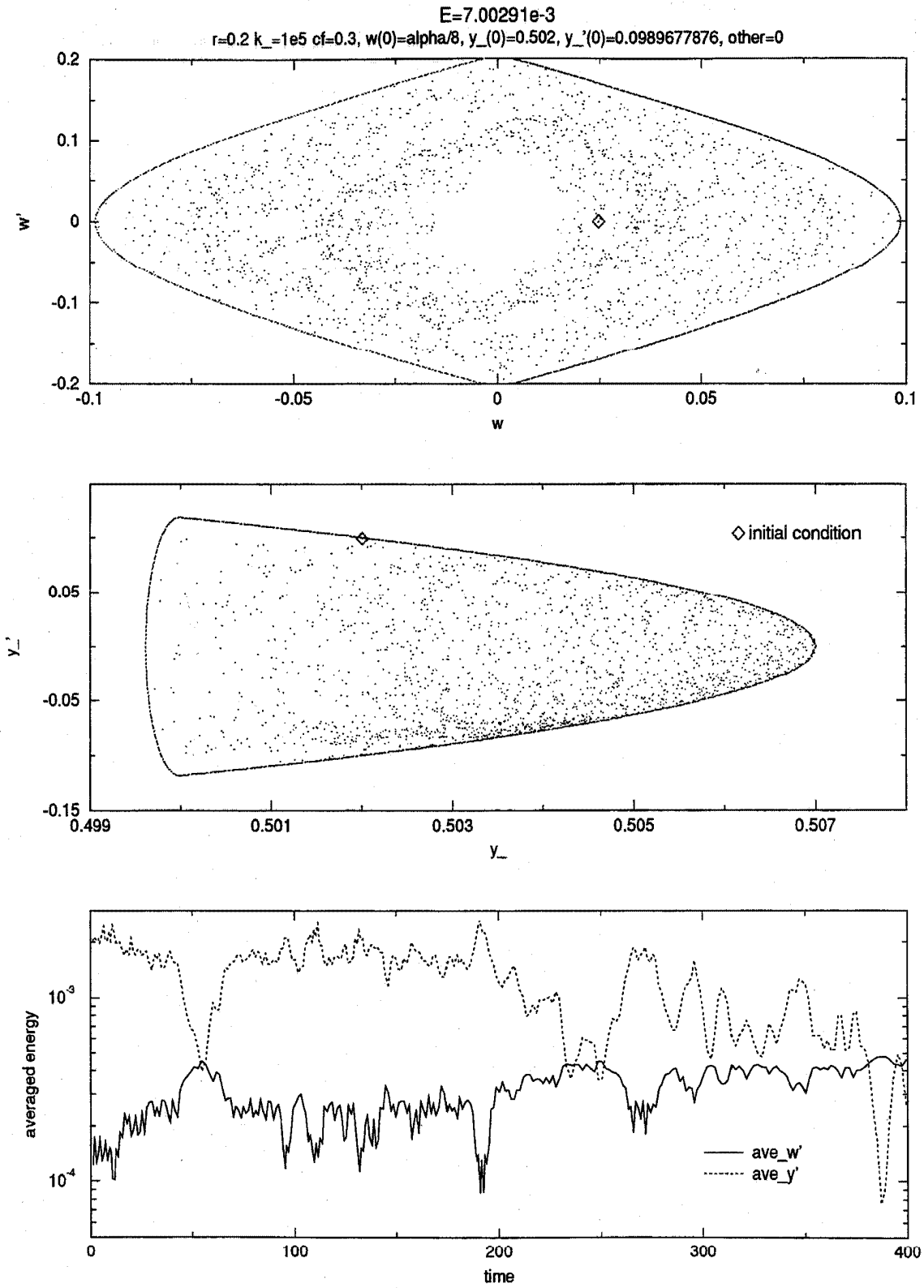
Figure 5.8: $r = 0.2, k_- = 1e5, \mu = 0.3$, typical initial condition set on given surface E

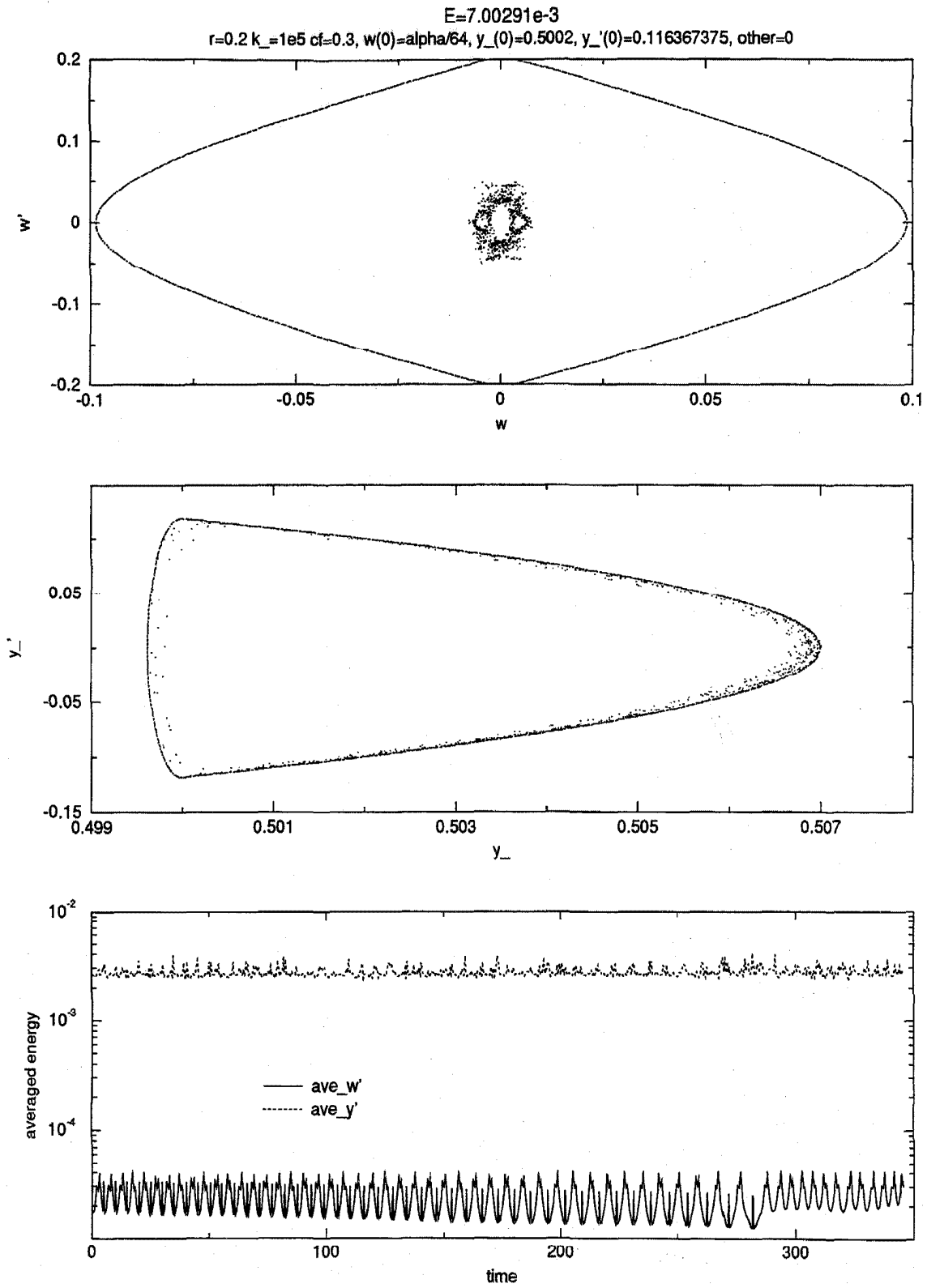Figure 5.9: $r = 0.2, k_- = 1e5, \mu = 0.3$, initial condition set near periodic solution
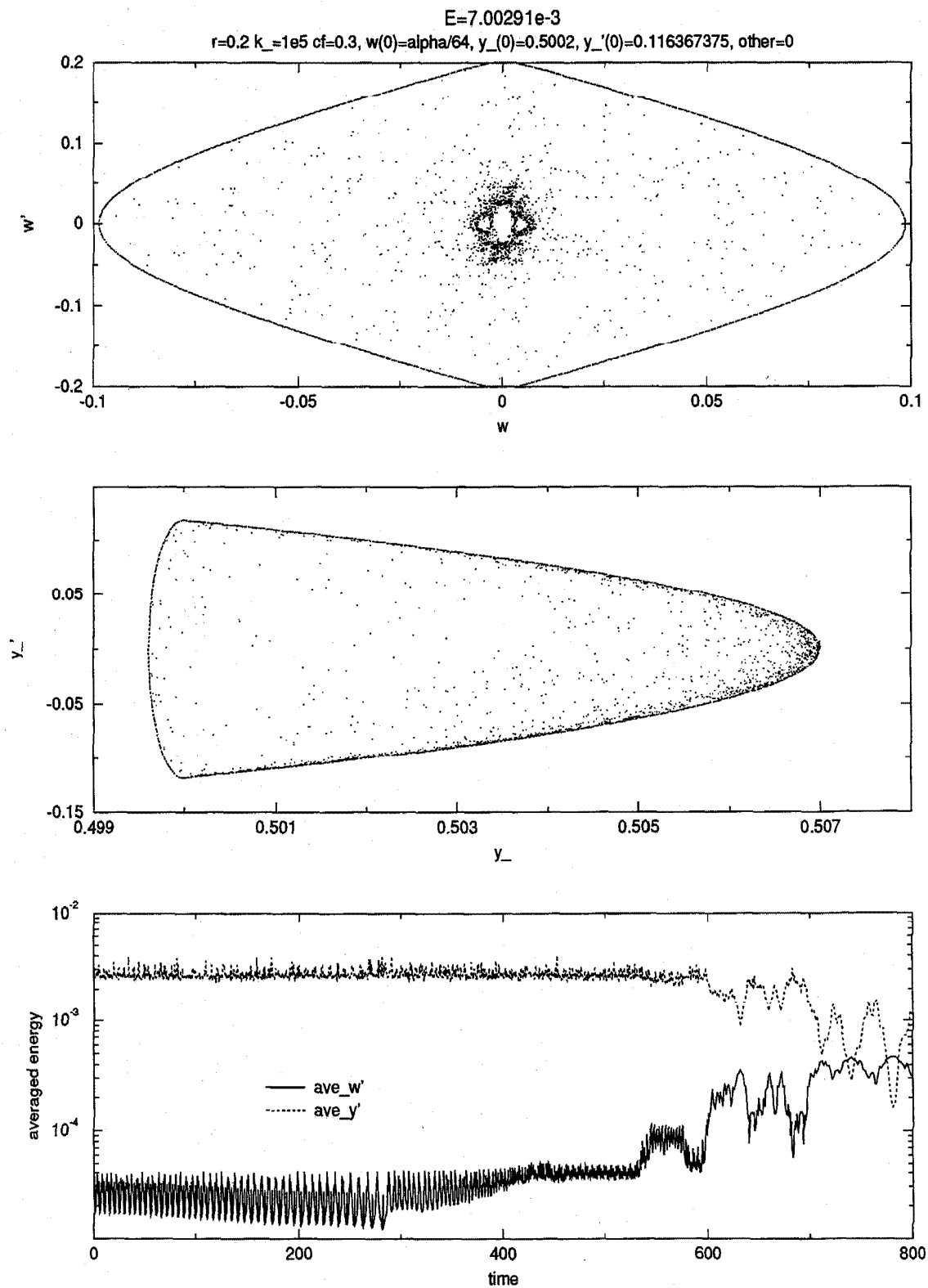
E=7.00291e-3
r=0.2 k_=1e5 cf=0.3, w(0)=alpha/64, y_(0)=0.5002, y_'(0)=0.116367375, other=0

Figure 5.10: $r = 0.2, k_- = 1e5, \mu = 0.3$, initial condition set near periodic solution

5.3.2 Chaos - other initial conditions

We studied in this thesis the dynamics of the block mainly for the initial conditions ic1 and ic2. Thus, we documented chaotic structure of the motion at a certain subset of the parameter space first for ic1 and ic2. Naturally, we have to ask whether such chaotic motion occurs for other initial conditions and where in parameter space. This is a very broad question. If we witness chaotic motion for ic1 at some point of the parameter space then obviously for another choice of initial conditions at the same point the motion may not be chaotic. Just take $y_0 = 0.5 - 1/k_-$ and set all other variables to zero. The block will merely sit there never moving at all. So, for a possibility of chaotic motion at a certain point of parameter space, we have to put enough energy into the initial conditions.

Initial conditions on given energy surface

We will look now at the dynamics of our system for the initial conditions on the fixed energy surface E. Pick a point in parameter space at which the system exhibits the Rock to vertical response type for the initial conditions ic1. For example, take $\mu = 0.3, k_- = 10^5$, and $r = 0.2$. The corresponding energy level for ic1 is E=7.002910e-03. Now alter the initial conditions while staying on the same energy level E. Avoid initial conditions resulting in an initial energy dissipation, i.e., initial conditions making the lowest corner move horizontally.

An initial condition set satisfying the above criterion is $y_0 = 0.502, y_0' = 9.8967787616e-02, w_0 = \alpha/8$, all other variables set to zero. The response of the system subjected to this initial condition set is presented in Figure 5.8 in the form of phase space plots. Comparing Figures 5.8 and 5.2, we see that the response at $\mu = 0.3, k_- = 1e5, r = 0.2$ is qualitatively same for the above initial condition set as for ic1.

We observed that at a specific point of parameter space the response was qualitatively the same for ic1 as for the different specific set of initial conditions on the same surface E. Numerical simulations show this to be true in general. Namely: Pick any point in parameter space where the initial conditions ic1 result in chaotic like motion. Let the energy level given by ic1 at that point be E. Then for almost any other initial condition set on E avoiding initial dissipation the response of the system is qualitatively same as for ic1. The system exhibits at the given point of parameter space *chaotic motion, with long time energy transfer if $\mu > 0$,* for almost any initial condition set on E avoiding initial dissipation.

Slight differences in the response to ic1 as opposed to other initial conditions on E may be in the direction of the initial energy transfer. Set ic1 is special in that it lies on the envelope of the

energy surface projected onto the w, w' plane. The ic1 trajectory will move inside the envelope which corresponds to an initial transfer of rotational kinetic energy to y kinetic energy. Other initial conditions may lie inside that envelope, as in Figure 5.8. Then the initial energy transfer may not be in the same direction as for ic1.

Initial conditions on a given energy surface near the periodic solution

We stated above that the response of the system is the same for ic1 as for *almost* any initial condition set on E avoiding initial dissipation. Now we consider the "not almost any" initial conditions on E, that is initial conditions which lie on E and avoid initial dissipation but do not result in qualitatively same response as ic1.

Such initial conditions lie in a direct vicinity of the periodic solution $w(t_-) = 0$ $\forall t_-$, when the block merely moves vertically. A specific example of the system's response to such initial conditions is shown in Figure 5.9 in the form of phase space plots. The block moves vertically with only slight angular motion. This kind of response is rather simple and predictable. The resulting Poincare map forms a simple geometric figure and the motion is not chaotic.

But wait! In Figure 5.10 we present the response of the system at the same point of the parameter space for the same initial conditions - only computed for longer time. Roughly at time 600 the response changes dramatically. The trajectories escape the direct vicinity of the periodic solution and start moving all over the energy surface. The response becomes chaotic, qualitatively the same as for ic1 and other initial conditions on a given E.

Numerical simulations show that the closer to the periodic solution we start, the longer it takes to escape the direct vicinity of the periodic solution. It is unclear whether there exists a small invariant subset of phase space containing the periodic solution or whether any trajectory, no matter how close initially to the periodic solution, will escape its vicinity at some finite time. The periodic solution itself never escapes of course - it is periodic. While we realize this is a good point for perturbation analysis of the system at small angles w, we have not done so yet.

For an interesting related observation look again at Figures 5.8 and 5.2. The trajectories move around the whole projected energy surface but visit less frequently the vicinity of the periodic solution. As time increases, the trajectories come closer to that vicinity, however, they never stay there long. Again, it is not clear whether the trajectories would come arbitrarily close to the periodic solution at some finite time or whether they forever avoid some invariant subset containing the periodic solution.

146

Various initial conditions - examples

We present now the response of the system to a few selected initial condition sets. While we realize this is not exactly a systematic approach to the study of chaos, the presented plots will at least show some types of chaotic motion not described on the previous pages. Notation ic $z(0) = z_0$ means an initial condition set ic, where the value of $z(0)$ is changed to z_0.

Figure 5.11 displays the response of the system to the initial condition set lying on the same energy surface as ic1, at the given point in parameter space. The system responds first with rather simple y and w oscillations. As time increases, the energy transfers very slowly but steadily from y oscillations to angular motion. Points in the Poincare map get scattered around indicating underlying chaotic structure.

Figure 5.12 shows a distinct geometric structure in the Poincare map. Points in the Poincare map are scattered again indicating chaos but this time they are confined to a certain geometric structure on the energy surface. Previously, the intersection points were scattered randomly over the whole energy surface when chaos was suspected. Roughly at time 120, motion seems to settle to steady state as is apparent from graphs of the averaged energies. The points are now confined to only a part of the geometric structure. However, later, at time 250, the points escape again and wonder around. This phenomena is quite common in our system in case of chaotic motion.

Figure 5.13 displays a rather simple type of response: rocking with slight vertical oscillations. The Poincare map creates a few simple lines with no indication of chaos. Now look at Figure 5.14, which shows the response to the same initial conditions and same parameters, only computed for a longer time. We see that at time 200 the response drastically changes. Points in the Poincare map jump out from the old simple lines and the vertical oscillation increases while the angular rotation decreases. Subsequent energy transfer is apparent and so is chaotic structure as the points in the Poincare map travel now randomly on the energy surface. The Poincare maps in the two figures are drawn at the same scale for comparison.

5.3.3   Chaos - conclusions

In certain subsets of parameter space and for certain initial conditions the considered dynamical system exhibits chaotic behavior. To support and document such claims we have computed numerically for specific orbits Liapunov exponents and Poincare maps. Positive Liapunov exponents indicate a sensitive dependence on the initial conditions. Scattered points in the Poincare map confirmed this and further displayed underlying chaotic structure.

It is hard to make *general* statements about where in the parameter space the considered sys-
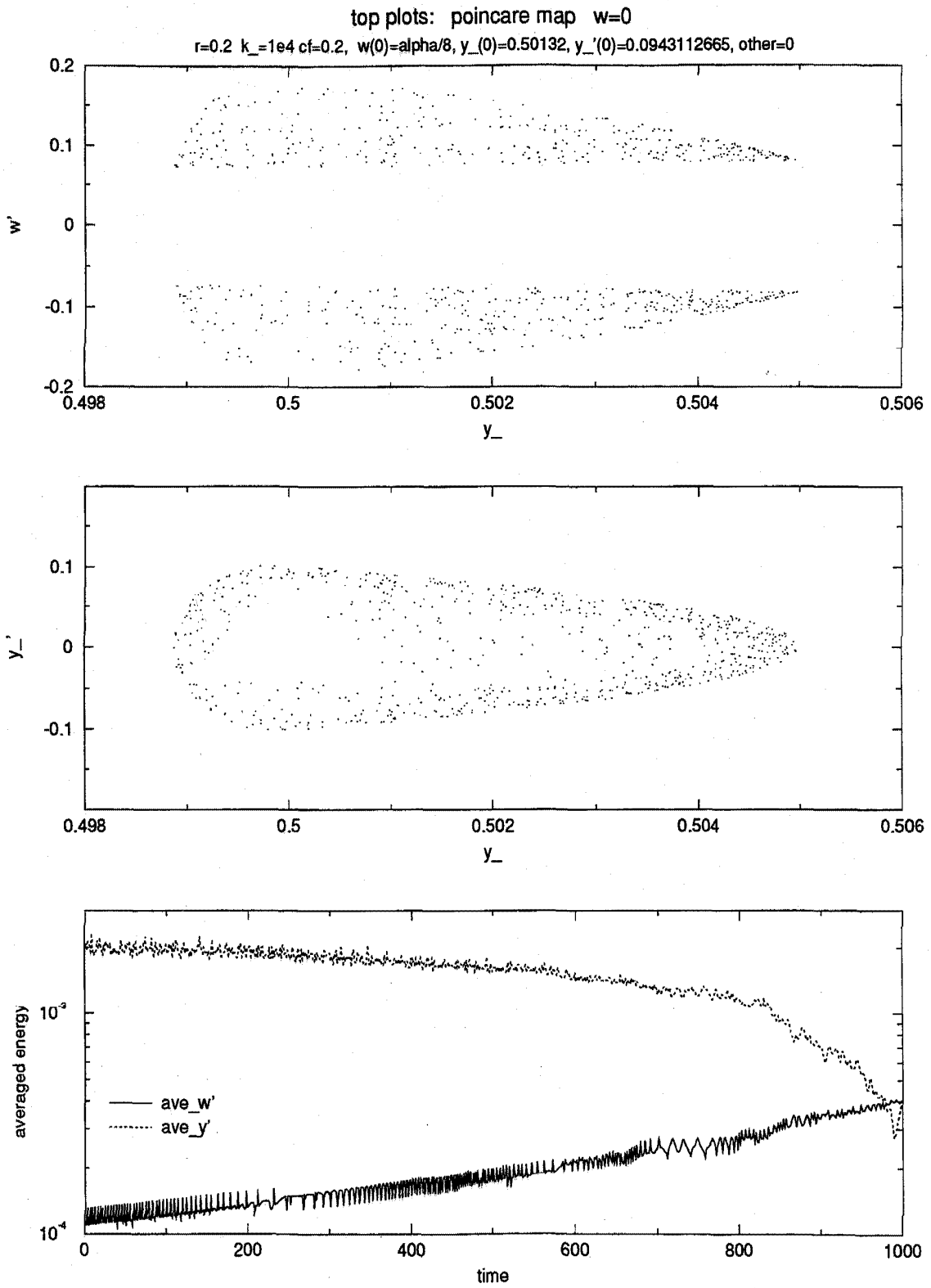
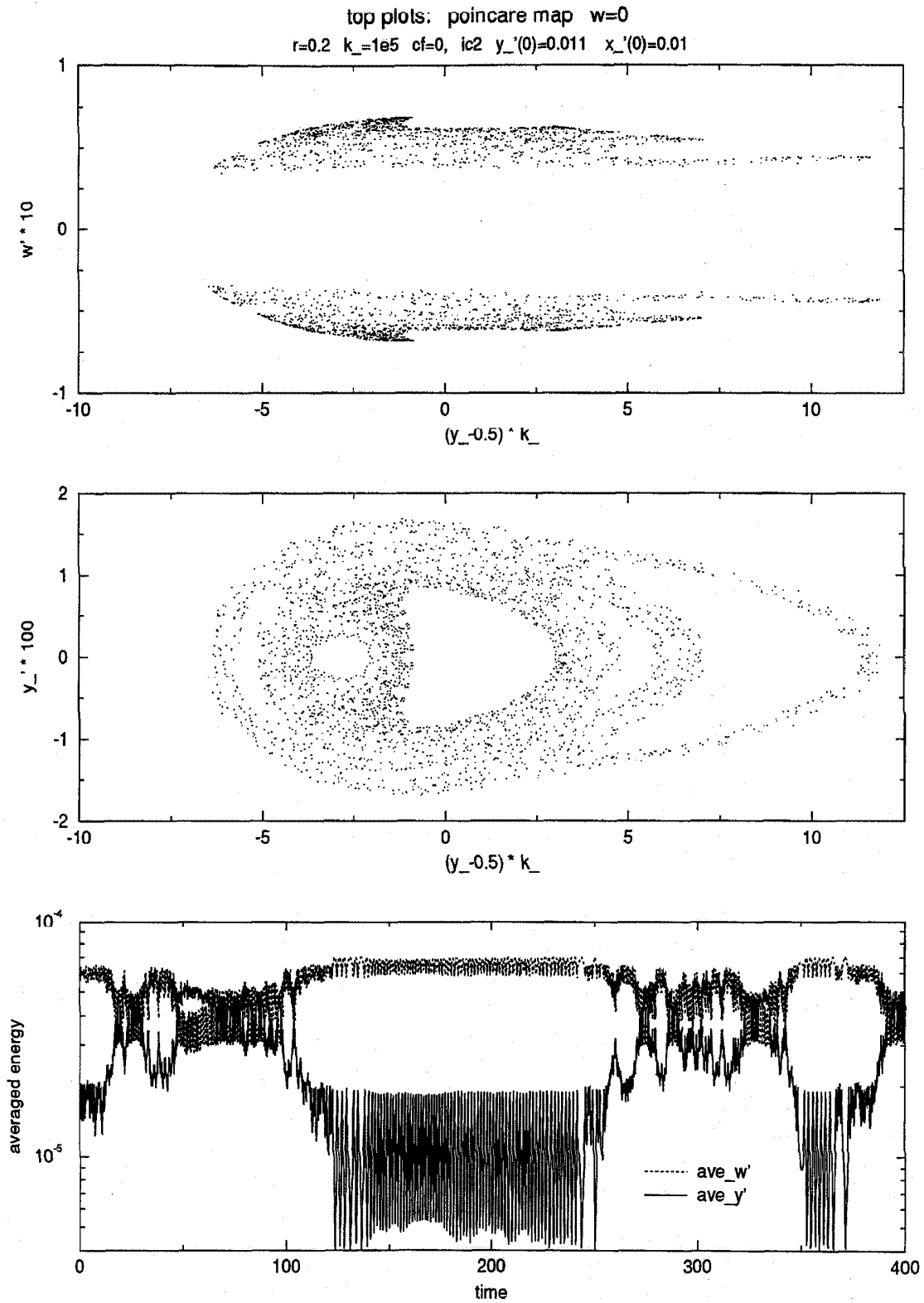Figure 5.11: Poincare map, $r = 0.2, k_- = 10^4, \mu = 0.2$, slow, long time energy transfer

Figure 5.12: Poincare map, $r = 0.2, k_- = 10^5, \mu = 0$, patterns

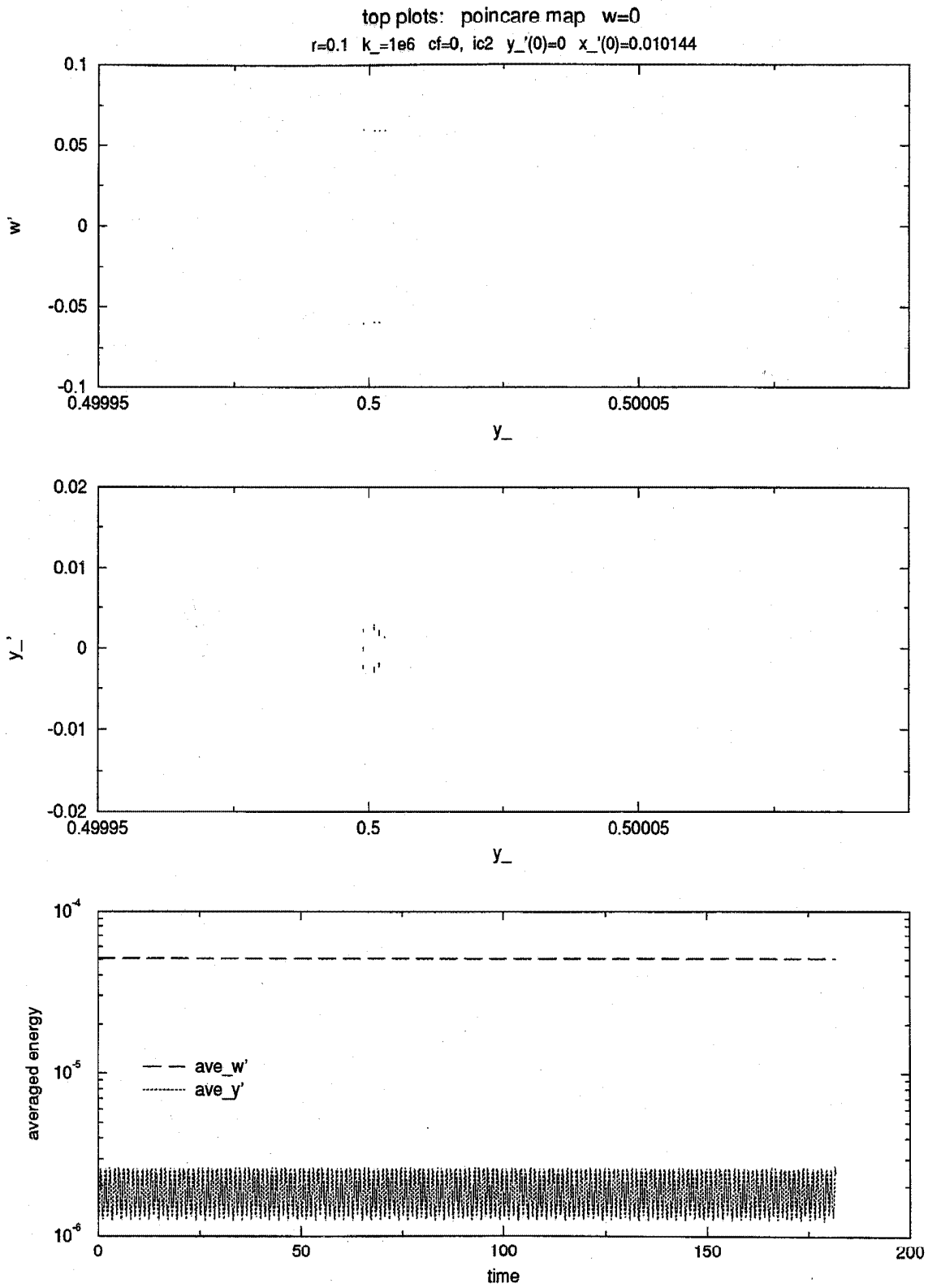Figure 5.13: Poincare map, $r = 0.1, k_- = 10^6, \mu = 0$, rocking

top plots: poincare map   w=0
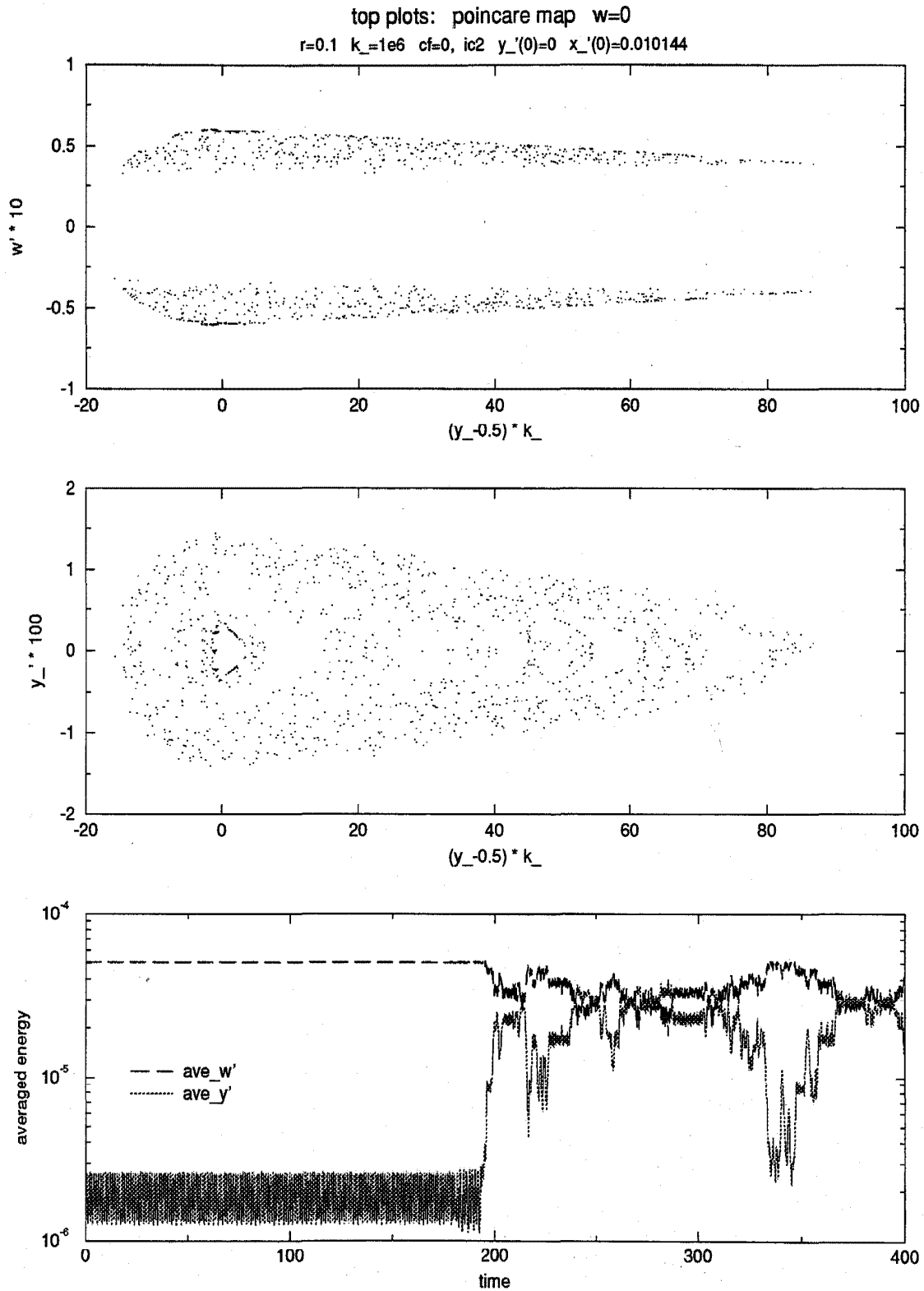
r=0.1 k_=1e6 cf=0, ic2 y_'(0)=0 x_'(0)=0.010144

Figure 5.14: Poincare map, $r = 0.1, k_ = 10^6, \mu = 0$, rocking changes to chaos

tem exhibits chaos and for what initial conditions. We shall try to do so - based on our limited observations.

Consider an arbitrary but fixed point p in the (μ, k_-, r) parameter space. Let a real constant E be an energy level given by the initial conditions at p. For a given p let $E_f(p)$ be the lowest energy level such that flight results for all initial conditions on $E_f(p)$ avoiding initial dissipation.

- Chaos and flight are closely related and no flight implies no chaos

- If $E < 0$, then no flight and consequently no chaos is possible

- if $E > E_f(p)$, chaotic motion results at point p for almost any initial conditions on E avoiding initial dissipation unless

  1. the block overturns

  2. energy is dissipated significantly

  the resulting chaotic trajectories seem to fill the whole surface E except possibly the direct vicinity of the periodic solution $w(t_-) = 0 \ \forall t_-$

- if $0 < E < E_f(p)$, the response of the system at p is

  1. simple predictable motion without flight or in vicinity of the periodic solution   or

  2. chaotic motion limited only to a subset of E (or a subset of an energy level lower than E if dissipation took place) possibly creating more complicated geometric figures

- we have not observed the presence of an invariant attracting chaotic set of complicated structure which repeats itself under resolution as in *Lorenz* [1984] (a strange attractor on a Cantor set)

The widely accepted definition of chaos, see for example *Wiggins* [1990] page 608, requires sensitive dependence and topological transitivity on a compact invariant set. We have shown quite convincingly sensitive dependence on the initial conditions. The energy surface E is compact. It is a preimage of a compact set (point) of a continuous function (total energy) from $\mathcal{R}^n$ to $\mathcal{R}$. Topological transitivity on E (or its subset) is likely, as seen in the presented computer simulations, but not certain.

Chapter 6

Conclusions

The dynamical system studied consists of a rigid, rectangular block moving on continuous, elastic foundation. Friction forces resist horizontal movement of the block on the foundation surface. The system is modeled in 2 dimensions allowing for general, unrestricted motion; the block can leave the foundation surface and fly, and at the same time it can rotate, move horizontally or vertically. The magnitude of the friction forces at a given moment determines whether the lowest corner of the block is prevented from horizontal travel or whether it slides resulting in energy dissipation.

At most two corners of the block can sink under the foundation surface at any given moment. Motion is observed only up to the point of overturning, that is when the block's diagonal becomes vertical. Otherwise there are no restrictions; the model is fully nonlinear and no simplifications assuming only small rotation angles or only tall blocks are made.

The parameters of the problem are reduced by dimensional analysis to the following three: the coefficient of friction μ, the aspect ratio $r = b/a$ and a non-dimensional stiffness $k_- = \frac{k\,ab}{mg}$, where b is the width of the block, a its height, k the original stiffness characterizing the elastic foundation, m the mass of the block, and g the gravitational constant.

A parametric study is carried out identifying the dominant types of response. Tendency to fly as well as block stability against overturning are also studied.

Dominant types of response

Steady rocking quasiperiodic motion, the block rocks back and forth, no flight, energy is conserved

Settle down strong transient energy dissipation, then the block settles in small vertical oscillations

Zero friction rock flight energy is conserved, chaotic motion, block rotates, moves vertically including flights

Rock to vertical typical for tall blocks on hard foundations, chaotic motion, long time energy transfer between different energy components, total energy practically conserved

Flight tendency

Flight tendency is high for a square block and decreases as the block becomes taller. Flight tendency is low for a soft foundation and increases as k_- increases. Recalling $k_- = \frac{kab}{mg}$, this shows that heavier blocks of the same dimensions are less likely to fly and bigger blocks of the same weight and aspect ratio are more prone to flight. At any given r, there exists a sufficiently high k_- such that the block flies unless special low energy initial conditions are chosen. For given initial conditions with sufficient energy, there exists a complicated transition zone between the region in the parameter space where the block never flies and the region where it always flies early.

Stability

Static stability of the block is studied. All equilibrium positions of the block in the considered angle range are found and determined to be stable or unstable. It is shown analytically that the block's vertical equilibrium position is stable only for k_- above a certain critical value, which increases with r. This suggests that the aspect ratio, not only mere height, may be a serious limiting factor in future attempts to construct super high buildings.

Dynamical analysis employing the described model shows that the stability of the block against overturning increases with the coefficient of friction for the considered initial conditions. This however, may be untrue for other initial conditions. Stability is further found to increase with k_-. Recalling $k_- = \frac{kab}{mg}$, this suggests that heavier blocks of the same dimensions are less stable and bigger blocks of the same weight and aspect ratio are more stable. The latter observation confirms work done by *Housner* [1963]. Finally, as expected intuitively, stability is found to decrease rapidly as the block becomes taller. There exists a sharp boundary in (k_-, r) parameter space separating a region where the block overturns and region where it does not for the considered initial conditions.

Chaos

In the final chapter, chaos is studied in the dynamics of the considered system. Chaotic motion occurs in certain subsets of parameter space and for certain initial conditions; roughly speaking, for initial conditions with sufficient energy and in subset of parameter space where k_- is high and r is low, i.e., tall block on hard foundation. When $\mu = 0$ chaos is found for all aspect ratios.

Liapunov exponents and Poincare maps are computed to provide numerical evidence for chaos

in the considered system. Poincare maps are computed at several points in the parameter space for various initial conditions to display different chaotic regimes. Strange attractors, i.e., chaos on attracting, invariant sets with Cantor structure, are not found.

Chaos was already reported in rigid block dynamics with *external forcing* by several authors. Numerical work presented in this thesis shows that chaos exists also in *free, unforced* dynamics of rigid blocks.

Parametric plots

Parametric plots of the block's response in the (k_-, r) parameter space for $\mu = 0.2$ are shown in Figures 6.1 and 6.2. These plots locate more precisely where in parameter space, various types of discussed response occur for considered initial conditions.

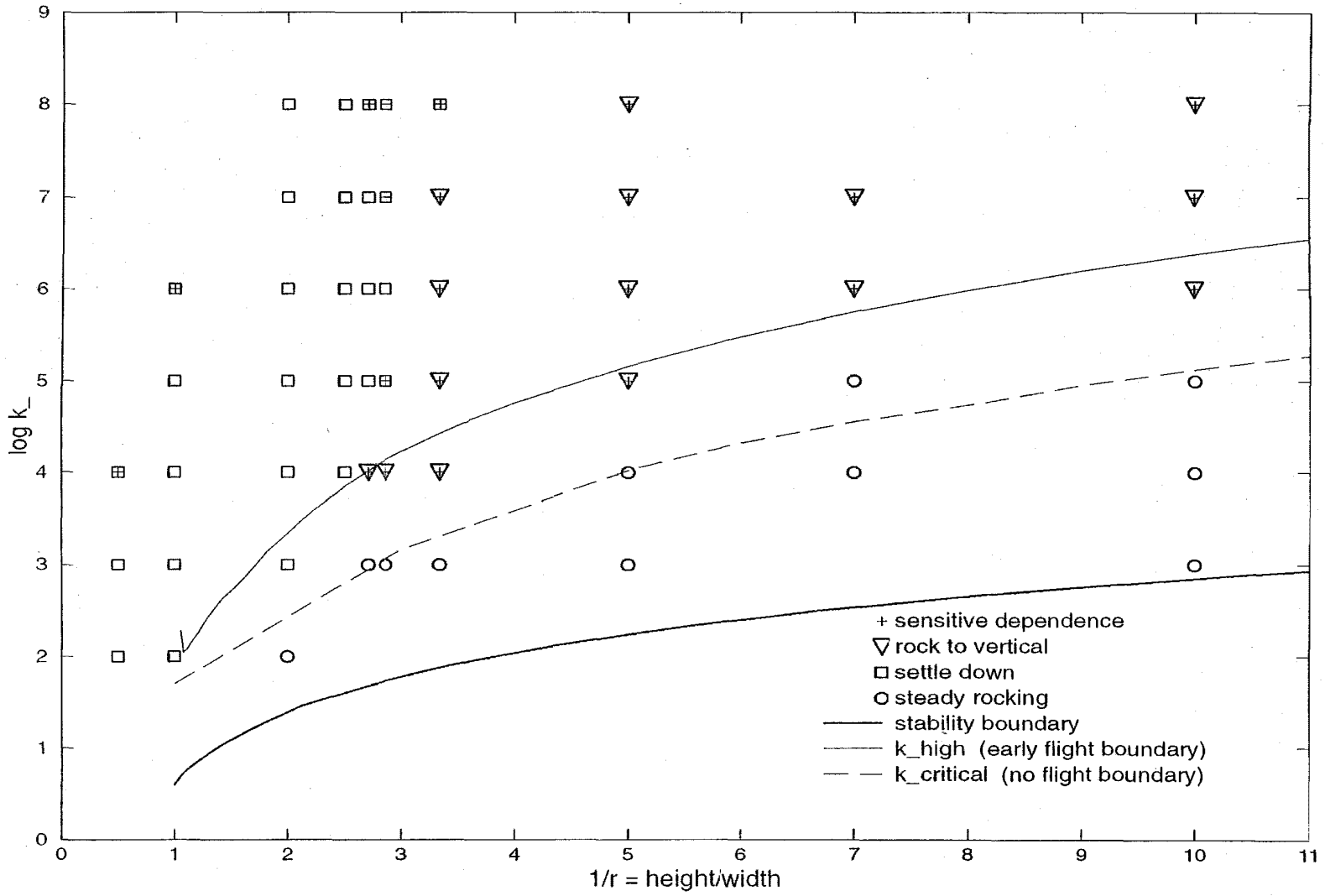response types in (k_,r) parameter space
cf=0.2,   initial conditions ic1

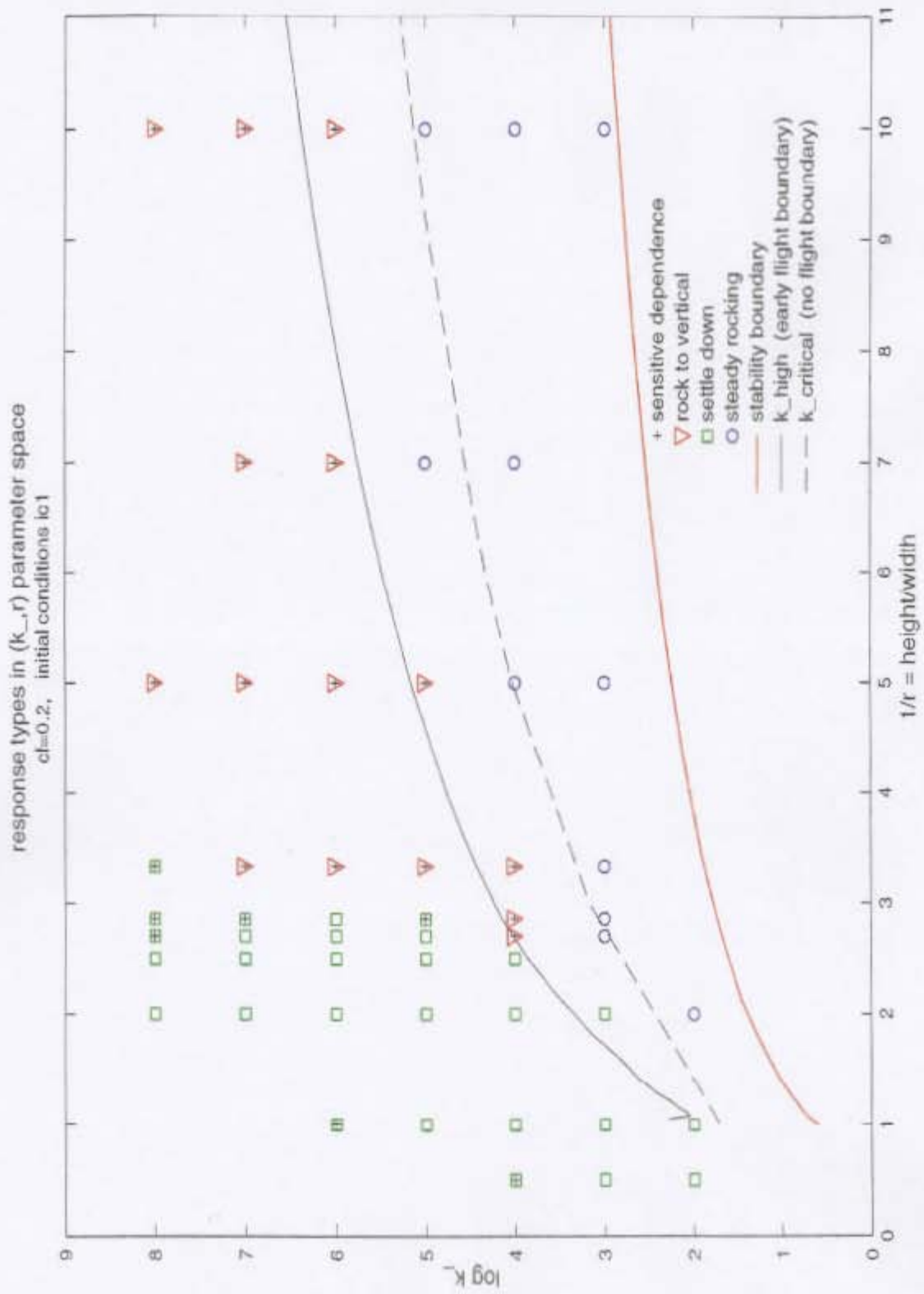Figure 6.1: Response in (k_-, r) parameter space at $\mu = 0.2$ for ic1

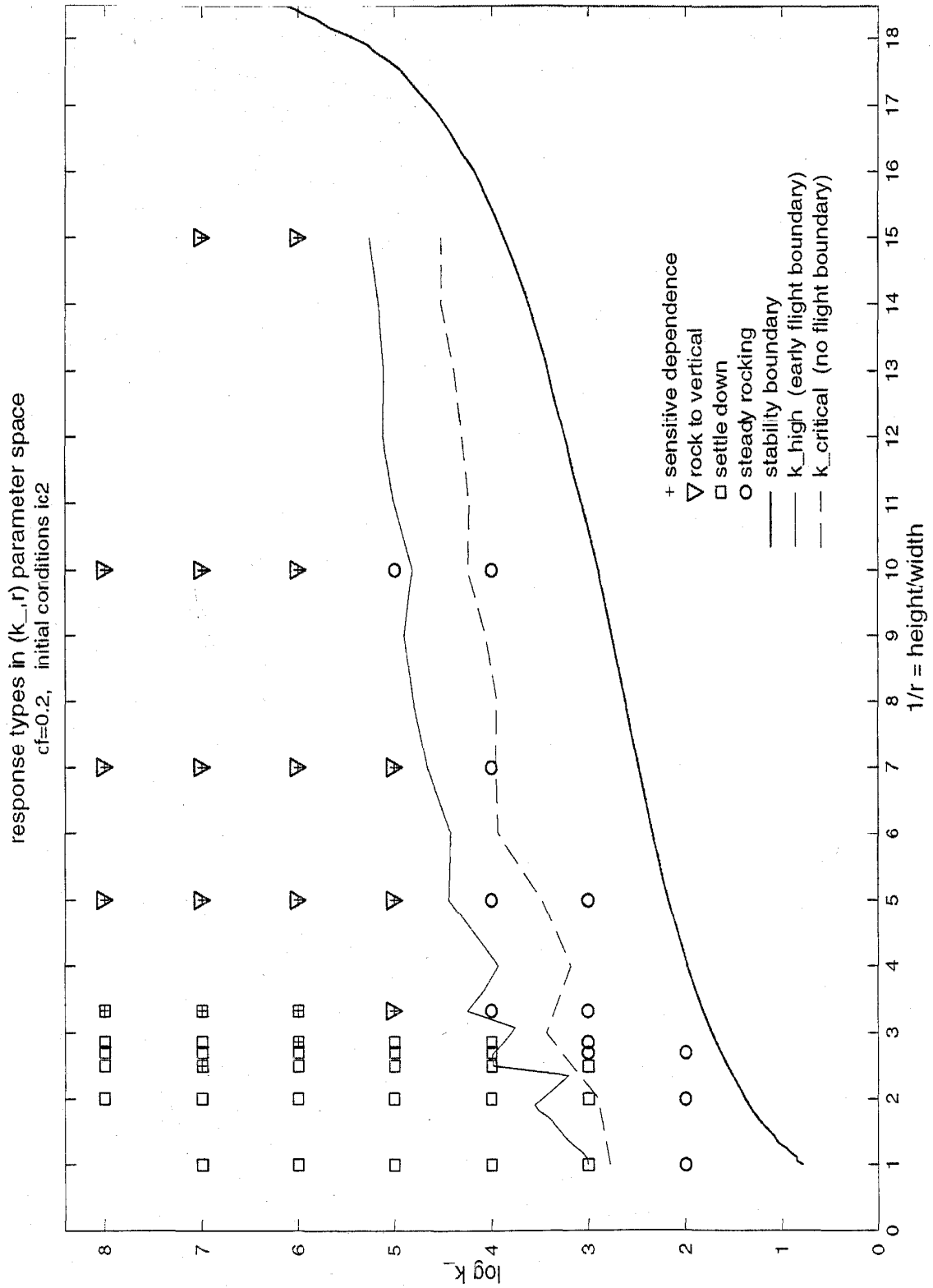Figure 6.1: Response in (k_-, r) parameter space at $\mu = 0.2$ for ic1

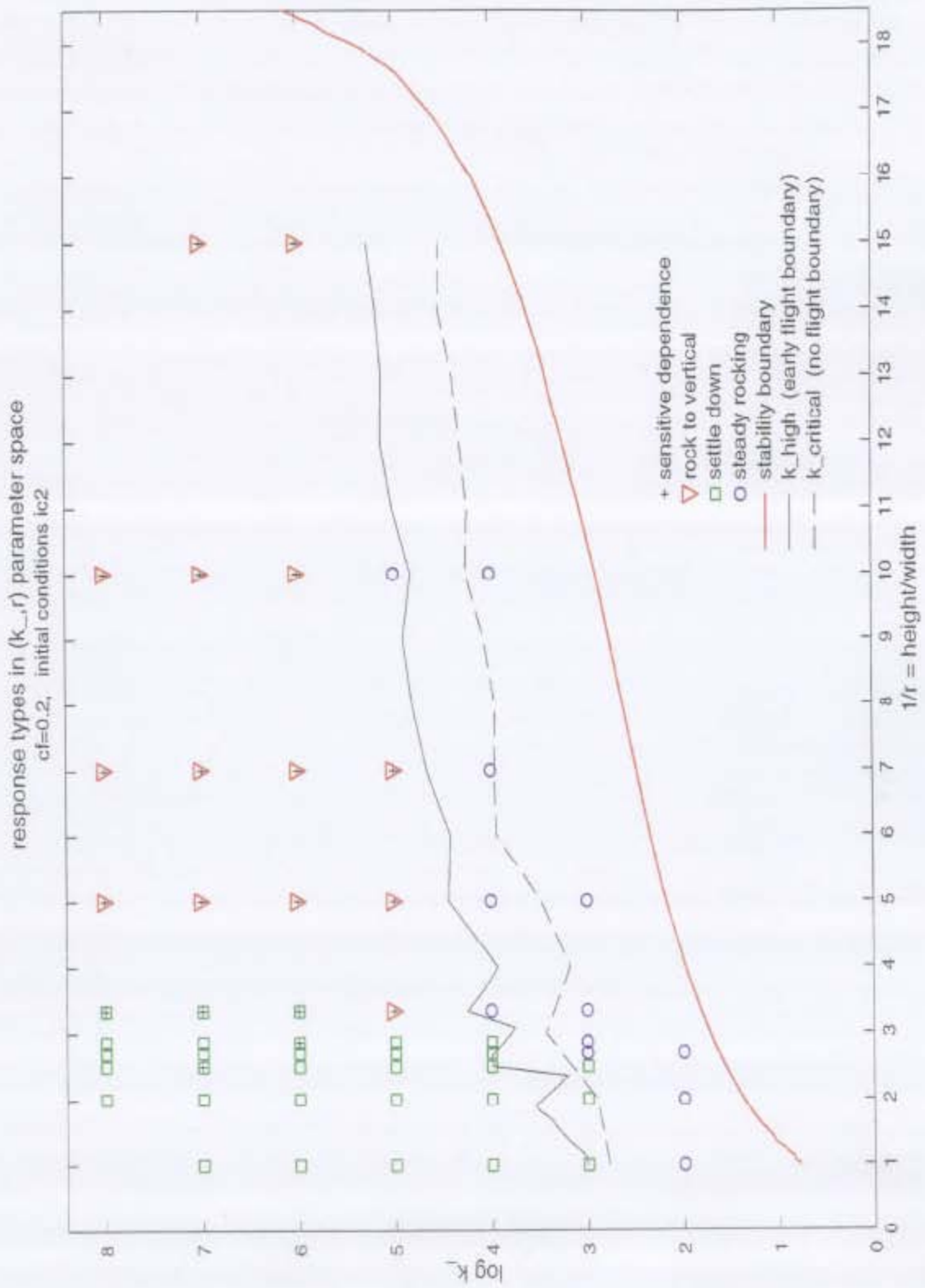Figure 6.2: Response in (k_-, r) parameter space at $\mu = 0.2$ for ic2

Figure 6.2: Response in (k_-, r) parameter space at $\mu = 0.2$ for ic2

Bibliography

Ames, W., W. Kuhn, and W. Rufeger, Computational chaos may be due to a single local error, *Journal Of Computational Physics*, *104*, 241–250, 1993.

Andreaus, U., Sliding uplifting response of rigid blocks to base excitation, *Earthquake Engineering and Structural Dynamics*, *19*(8), 1181–1196, 1990.

Aslam, M., W. G. Godden, and T. D. Scalise, Earthquake rocking response of rigid bodies, *Journal of Structural Division*, pp. 377–392, 1980.

Benettin, G., L. Galgani, A. Giorgilli, and J.-M. Strelcyn, Lyapunov characteristic exponents for smooth dynamical systems and for hamiltonian systems; a method for computing all of them, *Meccanica*, *9-20*, 1980.

Bruhn, B., and B. Koch, Heteroclinic bifurcations and invariant manifolds in rocking block dynamics, *Zeitschrift Fur Naturforschung*, *46*, 481–490, 1991.

Guckenheimer, J., and P. Holmes, *Nonlinear Oscillations, Dynamical Systems, and Bifurcations of Vector Fields*, Applied mathematical sciences. Springer-Verlag, 1983.

Hogan, S. J., The effect of damping on rigid block motion under harmonic forcing, *Proc. R. Soc. Lond.*, *437*, 97–108, 1992a.

Hogan, S. J., Heteroclinic bifurcations in damped rigid block motion, *Proc. R. Soc. Lond.*, *439*, 155–162, 1992b.

Hogan, S. J., Rigid block dynamics confined between side-walls, *Phil. Trans. R. Soc. Lond.*, *347*, 411–419, 1994a.

Hogan, S. J., Slender rigid block motion, *Journal of Engineering Mechanics*, *120*(1), 1994b.

Housner, G., The behavior of inverted pendulum structures during earthquakes, *Bulletin of the Seismological Society of America*, *53*, 404–417, 1963.

Jones, N. P., and H. W. ShentonIII, Generalized slide-rock response of rigid blocks during earth-quakes, in *Proceedings of Fourth U.S. National Conference on Earthquake Engineering*, vol. 3, pp. 31–40. 1990.

Koh, A. S., and P. D. Spanos, Harmonic rocking of rigid block on flexible foundation, *Journal of Engineering Mechanics*, *112*(11), 1165–1180, 1986.

Lorenz, E. N., The local structure of a chaotic attractor in four dimensions, *Physica*, *13D*, 90–104, 1984.

Matsui, K., M. Iura, T. Sasaki, and I. Kosaka, Periodic response of a rigid block resting on a footing subjected to harmonic excitation, *Earthquake Engineering and Structural Dynamics*, *20*(7), 683–697, 1991.

Parker, T. S., and L. O. Chua, *Practical Numerical Algorithms for Chaotic Systems*. Springer-Verlag, 1989.

Press, W. H., S. A. Teukolsky, W. T. Vetterling, and B. P. Flannery, *Numerical Recipes in C: The Art of Scientific Computing*. Cambridge University Press, second edn., 1992.

Psycharis, I. N., Effect of base uplift on dynamic response of SDOF structures, *Journal of Structural Engineering*, *117*(3), 733–754, 1991.

ShentonIII, H. W., Response of rigid bodies to base excitation, Ph.D. thesis, Johns Hopkins University, 1990.

Spanos, P. D., and A. S. Koh, Rocking of rigid blocks due to harmonic shaking, *Journal of Engineering Mechanics*, *110*(11), 1627–1642, 1984.

Wiggins, S., *Introduction to Applied Nonlinear Dynamical Systems and Chaos*, Texts in Applied Mathematics. Springer-Verlag, 1990.

Wolf, A., J. Swift, H. Swinney, and J. A. Vastano, Determining lyapunov exponents from a time series, *Physica*, *16D*, 285–317, 1985.

Yim, C.-S., and A. K. Chopra, Effects of transient foundation uplift on earthquake response of structures, Tech. Rep. UCB/EERC-83/09, University Of California, Berkeley, 1983.

Yim, C. S. S., and H. Lin, Chaotic behavior and stability of free-standing offshore equipment, *Ocean Engineering*, *18*(3), 225–250, 1991a.

Yim, S. C. S., and H. Lin, Nonlinear impact and chaotic response of slender rocking objects, *Journal of Engineering Mechanics, 117*(9), 1991b.

Zaremba, S., Theory of liapunov characteristic exponents, memo, Caltech, 1992.